Fatigue analysis of seam welds in lightweight aluminum structures

Vukić, Mislav

Master's thesis / Diplomski rad

2021

Degree Grantor / Ustanova koja je dodijelila akademski / stručni stupanj: **University of Zagreb, Faculty of Mechanical Engineering and Naval Architecture / Sveučilište u Zagrebu, Fakultet strojarstva i brodogradnje**

Permanent link / Trajna poveznica: https://urn.nsk.hr/urn:nbn:hr:235:072463

UNIVERSITY OF ZAGREB
FACULTY OF MECHANICAL ENGINEERING AND NAVAL ARCHITECTURE

MASTER THESIS

Mislav Vukić

Zagreb, 2021

UNIVERSITY OF ZAGREB
FACULTY OF MECHANICAL ENGINEERING AND NAVAL ARCHITECTURE

MASTER THESIS

Mentor:

Prof. dr. sc. Zdenko Tonković, dipl. ing.

Student:

Mislav Vukić

Zagreb, 2021

Hereby I declare that I have prepared this thesis independently, using the knowledge acquired during my studies and the cited literature. I would also like to point out that the work covered by this thesis has been supported by AVL-AST d.o.o. office in Zagreb, an official subsidiary of AVL GmbH with headquarters in Graz.

First of all, I would like to take this opportunity to thank the PTE department manager of the Zagreb office Mr. Nikola Naranča, for giving me the opportunity to work on an R&D project like this one, it has been a wonderful experience from which I learned a great deal. Many thanks go to Mr. Roman Baranja, for all his help in preparation of this master thesis, which he provided daily as a fantastic mentor of mine in the Zagreb office and without him all this wouldn't be possible. A big thank you also goes to Mr. Richard Tichy and Mr. Harald Pramberger who were present at all weekly meetings regarding this master thesis, as well as to all of the other colleagues in AVL, both in Zagreb and in Graz, who helped whenever it was needed, especially to the team in AVL Material lab which conducted the experimental investigations for the purposes of this thesis.

I would also like to thank Prof. Zdenko Tonković, who was my mentor at the faculty for the purposes of this master thesis, for his time, cooperation, patience and understanding. It was a pleasure to work with him, the same as with Prof. Ivica Garašić and his team at the Department of welded structures within the Faculty of Mechanical Engineering and Naval Architecture in Zagreb. They were in charge of the welding of the specimens for the experimental investigations and they were kind enough to do it with no charge since it was for the purposes of a master thesis, therefore I would like to express my gratitude for that.

Finally, I would like to thank my parents, Leda, and Miroslav, for always supporting me in my decision to study at the Faculty of Mechanical Engineering and Naval Architecture, never doubting my choices and always being there to help however they can.

Mislav Vukić

SVEUČILIŠTE U ZAGREBU
FAKULTET STROJARSTVA I BRODOGRADNJE
Središnje povjerenstvo za završne i diplomske ispite
Povjerenstvo za diplomske ispite studija strojarstva za smjerove:
Procesno-energetski, konstrukcijski, inženjersko modeliranje i računalne simulacije i brodostrojarski

Sveučilište u Zagrebu Fakultet strojarstva i brodogradnje	
Datum	Prilog
Klasa: **602 - 04 / 21 - 6 / 1**	
Ur.broj: **15 - 1703 - 21 -**	

DIPLOMSKI ZADATAK

Student: **Mislav Vukić** JMBAG: 0035204254

Naslov rada na hrvatskom jeziku: **Analiza zamora šavnih zavara u lakim aluminijskim konstrukcijama**

Naslov rada na engleskom jeziku: **Fatigue analysis of seam welds in lightweight aluminum structures**

Opis zadatka:

Nowadays, with the strong growing development of the hybrid and electric powertrains, the usage of lightweight materials plays a decisive role due to overall requirements for the general mass reduction and optimization for the whole vehicle and the powertrain components respectively. However, besides the reduced mass, the selected materials have to fulfil the overall strength criteria in order to ensure the structural integrity of the system, exposed to various types of load during the testing and homologation process so as during the vehicle operational lifetime respectively.

This master thesis will focus on the fatigue analysis of the seam welds joining extruded aluminum profiles, exposed to high cyclic loading. Extruded aluminum profiles are usually selected as a main structural element of the battery pack. Being one of the key elements of the electric powertrain, battery packs must be optimally designed and therefore the need for state-of-the-art analysis methods and processes is highly pronounced.

Based on everything said above in this study it is necessary to:

1. Study available literature and standards on the fatigue analysis of aluminum welded joints.
2. Investigate available finite element methods and tools for the weld fatigue analysis.
3. Design of the testing program and corresponding testing matrix.
4. Design and manufacturing of the test specimens.
5. Apply studied seam weld analysis procedures and compare to the experimental results.

During thesis preparation one must comply with the standard rules for preparation of master thesis. It is necessary to list all literature used and received assistance.

Zadatak zadan:	Datum predaje rada:	Predviđeni datumi obrane:
30. rujna 2021.	2. prosinca 2021.	13. – 17. prosinca 2021.

Zadatak zadao: Predsjednik Povjerenstva:

Prof. dr. sc. Zdenko Tonković Prof. dr. sc. Tanja Jurčević Lulić

CONTENTS

LIST OF FIGURES

LIST OF TABLES

NOMENCLATURE

Symbol	Unit	Description
a	mm	throat of the weld; crack length
a	-	numerical exponent
A	%	elongation
b	-	fatigue strength exponent
C	-	numerical constant
E	MPa	Young modulus
f	Hz	frequency
F	-	function of geometry, crack size and loading
F	N	loading force
ΔF	N	force range
F_{max}	N	maximum force
F_{min}	N	minimum force
$F_{unitary}$	N	unitary stress inducing force
G	-	sheet thickness influence factor
I	A	current
I	mm^2	moment of inertia
k	-	slope
K	-	stress intensity factor
ΔK	-	stress intensity factor range
ΔK_{th}	-	threshold stress intensity factor range
K_f	-	fatigue notch factor
K_f^*	-	reduced fatigue notch factor
$K_{f,\,r}$	-	Fatigue notch factor in the weld root
$K_{f,\,t}$	-	Fatigue notch factor in the weld toe
K_I	-	stress intensity factor for mode I
K_{Ic}	-	fracture toughness of the material
K_{II}	-	stress intensity factor for mode II
K_{III}	-	stress intensity factor for mode III
K_{max}	-	maximum stress intensity factor

K_t	-	stress concentration factor
m	-	numerical exponent
M	Nmm	applied moment
M_k	-	toe magnification factor
$M_{unitary}$	Nmm	unitary stress inducing moment
N	-	number of cycles
N_{end}	-	endurance cycle limit
N_f	-	number of cycles to failure
P	N	applied force
P_{max}	N	maximum force
P_S	%	survival probability
q	-	notch sensitivity
$q_{v,gas}$	l/min	shielding gas flow
R	-	stress ratio
R_m	MPa	ultimate tensile strength
$R_{p0.2}$	MPa	yield strength
s	-	support factor
S	MPa	stress
S_a	MPa	stress amplitude
t	mm	thickness
$T_{10/90}$	%	range of dispersion
U	V	voltage
v_{weld}	cm/min	welding speed
μ	-	friction coefficient
ν	-	Poisson's ratio
ρ	kg/m^3	density
ρ	mm	existing radius at the notch
ρ^*	mm	microstructural support length
ρ_f	mm	fictious notch radius
ρ_f^*	-	degree of cross sectional weakening
σ	MPa	stress
σ^*	-	surface stress ratio

$\Delta\sigma$	MPa	stress range
σ_a	MPa	stress amplitude
σ_A	MPa	fatigue strength for smooth structure
$\sigma_{A,\ notch}$	MPa	fatigue strength for notched structure
σ_f	MPa	fatigue effective notch stress
σ_f'	MPa	fatigue strength coefficient
σ_{hs}	MPa	hot spot stress
σ_l	MPa	lower surface remote stress
σ_m	MPa	mean stress
σ_{max}	MPa	minimum stress
σ_{min}	MPa	maximum stress
σ_n	MPa	nominal stress
σ_t	MPa	local notch stress
σ_u	MPa	upper surface remote stress

SUMMARY

Continuous advancements in the electrification of the whole automotive industry rely heavily on the use of lightweight materials. Due to the overall requirements for mass reduction that such rapid development imposes, lightweight materials such as aluminum play a major role in the optimization and development of powertrain components and vehicles while at the same time ensuring the structural integrity of the system.

In the introduction of this thesis a short overview of the four most common fatigue assessment methods is given which includes the description of the approaches based on nominal stress, structural hot spot stress, and effective notch stress as well as the crack propagation analysis. In the continuation of the thesis the focus will be on the fatigue assessment of weld seams joining extruded aluminum profiles with the use of modern-day fatigue assessment tools. A closer look will be given into the notch stress-based method behind *FEMFAT Weld* analysis tool and its benefits for the weld seam fatigue investigations. The fatigue assessment method for welded components proposed by *FEMFAT Weld* will be validated on an example of welded aluminum profiles from the literature before final experimental investigations begin. In the main focus of the work will be the high cycle fatigue testing of two different weld seams, I-seam butt weld and corner fillet weld, both made of extruded aluminum profiles. Along with the high cycle fatigue testing, additional microscopic measurements of the weld geometry and hardness will be performed. The results of such investigations will be used to conduct a thorough investigation of *FEMFAT Weld* in order to understand the notch stress methods that are being used and apply them in the desired way. The final results of fatigue assessment with the use of *FEMFAT Weld* analysis tool will be compared to the results from high cycle fatigue tests and certain conclusion will be drawn. In the end the work from this thesis will represent a detailed overview of *FEMFAT Weld* assessment tool and clear instructions on how to customize it to specific needs in respect to weld fatigue assessment.

Key words: fatigue assessment, seam weld, aluminum, *FEMFAT Weld*, notch stress

SAŽETAK

Neprestani napredak u elektrifikaciji cijele automobilske industrije uvelike se oslanja na korištenje lakih materijala. Zbog općih zahtjeva i potreba za smanjenjem mase koje nameće takav napredak, laki materijal kao što je aluminij igraju bitnu ulogu u optimizaciji i razvoju komponenti kako pogonskog sklopa tako i cijelog vozila, dok u isto vrijeme moraju osigurati strukturalni integritet cijelog sustava.

U uvodu ovog diplomskog rada dan je kratak pregled četiri najčešće metode procjene zamora koji uključuje opis pristupa temeljenih na nominalnom naprezanju, strukturnom „hot spot" naprezanju i efektivnom zareznom naprezanju, kao i opis analize propagacije pukotine. U nastavku rada fokus će biti na procjeni zamora šavnih zavara koji spajaju ekstrudirane aluminijske profile uz korištenje suvremenih alata za procjenu zamora. Detaljnije će se razmotriti metoda koja stoji iza *FEMFAT Weld* simulacijskog alata, a temelji se na zareznom naprezanju, kao i njene prednosti u procjeni zamora. Metoda procjene zamora za zavarene komponente koju predlaže *FEMFAT Weld* bit će provjerena na primjeru zavarenih aluminijskih profila preuzetom iz literature, prije samog početka eksperimentalnih ispitivanja. U glavnom fokusu rada bit će ispitivanje visokocikličkog zamora dvaju različitih šavnih zavara izrađenih od ekstrudiranih aluminijskih profila, sučeonog I-zavara i kutnog zavara. Uz visokocikličko ispitivanje zamora, izvršit će se i dodatna mikroskopska mjerenja geometrije te mjerenje tvrdoće zavara. Rezultati tih istraživanja poslužit će za provedbu temeljitog istraživanja *FEMFAT Weld* alata kako bi se bolje razumjele metode zareznih naprezanja koje se koriste kako bi ih se moglo primijeniti na željeni način. Konačni rezultati procjene zamora korištenjem *FEMFAT Weld* alata usporedit će se s rezultatima ispitivanja visokocikličkog zamora te će se izvući odgovarajući zaključci. Ovaj diplomski rad na kraju će predstavljati detaljan pregled *FEMFAT Weld* simulacijskog alata i jasne upute kako ga prilagoditi specifičnim potrebama u pogledu procjene zamora zavarenih spojeva.

Ključne riječi: procjena zamora, šavni zavar, aluminij, *FEMFAT Weld*, zarezno naprezanje

1 INTRODUCTION

In recent times, automotive industry is going through a major rehaul. In the last couple of decades, global warming has raised many concerns about the future of vehicle transport in regards of fuel consumption and CO_2 emissions. Each year worldwide vehicle regulations are getting stricter than ever before, see [Fig. 1], what forced the whole industry to find new solutions in terms of vehicle development.

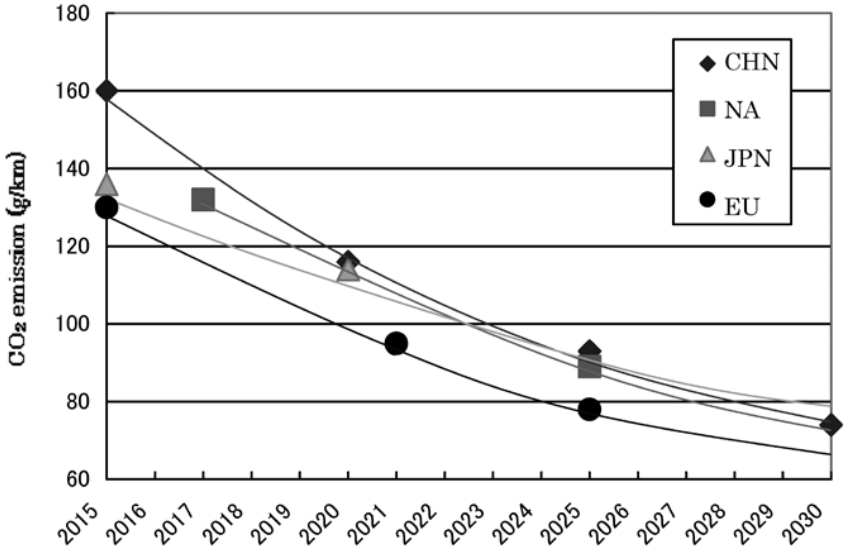

Figure 1: Diagram of strengthening standards on CO_2 emissions [1]

Besides the harsh regulations, hard and quality competition has forced vehicle manufacturers to be more cost effective. In order to accomplish that, saving time, costs, material and reducing weight is needed. From an engineering point of view, weight reduction in structural components of the vehicle is crucial in order to reduce fuel consumption, tire wear, noise and to enhance driving characteristics. All these effects are very appealing to the customer, but they must be accomplished while retaining the same standard of quality, functionality, service life and safety of the final product. To make weight reduction even harder, the evolution of the consumer electronics industry in recent years has led to an increase of the various equipment that has to be installed in an average vehicle. Naturally, all the electronic equipment increases the total weight of the vehicle by some margin as well. Considering all the mentioned parameters, vehicle manufacturers have turned to aluminum in the building of vehicles, more so than ever before.

The need and desire for the use of aluminum alloys in automotive industry is rising constantly from 1975 and this rise is expected only to increase in the coming years, see [Fig. 2]. This increase means that the modern vehicle bodies are comprised of several different materials and that many structural steel components are more and more often being replaced with aluminum or even some newer composite materials. According to Naito et al. [3], combination of steel and aluminum in modern vehicle bodies provides a great solution for reducing the weight of the final product without compromising the structural strength, quality, and safety requirements.

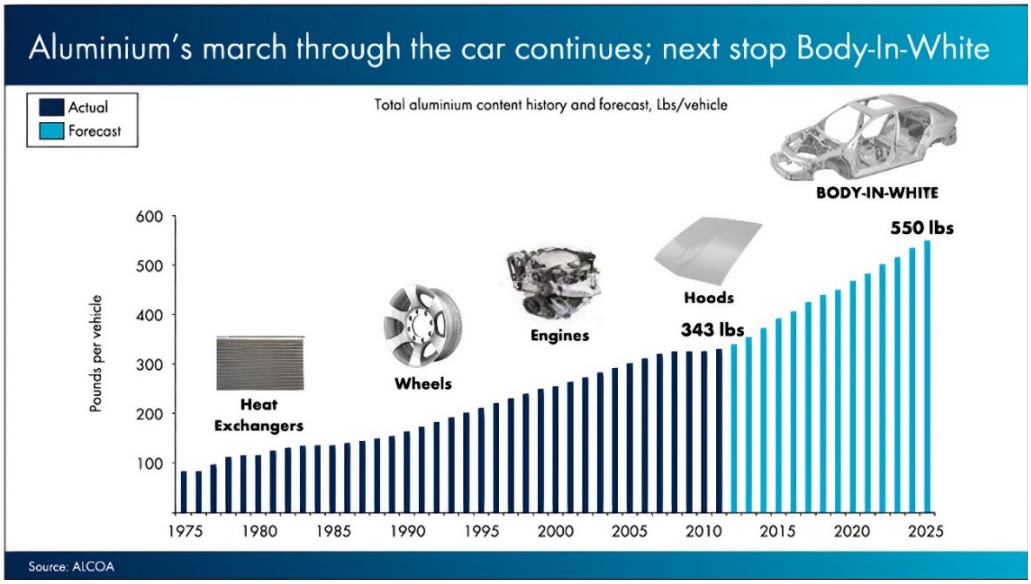

Figure 2: Diagram of a rise in aluminum content per vehicle over the years [2]

In comparison with steel, which has been the main material for the automotive industry a very long time, aluminum has a better strength to weight ratio. Therefore, although steel has a higher tensile strength and it is generally much stronger, it is almost 3 times denser than aluminum, and exactly the aluminums lightness is what provides the opportunity to drastically reduce the weight of the final product. Besides that, aluminum is more malleable than steel, which means it can be easily used for bending in all kinds of shapes and for extruding complicated cross sections without it starting to break or crack. As a final advantage over steel, we should mention that aluminum is very easy to recycle which makes it more cost efficient.

Aluminum alloys used in the automotive industry can be classified in several categories depending on the manufacturing technology (casting, extrusion or rolling alloys) and vehicle parts for which they are used. What this actually means is that a modern-day vehicle can mostly

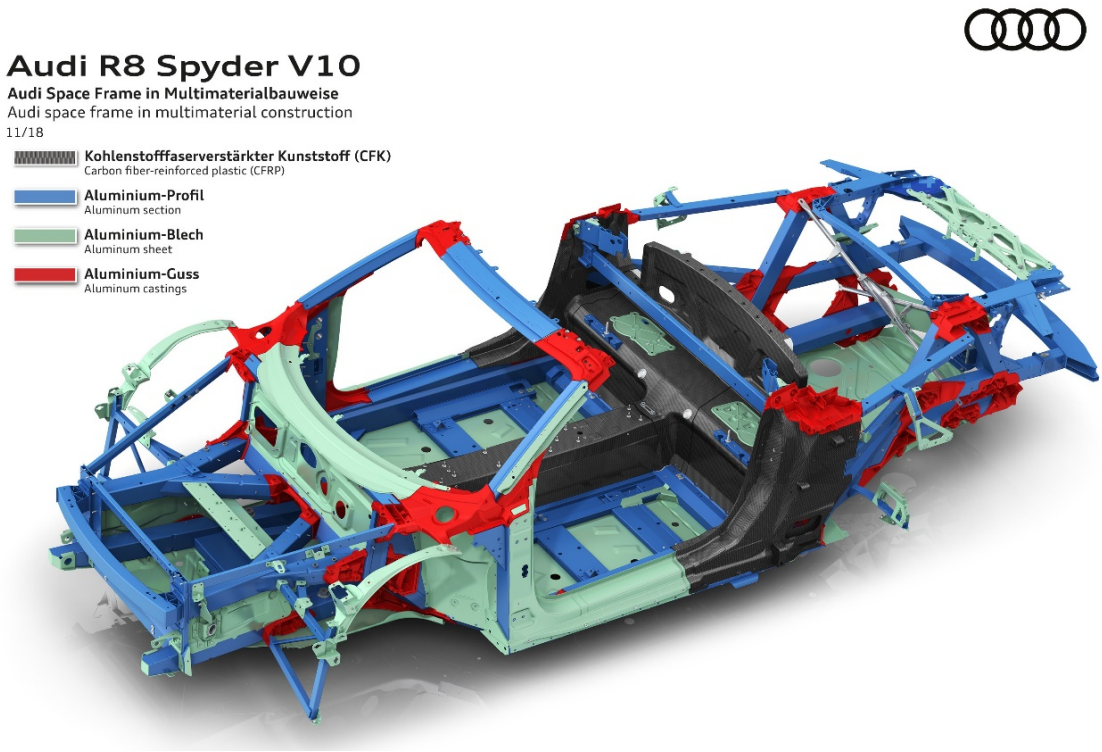

Figure 3: Audi R8 Spyder V10 space frame in multi-material construction [4]

be comprised of aluminum components that are produced with different technologies and alloys, in order to get the most beneficial properties from each shape and/or alloy composition. An example of such a vehicle body is depicted in [Fig. 3].

As it can be seen from [Fig. 3], extruded aluminum components are crucial for the structural integrity of a vehicle. In comparison to steel, this type of aluminum components has multiple advantages, but most importantly, it offers the possibility to improve both safety and performance of the vehicle while simultaneously reducing its mass. Some of the possible benefits of weight reduction are better acceleration and handling, shortening of the breaking distance, greater driving comfort and even better pedestrian protection. Also, according to the research done by EAA [5], at equal energy absorption, use of extruded aluminum alloys provides weight savings of around 40% in comparison to steel components because aluminum can absorb almost twice the crash energy than steel. Furthermore, thanks to the higher allowable material thickness, aluminum structures show extreme rigidity, so when combined with the possibility of extruding complicated shapes with different cross sections, it is possible to even improve the stiffness of a vehicle structure while reducing the weight by almost 50% in comparison to the available steel solutions.

As it was already mentioned, fuel consumption and CO_2 emission requirements are being reduced yearly, so it is no surprise that the process of electrification is rapidly taking over the automotive industry. Rising development of hybrid and electric powertrains provides a solution for the future of the automotive industry once the fossil fuel era comes to an end. However, this puts more challenges in front of vehicle manufacturers in terms of weight reduction and vehicle safety. In electric vehicles, battery packs are there to replace the fuel tank, and as it is with fuel, batteries present a flammable hazard as well. Therefore, it is of the most importance to prevent any kind of protrusion into the battery pack because such protrusions can have disastrous consequences. When all of the aforementioned benefits that aluminum offers, such as high strength to weigh ratio, lighter weight, and great energy absorption, are considered, it is no wonder that aluminum found a wide application in the housings for electric motors and electric batteries. Besides being used for the outer housing, extruded aluminum is commonly used for the crash structure inside the battery pack, an example of which is depicted in [Fig. 4]. Thanks to its great energy absorption, it provides a safety structure that ensures the structural stability of the battery pack in the event of a crash of any kind.

Figure 4: Audi e-tron 55 quattro integrated crash structure of the battery pack [6]

Vehicle bodies, housings for electric motors, battery packs with incorporated crash structures and many other vehicle components are often manufactured with the use of welding technology. Due to long and extensive welding experience in many automotive manufacturing companies and since the technology is very cost effective, welding seems to be the joining technology of choice for the automotive industry.

However, from a fatigue point of view, using welds as a main joining method for these structures is far from optimal. Whether the components are made from steel or aluminum, welding processes can introduce many defects into the structure that can lead to fatigue cracks under cyclic loading, and considering the recent trends in weight reduction, even if fatigue wasn't a critical failure mode for some of the components, reducing the weight of those components may cause fatigue to become one.

This leads to the conclusion that fatigue testing of vehicle components is an important part of automotive industry. To accomplish all the safety, regulatory and functional requirements for the final product, many welded structures must be subjected to fatigue testing even before the assembly begins. Along with the actual testing, most likely some finite element analyses of the tested component will also be conducted. Thanks to the enormous increase in computing power and great quality of modern finite element software, very detailed results can be obtained through such analyses. But to estimate fatigue life correctly, a suitable fatigue assessment method must be used for the finite element analyses results. This way, any premature failure or accident with the final product can be avoided.

With all things considered, the main focus of this master thesis will be the fatigue analysis of seam welds joining extruded aluminum profiles while exposed to high cycle loading. Over the years, it has been shown that extruded profiles are usually the main structural components of the battery pack, as it was already mentioned. Battery packs, as the biggest part of the electric powertrain, play the crucial role in structural stability of the whole powertrain and therefore they need to be assessed using the most accurate methods available. Investigation of applicable fatigue assessment methods will be conducted, and most recent fatigue element analysis methods will be used along with the results of actual fatigue tests carried out on welded aluminum specimens. Results of both, the experiment and finite element analysis, will be compared and the whole thesis will represent the basis of a methodology for the fatigue assessment of welds in future work and projects for simulation departments in AVL List GmbH.

2 FATIGUE LIFE ASSESSMENT METHODS

Fatigue is defined as a process during which an increasing number of cycles results in the accumulation of damage in a material that is subjected to fluctuating stresses and strains, a definition according to Almar-Næss [7]. This damage accumulation can eventually lead to a fracture and that is the most significant feature of fatigue. Basically, the load causing the fatigue fracture is not large enough to cause immediate failure so instead, failure occurs after a certain number of load fluctuations have been experienced i.e., after the accumulated damage has reached a critical point.

There are many approaches and theories that can be applied in order to assess the fatigue life of a certain component. Over the years, there have been many reviews and summaries of the existing fatigue life assessment methods since fatigue is a very complicated topic and an engineering problem that requires constant progress. However, from all of the available literature, it can be found that there are some theories used more often than others.

The most widespread fatigue assessment approach is the stress-based approach. With the use of this approach, the fatigue assessment of a specific component is done by comparing the design stresses with allowable stresses by means of stress-life curves, otherwise known as S-N or Wöhler curves. In these curves, the fatigue life (number of cycles N) is related to the applied stress range $\Delta\sigma$ or the stress amplitude σ_{a}. Each S-N curve may be based on different stress such as nominal, structural hot spot or effective notch stress which results in three different fatigue assessment methods. If no S-N curve for a given component or a material is available, the curves provided by design codes and standards such as Eurocode 9 [8], IIW [9], ECCS [10] etc. must be used. For metals, fatigue test data usually follow straight lines in a $\log S - \log N$ plot and those lines can be described with Basquin's law [11], which may be written as

$$\sigma_{\mathrm{a}} = \sigma_{\mathrm{f}}'(2N_{\mathrm{f}})^{b}\,, \tag{1}$$

where σ_{f}' is the fatigue strength coefficient, b is the fatigue strength exponent and N_{f} is the number of cycles to failure.

The three already mentioned methods are intended for application at the design stage in order to avoid fatigue failure during the design life of a component. However, there are methods with different approaches to fatigue assessment. One of these methods, also commonly used, is the crack propagation analysis. Crack propagation analysis is not generally used for design but for assessing known or assumed flaws in the component or the material.

This chapter will cover the description of the four most commonly used fatigue assessment methods. However, before introducing the approaches based on nominal stress, structural hot spot stress, and effective notch stress as well as the crack propagation analysis, a short overview of the relevant features of fatigue in welds is given.

2.1 Relevant features of fatigue in welds

Welding is a joining process that is affected by a lot of factors driven either by the welder, geometry of the components to be welded or metallurgical effects that occur during the process. With the development of technologies and the increasing use of welding robots, especially for mass produced structures, various influences have been minimized in order to maintain uniform weld quality. Despite of that, very often various structures are welded by hand, especially if they are some types of product prototypes, primarily due to lower costs of welding for a small series of welded structures. This means that mistakes in welding are common and weld quality is not always as uniform as it should be. If we add to this the fact that welded structures are often subjected to high cycle fatigue due to the longevity of their use, we can safely say that it is very important to know which errors or phenomena caused by welding affect the fatigue life most significantly.

Before the welding process even starts, it is necessary to choose the right filler material and shielding gas as well as to set a number of parameters such as current, voltage, travel speed, shielding gas flow etc., and each of these things can affect the quality of the weld in its own way. In addition to all of this, there are a number of other phenomena that can occur as a result of welding itself. Some of these phenomena according to Mathers [12] include distortion of the components that are welded together, incomplete fusion of the weld material with the base material, incomplete or excessive penetration of the weld, undercuts, porosity in the weld material, lack or excess of the weld material and many more.

All of the aforementioned defects can occur during the welding process and have an influence on the fatigue life of the welded structure. More often they will cause failures than they will positively affect the structures. However, in respect to fatigue, some defects are more important to look out for than others. Hence, in this chapter, a brief overview of the most important defects relevant for fatigue life is presented.

2.1.1 Crack-like defects

As already mentioned, welding can have many different negative effects on a structure for various reasons but maybe the most dangerous defects that can turn up are crack-like defects. Cracks are a defect that is most likely to significantly shorten the service life of a welded structure. With that in mind, it can be stated that the fatigue life of a welded structure is governed by the initiation and growth of one or more cracks. They don't need to necessarily start as large cracks, it is enough for the weld to have some common defects such as incomplete fusion or undercuts and these defects will act like stress concentrators which will shorten the time needed for crack initiation. When the crack appears, it needs some time to propagate and when it reaches its critical length, rapid failure occurs. Needless to say, this is something that is preferred to be avoided but, in most cases, cracks are inevitable because their form and position is often unknown and hard to spot. This is the reason why it is important to design welded structures in such a way that the possibility of a crack initiation is reduced to a minimum so that even if cracks cannot be fully avoided, their initiation can be postponed as long as possible. A good design with visual control of the welds along with the fatigue tests of welded structures can easily result in a long service life.

2.1.2 Residual stress

During the welding process, a significant amount of heat is transferred into the material in the close proximity of the weld. Since all metal materials and their alloys soften and expand at high temperatures, there is always some contraction that occurs in the weld material when cooling down to room temperature after welding. It is precisely this contraction of the material that leads to residual stress and distortion of the welded structure. Therefore, it is safe to say that residual stresses are an unavoidable occurrence in welded structures, as stated by Mathers [12], influenced by local geometry, global constraints, and the welding sequence, and they can vary from insignificantly low to very high stresses. If the distortion of the welded structure is local and evenly distributed, so are the residual stresses and the structure can be used for its purpose regardless of the residual stresses. However, sometimes the distortion can be so severe and with such a complicated multidirectional distribution of the residual stresses that the whole welded structure may be unusable for its intended purpose. In some cases, the residual stresses can even reach the magnitude of yield stress which is far from optimal for the welded structure in question in respect to the fatigue life.

Residual stresses basically act as an additional mean stress which means that the stress range applied to the welded structure won't change but the actual ratio of the minimal and maximal stress will be different from the applied stress ratio R. However, it is assumed that the residual stresses, especially those that go as high as yield stress magnitude, increase the mean stress at the weld to such a level that the influence of the applied stress ratio R is insignificant. This is the reason why it is usually said that welded structures are insensitive to the stress ratio R, see Maddox [13]. Even though they are inevitable, residual stresses can be removed from welded structures with stress relieving procedures. Through these procedures, the weld and basic material are heated to a certain temperature and then slowly cooled down in order to avoid the effect of instant cooling that causes the distortion and residual stresses after welding. However, these methods can't be applied every time, for various reasons, so very often welded structures are left in as-welded state. Therefore, it is of the most importance to account for the possible residual stresses in the welded structure before the assessment of the fatigue life is conducted.

2.1.3 The heat affected zone

As it was already stated, welding is a process that requires a significant heat input which is then largely absorbed by the base material. During welding, the heat is needed in order for welding material to melt and to achieve fusion with the base material but the whole area around the weld is affected by the immense heat that is produced. This heat input causes changes in the microstructure of the base material in the area around the weld, often called the heat affected zone (HAZ). Not only that the microstructure can change, but also different properties of the base material gained by postproduction heat treatments can be nullified after welding. All things considered, base materials may face a great reduction in strength because of the welding process which can have drastic consequences on the fatigue life of the welded structure. Possible solution of the strength reduction problem is to apply post weld treatments on welded structures to improve their fatigue life, which was investigated by Pinho-da-Cruz et al. [14]. They investigated what is the impact of post weld T6 heat treatment on fatigue strength for single lap welded elements and the conclusion was that this heat treatment improved their fatigue strength drastically. Hardness of the HAZ was recovered to the original value of the base material, microstructure was improved, and residual stresses were relieved. Therefore, removing the HAZ from the welded structure will most definitely cause an increase in fatigue strength.

2.2 Nominal stress approach

The assessment of fatigue strength and service life, usually up to the final fracture, with nominal stress approach, according to Radaj et al. [15], is a procedure in which the nominal stress amplitudes at the critical cross section of the component being analyzed, are compared directly with the allowable stress amplitudes from an existing, nominal S-N curve. The acting forces and moments can also be introduced directly into the diagram instead of the nominal stresses, in cases when it is not possible to meaningfully define them.

The nominal stress approach for the assessment of fatigue strength and service life of welded components shares the same procedure as the approach for the non-welded components, see Radaj et al. [15]. The only difference is in the main parameters that are influencing the S-N curve. In the case of welded components, the nominal S-N curve depends on material, notch class of the weld and weld quality class while in the case of non-welded components the most influential parameters for the nominal S-N curve are material, geometry, and surface parameters. The main procedural steps, as well as the main parameters in the case of welded components, are visually represented with the graph in [Fig. 5].

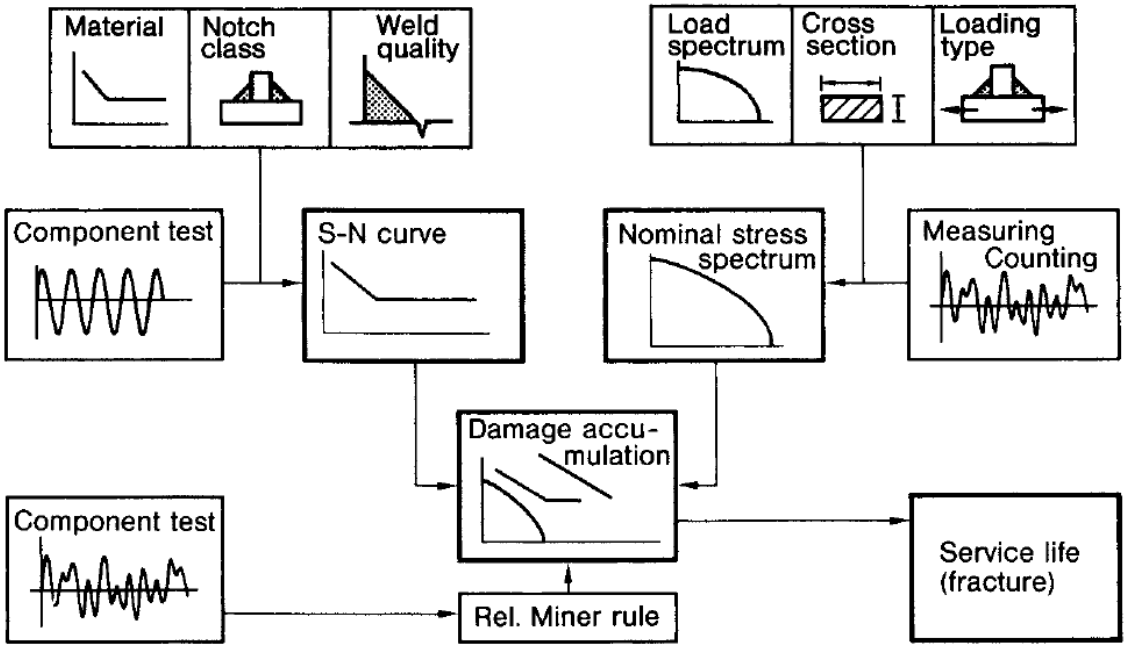

Figure 5: Main parameters and procedural steps controlling the nominal stress approach for welded components according to Radaj et al. [15]

Notch or detail classes, often called fatigue or FAT classes, as well as weld quality classes are assigned to sets of uniform design S-N curves which are generally linearized, parallelized and equidistantly positioned in logarithmic scales of the parameters S and N. An example of such a set of S-N curves is shown in [Fig. 6]. The welded joints are graded according to their shape, type of weld, loading type and quality of manufacture. They are then allocated to the detail classes representing the design S-N curves based on the result of relevant fatigue tests. Also, the detail classes are usually defined through the fatigue strength at $N = 2 \times 10^6$ cycles.

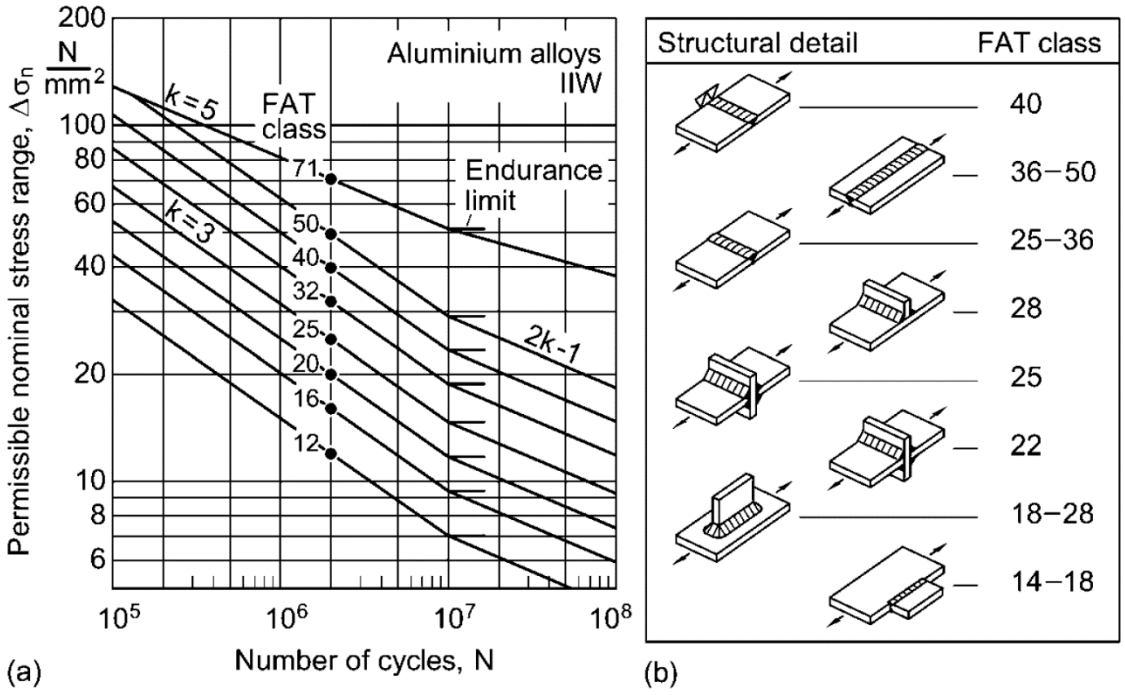

Figure 6: Design S-N curves for aluminum alloys given in IIW [16]: (a) permissible range of nominal stress, (b) notch classes for different welded joints

Considering all of the information presented so far, we can safely say that in the nominal stress approach, all information about the local stress distribution at the expected failure site is included in the nominal S-N curve. Furthermore, a nominal S-N curve is always connected to a specific geometry and load configuration. With this in mind, when using nominal stress approach, a detail class in the standard used, must be as similar as possible to the weld joint that is currently being analyzed. Reason for this is that each detail category possesses an S-N curve with the allowable stress for that specific weld joint type which is then compared to the nominal stress of the analyzed welded component, as it was mentioned in the beginning of this chapter.

The nominal stress from the welded component that is being analyzed can be found in multiple ways. The simplest one is by using the basic principles of strength of materials i.e., analytical equations, depending on the type of geometry and loading. Besides the analytical approach, stress can be acquired from a finite element analysis or from strain measurements at the actual specimen of the component where the most important thing is that the measurements are taken somewhere away from the weld in order to find the true nominal stress without any influence of local stress concentrations. However, if large stress concentrations are present, nominal stress must be multiplied by a certain stress concentration factor to account for those stress concentrations, if they are not already included in the nominal S-N curve.

All things considered, nominal stress approach is applicable only if the weld joint that is being analyzed is geometrically simple. As soon as the geometry of the weld or the component gets more complicated, there is a great chance that such joint is not defined in the existing standards from which nominal S-N curves are taken from.

Nevertheless, the nominal stress approach is the basis of fatigue assessment in many areas of mechanical and structural engineering such as construction of bridges, cranes, vessels, pipes, rail vehicles, ships and many more. The approach is also incorporated in the relevant design codes. However, according to Radaj et al. [15], areas of engineering with exceptionally high demands for lightweight design and damage tolerance, commonly do not use this approach, the preference being for local approaches. These areas are primarily automotive and aircraft engineering and as a preference over the nominal stress approach, they have introduced different local approaches in their assessment procedures.

2.3 Structural hot spot stress approach

As presented in the previous chapter, nominal stress is easy to define in cases where simple welded structures are being analyzed. However, in real life applications, welded structures are seldom simple. As stated by Maddox [17], various stress concentrations due to geometrical discontinuities, non-uniform stress distribution and stress gradients through the thickness of the welded structure can reach such a level of complexity that the nominal stress is no longer so easy to define. Therefore, new approaches have been developed with structural hot spot stress being one of them. In the literature this approach can be found under several names such as structural stress, geometrical stress, hot spot stress or as a combination of the above. According to IIW [9], the structural stress at the "hot spot" of the weld i.e., critical point of the weld, is named structural hot spot stress so this nomenclature will be followed in this thesis.

The structural hot spot stress approach is an extension of the nominal stress approach in the sense of using the S-N curves obtained from tests conducted with actual welded joints. The difference between the two approaches is in the stress range used for the assessment of the welded structure. Instead of using the nominal stress range, structural hot spot stress approach focuses on the structural stress range at the "hot spot" of the weld. The structural stress is the actual stress in the structure which means it doesn't include the stress raising effect caused by the weld profile as depicted in [Fig. 7].

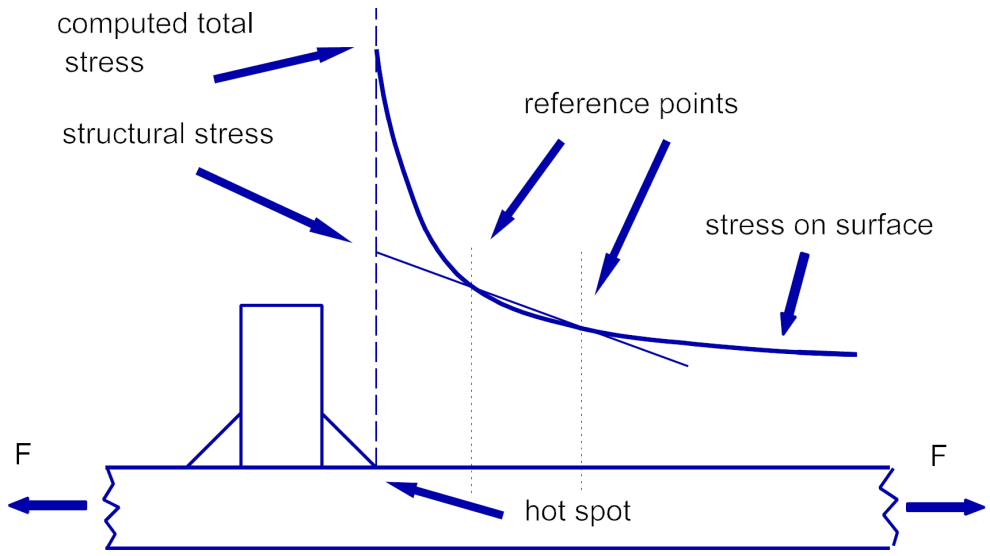

Figure 7: Definition of structural hot spot stress according to IIW [9]

It is a combination of membrane and bending stresses with a linear distribution through the thickness of the structure. Although it doesn't include stress concentrations due to the weld profile, structural stress includes all stress concentrations caused by loading parameters and geometry of the joint in question. Therefore, by using structural hot spot stress, number of detail categories i.e., standard S-N curves, can be significantly reduced in comparison with the nominal stress approach.

Strictly speaking, the structural hot spot stress approach is suited for the fatigue assessment of the weld toe and it is not applicable for the fatigue failure starting from the weld root. According to IIW [9], the approach may be used for the assessment of other crack initiation sites such as weld root by using the structural hot spot stress at the surface of the welded structure as an indication of the stress in the region of interest. However, this must be used with caution since in such cases the S-N curves used for verification are heavily dependent on the geometric and dimensional parameters and can be used only in the certain range of these parameters. For the purpose of this thesis, the structural hot spot stress approach will be considered as only applicable for the weld toe fatigue failure.

As it can be seen in [Fig. 7], structural hot spot stress is actually a fictious value which means it has to be found either by means of extrapolation of the stress at the surface in the vicinity of the weld toe, by linearization of the stress through the thickness of the plate or by means of specifically adapted parametric equations. Either way, whichever method for the calculation is chosen, structural stresses at certain reference points must be obtained in order to calculate the structural hot spot stress. These reference point stresses are used in order to capture the stress distribution in the area approaching the weld and can be found either by calculation or by conducting measurements. This thesis will focus on extrapolation procedures of surface stresses which are basically the same for both, experimental measurement, and calculation.

The original method of finding the structural hot spot stress is by measuring strains at different reference points at the surface ahead of the weld toe. For the measurement, strain gauges are used, and placed both, perpendicular and parallel to the weld toe since both contribute to the structural stress perpendicular to the weld toe. Naturally, the placement of the strain gauges depends on the chosen extrapolation method. From the measured strains, structural stresses at the reference points are calculated which are then used for the extrapolation of the structural hot spot stress at the weld toe.

The second approach to obtaining the surface structural stresses at the reference points is by the means of finite element analysis. This method is used more and more often in today's world since it is much faster, simpler to conduct and more cost effective. Also, strain gauges have certain limitations in regard to their length and applicability for smaller plate thicknesses. However, if structural hot spot stress is chosen as a main fatigue assessment method for research purposes of any kind, it is always beneficial to use both, strain measurement and finite element approach, for the sake of result verification.

So, the procedure is first to define the reference points and then to calculate the structural hot spot stress using extrapolation to the weld toe from the stresses of those reference points. Regardless of how these reference point stresses were obtained i.e., via measurement or finite element analysis, the procedure is the same. There are several extrapolation methods available and depending on the method there may be from one to three reference points.

The IIW document [9] distinguishes two different types of "hot spots" and describes different extrapolation methods for each type. Type "a" is a "hot spot" where reference points can be related to the plate thickness i.e., stress distribution depends on it. Type "b" "hot spots" on the other hand refer to cases where the stress distribution is not influenced by the plate thickness. In order to find the structural hot spot stress for type "a" "hot spot", IIW [9] proposes three different extrapolation equations depending on the mesh quality of the finite element grid. If fine mesh with element length of maximum $0.4\ t$ at the "hot spot" is used, two reference points at $0.4\ t$ and $1.0\ t$ must be assessed and used for linear extrapolation according to the following equation:

$$\sigma_{\mathrm{hs}} = 1.67 \cdot \sigma_{0.4\cdot \mathrm{t}} - 0.67 \cdot \sigma_{1.0\cdot \mathrm{t}} \,. \tag{2}$$

In case of thick-walled structures or when steep stress gradients occur, the same fine mesh can be used with quadratic extrapolation at three reference points $0.4\ t$, $0.9\ t$ and $1.4\ t$ with equation being as follows:

$$\sigma_{\mathrm{hs}} = 2.52 \cdot \sigma_{0.4\cdot \mathrm{t}} - 2.24 \cdot \sigma_{0.9\cdot \mathrm{t}} + 0.72 \cdot \sigma_{1.4\cdot \mathrm{t}} \,. \tag{3}$$

Finally, if the assessed structure has a coarse mesh with elements of higher order and length equal to the plate thickness at the "hot spot", linear extrapolation with two reference points at $0.5\ t$ and $1.5\ t$ is recommended:

$$\sigma_{\mathrm{hs}} = 1.50 \cdot \sigma_{0.5\cdot \mathrm{t}} - 0.50 \cdot \sigma_{1.5\cdot \mathrm{t}} \,. \tag{4}$$

For type "b" "hot spots", two different extrapolation methods are proposed by the IIW document [9], first being the quadratic extrapolation at three reference points 4 mm, 9 mm and 12 mm away from the "hot spot" if fine mesh with maximum element length of 4 mm at the "hot spot" is used. The corresponding equation goes as follows:

$$\sigma_{\mathrm{hs}} = 3 \cdot \sigma_{4\ \mathrm{mm}} - 3 \cdot \sigma_{8\ \mathrm{mm}} + \sigma_{12\ \mathrm{mm}} . \tag{5}$$

When coarse mesh is used, with higher order elements having length of 10 mm at the "hot spot", reference points are to be placed at the middle of the first two elements with linear extrapolation according to the following equation:

$$\sigma_{\mathrm{hs}} = 1.5 \cdot \sigma_{5\ \mathrm{mm}} - 0.5 \cdot \sigma_{15\ \mathrm{mm}} . \tag{6}$$

Graphical overview of the aforementioned reference points at different types of meshing is given in [Fig. 8].

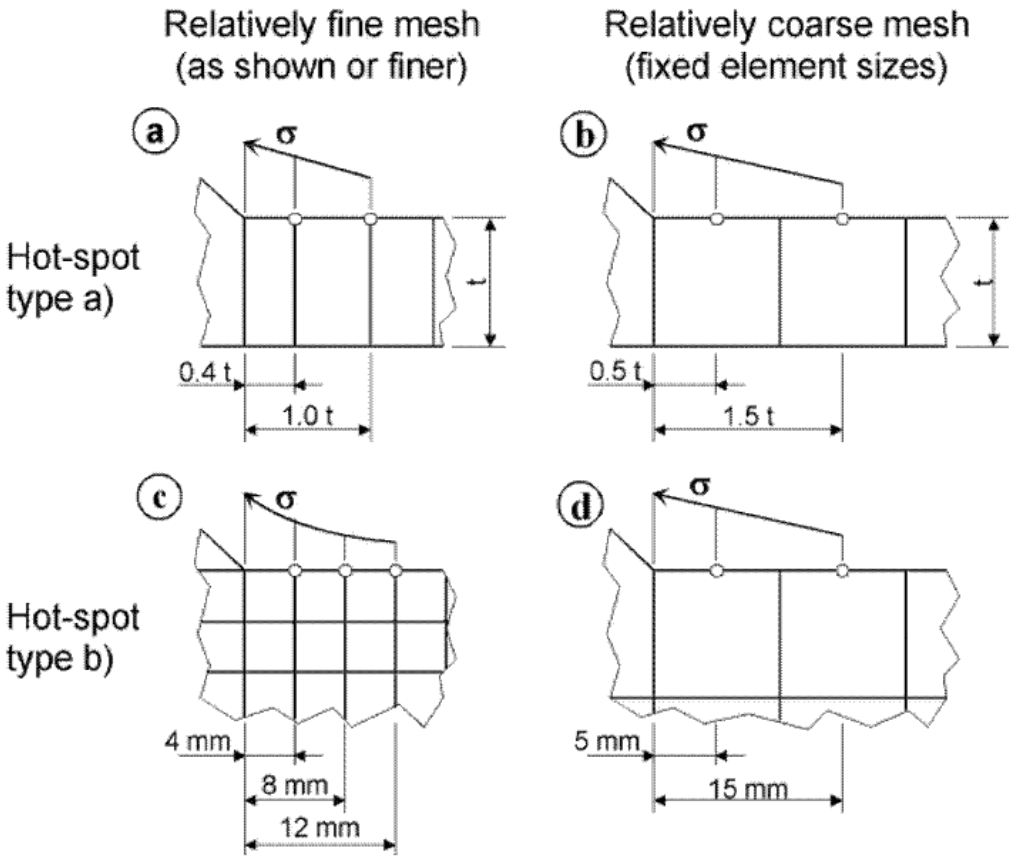

Figure 8: Reference points at different type of meshing according to IIW [9]

Besides the IIW document there are many other recommendations for the placement of the reference points. For example, the DNV document [18] recommends two different methods for the extrapolation of the structural hot spot stress at the weld toe. The first one is to place the reference points at $0.5\ t$ and $1.5\ t$ from the weld toe, while the other one proposes to use only the reference point at $0.5\ t$ with a multiplication factor of 1.12 in order to obtain the structural hot spot stress at the weld toe.

All of these methods are applicable for the use of either shell or solid elements for the finite element analysis but the one difference that must be clarified between these approaches is the position of the "hot spot", see [Fig. 9]. Although the weld geometry can be modelled with both element types, its modelling is often avoided when using shell elements in order to keep the model as simple as possible. So, if solid elements are used, then the weld geometry is modeled, and the "hot spot" is indeed at the weld toe. However, if shell elements are used for the modeling of the grid, that usually means the weld geometry isn't modelled in which case IIW [9] recommends that the extrapolation be conducted to the intersection point of the shell elements in order to avoid stress underestimation due to the missing stiffness of the weld geometry.

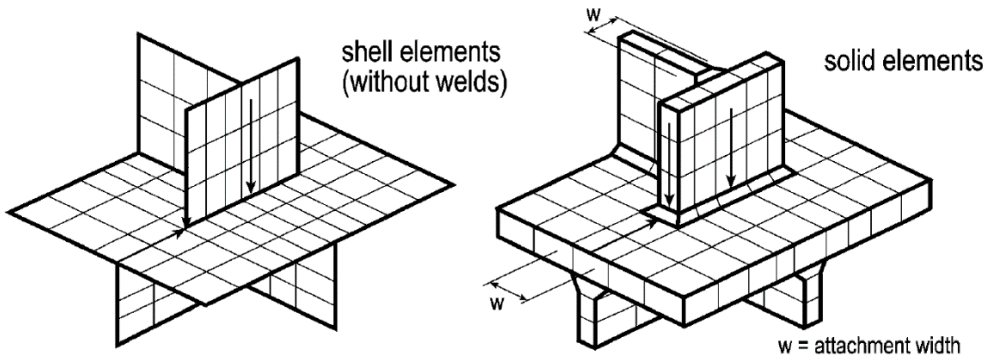

Figure 9: "Hot spot" placement in respect to meshing approach [9]

Structural hot spot stress approach offers many different possibilities for the assessment of welded structures but there are still several difficulties involved. Research by Lee et al. [19], has shown that the results depend not only on how the "hot spot" is defined but also on the modelling of the structure. Depending on the geometry and loading conditions using linear or quadratic extrapolation can yield different results with element type and mesh density also having an impact on the final results, as Tveiten [20] has shown. All in all, a uniform and schematic structural hot spot stress approach is hard to define.

2.4 Effective notch stress approach

When choosing either nominal or structural hot spot stress approach for fatigue assessment of structural components, the effect of all or at least some of the stress concentrations found in the structure is already included in the respective S-N curves. Both approaches are used in order to bypass the local stress at the most critical site where the crack initiation is expected. However, the effective notch stress approach deals with that local stress as the main indicator for the fatigue life of the structural component. This local stress at the expected failure site of the structure is used together with one material dependent S-N curve, therefore the effective notch stress approach has the benefit of having the same S-N curve, regardless of how the geometry of the structural component looks like. This is the main reason why this approach is becoming more attractive to the engineering world and various methods have been developed in order to apply this to welded structures. The most prominent one being the effective notch stress approach according to Radaj [21] with fictious notch rounding.

Based on Radaj [15], the fatigue strength of a welded structure is highly dependent on the notch effects i.e., stress concentrations and strength reductions, that can occur as a consequence of the welding process. The simplest fatigue assessment based on the notch effect refers to the design requirement in respect to the endurance limit, meaning that fatigue failures must be avoided regardless of the demands on service life of the structure. Accordingly, an assumption must be made that no significant plastic deformation will occur at the notch i.e., the notch effect can be approximated as purely elastic in terms of stresses. Therefore, the local stress conditions at the notch are decisive for the fatigue strength of the whole welded structure.

The local notch stress, as well as any other local stress σ_{t}, can be related to the nominal stress σ_{n} with a linear relationship according to the following equation:

$$\sigma_{\mathrm{t}} = K_{\mathrm{t}} \cdot \sigma_{\mathrm{n}} \,, \tag{7}$$

where K_{t} stands for the elastically calculated stress concentration factor. This factor represents the effect of stress concentration caused by a certain notch on the overall stress distribution of the analyzed structure. Very often, the stress concentration factor can be found in various handbooks, such as *Peterson's Stress Concentration Factors* [22], depending on the loading conditions and the geometry of the structure. If K_{t} can't be obtained from a manual of sorts, then it must be calculated via finite element analysis or by conducting an experimental investigation. Whichever method is chosen, the local stress peak could be very hard to measure,

sometimes even impossible. When using finite element analysis for modelling a rather complicated welded structure, it is very hard to incorporate all of the details, radii and notches that determine the local stress into the global model of the structure. Therefore, very often a detailed sub-model must be created in order to calculate the stress concentration factor for the welded structure in question which can be time consuming. Another problem is the geometry of the weld itself which can vary significantly from weld to weld. Furthermore, local weld geometry may also vary a lot along the weld seam, so it is rather difficult to model correct angles and radii of the weld, as well as to approximate a reasonable weld toe radius.

It would be simple to assume that local and nominal fatigue stresses e.g., fatigue strengths, can also be related via the same stress concentration factor K_t, meaning that both, smooth and notched structures have the same fatigue lives if ratio of their stresses is equal to K_t. To put it visually, on a plot of stress amplitude S_a versus life cycles N_f, the notch should have such an effect that it would reduce the stress amplitude for any given life by the same factor K_t. However, research has shown that this isn't always true as it can be seen from [Fig. 10]. According to Dowling [23] the notch has less of an effect on fatigue life of the welded structure than it can be expected from looking at K_t. In order to account for these differences, a special stress concentration factor, the fatigue notch factor K_f, is introduced in fatigue design.

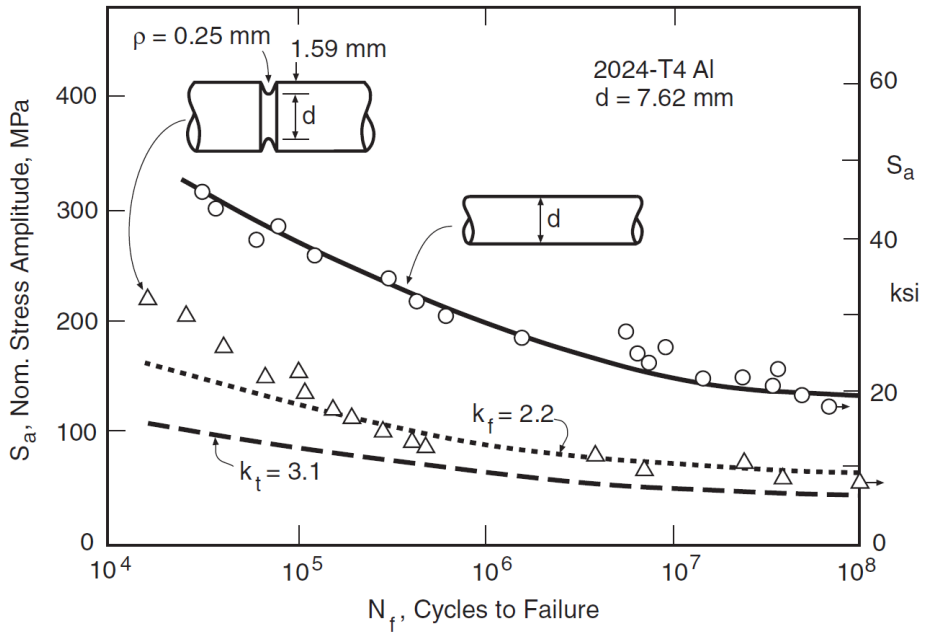

Figure 10: Effect of a notch on the S-N behavior of an aluminum alloy and comparison with strength reductions by K_t and K_f according to Dowling [23]

The fatigue notch factor K_f is the is the main parameter that defines the fatigue effective stresses within the effective notch stress approach. The relation between the fatigue effective notch stress σ_f and the nominal stress σ_n can be presented as the following equation shows:

$$\sigma_\mathrm{f} = K_\mathrm{f} \cdot \sigma_\mathrm{n} \,, \tag{8}$$

and the fatigue notch factor K_f is then defined as:

$$K_\mathrm{f} = \frac{\sigma_\mathrm{A}}{\sigma_{\mathrm{A,\,notch}}} \,, \tag{9}$$

where σ_A and $\sigma_{\mathrm{A,\,notch}}$ are the fatigue strengths of a smooth and notched structure respectively.

There may be several reasons for the different values of the stress concentration factor and the fatigue notch factor. According to Dowling [23] one of the main causes for this difference is related to the stress gradient $\mathrm{d}\sigma/\mathrm{d}x$ which decreases rapidly with increasing distance from the notch and since crack propagation from the surface is fairly unpredictable, how fast will the fatigue failure occur depends on the stress region to which the crack will propagate i.e., it can propagate to a region with decreasing stress which will result in slower propagation and longer fatigue life. Also, statistically speaking, the whole area of smooth surface is much larger than the notch area at the structure and the chances for a defect that will initiate the crack are much greater at a larger area.

There is a number of different approaches for the calculation of K_f such as the critical distance approach by Lawrence et al. [24] from the stress concentration factor on the basis of microstructural support hypothesis conceived by Peterson [25, 26] or the fictious notch rounding approach by Radaj [21] from the stress concentration factor on the basis of the microstructural support hypothesis conceived by Neuber [27, 28, 29]. The important thing to note is that all existing equations must be regarded as empirical estimations because there are many different effects that are causing the difference between K_f and K_t and it is very hard to include them all together in the equations at the same time.

In order to corelate the aforementioned factors, a new parameter called notch sensitivity q had to be introduced. According to Thum and Buchmann [30], the stress concentration factor and the fatigue notch factor can be related through the following expression:

$$K_\mathrm{f} = 1 + q \cdot (K_\mathrm{t} - 1) \,. \tag{10}$$

From the equation (10) it can be seen that the maximal fatigue notch factor is obtained for notch sensitivity equal to $q = 1$ i.e., $K_\mathrm{f} = K_\mathrm{t}$, which means that the maximum notch effect is achieved.

On the other hand, if notch sensitivity is equal to $q = 0$, that leads to the fatigue notch factor of $K_\mathrm{f} = 1$ which means that the notch has absolutely no effect on the fatigue behavior of the welded structure in question. There are many different interpretations on how to evaluate q by many different authors, including the already mentioned Peterson [26] but for the purposes of this thesis, focus will be put on the proposal by Neuber [27, 28] because it is in direct relations with the already mentioned effective notch stress approach by Radaj [21].

In order to avoid unrealistically high stress concentration factors for sharp notches, suggestion by Neuber was to use the stress averaged over a small, material dependent parameter denoted substitute microstructural support length ρ^*. When this is applied to welded structures with a notch and in the light of fatigue assessment, the relation between the microstructural support length and the fatigue effective notch stress is defined through the fatigue notch factor as follows:

$$\sigma_\mathrm{f} = K_\mathrm{f} \cdot \sigma_\mathrm{n} = \frac{1}{\rho^*} \int_{x=0}^{x=\rho^*} \sigma(x)\mathrm{d}x \,, \tag{11}$$

with the visual representation of microstructural support length concept depicted in [Fig. 11].

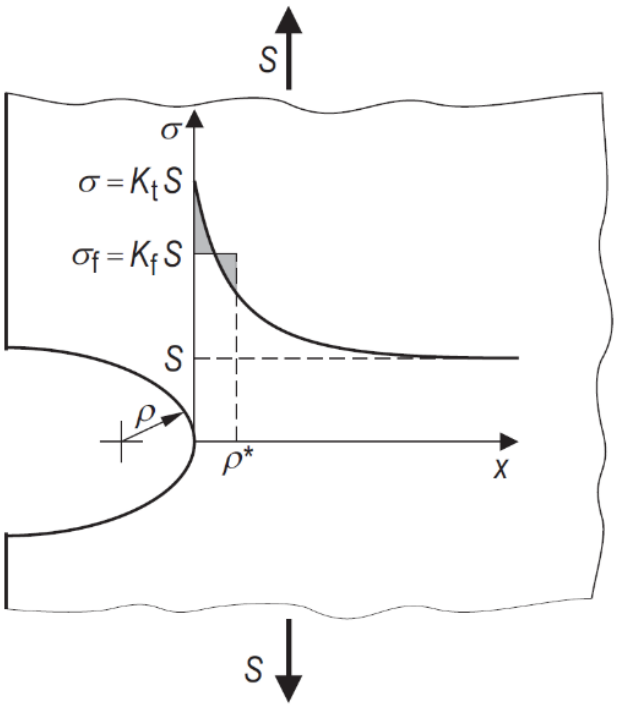

Figure 11: Relation between the fatigue notch factor σ_f and the microstructural support length ρ^* with $S = \sigma_\mathrm{n}$ and $\sigma = \sigma_\mathrm{t}$ from Mann [31]

In regard to the mentioned notch sensitivity q, for incorporating the microstructural support length concept into its calculation Neuber proposed the following:

$$q = \frac{1}{1 + \sqrt{\frac{2 \cdot \rho^*}{\rho}}}, \tag{12}$$

where ρ is in fact the radius at the notch of the welded structure. By observing the equation (12) and its possible values, it can be seen that the smaller the notch radius ρ becomes, the smaller will notch sensitivity q be. This also means that the fatigue notch factor will have less influence on fatigue behavior of the welded structure with smaller notch radii ρ. Large ρ on the other hand will cause q to approach the value of 1 and equalize the fatigue notch factor with the stress concentration factor. While the stress concentration factor increases for the smaller notch radii, from this comparison it is possible to see that the smaller the notch radius, the larger is the effect of notch sensitivity on decreasing the fatigue notch factor. Notch sensitivity q calculated with the equation (12) can be used together with equation (10) in order to see how the factors K_f and K_t relate to each other for the welded structure that is being analyzed.

According to Radaj [21], in order to obtain the fatigue effective maximum notch stress resulting in the respective fatigue notch factor of the welded joint in question, sharp notch in the cross section of the model has to be factiously rounded to a certain value. Hence, the version of effective notch stress approach proposed by Radaj is called fictious notch rounding approach. The fictious notch radius ρ_f of the notch at the welded structure is given by the following equation suggested by Neuber:

$$\rho_\mathrm{f} = \rho + s \cdot \rho^* , \tag{13}$$

where ρ is the existing radius at the notch of the weld, ρ^* is the substitute microstructural support length and the support factor s accounts for the assumed strength hypothesis and loading type. Typical values for the support factor s can be found in [21, 28] and they lie between 1 and 3. This approach was originally proposed to be used for any radius at the notch, but it has mainly been applied as a worst-case scenario approach with the real notch radius ρ equal to zero. Radaj [21] found that when applying a radius of $\rho = 0$ mm to the equation (13), with assumptions of $\rho^* = 0.4$ mm and $s = 2.5$ for alternating fatigue tests on notched bars, the fictious notch radius results in $\rho_\mathrm{f} = 1$ mm. This showed to be an approach that provided a reasonable agreement for welded joints in structural steel. What makes this approach highly attractive, is the fact that the

real notch radius can be conservatively assumed as $\rho = 0\,\text{mm}$ which solves the highly complicated problem of finding the value for the existing radius at the notch of the welded structure. Another major benefit of this approach is that it can be used for the assessment of both, weld toe and weld root fatigue failure. With this in mind for the welded joints in aluminum, Radaj et al. [15] proposed $\rho^* = 0.1\,\text{mm}$ and $s = 2.5$ i.e., the fictious notch radius of $\rho_\text{f} = 0.25\,\text{mm}$, for the worst-case considerations of the fatigue notch factor for 5083 aluminum alloy. According to IIW [9], fictious notch radius of $\rho_\text{f} = 1\,\text{mm}$ should be used for aluminum 2000 series, while Neuber [28] suggests $\rho^* = 0.1 \ldots 0.2\,\text{mm}$ for the 5083 aluminum alloy which would, according to Radaj's principle, result in $\rho_\text{f} = 0.25 \ldots 0.5\,\text{mm}$, which was confirmed by Sonsino et al. [32]. All of the listed values were determined for plate thicknesses of $t = 5\,\text{mm}$ and/or $t = 25\,\text{mm}$.

The main procedure of this approach is first to determine the structural stresses at the weld toe and root of the welded structure without considering the notch effect. After that, a cross-sectional model of the weld has to be devised to which the resulting stresses from the first step need to be applied and in which factiously rounded notches have to be included. The results from the cross-sectional model are then used for the determination of the fatigue notch factors. When the real notch radius ρ is enlarged to the fictious notch radius ρ_f as described, the fatigue notch factor can be determined directly from the fatigue effective notch stress σ_f i.e., the effective notch stress analysis is performed for the enlarged notch radius which means the averaging process from [Fig. 11] can be avoided through modified equation (8):

$$K_\text{f} = \frac{\sigma_\text{f}}{\sigma_\text{n}} \tag{14}$$

if the nominal stress σ_n can be properly defined.

With respect to everything presented so far, main problem of the fictious notch rounding is that it can cause large undercuts, also fictious, which can then result in an unrealistically large notch stress, especially when applied to weld joints with low plate thickness. In order to reverse this effect, certain correction of the calculated fatigue notch factors must be conducted. According to Radaj et al. [15] the weaking of the cross section can be considered in fatigue notch factors by means of a reduction factor resulting from tensile and bending stress increase in the equally unnotched plate. This reduction factor depends on the type of loading and the severity of the cross-sectional weaking with different examples of the undercuts given in [Fig. 12].

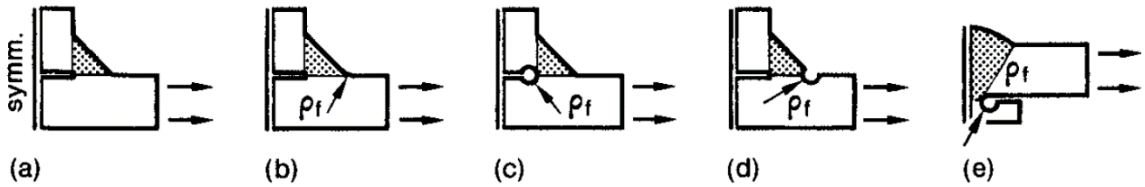

Figure 12: Undercut caused by fictious notch rounding according to Radaj et al. [15]: (a) sharp notches without rounding, (b) toe rounded notch without undercut, (c) root rounded notch with undercut, (d) toe rounded notch with undercut, (e) root rounded notch without undercut of the load-carrying cross section

Fictious notch rounding at the weld toe without root undercut. see [Fig. 12 (b)], results in virtually unchanged cross section in comparison with the sharp notched cross section seen in [Fig. 12 (a)], therefore no correction is needed. On the other hand, when rounding with undercut is applied at the weld root or at the weld toe, see [Fig. 12 (c)] and [Fig. 12 (d)] respectively, significant weakening of the welded cross section occurs, and correction is required. However, when undercut is applied in low stress regions of the cross section as in [Fig. 12 (e)], there is no increase of the notch stress since the weaking is applied on a non-load carrying element. For the single sided notch i.e., fictious notch rounding with undercut on one side of the welded element, the following equation is applied for the fatigue notch factor correction:

$$K_{\mathrm{f}}^{*} = \frac{\left(1-\rho_{\mathrm{f}}^{*}\right)^{2}}{1+\rho_{\mathrm{f}}^{*}\cdot\left(1+\sigma^{*}\right)}\cdot K_{\mathrm{f}}\,, \tag{15}$$

where K_{f} and K_{f}^{*} are the original and reduced fatigue notch factor, respectively, ρ_{f}^{*} presents the degree of cross-sectional weakening which is equal to:

$$\rho_{\mathrm{f}}^{*} = \frac{\rho_{\mathrm{f}}}{t}\,, \tag{16}$$

and σ^{*} is the surface stress ratio calculated according to the following equation:

$$\sigma^{*} = \frac{\sigma_{\mathrm{l}}}{\sigma_{u}}\,, \tag{17}$$

where σ_{l} and σ_{u} are the remote stresses at the lower and upper surfaces of the welded element, respectively. According to Radaj et al. [15], in cases where the fictious notch rounding is done on both sides of the welded element, a slightly different term must be used for the fatigue notch factor reduction:

$$K_{\mathrm{f}}^{*} = \frac{2\cdot\left(1-\rho_{\mathrm{f}}^{*}\right)^{2}}{2-\rho_{\mathrm{f}}^{*}\cdot\left(1+\sigma^{*}\right)}\cdot K_{\mathrm{f}}\,. \tag{18}$$

When using the effective notch stress approach, regardless of the approach version that is applied, the question arises as to which stress should be used for the fatigue assessment, maximum principal stress or a type of equivalent stress like Tresca and von Mises. All of the three mentioned theories can be seen in [Fig. 13] where they are compared.

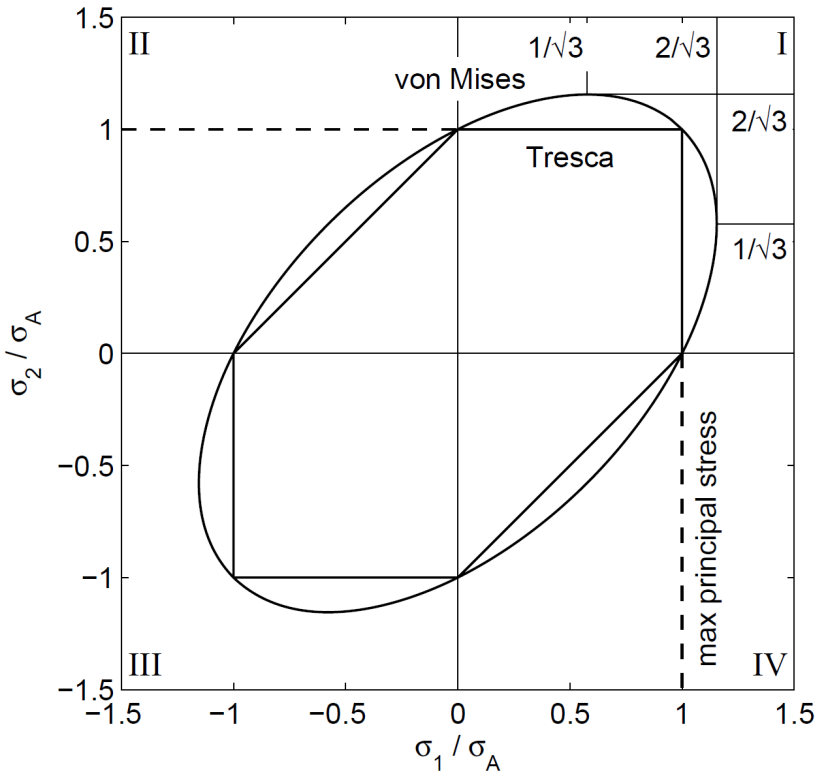

Figure 13: Maximum principal, von Mises and Tresca surfaces [31]

Looking at the [Fig. 13] it can be seen that the least and most conservative theory between the three, differs from one quadrant to another. For example, in quadrant I, the von Mises theory is the least conservative while the other two theories are equal but the margin between these two and von Mises is not large. In quadrants II and IV, however, the von Mises theory is far more conservative than the maximum principal stress theory. The additional problem with the von Mises equivalent stress theory is that the spot with the highest stress can be in compression and in that case the negative sign of the stress will be lost, which means that this won't be the spot most critical to fatigue. According to Mann [31] the maximum principal stress theory is used more often with the structural hot spot stress approach while different local approaches usually opt for von Mises equivalent stress theory.

2.5 Crack propagation analysis

The crack propagation analysis has a quite different approach to fatigue assessment in comparison with the three methods previously introduced. While all three methods, nominal stress, hot spot stress and effective notch stress, approach the fatigue assessment in a way of assuming where will the crack initiate and no specific data of the crack is needed to conduct an assessment, the crack propagation analysis requires a crack to already exist in order to follow and assess its propagation over some time. To put it simply, usual application of the crack propagation analysis would be to detect a crack at the beginning and then check if it will grow to a critical size before the next inspection with repeating the procedure until the critical size is reached. Therefore, as already mentioned, this requires an initial crack or a crack-like defect to be present, otherwise this approach wouldn't be applicable.

Since knowing the location of the crack is a requirement in this approach, it is only logical that the geometry of a crack is also an influential parameter. Cracks can be very different in shape and size and large differences between cracks can transfer into large differences in fatigue life i.e., behavior of the crack is depending on its size and shape. Miller et al. [33] have given a classification of cracks according to their size which divides them into geometrically short and geometrically long cracks. To which category will the crack be classified depends not only on its size but also on the loading conditions. Geometrically short cracks are cracks that are larger than a couple of grains in the material but still small in comparison with the plastic zone of the material around the tip of the crack. Hence, a crack is considered geometrically large when it is large in comparison with the plastic zone around the crack tip. However, when large enough load is applied, a geometrically long crack can behave like a short one.

In regard to the crack behavior, according to the linear elastic fracture mechanics from Lee et al. [34], there are only three basic crack loading modes, as depicted in [Fig. 14]. These three modes are basically idealized planar crack problems where stresses and strains can be expressed in terms of in-plane x and y coordinates. In mode I, also named opening or tensile mode, the in-plane stresses and strains around the crack tip are symmetrical with respect to the x axis. If the crack is subjected to mode II, the sliding or in-plane shearing mode, stresses and strains are anti-symmetrical in respect to the x axis. Finally, in mode III, the tearing or anti-plane shearing mode, the out-of-plane stresses and strains are anti-symmetrical in respect to the x axis. Stress field in the area around the crack tip for each of the three modes can be completely described with the stress intensity factors K_{I}, K_{II} and K_{III}.

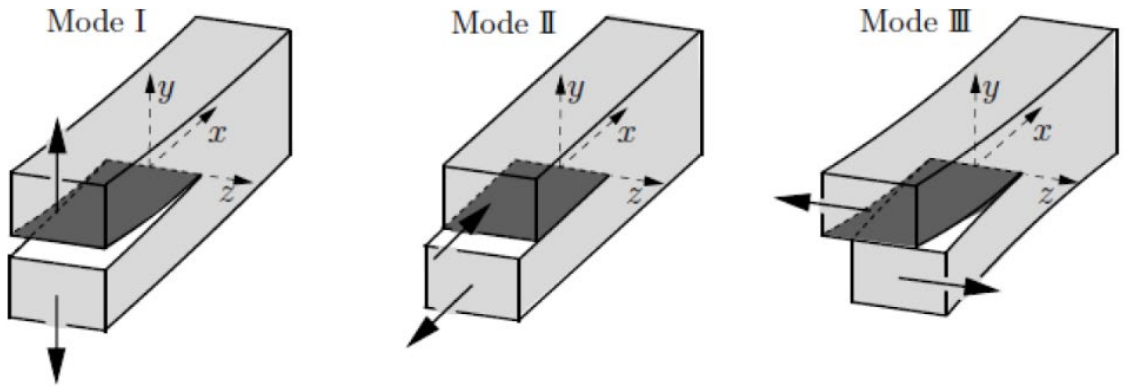

Figure 14: Three basic crack loading modes from [35]: Mode I, Mode II and Mode III

Values of these three stress intensity factors can be found in various handbooks, such as the one by Tada et al. [36], but for relatively simple geometric configurations. Very often, mode I is the most dominant in crack behavior so the other two modes can be neglected, which means the stress intensity factor can be denoted with K and defined according to the following equation:

$$K = F \cdot \sigma \cdot \sqrt{\pi \cdot a}\,, \tag{19}$$

where F is a function of geometry, crack size and loading, σ is the applied stress and a is the crack length. According to Lee et al. [34], equation (19) can be used for both, center-cracked, and edge-cracked elements. As fatigue is not a static problem but is caused by variable stress loading, equation (19) needs to be updated, with K and σ being replaced by their respective ranges and thus forming the equation:

$$\Delta K = F \cdot \Delta\sigma \cdot \sqrt{\pi \cdot a}\,, \tag{20}$$

where ΔK stands for stress intensity factor range and $\Delta\sigma$ is the applied stress range.

Considering that the presented stress intensity factor K describes the stress field around the crack tip, it can be assumed that this factor is in direct relation with the propagation of the crack. Behavior of the crack propagation itself i.e., the speed of the propagation, is usually plotted with the crack propagation rate $\mathrm{d}a/\mathrm{d}N$. When combined with the stress intensity factor range ΔK and by using logarithmic scale on both axes, a plot similar to the one depicted in [Fig. 15] can be obtained for long cracks in metal materials. From the plot it can be clearly seen that the crack propagation can be divided into three characteristic phases with the first one being the near threshold behavior. Below the threshold stress intensity factor range ΔK_{th}, the long crack will not propagate. If it would stay under this limit, crack failure would never occur. However,

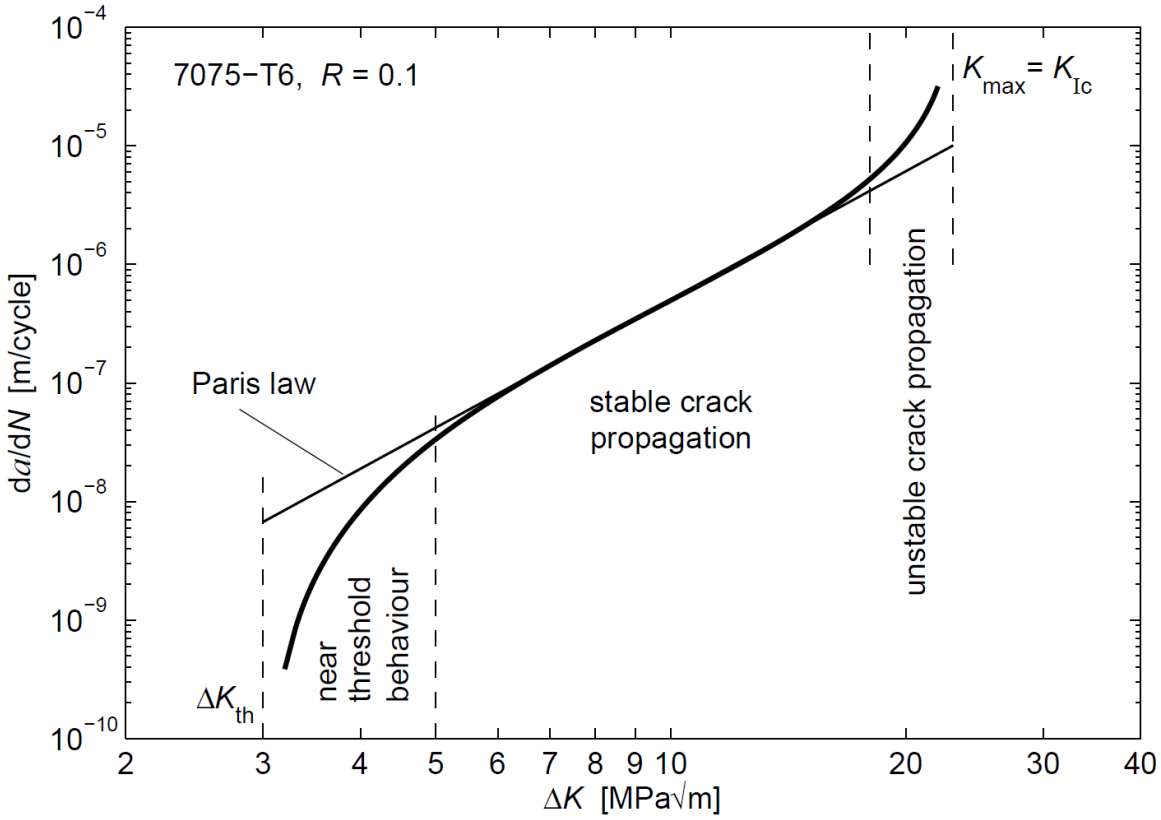

Figure 15: Principal propagation behavior of a long crack and Paris's law from [31]

when the stress intensity factor range exceeds the threshold limit, the crack will slowly start to propagate. In the beginning this will be a low propagation rate, but it would rapidly increase. Eventually, the crack propagation rate would reach the straight part of the plotted curve with a logarithmically linear behavior. This is the second characteristic phase of crack propagation called the stable crack propagation phase or more often referred to as Paris's law. During this stable crack propagation phase, the crack propagation rate can be found by using the simple expression proposed by Paris et al. [37]:

$$\frac{\mathrm{d}a}{\mathrm{d}N} = C \cdot (\Delta K)^m \,, \tag{21}$$

where C stands for a numerical constant that defines the vertical position of the curve while m is a numerical exponent that defines the slope of the curve. After a long second phase of crack propagation, follows a third and final phase called unstable crack propagation. In this final phase the crack propagation rate will start to rapidly increase as the stress intensity factor increases. Eventually, when $K_{\max}$ reaches the fracture toughness of the material K_{Ic}, unstable crack propagation will occur and within a few cycles a sudden fracture would follow.

Aforementioned Paris's law, given with the equation (21), describes only the stable crack propagation phase which means it is not the most suitable solution for the regions near the threshold stress intensity factor range ΔK_{th} and fracture toughness of the material K_{Ic}. With this in mind, a large number of different crack propagation laws was developed through history and each of them is trying to describe one or more of the three mentioned crack propagation phases. However, including two or even all three phases into one single assessment equation can be very difficult. Many different parameters can be unknown, so it is not uncommon for Paris's law to still be the preferred method because of its simplicity and ease of use. Dijkstra et al. [38] provided a great summary of many different crack propagation equations but for the purposes of this thesis, crack propagation analysis won't be utilized so no other laws except Paris's will be included in this overview. Except being suitable only for stable crack growth, Paris's law is also applicable only for long cracks. In order to assess geometrically short cracks, other approaches such as the one proposed by El Haddad et al. [39] or by Härkegård [40] must be considered.

The main characteristic of welded joints, in respect to cracks, are the sharp notches at the weld toe and weld root, even more so when they are combined with an undercut or any other weld defect. When applied to welded joints it could be assumed that crack propagation analysis accounts for the sharp notches within the stress intensity factor K. However, cracks starting from the weld toe are subjected to a fast-decreasing stress field i.e., high stress gradient, and the crack propagation analysis in its original form doesn't account for the stress concentrations resulting from such notches.

The influence of multiple geometric parameters such as the shape and size of the crack, thickness, and width of the component, are included in the crack propagation analysis via the geometry factor F. In order to account for the local stress concentrations arising from welding, a new factor was introduced by Maddox [41] called the weld toe magnification factor M_{k}, among other factors for additional stress raising effects not included in F. According to Bowness et al. [42], M_{k} is defined as the ratio of the stress intensity factor of a crack in a plate with welded attachment i.e., including weld toe, and the stress intensity factor of the same crack in a plate without the attachment subjected to the same loading:

$$M_{\mathrm{k}} = \frac{K_{(\text{plate with welded attachment})}}{K_{(\text{plate without welded attachment})}}. \tag{22}$$

In order to apply the weld toe magnification factor M_k and include it into the crack propagation analysis, equation (20) for the stress intensity factor range ΔK needs to be modified to the following:

$$\Delta K = M_k \cdot F \cdot \Delta\sigma \cdot \sqrt{\pi \cdot a}\,. \tag{23}$$

As already mentioned, the influence of the stress concentration such as weld toe is decreasing by getting further away from the sharp notch. So, when the crack propagates, it will move away from the stress peak caused by the sharp notch and therefore this stress will have less influence on further propagation. This means that the weld toe magnification factor M_k can't be a constant value and instead it needs to be expressed as a function of loading conditions and geometry of the crack. Naturally, depending on the complexity of the crack and its parameters, equations needed to calculate M_k can become very complicated. Some examples of the said equations can be found in [42].

Even though there are cases that can only be dealt with by applying the crack propagation analysis, such as back-tracing of failures, definition of inspections during the service life, definition of tolerable crack sizes and flaws etc., the crack propagation analysis is rarely suitable for determination of fatigue strength or service life, according to Radaj et al. [15]. Main reason for that are many different assumptions that need to be introduced in the analysis regarding the initial crack size, shape, and general material parameters. Besides that, the crack initiation phase, as a part of service life, is completely neglected by the crack propagation analysis because of its fundamental assumption that the crack must exist at the beginning of the analysis. Therefore, this approach can't fully substitute any of the approaches introduced so far in this thesis.

3 INTRODUCTION TO *FEMFAT 5.4*

In regard to the introduction of this thesis, electrification in the automotive industry has triggered major changes. New possibilities for saving weight had to be explored while maintaining the same level of quality, safety, and strength of the final product. With all that in mind, fatigue requirements have quickly been turned into a major feature from an engineering point of view. Therefore, different software solutions have been developed over the years in order to simplify and speed up the process of fatigue assessment and determination of other fatigue related characteristics.

For the purpose of this thesis, software program called *FEMFAT* has been used as it is also one of the main tools used for fatigue assessment in various departments of AVL List GmbH. In this chapter a short overview of the main features of the software is given in order to clarify the work described in further chapters of this thesis.

FEMFAT is a universally applicable software program for the fatigue assessment of statically or dynamically loaded components and structures developed at Engineering Center Steyr GmbH & Co KG, or ECS for short, see [43]. It can be used for the determination of damage, fatigue life and safety factors for any given component or structure which enables the engineers to identify the weak spots and make changes accordingly in an early stage of product development. However, in order for *FEMFAT* to be utilized, a finite element analysis must be conducted first since *FEMFAT* works by reading out the stresses from the finite element analysis results and uses them for its own calculations. Therefore, it is important to note that for all of the finite element analyses conducted in this thesis, *Abaqus 2019.HF4* simulation program was used. Furthermore, two main files obtained from the finite element analysis as the most important ones for *FEMFAT* simulations are the input (*.inp) file and the output database (*.odb) file. From these two files, *FEMFAT* can obtain all the information it needs for a successful fatigue assessment so all that remains is to define all the necessary parameters that have an influence on the final results depending on what the user needs to analyze. In respect to this, *FEMFAT* offers a number of different methods and approaches for solving various fatigue related problems through the modules that are incorporated in the software. Each module has its own characteristic features, but the work of this thesis is focused on fatigue analysis of the welds, therefore *FEMFAT Basic* and *FEMFAT Weld* modules will be introduced in more detail and eventually used for the assessment.

3.1 *FEMFAT Basic*

Graphical user interface of the *FEMFAT 5.4*, version of the program used for the purposes of this thesis, is depicted in [Fig. 16]. Depending on the type of simulation the user wants to perform, several different modules such as *FEMFAT Basic*, *FEMFAT Plast*, *FEMFAT Max*, *FEMFAT Weld*, *FEMFAT Heat*, *FEMFAT Spectral* etc., are available in *FEMFAT*.

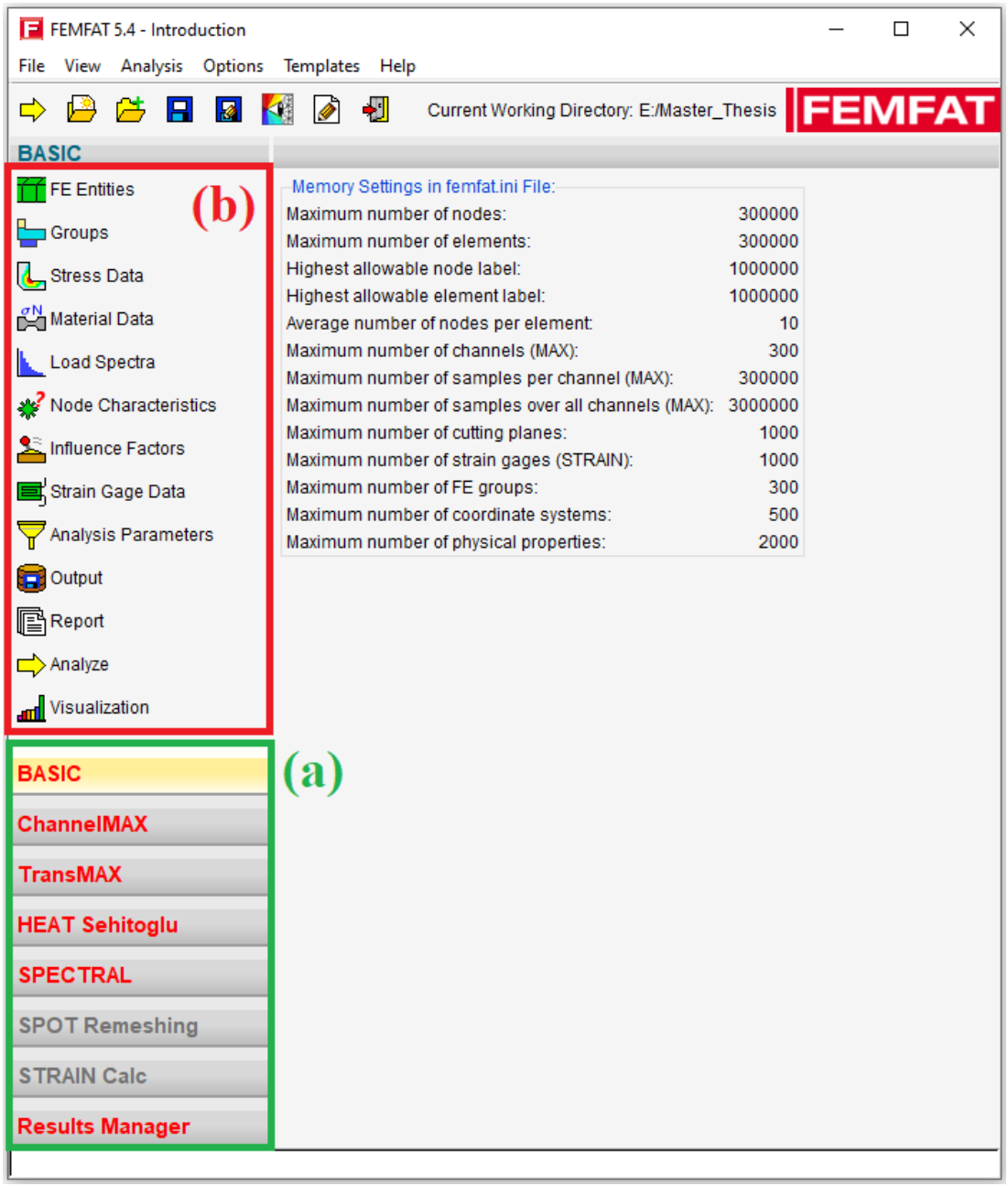

Figure 16: Graphical User Interface of *FEMFAT 5.4*: (a) different *FEMFAT* modules, (b) main menu tabs for *FEMFAT Basic*

Some of the mentioned modules can be seen in [Fig. 16 (a)] while the main menu items of the module *FEMFAT Basic* are depicted in [Fig. 16 (b)]. The first item on the said menu list is the *FE Entities* tab where the geometry of the model needs to be loaded into *FEMFAT*. For this either the *.inp or the *.odb file from the previously conducted finite element analysis can be used. This tab also offers the option to define the position of the weld in the model but more detail on that will be given in chapter 4.4. The *Groups* tab offers the possibility to choose only a part of the model, a group consisting of elements and/or nodes, for which the simulation will be conducted which can be cost effective and time saving when very large models are in question. The next step in preparing the FEMFAT simulation is to assign the stress data from the finite element analysis and the material properties to the already loaded model geometry, which can be done through the tabs *Stress Data* and *Material Data* respectively. For the stress data, the *.odb file containing the stress results from the finite element analysis can be used and loaded in *FEMFAT* in different ways, as stress amplitude, mean stress, lower and upper stress level or as a constant stress which offers various different possibilities for the fatigue assessment. Material data can also be loaded through an existing file containing the material properties or it can be created directly in *FEMFAT Basic*. Through the *Load Spectra* tab, the load spectrum type can be assigned and adapted for different loading steps and wanted number of cycles while the *Node Characteristics* tab offers the user a possibility to assign various parameters, including the material properties, to different node groups.

FEMFAT provides a range of options for quickly performing parameter studies or comparative investigations of a variety of influence factors which are depicted in [Fig. 17]. Many of these factors were used during the work of this thesis which is the main reason for their more detail description. From [Fig. 17 (a)] it can be seen that these influence factors are divided in four main categories: *General Factors*, *Surface Treatment*, *SPOT* and *WELD*, of which the latter will be described separately in chapter 3.2. Some of the main *General Factors* include the influence of stress gradient and mean stress on the endurance stress limit, the endurance cycle limit, and the slope of the S-N curve. Furthermore, the effect of plastic deformations caused by local stresses exceeding the material yield strength can also be included into the analysis if *FEMFAT Plast* is enabled. The final influence factor that is enabled by default in *FEMFAT* is the modification of the Haigh diagram as a consequence of the stress gradient in the material. Among other influence factors that can be enabled by the user, the one used most for further work in this thesis is the *Statistical Influence* factor in [Fig. 17 (b)], which enables the analysis

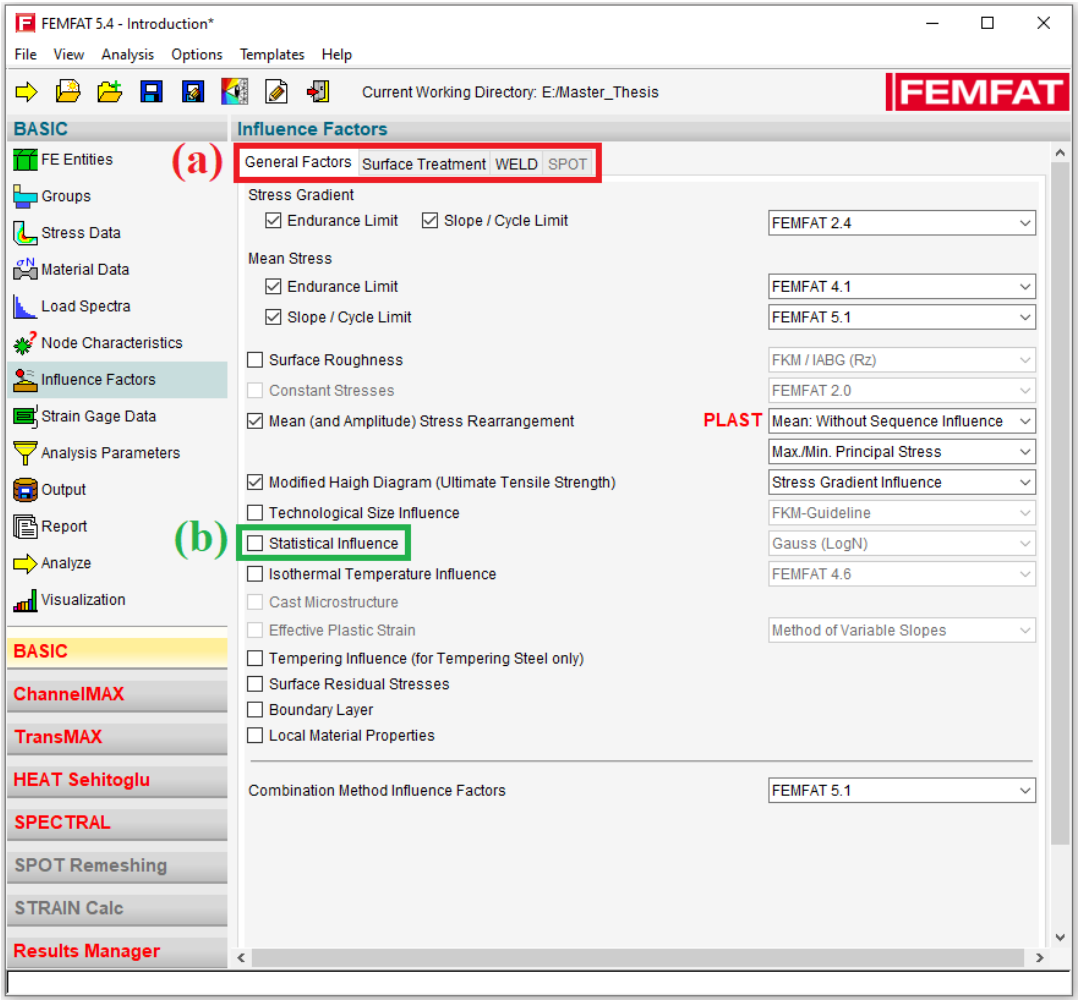

Figure 17: Interface of the *Influence Factors* tab in *FEMFAT Basic*: (a) main groups of influence factors, (b) non-default statistical influence factor

to be performed for any arbitrary value of the survival probability. When disabled, *FEMFAT* uses the survival probability of $P_S = 90\%$ for its calculations. In order to avoid any errors during the analysis it is recommended to always check the influence factors before proceeding with the next tab on the list.

To continue with the main menu list, *Strain Gauge Data* tab can be used when certain measurements of the strains are available in order to process the data and directly compare it to the finite element analysis, however this option wasn't used for this thesis because no strain measurements were conducted. *Analysis Parameters* tab is the one where the main target of the analysis is chosen by the user, whether the aim is to calculate damage, safety factor or just compare the strain measurements given in the previous tab. Whichever simulation target is chosen for the analysis, *FEMFAT* offers several procedures for the calculation based on various

different approaches or standards. The main calculations conducted in this work will be focused on the damage calculation from which the number of cycles to failure can be obtained. Finally, when all the main steps described so far are finished, all that is left is to define the wanted parameters and their format for the output file through the *Output* tab as well as to choose the data that will be written into a *FEMFAT* report file through the tab named *Report*. The analysis can then be started within the *Analyze* tab and when the simulation is finished, the results can be viewed by *FEMFAT Visualizer* or within the *Visualization* tab. From there, results such as position of the critical node, local S-N curve, and local Haigh diagram, can be easily obtained.

All of the steps mentioned here were important for further work in this thesis, but with welded aluminum structures being in the focus, a more detail description of the capabilities and options behind *FEMFAT Weld* is given in the next chapter for better understanding of the topic.

3.2 *FEMFAT Weld*

Throughout the engineering industry, finite element method (FEM) has been used for many years as the generally accepted approach for the assessment of stresses and strains in complex structures, including welded structures as well. Since welded structures show substantially lower loading capacity when under dynamic loads in comparison with non-welded structures, it is no surprise that the assessment of stresses in the weld area is of great importance, especially in respect to the fatigue life of the structure. As it has been presented through chapter 2, various standards and literature references offer a multitude of different assessment approaches for fatigue life. However, not all of these approaches can be applied to every possible structure, and when assessing the weld area with FEM, various difficulties can be encountered during the process. Maybe the main issue is that standards generally do not provide much information for the assessment of FEM results for welded structures. Analyzing the FEM results for complex structures can often be time consuming with a lot of manual assessment needed, which often means that weld geometry and stress conditions must be dissolved to simpler cases for a successful assessment. Besides that, different approaches in modelling of the weld area, often lead to different stress results. A lot of other issues can be found but in order to provide a solution for these problems, *FEMFAT Weld* module has been introduced as an extension of *FEMFAT Basic*. It is also based on the results of finite element analysis but offers a lot of possibilities for the assessment of dynamically loaded complex welded structures, some of which will be introduced in this chapter.

3.2.1 Weld modelling guidelines in FEMFAT Weld

It was already mentioned that the modelling approach of the weld area can have a significant effect on the final results of the simulation and many studies have been conducted in order to compare different modelling approaches and their benefits. Tveiten et al. [44] compared the results of fatigue assessment with hot spot stress approach between three different types of finite element models: solid model with detailed weld geometry, shell model with idealized weld geometry represented with inclined shell elements and shell model with no weld geometry. The comparison of the results showed that no significant advantage or better quality of results was obtained with detailed weld modeling. In fact, shell elements without the weld geometry showed reliable results with great numerical efficiency. The logic behind *FEMFAT Weld* is pretty similar, to use simple finite element models without weld geometry for an automated assessment of fatigue life parameters such as damage or safety factors.

In order to get the most reliable results possible from using *FEMFAT Weld*, certain guidelines are given by ECS in regard to the modelling of the weld area that is being assessed. Both, modelling with shell (2D) elements and solid (3D) elements is defined in these guidelines, but the focus of this thesis will be on the shell modelling approach. Reason for this is that in most cases, modelling of the whole welded structure is carried out with shell elements so it is preferable to investigate the same modelling approach for the weld area as well.

Following the instructions from the mentioned guidelines, attention must be paid to the way the finite element grid is modelled i.e., to ensure a certain mesh size in the model for the finite element analysis. According to *FEMFAT Weld* recommendations in [45] all elements that are connected to a weld start or end node must have an edge length of:

$$L = 2 \cdot t\,, \tag{24}$$

where t stands for sheet thickness of the welded structure. The look of correctly meshed weld joint is depicted in [Fig. 18] where it can be seen that the element quality defined with equation (24) is kept throughout the whole length of the weld and for all the elements connected with at least one of the weld nodes. The reason for such mesh size is to avoid unrealistically high stress singularities to be included in the assessment of welds. In such cases where this kind of mesh size can't be met or is willingly disregarded for other reasons, the automatic stress correction needs to be enabled within the *FEMFAT Weld* module which is described in chapter 3.2.2.4. As it can be clearly seen from [Fig. 18], *FEMFAT Weld* is able to distinguish the nodes that make

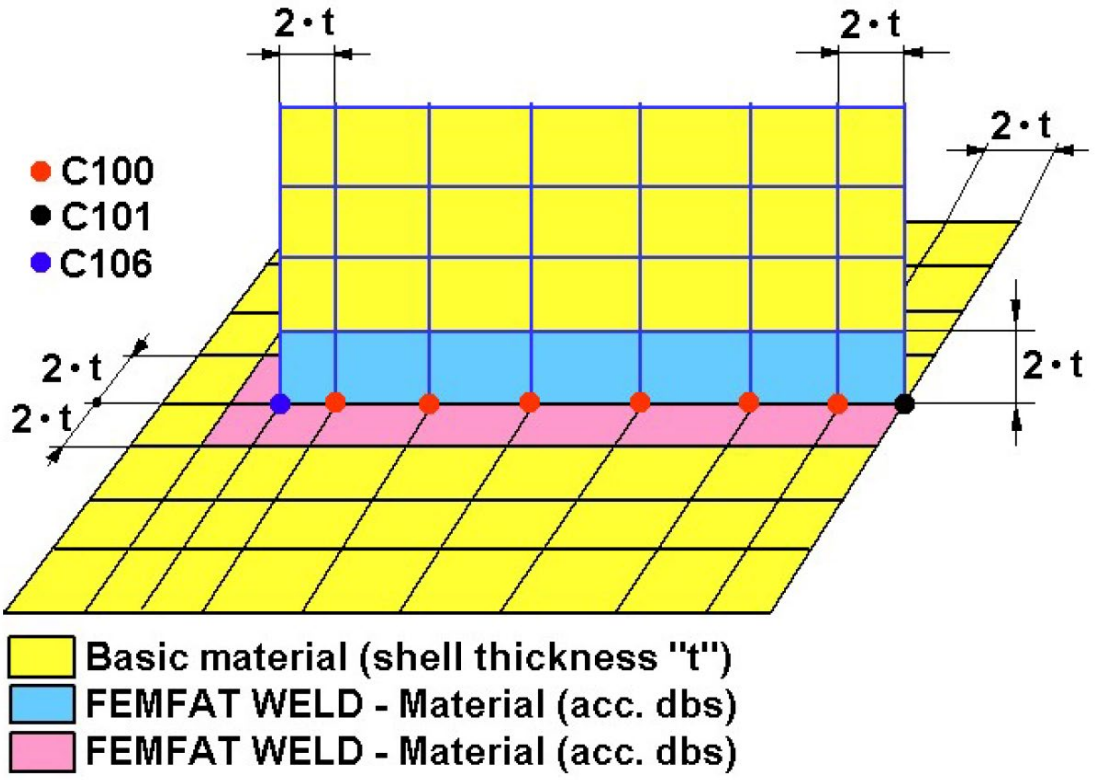

Figure 18: Mesh modelling recommendations according to *FEMFAT Weld* [45]

up the weld based on their location in the weld seam itself. Therefore, different node attributes are assigned to each node depending on its position in the weld. Node attributes are assigned with node color labels in the format of Cxxx and they differ between simple welds and combined welds i.e., multiple mutually intersecting weld seams of different type. Node color labels for simple welds that are predefined in *FEMFAT Weld* are given in [Table 1].

Table 1: Predefined node color labels in *FEMFAT Weld* [45]

Weld node color label	reserved for
C100	simple weld node
C101	simple weld end non-boxed
C102	simple weld end boxed
C106	simple weld start non-boxed
C107	simple weld start boxed

Besides recognizing the nodes that make up the weld and assigning them each a node color label, when the user defines the weld position, *FEMFAT Weld* also recognizes all of the elements in the vicinity of the defined weld and assigns them the weld material properties based on the data available in the weld database. The weld database, a *.dbs file that comes with the software, is the main source of data for *FEMFAT Weld* since it contains information about Haigh diagrams, S-N curves, influence of various parameters on the weld and most importantly, it contains notch factors for numerous predefined weld joints. Two weld databases are provided with the software, one for aluminum, which is used for the work in this thesis, and the other one for steel weld joints. So, when the user imports the base material properties of the finite element model loaded into *FEMFAT Basic* and defines the weld position, *FEMFAT Weld* uses the endurance stress limit of the base material for determining the notch stress endurance limit of the weld material. This is done by means of a polygon course defined with the data from the weld database given in [Table 2] and graphically presented in [Fig. 19] for aluminum joints.

Table 2: Polygon course definition of weld fatigue strength from base material strength for normal stresses in aluminum joints

Fatigue limit of base material [MPa]	0	76	105	265	5000
Notch fatigue strength of weld material [MPa]	0	72	110	110	110

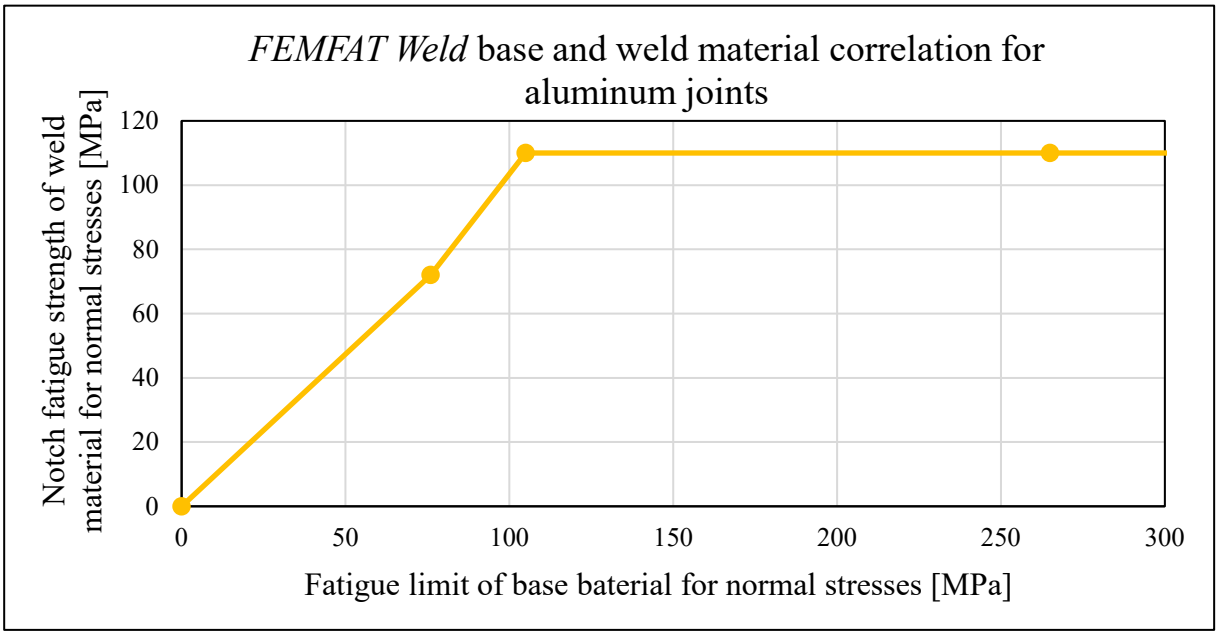

Figure 19: *FEMFAT Weld* base and weld material correlation diagram for aluminum joints

In case the current base material endurance stress limit lies between two points of the polygon course, linear interpolation is performed. Besides the correlation for the normal stresses which has been presented here, the weld database contains the data for shear stress dependency between the base and the weld material as well.

The important thing to note is that in the weld database it is assumed that the base material alternating stress limits i.e., endurance stress limits, are given with reference to survival probability of 90%, but the weld notch stress limits defined from the polygon course refer to a survival probability of 50%. Therefore, the user needs to be careful when importing the base material data into *FEMFAT Basic* to keep everything in line with the data in the database. Furthermore, if the statistical influence from [Fig. 17 (b)] is enabled and the survival probability for the analysis defined in the *Analysis Parameters* tab of *FEMFAT Basic* is not equal to 90%, the alternating stress limit of the base material is first recalculated for 90% survival probability and only then is the polygon course procedure applied.

3.2.2 FEMFAT Weld interface

When the modelling of the welded structure is finished with respect to the aforementioned modeling guidelines defined in [45] and described in the chapter 3.2.1, the welded structure geometry can be loaded into *FEMFAT Basic*. Of course, it is advisable to conduct a finite element analysis before loading the model geometry into *FEMFAT Basic*, just to make sure that the simulation gives reliable stress results for that given geometry, especially when welded structures are in question. Namely, as it can be concluded from everything presented so far, both *FEMFAT Basic* and *FEMFAT Weld* use a large number of different factors for various influences which can make it difficult to recognize an error in their final calculation. On the other hand, in FEM tools such as *Abaqus 2019.HF4*, it is always easy to compare the stress results with expected results obtained either through empirical or analytical knowledge. In the end, the results of the FEM analysis are in any case required to perform calculations in *FEMFAT* in general. So, with the geometry of the model loaded in *FEMFAT Basic*, user can define the position of the weld or welds in the whole welded structure by using *FEMFAT Visualizer*. The exact process of defining the weld through this tool will be described in chapter 4.4 by using a specific welded structure. Once the weld position is defined and the weld type is chosen, *FEMFAT Weld* automatically recognizes all of the nodes and elements characterizing the defined weld and stores the data in the weld definition file (*.wdf). All of the information about

already mentioned node attributes and weld material properties are stored in this file through the weld database that is chosen for the weld definition. However, this alone isn't enough for *FEMFAT Basic* to automatically include *FEMFAT Weld* into the calculation, this must be done by the user through the *FEMFAT Basic* interface. As described in chapter 3.1, the *FEMFAT Weld* module is one of the main groups of influence factors which needs to be enabled by the user when necessary. The interface of the *FEMFAT Weld* module is depicted in [Fig. 20] and it can be seen that various parameters can be enabled or disabled through the interface depending on the purpose and defined conditions of the analysis. One of which is the possibility to choose between several assessment methods as well as to change the weld database used for the definition of the weld in the geometry model of the welded structure.

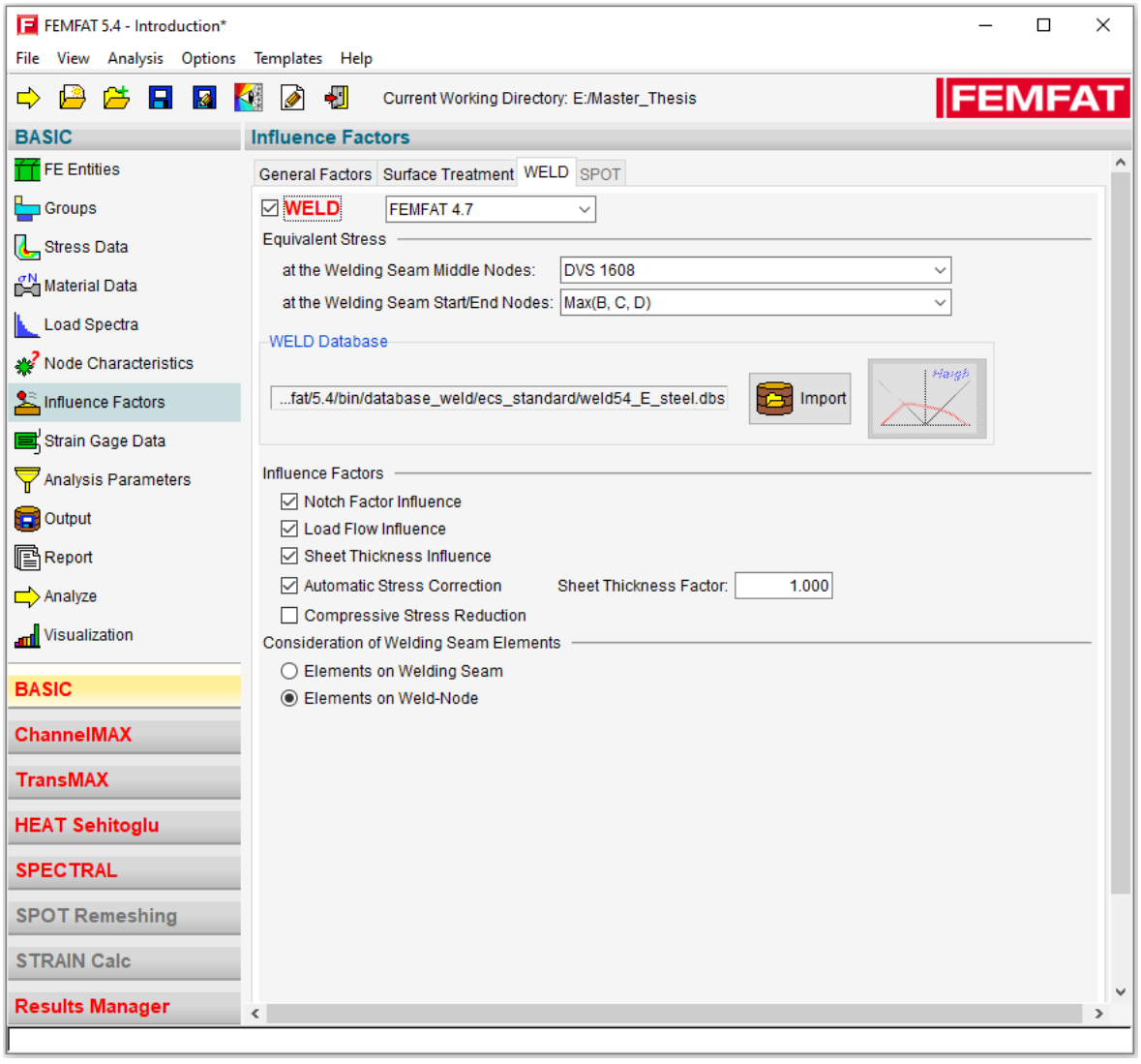

Figure 20: *FEMFAT Weld* module user interface

Among the mentioned assessment methods, even methods based on standards such as Eurocode 3/9 and BS 7608 can found, but all of them were developed on the basis of the FEMFAT 4.7 evaluation method which is used as default in *FEMFAT Weld*. This method first determines the membrane and bending stress components from the stresses of both, bottom and top of the evaluated element. These stresses are then multiplied by the corresponding notch factors for tension/compression, bending and load flow from the weld database and added together to form an overall notch stress. Precisely because of the nature of this assessment method, following the modelling guidelines from chapter 3.2.1 ensures that that the stresses used for the calculation with notch factors, do not already include local stress concentrations caused by the geometry of the weld toe or the weld root.

With that said, there are some influence factors that are specific for the *FEMFAT Weld* module and they are clearly shown in [Fig. 20]. Whether or not to use these influence factors depends entirely on the user, so a short overview of the most important factors will be given here.

3.2.2.1 Notch Factor Influence

The weld notch factors represent the most important influence parameter for the fatigue assessment of welded structures using *FEMFAT Weld* module. For this reason, notch factor influence is enabled by default when *FEMFAT Weld* is activated. In cases when notch factor influence is disabled, any calculations done this way will be using the values of 1.00 for all the notch factors. The weld notch factors are stored in the weld database file with maximum three digits and they are unique for each type of weld joint because the notch effect i.e., local stress concentration caused by the weld geometry differs between each and every weld joint type. They are calculated by detailed finite element modeling of the respective joint type with weld geometry included and then saved into the weld database in a specific format. An example of the format in which every weld joint is defined in the weld database is presented in [Fig. 21] through the example of a simple one-sided T-joint fillet weld with root undercut.

There are several important pieces of information that can be drawn out for each weld joint from the database file with the first one being the unique number designation i.e., SID number of the weld joint shown in [Fig. 21 (a)]. Other important designations for each weld joint are the element material numbers i.e., MAT numbers which can be found in [Fig. 21 (b)]. As the weld nodes are given node color labels according to their position in the weld [Table 1], so are the weld elements assigned with their own material number referring to the orientation of each

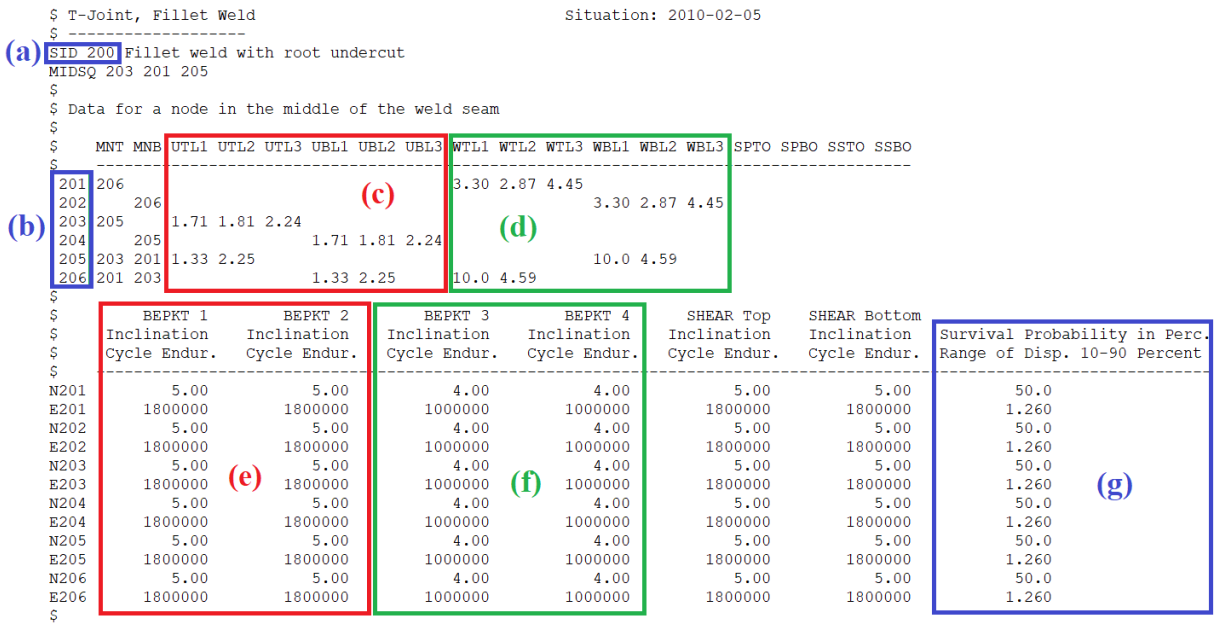

Figure 21: Format of the weld database for nodes in the middle of the weld: (a) SID number, (b) material property labels, (c) weld toe notch factors, (d) weld root notch factors, (e) weld toe S-N curve slope and endurance limit, (f) weld root S-N curve slope and endurance limit, (g) S-N curve survival probability and range of dispersion

weld element and its position in relation to other weld elements of the same weld joint. For shell (2D) elements these material numbers, also known as material property labels, can be in the range from 1 to 9999 but, the same as the SID number, they have to be unique for each weld joint. The allocation of the calculated notch factors is done by means of material property labels i.e., through MID number *FEMFAT Weld* knows which notch factor is characteristic for which weld element.

Notch factors are calculated for the weld toe and/or weld root, depending on the geometry of the weld and the existence of one or both stress concentration points typical for welds. For each of these points, weld toe or weld root, there can be a maximum of four notch factors for each of the three possible load cases. All of the notch factors are divided into columns which are filled according to the corresponding material property labels. For better understanding of the notch factors allocation, some designations need to be explained. First thing that distinguishes the notch factors is the location in the weld to which they refer to, weld toe or weld root. Designation for weld toe (ger. *Nahtübergang*) is U while weld root (ger. *Nahtwurzel*) is marked with W. Second differential parameter is to which side of the material property label does the notch factor refer to, top or bottom, designated with T and B respectively. Finally, as mentioned

earlier there are three possible load cases that can have different notch factors and they are denoted by LC1 (tension/compression), LC2 (bending) and LC3 (load flow). An example of the format in which the notch factors are written in the weld database for each weld joint can be seen for both, weld toe and weld root notch factors, in [Fig. 21 (c)] and [Fig. 21 (d)] respectively. So, for example, a column designation of UBL2 means that the notch factors in that column refer to the weld toe, for the bottom of the corresponding material property label and are representing the second load case i.e., bending.

In addition to the notch factors, each weld joint in the weld database contains the information needed to generate a local S-N curve for both, weld toe and weld root of the joint in question. For its definition, three values are needed, endurance stress limit, endurance cycle limit and the slope of the S-N curve itself. Since the endurance stress limit gets calculated using the weld notch factors for the respective joint in the combination with the Haigh diagram data that can be found in the weld database for the used material, only the other two values need to be defined for each weld joint in particular. Figures [Fig. 21 (e)] and [Fig. 21 (f)] show how these two values are listed in the weld database for the weld toe and weld root of the specific weld joint respectively. Normal stress S-N curves can be defined for a total of four assessment points, two for the weld toe and two for the weld root, each of the regions having one for the top and the other for the bottom of the corresponding material property label.

Regarding the values of the survival probability P_S and the range of dispersion $T_{10/90}$ between 10% and 90% survival probability, for the fatigue assessment of all weld joints in the weld database their values are by default set to $P_S = 50\%$ and $T_{10/90} = 1.26$. However, these values can be specified and changed for each weld joint individually in the section of the weld joint data depicted in [Fig. 21 (g)].

In the chapter 3.2.1, while introducing the modelling guidelines it was pointed out that *FEMFAT Weld* distinguishes weld nodes based on their position in the weld seam. Different node color labels are assigned for weld nodes in the middle of the weld seam and for the weld nodes at the start or end of the weld seam, all according to [Table 1]. Such a distinction is also transferred to the weld database in the sense that for each weld joint different notch factors are defined for the nodes in the middle of the weld seam and for the nodes at the start or end of the weld seam. In respect to that, all of the data introduced so far and presented in [Fig. 21] refers to the weld nodes in the middle of the weld seam. The format of the weld joint data referring to the weld nodes at the start or end of the weld seam is given in [Fig. 22].

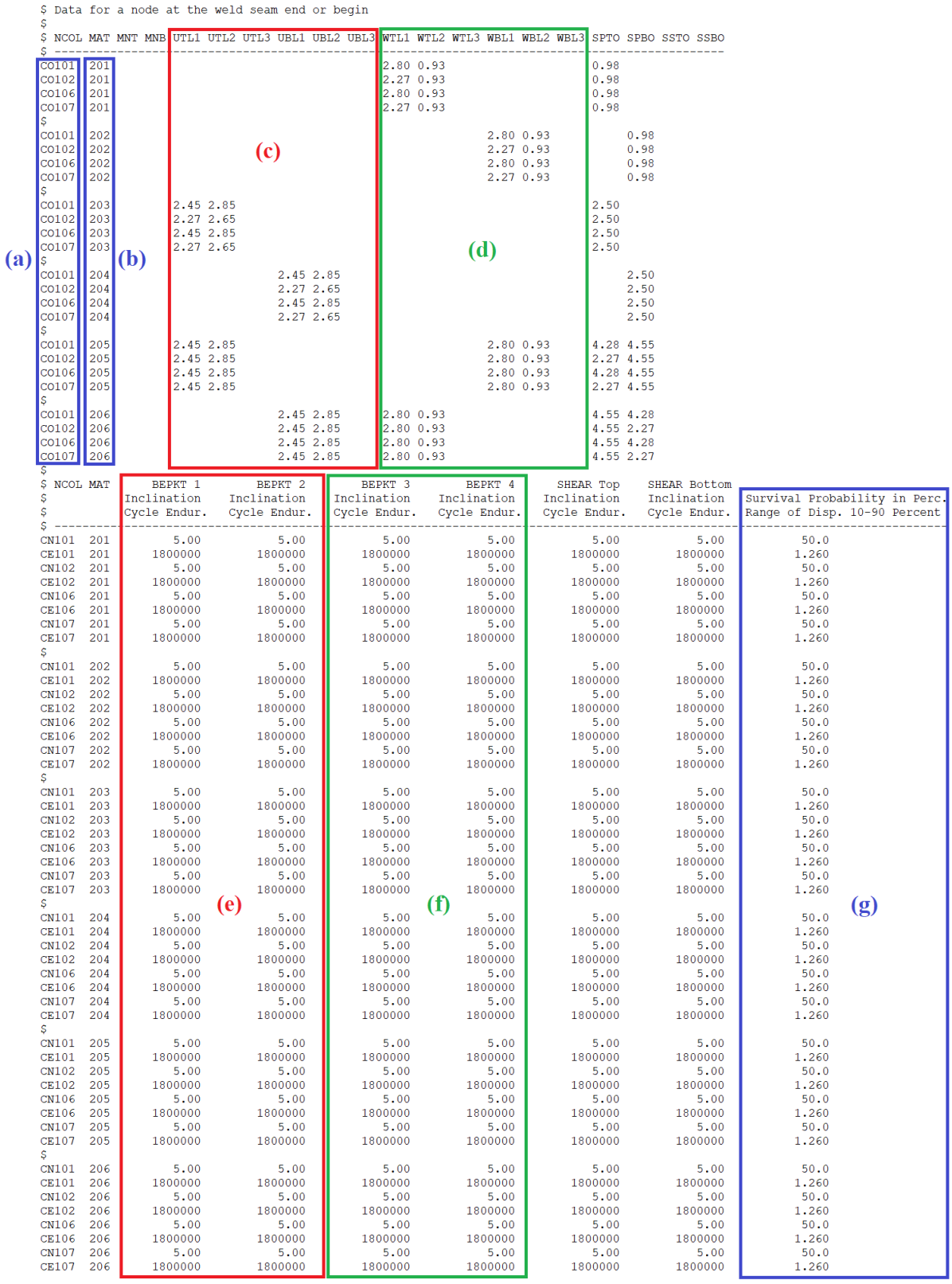

Figure 22: Format of the weld database for nodes at start/end of the weld: (a) node color labels, (b) material property labels, (c) weld toe notch factors, (d) weld root notch factors, (e) weld toe S-N curve slope and endurance limit, (f) weld root S-N curve slope and endurance limit, (g) S-N curve survival probability and range of dispersion

Color node labels mentioned in the chapter 3.2.1 can be seen in [Fig. 22 (a)] and together with the material property labels, see [Fig. 22 (b)], they define the position in the weld seam to which each notch factor or other value e.g., slope, refers to. Notch factors for weld toe and weld root are presented in figures [Fig. 22 (c)] and [Fig. 22 (d)] respectively, with data for the slope and endurance cycle limit of the local S-N curve for the weld toe in [Fig. 22 (e)] and for the weld root in [Fig. 22 (f)]. Finally, the values for survival probability and range of dispersion for the weld nodes at the start or end of the weld seam are given in [Fig. 22 (g)].

All of the data presented here constitute a set of information needed for the definition of a weld joint in the weld database. Even though there are a fair amount of different weld joints already defined in the weld database by *FEMFAT*, there are still a lot of weld joints that can appear in modern day welded structures that don't have their definition inserted into the weld database. Since it would never be possible to have all the existing weld joints defined within one file, this particular weld database was created in such a way that it can be easily extended by the user. Following all of the rules and recommendations presented so far with a few additional procedures, each *FEMFAT* user can create his own weld joint and include it in the database. With this being an option, it is possible to create highly specific weld joints for the use in specific areas of application depending on the user's area of expertise. Since the procedure of extending the weld database was used for the purpose of this thesis, the procedure itself will be described in more detail in chapters to come.

3.2.2.2 Load Flow Influence

As it was already described in the chapter 3.2.2.1, up to three notch factors can be defined per one assessment point i.e., weld node, at any given weld element. This is of course valid only for normal stresses and even though all of the parameters in the weld database exist for both, normal and shear stresses, work in this thesis will be focused only on normal stresses. Anyway, these notch factors are applied in one of the three mentioned load cases, with load case LC1 and LC2 acting in the assessed element and load case LC3 acting through the neighboring element. In cases when load flow influence is enabled through the *FEMFAT Weld* module and FEMFAT 4.7 is used as the assessment method, notch factors from the database are directly multiplied with the corresponding stress components and added together to form a notch stress. This means that the effective notch factor is always smaller or equal to the largest of the three notch factors available for the assessment point in question. If the load flow influence is disabled, the largest

of all the notch factors available in the weld database will be used for the further calculations, regardless of the position or load case for which this notch factor is defined.

3.2.2.3 Sheet Thickness Influence

All of the notch factors that can be found in the database are defined for the sheet thickness of 10 mm. However, sheet thickness has a large influence on the notch effect and thus fatigue life of the whole welded structure, which means that the notch factors from the weld database need to be corrected for the sheet thickness of the welded structure that is being assessed. This correction is performed through a polygon course, quite similar to the one mentioned in chapter 3.2.1. Polygon line for the sheet thickness correction is defined in the weld database with data given in [Table 3] and visually represented in [Fig. 23]. Linear interpolation is performed when sheet thickness lies between two points of the polygon line. Weld database contains the data for sheet thicknesses all the way up to 1000 mm but values up to 50 mm presented here are more than enough for the purposes of this thesis.

Table 3: Polygon course definition of sheet thickness factor for weld joints

Sheet thickness t [mm]	0.0	1.0	4.0	8.0	10.0	13.0	15.0	50.0
Sheet thickness factor G	0.51	0.56	0.72	0.95	1.00	1.07	1.11	1.65

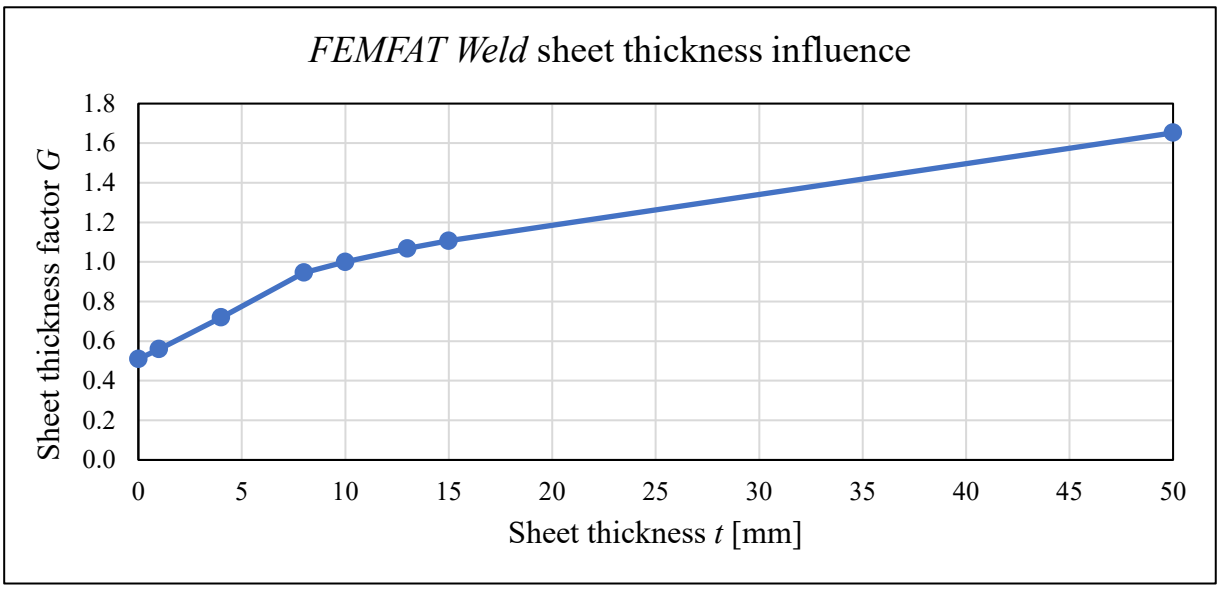

Figure 23: *FEMFAT Weld* sheet thickness influence diagram

3.2.2.4 Automatic Stress Correction

When modelling guidelines presented in the chapter 3.2.1 can't be accomplished, for whatever the reason, the automatic stress correction factor needs to be enabled to ensure more accurate fatigue assessment. When this influence factor is activated, the stresses in the weld or neighboring elements are not utilized, but instead the stresses of elements located at the assessment distance from the weld are used. This assessment distance should be chosen in such a way that the assessment point lies approximately at the weld toe. The aim of this stress correction factor is basically to minimize the influence of size and quality of weld elements with regard to damage calculation. However, the automatic stress correction works differently for fine and coarse meshes of the finite element model being assessed. It also differs for the assessment of the weld nodes in the middle of the weld seam and for the weld nodes at the start or end of the weld seam. All of that means that automatic stress correction introduces more unknown procedures that would need investigating before using them with full certainty in their correctness. Therefore, for the purposes of this thesis, modelling guidelines will be followed, and automatic stress correction will be avoided just for the sake of keeping the assessment procedure as simple as possible and excluding as many additional influence factors as possible.

3.2.2.5 Rest of the influence factors and considerations

The last influence factor that can be included into the assessment via *FEMFAT Weld* module is the compressive stress reduction which, when enabled, reduces the compressive stress component of the stress cycle by 40%. This results in a new amplitude stress which is then used for the assessment. Since compression load cases won't be analyzed through this thesis, detail analysis of this influence factor won't be necessary.

The final parameter to be considered in regard to the *FEMFAT Weld* module is the choice of what is considered to be a weld seam element. In *FEMFAT Weld* a weld is defined as a connection between two weld nodes if at least one weld element which contains both of the nodes, exists. Through the interface depicted in [Fig. 20], user can select whether *FEMFAT Weld* uses only the weld elements attached with an edge to the weld seam or to also include the weld elements that are connected to the weld seam by only one weld node. For including as many weld elements as possible and to avoid unassessed elements in close proximity to the weld, for this thesis it will be preferable to use the second option for the weld assessment.

4 VALIDATION OF *FEMFAT Weld* ASSESSMENT METHOD

Throughout the whole chapter 3, various properties of *FEMFAT* software have been introduced, especially in regard to the *FEMFAT Basic* and *FEMFAT Weld* modules of the program. Before using these modules as a possible solution for the fatigue assessment in this thesis, some additional conclusions about the method can be drawn through the process of method validation. Therefore, fatigue assessment using *FEMFAT Weld* as the main tool has been applied to a specific example found in the literature research in order to see how well does the procedure work. The example that was found most appropriate for this validation in respect to the topic of this thesis was taken from the doctoral thesis by Mann [31]. Through this chapter the whole process of the assessment using many of the parameters from chapter 3 will be described.

4.1 Literature example data

The work done by Mann [31] was for the most part based on a simple welded T-joint of two aluminum hollow sections. To be specific, welded T-joints made from extruded 6082-T6 aluminum alloy profiles with rectangular hollow cross section (RHS) were produced and fatigue tested. The geometry of the welded specimens used in [31] is given in [Fig. 24] and exactly that geometry was used for *FEMFAT* Weld validation purposes.

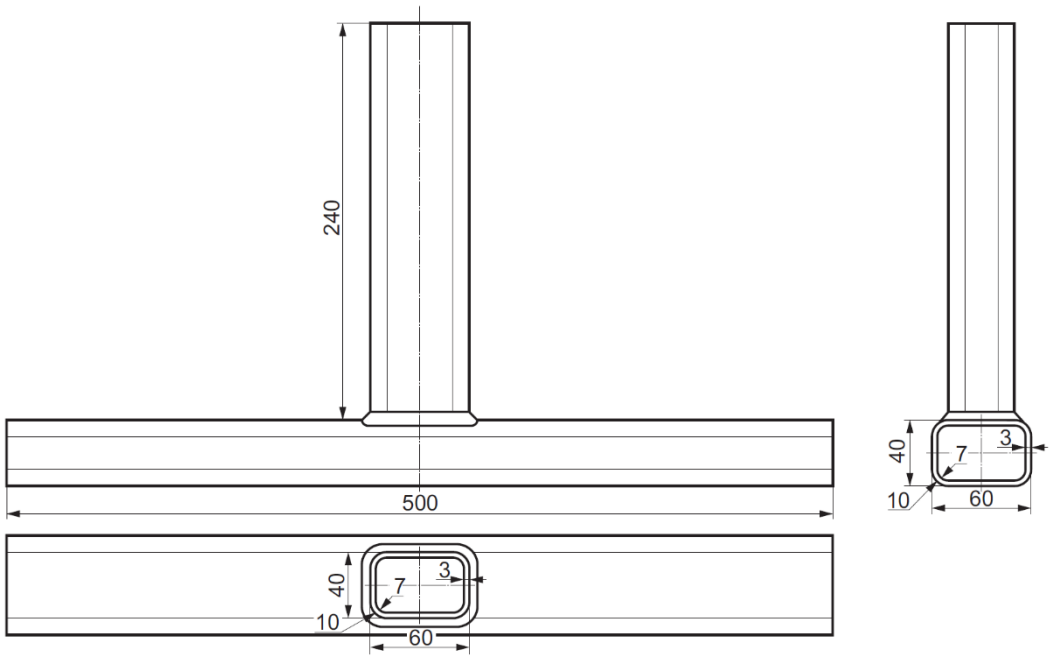

Figure 24: Drawing of the T-joint from Mann [31] used for *FEMFAT Weld* validation

The extruded aluminum profiles were welded together by a robotic welding procedure with the use of ER 5183 as a filler material. The weld itself is a simple T-joint fillet weld seam along the entire circumference of the vertical extruded profile, cleaned after the welding and without any other post-weld surface treatments. The specimens were subjected to 4-point bending tests at the stress ratio of $R = 0.1$, with the setup depicted in [Fig. 25].

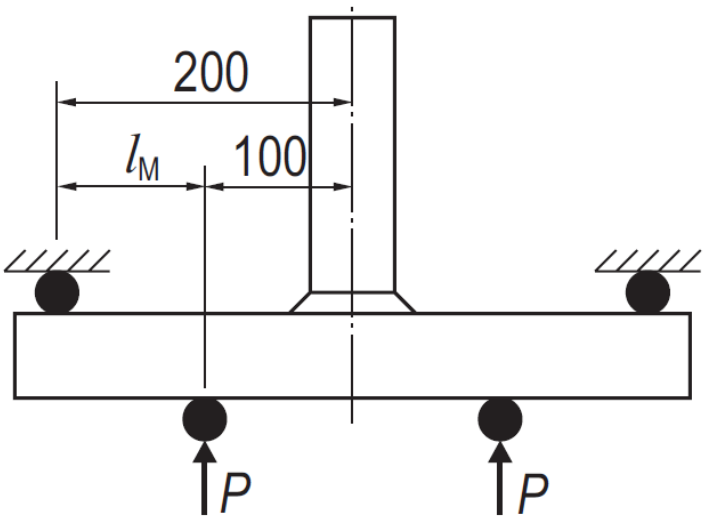

Figure 25: Loading setup of the T-joint from Mann [31] used for *FEMFAT Weld* validation

In respect to the fatigue testing, the specimens were tested at two different load levels to obtain results for both, lower and higher number of cycles. Stress data used for the testing was taken from Mann [31] and it is presented here in [Table 4].

Table 4: T-joint nominal stress data from Mann [31] used for *FEMFAT Weld* validation

	R	$\Delta\sigma$ [MPa]	σ_a [MPa]	σ_m [MPa]
Load level 1	0.1	50	25	30.5
Load level 2	0.1	100	50	61.1

During testing it was found that cracks tend to initiate at the weld toe in one of the four corners of the circumferential weld seam. Considering those areas represent the areas of the highest local stress concentration in the whole specimen, such behavior could have been expected.

4.2 Finite element model preparation

With all of the necessary data from Mann [31] acquired, the next step was to apply this data and prepare a finite element model which would be used for validation purposes. According to the geometry presented in [Fig. 24] a complete 3D CAD model of the welded specimen was created using *SOLIDWORKS 2020* software, see [Fig. 26]. The weld geometry wasn't included in the model in order to test the possibilities of weld joints defined through *FEMFAT* weld database.

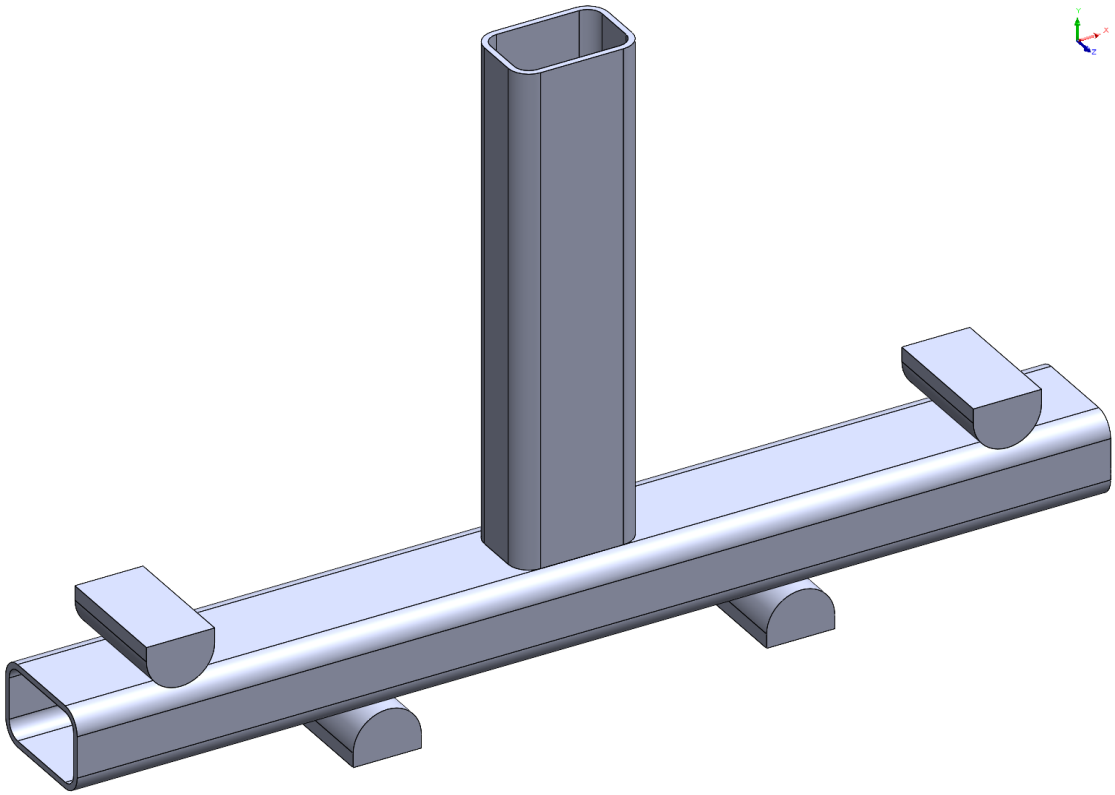

Figure 26: CAD model of the welded specimen for *FEMFAT Weld* validation

The geometry and material information for the loading pins used to conduct the 4-point bending test was taken from the work by Tveiten et al. [46], which was done in cooperation with the thesis by Mann [31]. Hence, cylindrical pins made of steel with the diameter of $d = 33$ mm were used in fatigue testing and consequently in the model.

With the geometry of the welded specimen fully defined, it was in order for the model to be prepared for the finite element analysis. For preprocessing of the CAD model, *ANSA v20.1.2* was used where the final finite element model presented in [Fig. 27] was prepared for the finite element analysis that was eventually conducted using *Abaqus 2019.HF4* simulation tool.

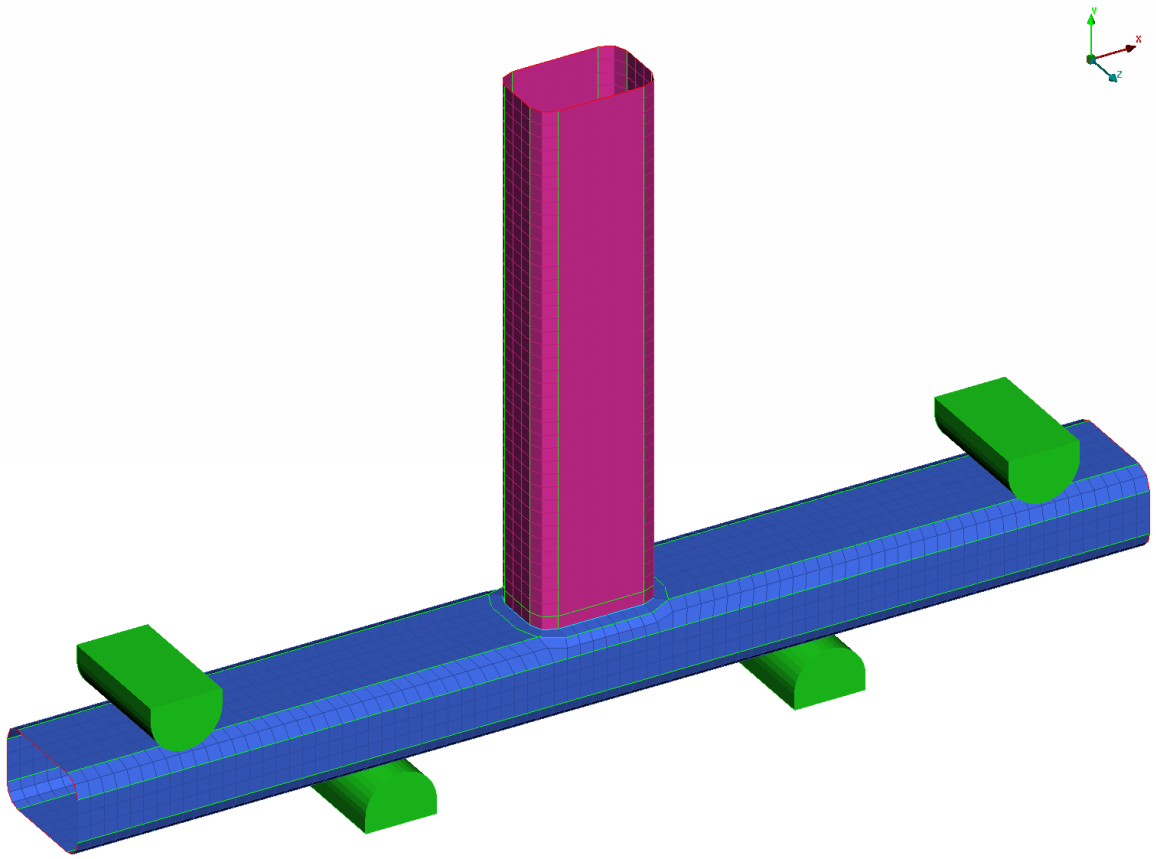

Figure 27: Finite element model of the welded specimen for *FEMFAT Weld* validation

From [Fig. 27] it can be clearly seen that two different modelling approaches were used for the purpose of FE model creation. Aluminum profiles of the welded specimen were modeled as shell sections with the use of first order quadratic shell elements, designated with S4 (4-node general-purpose shell). Since solid components and curvatures are hard to define with shell elements, steel loading pins were modeled as solid sections and meshed with second order tetrahedral solid elements, designated with C3D10M (10-node modified tetrahedron). However, the most important thing to point out is that the shell mesh of the welded specimen was created by following the modelling guidelines introduced in the chapter 3.2.1 so that the FE model could be used for *FEMFAT Weld* assessment as well. The contact between the loading pins and the outer surface of the horizontal hollow section was defined using the *Contact Pair* formulation, with hollow section surface being the master and loading pins being the slave surface. Friction between the two components was defined using the friction coefficient between steel and aluminum with the value of $\mu = 0.61$ according to *Marks' Standard Handbook for Mechanical Engineers* [47]. Boundary conditions were defined through different

reference points that referred to different sets of surfaces via the *Kinematic Coupling* formulation. In total, four boundary conditions were defined, two for the top side pins that are fixed and two for the bottom side pins that could move only in the y axis direction. Regarding the loading conditions, the force that needs to be applied to the bottom side pins in order for the stresses from [Table 4] to realize, can easily be calculated using the beam theory:

$$\sigma = \frac{M}{I} \cdot y\,, \tag{25}$$

with y being the maximum distance from the center of the hollow profile to its edge along the axis around which the moment M acts. According to [Fig. 25] it can be easily understood that the 4-point bending applies the bending moment of $M = P \cdot l_{\mathrm{M}}$ to the center of the welded specimen. With this in mind, equation (25) can be reformulated to:

$$\sigma = \frac{P \cdot l_{\mathrm{M}}}{I} \cdot y\,, \tag{26}$$

and the required force can now be explicitly expressed directly from the equation (26):

$$P = \frac{\sigma \cdot I}{y \cdot l_{\mathrm{M}}}. \tag{27}$$

With moment of inertia $I = 125830\ \mathrm{mm}^4$ obtained from Mann [31], and values $y = 20\ \mathrm{mm}$ and $l_{\mathrm{M}} = 100\ \mathrm{mm}$, the maximum applied force can be calculated for the maximum nominal tensile stress in the specimen, $\sigma_{\mathrm{max}} = 111.1\ \mathrm{MPa}$ from [Table 4]. Applying all of these values to equation (27) gives the value of $P_{\mathrm{max}} \approx 7000\ \mathrm{N}$ for the maximum applied force. Since the stress distribution in these calculations is strictly linear, force values per one loading pin for both load levels can be easily obtained and are presented in [Table 5].

Table 5: Welded specimen loading forces used for *FEMFAT Weld* validation

	R	ΔF [N]	F_{min} [N]	F_{max} [N]
Load level 1	0.1	3150	350	3500
Load level 2	0.1	6300	700	7000

All of the four presented force levels were applied to the finite element model in sequential order, with each one acting in a different step of the simulation. This way, stress results for each force level can be used separately for *FEMFAT Weld* fatigue assessment.

As it was already mentioned through previous chapters, finite element analysis of the described model was conducted in *Abaqus 2019.HF4* as a simple static and linear simulation. Therefore, only basic material properties for linear behavior were needed for the model geometry. For the simulation in question, material data from [Table 6] was used.

Table 6: Material properties used for the FE model in *Abaqus 2019.HF4*

Material	E [MPa]	ρ [kg/m^3]	ν
Aluminum	210000	2700	0.3
Steel	70000	9850	0.3

4.3 FEM static linear analysis results

An adequate finite element model was created with all the data presented so far in chapter 4, and the simulation was successfully conducted. With the areas of contact between the welded specimen and the loading pins creating high local stress concentrations, to avoid result misinterpretation, only the area around the weld is presented with the Max. Principal stress distribution in [Fig. 28]. The figure also nicely shows the mesh created according to the guidelines from chapter 3.2.1.

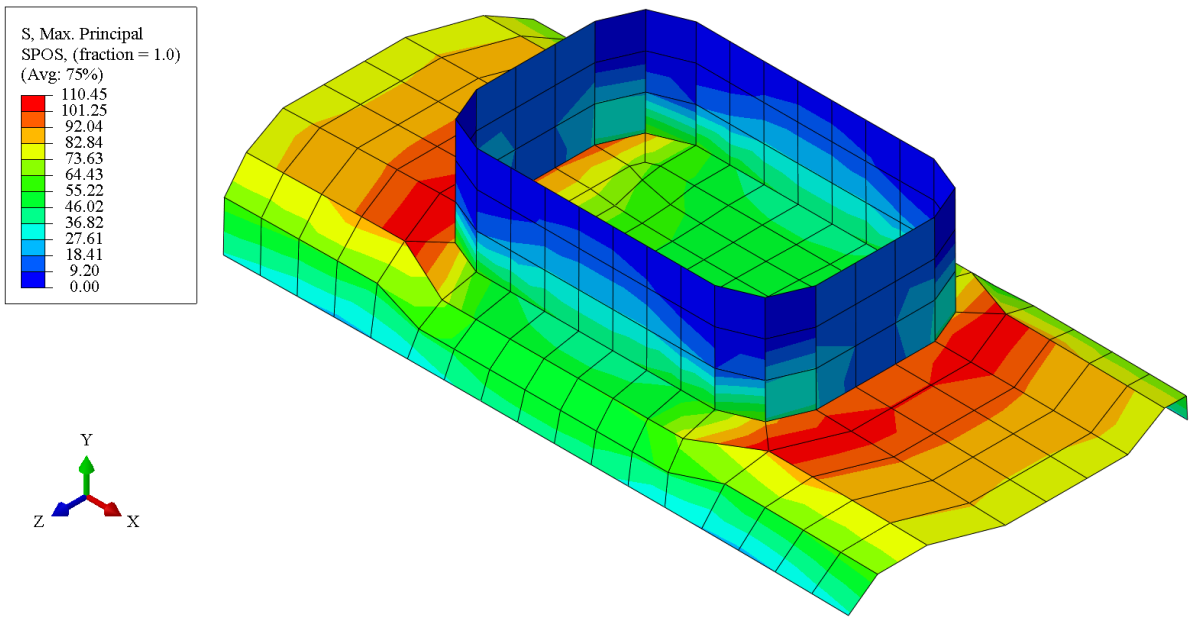

Figure 28: Max. Principal stress distribution in the weld area of the literature example

Obtained results show that the most critical areas of the specimen are in fact the corners of the weld seam, as it was expected. Since the loading conditions of the 4-point bending test are symmetrical in respect to the center of the specimen, so are the results, which show similar stress values at all four corners of the weld seam. As it was advised in the chapter 3.2.2, a comparison of the FEM stress results with the expected analytical stresses was done. For each of the four different forces that were applied to the loading pins during the simulation, resulting Max. Principal stresses were compared to the maximum expected analytical stress that could be calculated from the mean and amplitude stresses in [Table 4] or by using the equation (26). Final comparison is given in [Table 7] from which it is clearly seen that there are virtually no differences between the analytical and FEM results.

Table 7: Comparison of analytical and FEM stress results

Step ID	F [N]	$\sigma_{\text{max, analytical}}$ [MPa]	$\sigma_{\text{Max. Principal, FEM}}$ [MPa]
1	350	5.50	6.13
2	700	11.10	11.11
3	3500	55.50	55.30
4	7000	111.10	110.45

Such great correlation between expected and simulated results just shows that the mesh used in this case can provide reliable results even though it is rather course. With this in mind and considering that the mesh was created by following specifically defined modelling guidelines from chapter 3.2.1, there is no need to conduct a convergence analysis. By reducing the size of the elements, only a larger local stress concentration would be obtained in the most critical areas i.e., weld seam corners, while the nominal stress in the area around the weld would remain the same. This may be beneficial for some investigations, however, in this case, a model that already includes large stress concentrations can give unrealistic results when combined with *FEMFAT Weld* fatigue assessment method that will be performed.

4.4 *FEMFAT Weld* fatigue assessment with existing weld joints

The main reason for avoiding a simulation model with detailed weld geometry, besides the obvious reason of keeping the model as simple as possible, was to investigate the fatigue assessment procedure based on using weld joints from the *FEMFAT* weld database. The whole database of weld joints was thoroughly checked in order to find the weld joint that would suit best to the literature example that was chosen for validation purposes. Two possible solutions were found, with both of them graphically depicted in [Fig. 29] from which characteristic material property labels, as well as the unique SID number, for each of the presented joints can be noticed. This type of visual representation of the weld joint is important for understanding how the weld elements i.e., material property labels, are positioned in relation to each other. Furthermore, even notch factors for each weld joint are allocated to specific material property labels which makes them an important part of the fatigue assessment procedure. Such a sketch exists for each weld joint defined in the weld database and can be found in [48].

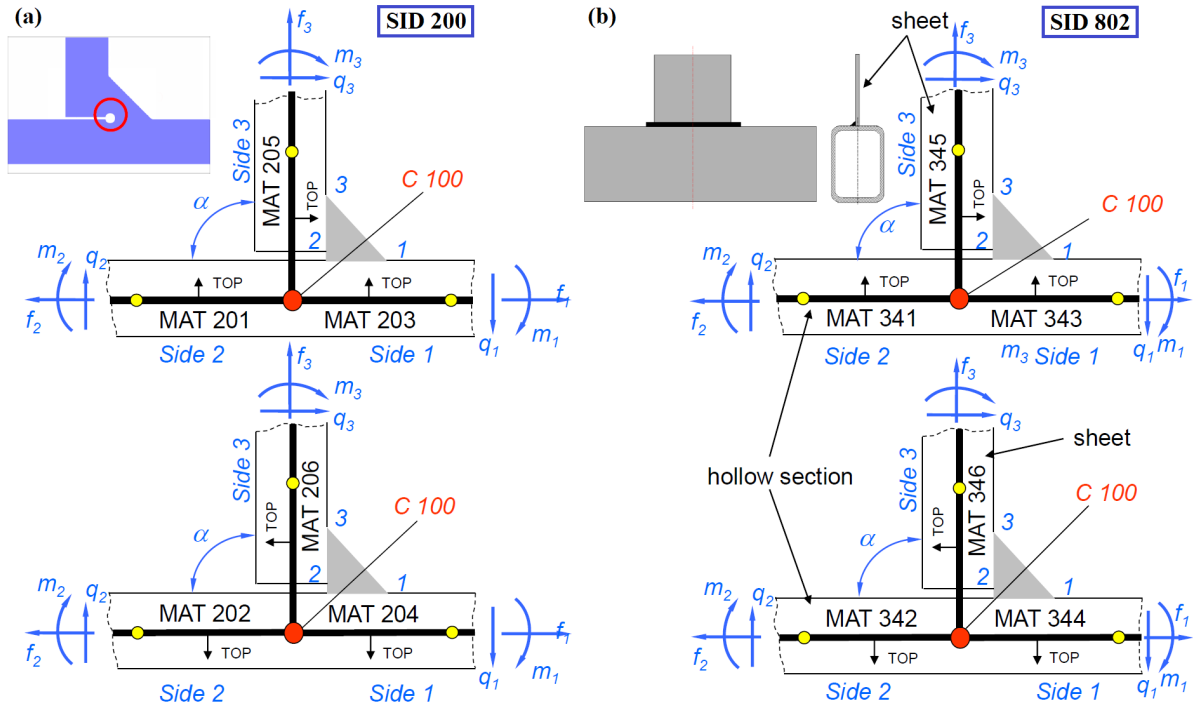

Figure 29: Weld joints chosen for the fatigue assessment from the database [48]: (a) one-side fillet weld with root undercut, (b) T-joint fillet weld at hollow section

These two weld joints are far from an ideal representation of the weld seam that can be found in the presented literature example. The first chosen weld joint shown in [Fig. 29 (a)] is a simple

fillet weld between two metal sheets, while the second one presents a similar connection between one sheet and one hollow section, see [Fig. 29 (b)]. Since no weld joint with a circumferential connection of two extruded profiles exists, these two will be tested to see how reliable, or unreliable results, can they provide compared with the test results from Mann [31].

When both, model geometry and FEM results, are ready and available, they can be loaded into *FEMFAT Basic* and a desired weld joint from a desired weld database, in case there are multiple databases, can be assigned to the geometry model with the help of *FEMFAT Visualizer*. Defining the weld joint at the welded specimen geometry is presented in [Fig. 30] with several main characteristics of the process.

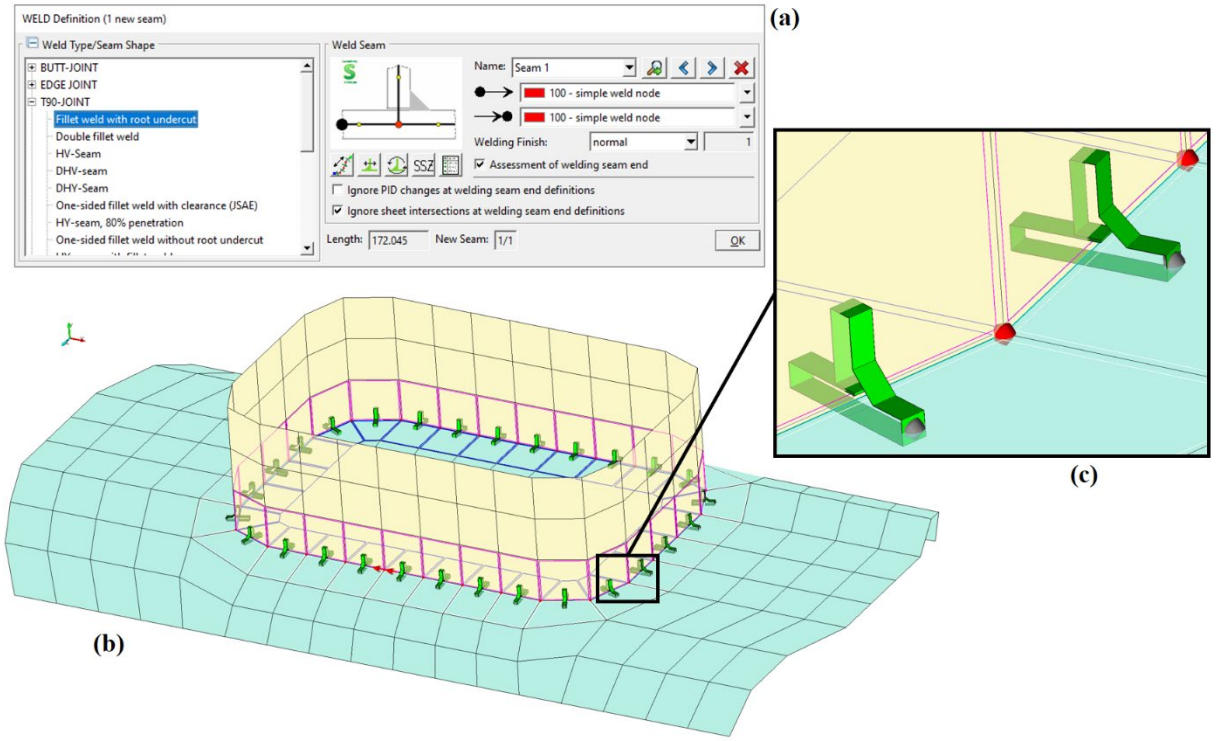

Figure 30: Defining a weld joint in *FEMFAT Visualizer*: (a) weld definition window, (b) visual preview of the chosen weld joint, (c) detailed view of the weld joint

By choosing a desired line at the geometry along which the weld will be positioned, a window for selecting the exact type of the weld joint is opened, see [Fig. 30 (a)]. Through this window, various parameters can be set such as orientation of the weld, direction of welding, assessment of weld seam start/end, surface finish of the weld etc. When the desired weld joint is chosen, a preview of the weld joint will automatically appear at the specimen geometry, see [Fig. 30 (b)].

Also, *FEMFAT* will automatically recognize the position of each weld node and assign corresponding node color labels which can be seen from [Fig. 30 (c)] where red points for nodes in the middle of the weld seam are visible. Node color labels can also be manually adjusted for each weld node through the weld definition window if necessary.

Since fatigue assessment in *FEMFAT Weld* implies a dynamically loaded welded structure, a different set of material data from the one used earlier, see [Table 6], is needed. For the validation purposes with the literature example, material data for 6082-T6 aluminum alloy from AVL material library was used and shown in [Table 8].

Table 8: Material data for 6082-T6 aluminum from AVL material library

	Static [MPa]		Fatigue, $P_S = 50\%$ [MPa]	
Strengths	UTS R_m	Yield $R_{p0.2}$	Pulsating	Alternating
Tension	300.0	255.0	170.9	107.7
Compression	300.0	255.0	0.0	107.7
Bending	357.9	305.5	181.2	129.8
Shear	173.1	147.1	107.9	62.0

Finally, using all the data listed so far in chapter 4, and abiding the procedures described in chapter 3, fatigue assessment of the literature example was realized. Multiple iterations of the simulation were processed with different additional *FEMFAT Weld* factors investigated for the purpose of better understanding the assessment method itself. Both of the presented weld joints were assessed and their results can be found in [Table 9] together with the fatigue testing results from the literature example by Mann [31]. Each weld joint was simulated for a damage calculation at two different load levels with nominal stress ranges taken as a reference value for the creation of corresponding S-N curves for each of the joints, see [Fig. 31]. The slope of each S-N curve was obtained from *FEMFAT Weld* results where the slopes weren't calculated but taken from the weld database for each weld joint depending on the critical location. The slope for the fatigue testing results from Mann [31] was simply calculated by the following equation:

$$k = \left| \frac{\log_{10}(N_{f2}) - \log_{10}(N_{f1})}{\log_{10}(\Delta\sigma_2) - \log_{10}(\Delta\sigma_1)} \right|. \tag{28}$$

Table 9: *FEMFAT Weld* fatigue assessment results for the literature example

	$\Delta\sigma_n$ [MPa]	N_f [cycles]	k
Mann, T., Fatigue testing results [31]	50.0	$1.769 \cdot 10^6$	4.6
	100.0	$7.158 \cdot 10^4$	
FEMFAT Weld, One-side fillet weld with root undercut	50.0	$1.699 \cdot 10^7$	4.0
	100.0	$1.034 \cdot 10^6$	
FEMFAT Weld, Fillet weld at hollow section	50.0	$4.288 \cdot 10^7$	4.1
	100.0	$2.432 \cdot 10^6$	

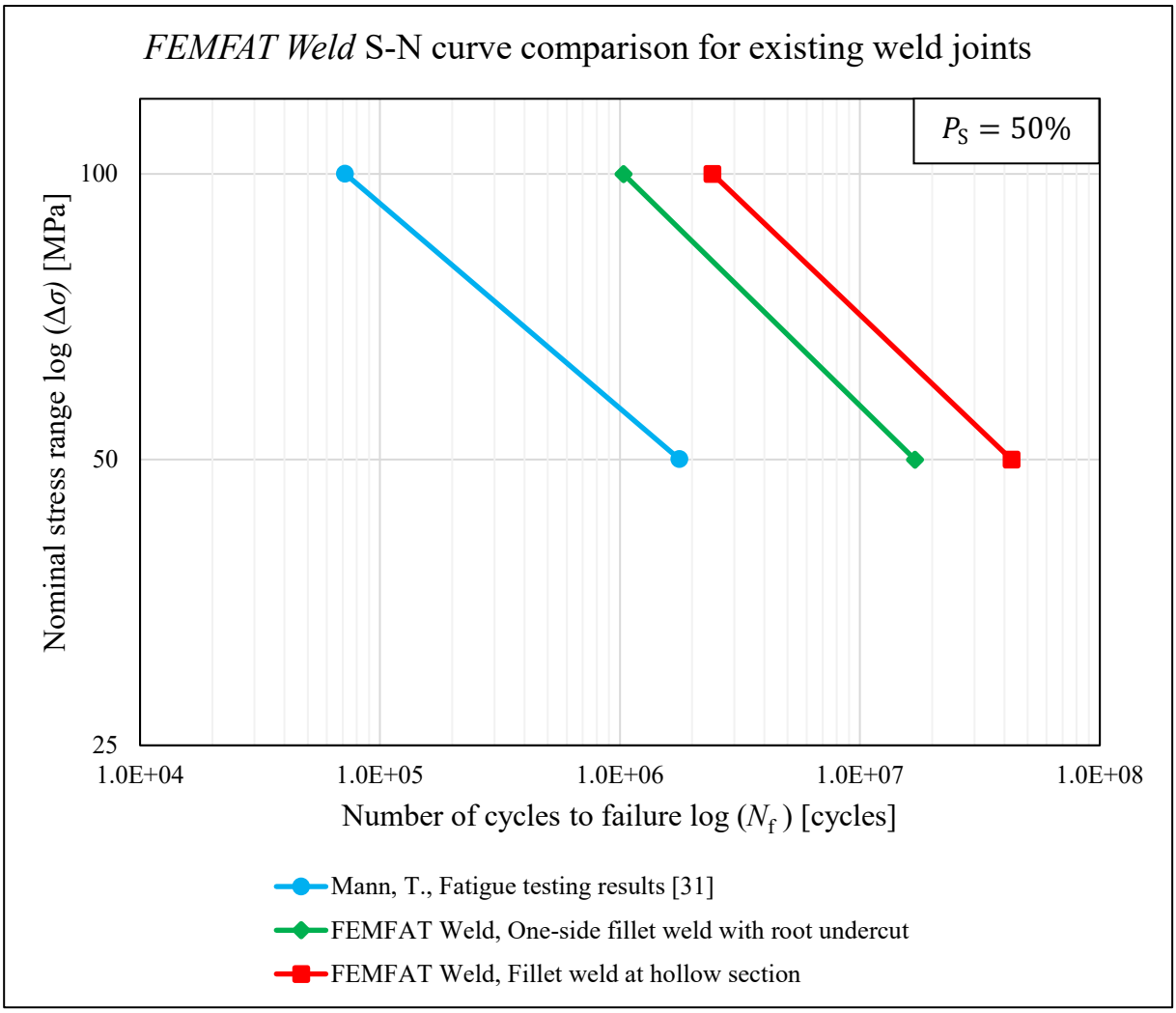

Figure 31: S-N curves for *FEMFAT Weld* fatigue assessment of the literature example

Regarding the slopes of all three S-N curves it can be concluded that they are matching quite good with differences only visible through the numerical values rather than graphical representation. However, regarding the number of cycles to failure, S-N curves of both weld joints that were taken from the weld database show far less conservative results than fatigue testing conducted by Mann [31] with the fillet weld at a hollow section showing the least conservative behavior i.e., the longest fatigue life for the welded specimen, in between all three presented curves. What this basically means is that the notch factors that would faithfully represent the fatigue life of the welded specimen according to fatigue testing, would need to be higher than the notch factors characteristic for both weld joints used in this assessment. Higher notch factors would result in higher notch stresses which would be reflected on fatigue life by reducing it. It is worth mentioning that all three curves from [Fig. 31] are valid for the survival probability of $P_S = 50\%$.

It was already mentioned that during the fatigue testing of the welded specimen it was found that the crack initiated at the weld corner with weld toe being the critical area for crack initiation. However, according to *FEMFAT Weld* results, the critical point of the welded specimens in respect to fatigue, for both weld joints that were assessed, was indeed the weld root. This could be explained by looking at the values of the notch factors for both weld joints (see [Fig. 21] for notch factors of the fillet weld joint between two metal sheets), which shows that in both cases, notch factors for the weld root are significantly higher than the notch factors for the weld toe. So, in a situation where nominal stresses are similar in the whole area around the weld, especially on the top and bottom of shell element that is being assessed, higher notch factors would determine the critical point of the weld, which might not be the real or expected crack initiation source.

All in all, final conclusion of the first fatigue assessment for the literature example would be that there is no existing weld joint in the weld database that can faithfully represent the behavior obtained from fatigue tests. Therefore, a new weld joint must be created i.e., weld database needs to be expanded, and that is exactly what will be done. This way, additional knowledge about the software will be gathered and simplicity of the new weld joint creation will be tested.

4.5 Extending the weld database in *FEMFAT Weld*

In order to create a new weld joint that can be included into the existing weld database, certain steps to follow and recommendations to consider have been defined by *FEMFAT*. The main idea behind the possibility of expanding the weld database is to combine the experimental data from fatigue measurements with finite element modelling and fatigue assessment in *FEMFAT Weld*, all for the purpose of defining a specific weld joint i.e., calculating the joint specific notch factors, that can speed up the process of fatigue assessment in the future.

First step in expanding the weld database is to determine the exact weld geometry and include it into a detailed CAD model of the welded specimen in question. To measure the weld geometry in detail, microscopic measurement must be applied to a cross section of the weld joint that is being analyzed. Therefore, it is recommended that the CAD model with detailed geometry of the weld joint in question is also created as a two-dimensional cross section from which the measurements were taken. However, another approach of defining the weld geometry was utilized for the purposes of this literature example and that is to simply assume an idealized weld shape with basic weld geometry that is used in visual representations of a fillet weld such as the ones given in [Fig. 29]. The complete CAD model with the detailed weld geometry is depicted in [Fig. 32 (a)], with simplified weld cross section along the shorter side of the vertical aluminum profile given in [Fig. 32 (b)]. A simple fillet weld with the throat of the weld i.e., distance between the root and the face of the weld, of $a = 3$ mm was used. In order to avoid sharp notches at weld toes and the weld root, *FEMFAT* recommendation for modeling with reference radii was applied, which states that the radius at the weld toe and the weld root can be approximated from sheet thickness t with the following expression:

$$\rho_{\mathrm{f}} = \frac{t}{10}, \tag{29}$$

which defines a fictious radius of $\rho_{\mathrm{f}} = 0.3$ mm for the welded specimen depicted in [Fig. 32].

This simplified approach of weld geometry definition was used even though the detailed cross section weld measurements for the welded specimen from [Fig. 24] can be found in an article by Tveiten et al. [46]. These values weren't used for validation purposes because of different cross sections that could be found along the weld seam that goes all around the circumference of the vertical extruded profile. Because of the large curvature of the edges of the used extruded aluminum profiles, different shape of the weld is achieved along the longer side of the extruded profile and in the corner of the weld than with the shorter side of the extruded aluminum profile.

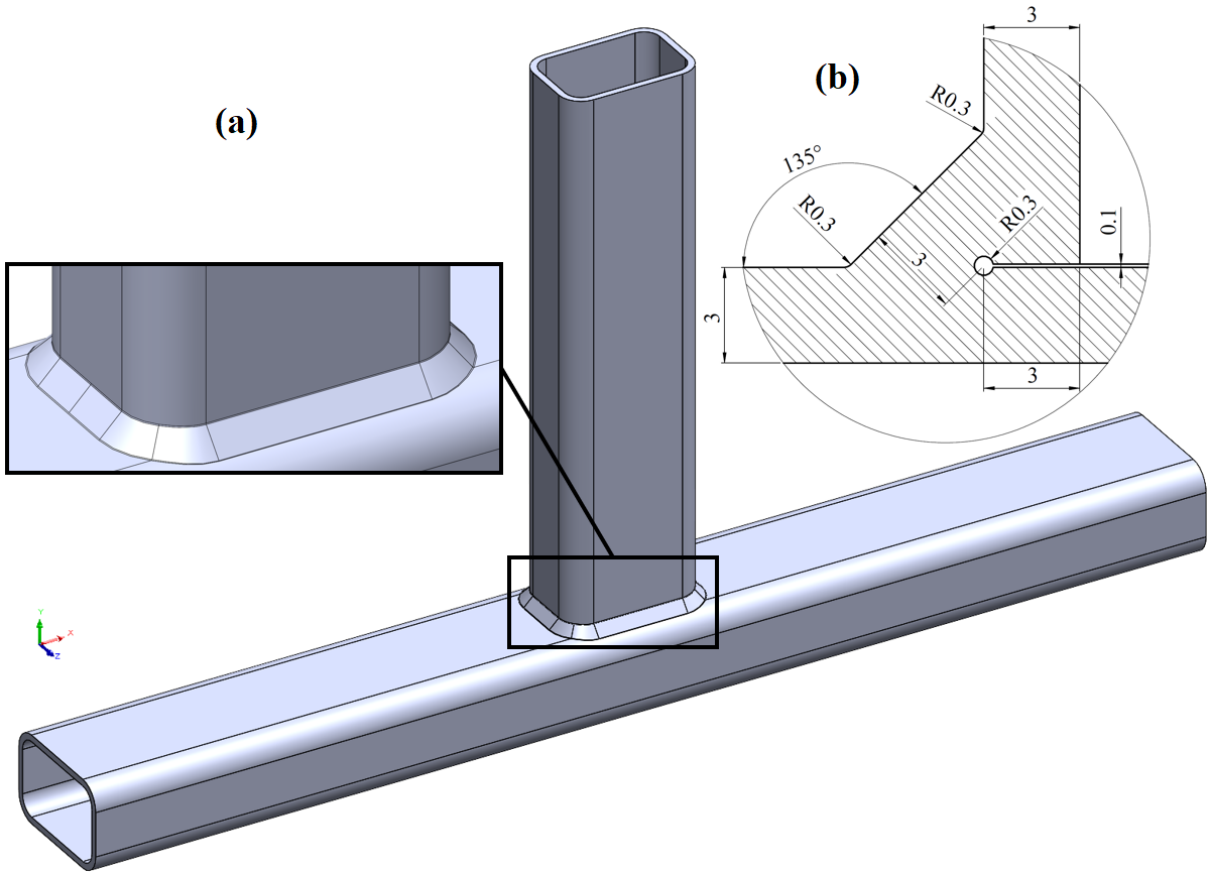

Figure 32: Welded specimen for *FEMFAT Weld* validation: (a) CAD model with detailed weld geometry, (b) cross section of the weld along the short side of the hollow section

Geometry of the variable weld seam cross section specific for this literature example can be seen in [Fig. 33] where three different cross sections at three characteristic places of the weld seam are presented. The first cross section in [Fig. 36 (a)] is situated along the shorter side of the vertical extruded profile with the weld surface of the horizontal profile in the cross section being completely straight. The second one, see [Fig. 36 (b)], is the cross section at an angle of 45° in respect to $x - y$ plane, passing through the middle of the weld seam corner and it already includes the curved edge of the horizontal profile. The final weld seam cross section depicted in [Fig. 36 (c)] shows the shape along the longer side of the vertical extruded profile with the steepest curvature change of the horizontal profile edge. So, going from the first cross section before the weld seam corner, to the third one it can be seen that the edge curvature of the horizontal extruded profile gets more and more pronounced, thus changing the weld seam shape. To avoid this, simple geometry was used even though that isn't a direct *FEMFAT* recommendation, besides the reference radii determination which is. However, with this model

being used only for validating the process of weld database extension rather than conducting the exact notch factor calibration for the welded specimen in question, it will suffice. The simplicity assessment of this process in respect to entering new data i.e., new notch factors, into an existing weld database is in the main focus.

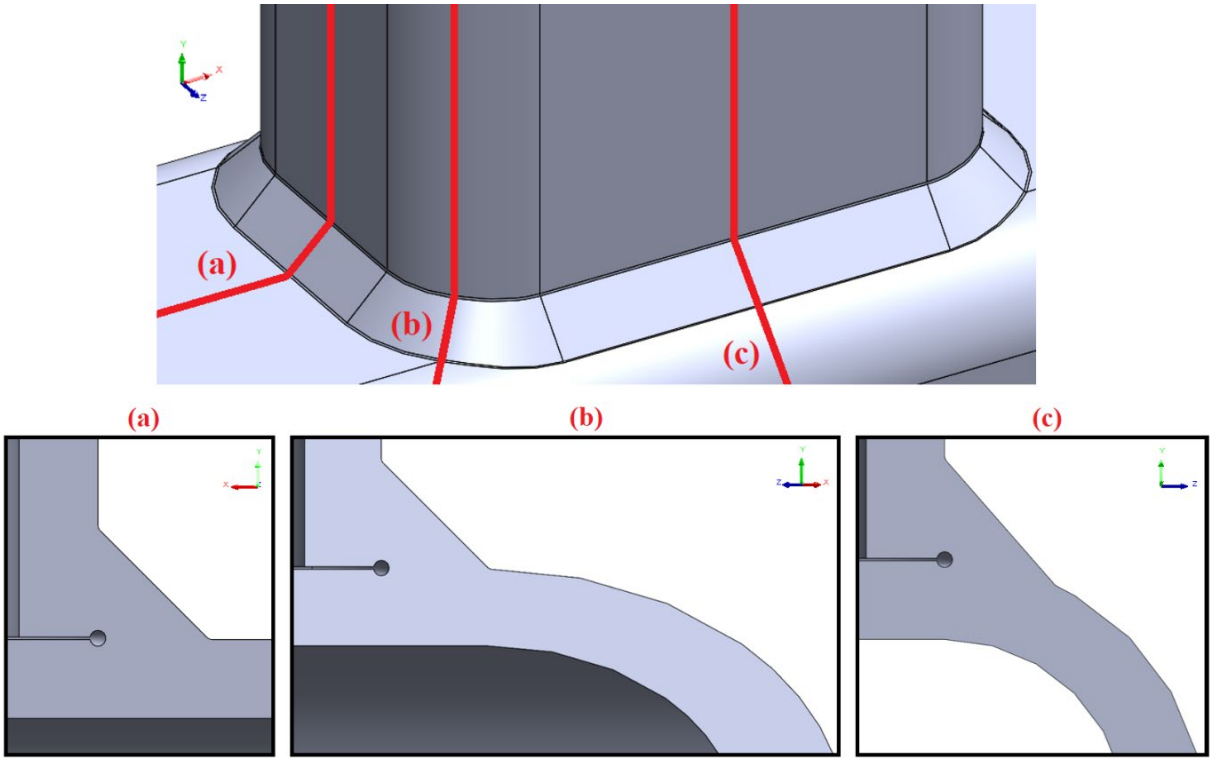

Figure 33: Different cross sections of the weld along the weld seam: (a) cross section along the short side of the vertical profile, (b) cross section in the middle of the weld seam corner, (c) cross section along the long side of the vertical profile

With the model geometry completely defined, the step that follows is to create an element mesh for the finite element analysis to be conducted. However, opposed to the meshing guidelines for fatigue assessment using *FEMFAT Weld* where coarse mesh is preferred, for notch factor determination of the new weld joint, the mesh needs to be as fine as possible to include all local stress concentrations that can appear due to the weld geometry. This is only logical because the determination of new notch factors doesn't include any fatigue related loading conditions, on the contrary, it is done using static and linear finite element analysis. For the FE model of the welded specimen only half of the geometry depicted in the [Fig. 32 (a)] has been used and the final mesh of the weld area can be seen in [Fig. 34] from both sides of the halved specimen.

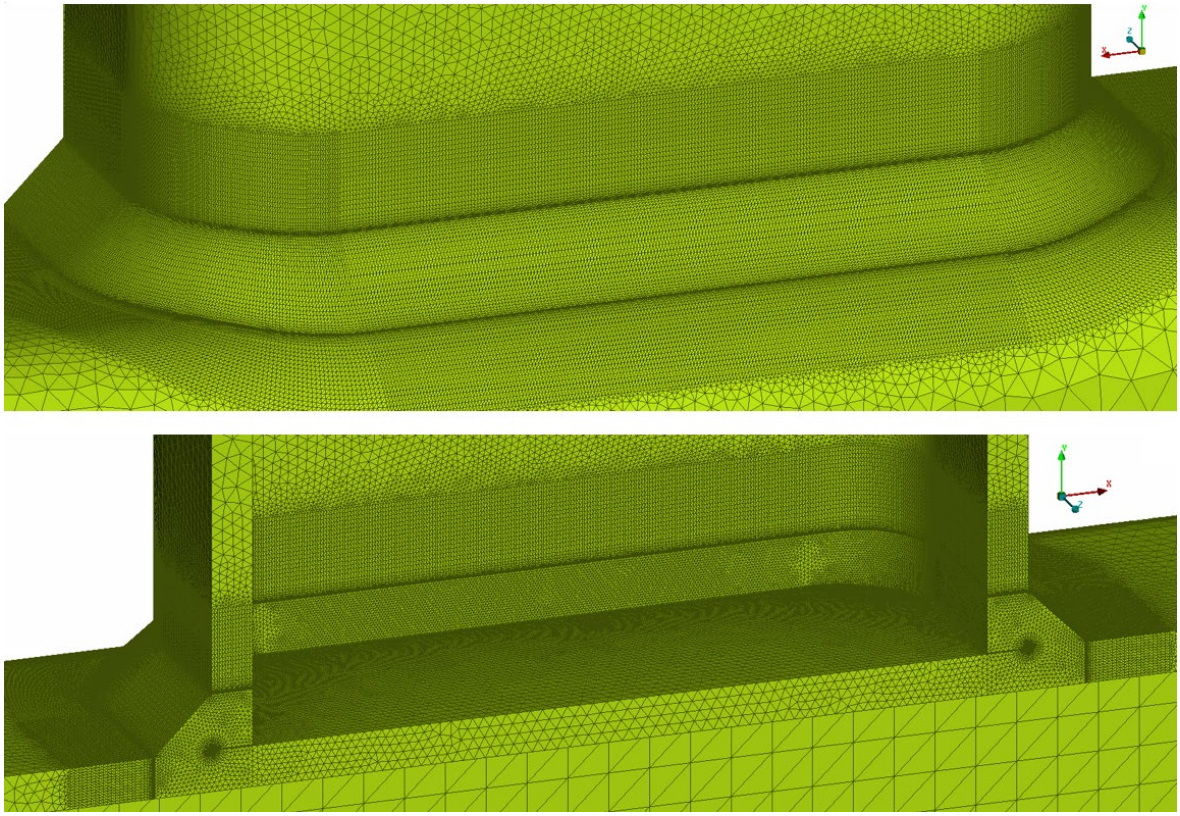

Figure 34: FE model with detailed weld geometry for *FEMFAT Weld* validation

Only half of the geometry model was used in order to save computation time needed to analyze this highly detailed FE model which was meshed using the second order tetrahedral solid elements (C3D10M). This was done on the account of symmetrical geometry, boundary and loading conditions in respect to $x - y$ plane. Elements are densely distributed in the whole area of the weld seam and through the thickness of the material, especially in the weld root and both weld toes to ensure reliable results which will show high local stress concentrations in these areas. The reason for going with a 3D model for the finite element analysis, rather than creating a 2D cross section like *FEMFAT* guideline would suggest, was in fact that the weld cross section changes shape in different parts of the weld seam, as already explained.

As it was mentioned in chapter 3.2.2.1, notch factors are distributed in the weld database in respect to the corresponding load case for which they are calculated. So, in the reverse scenario, for the determination of new notch factors, adequate load cases need to be defined in order for them to be applied to the finite element model of the weld joint that is being added to the weld database. Load cases are defined in such a way that the necessary information for weld database extension is obtained. In the case of a T-joint fillet weld, according to [49], there are six different

load cases that need to be defined to evoke stresses in the root and the toe of the base plate and the web plate of the joint. For the weld joint from the literature example, the base plate would be the horizontal extruded aluminum profile while the vertical profile would serve as a web plate. The six needed load cases for notch factor determination in a T-joint fillet weld can be seen in [Fig. 35].

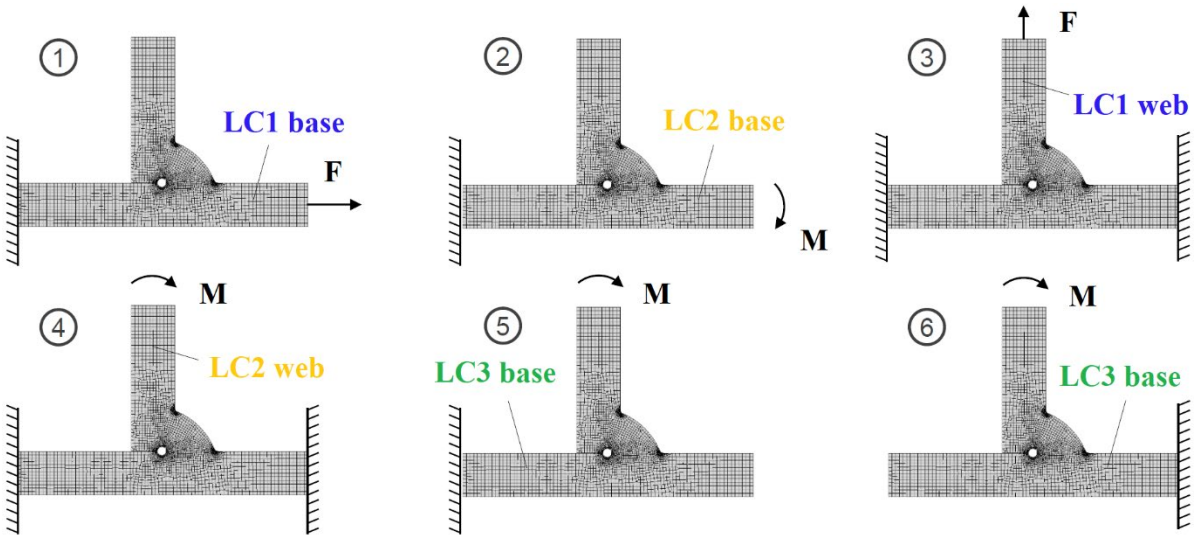

Figure 35: Load cases for tension (LC1), bending (LC2) and load flow (LC3) used for notch factor determination in a T-joint fillet weld

In accordance with the three main load cases existing in the weld database and by looking at [Fig. 35], it can be seen that each part of the T-joint fillet weld needs to be individually analyzed by first two load cases, LC1 and LC2, while the third load case, LC3, is observed only in the base plate of the joint but for two different scenarios, hence a total of six load cases. To avoid confusing the main load cases with the load cases for notch factor determination and to understand their mutual correlation, nomenclature presented in [Table 10] will be used in this paper from this point on.

Table 10: Load case nomenclature in accordance with [Fig. 35]

Main	LC1 (tension)		LC2 (bending)		LC3 (load flow)	
[Fig. 35]	1	3	2	4	5	6
Auxiliary	lc1	lc3	lc2	lc4	lc5	lc6

With the weld geometry meshed, all of the six presented load cases can be applied with six different simulations to conduct. From each load case, stresses in the root and the weld toe of the weld seam can be obtained in order to calculate notch factors for the weld joint in question. Notch factors are calculated using the equation (14) with σ_f being the notch stress read directly from the weld toe or the weld root, and σ_n being the nominal stress at a certain distance away from the local stress concentration, either weld toe or weld root. According to *FEMFAT* recommendations, no specific distance is given for notch factor calculations, but it should be the distance after which the stress doesn't change much. Several distances have been analyzed for the purpose of this calculation and they are all presented in [Fig. 36] at the cross section of the FE model along the short side of the extruded aluminum profile. The stresses were taken from the top surface of the horizontal profile for the bottom weld toe and weld root, and from the top surface of the vertical profile for the other weld toe. From the same figure it can be seen that the mesh was designed in such a way that reading out the stresses at certain distances can be as easy as possible even with the cross sections changing along the weld seam. As it could be expected, notch factors showed to be falling in value when increasing the distance from the notch and they were expected to achieve an approximately constant value at a certain distance i.e., when distance would increase further, the notch factors wouldn't change much.

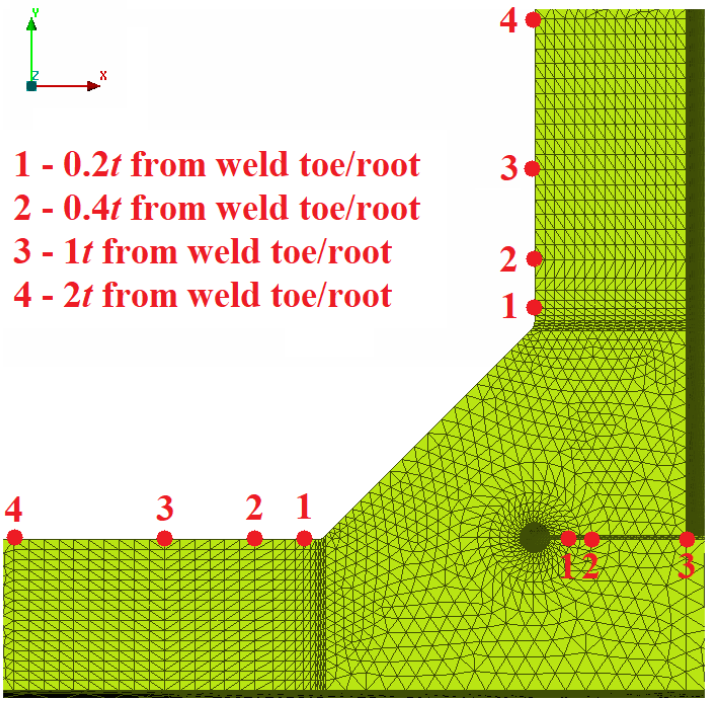

Figure 36: Distances from the weld toe/root for notch factor calculation

However, for the weld joint in question, notch factor values didn't converge to a constant value, at least not before the distance of $2t$ from the notch. Calculated notch factors kept decreasing for each change of the distance. Considering that all of the six load cases showed for the critical point to be somewhere in the corner of the weld seam, the ever-decreasing notch factors could be explained with a better look at the geometry of that corner.

Unlike the cross section depicted in [Fig. 36] where horizontal extruded profile of the joint is flat, at the corner of the weld seam, the edge curvature of the horizontal extruded profile starts immediately after the weld notch or at a very small distance from it, depending in which part of the corner is the critical point situated. From [Fig. 33] it can be seen that as the weld seam progresses through its corner, the transition from the weld to the base material of the horizonal extruded profile is getting smoother because of the edge curvature. When trying to read out the stress at a distance of $1t$ or $2t$ from the notch, the curvature is already so pronounced that the stress just continues to decrease because of the shape of the geometry. Because of this effect, the notch factors couldn't possibly achieve a constant value. So, through numerous iterations and investigations, it has been concluded that the distance of $1t$ from the notch effect can be used to get satisfactory results for notch factors since the stress decrease between points at $1t$ and $2t$ distance is relatively small in comparison to the maximum stress at the notch.

Additional thing to look after when calculating notch factors is the need for correction of each notch factor that is calculated using the notch stress obtained from a notch with an undercut, as it was described in chapter 2.4. Therefore, for the weld joint from the literature example, the correction was conducted using the equation (15) for weld root notch factors from all six load cases. Finally, for the calculation of the notch factors *FEMFAT* recommends the use of principal stresses S11 and S22 depending on the load case, but since the notch factors in the weld joint presented here were acquired from a 3D model rather than a 2D cross section, Max. Principal stresses were used for the calculation of notch factors which are given here in [Table 11].

Table 11: Notch factors for a T-joint fillet weld between two extruded profiles

	lc1	lc2	lc3	lc4	lc5	lc6
Weld toe	2.45	2.69	4.91	6.06	–	5.79
Weld root	2.52	2.76	2.47	3.08	2.81	-

The reason for load cases lc5 and lc6 to have only one notch factor defined rather than two like other load cases, can be noticed from [Fig. 35]. These load cases describe load flow through the weld joint and the boundary conditions are set in such a way that in lc5 load flows through the root of the weld and in lc6 the load flows through the weld toe, hence such distribution of notch factors. All of the notch factors calculated with the described procedure and already presented in [Table 11] are valid only for the weld nodes in the middle of the weld seam i.e., the effect of start or end of the weld wasn't investigated. In order to acquire these notch factors, additional investigations must be performed.

When the notch factors for the investigated weld joint are finally calculated, they can be integrated into the weld database according to *FEMFAT* guidelines that were also presented in this thesis. In order to integrate the notch factors from [Table 11] into the weld database, a new weld joint in the database has been created with a unique SID number 210, see [Fig. 37 (a)], and material property labels from MAT 901 to MAT 906, also specific for this joint only, see [Fig. 37 (b)]. The newly created joint is completely defined for weld nodes in the middle of the weld seam, and it can be seen in standard weld database format in [Fig. 37].

```
$ T-Joint at two Hollow Sections, Fillet Weld  (Master Thesis MV)              Situation: 2021-09-09
$ ------------------------------------------------------------
(a) SID 210 T-Joint at two hollow sections, fillet weld
MIDSQ 903 901 905
$
$ Data for a node in the middle of the weld seam
$
$    MNT MNB UTL1 UTL2 UTL3 UBL1 UBL2 UBL3 WTL1 WTL2 WTL3 WBL1 WBL2 WBL3 SPTO SPBO SSTO SSBO
$    ------------------------------------------------------------------------------------
  901 906                  (c)              2.52 2.76 2.81
  902     906                                          2.52 2.76 2.81
(b) 903 905      2.45 2.69 5.79                    (d)
  904     905                  2.45 2.69 5.79
  905 903 901 4.91 6.06                                 2.47 3.08
  906 901 903                  4.91 6.06        2.47 3.08
$
$        BEPKT 1         BEPKT 2         BEPKT 3         BEPKT 4       SHEAR Top     SHEAR Bottom
$     Inclination     Inclination     Inclination     Inclination     Inclination     Inclination   Survival Probability in Perc.
$     Cycle Endur.    Cycle Endur.    Cycle Endur.    Cycle Endur.    Cycle Endur.    Cycle Endur.  Range of Disp. 10-90 Percent
$    ------------------------------------------------------------------------------------------------------------------------
N901         4.60            4.60            4.10            4.10            5.00            5.00            50.0
E901      1800000         1800000         1800000         1800000         1800000         1800000          1.260
N902         4.60            4.60            4.10            4.10            5.00            5.00            50.0
E902      1800000         1800000         1800000         1800000         1800000         1800000          1.260
N903         4.60            4.60            4.10            4.10            5.00            5.00            50.0
E903      1800000   (e)   1800000         1800000         1800000         1800000         1800000          1.260
N904         4.60            4.60            4.10            4.10            5.00            5.00            50.0
E904      1800000         1800000         1800000         1800000         1800000         1800000          1.260
N905         4.60            4.60            4.10            4.10            5.00            5.00            50.0
E905      1800000         1800000         1800000         1800000         1800000         1800000          1.260
N906         4.60            4.60            4.10            4.10            5.00            5.00            50.0
E906      1800000         1800000         1800000         1800000         1800000         1800000          1.260
$
```

Figure 37: Weld database for a T-joint fillet weld between two extruded profiles: (a) SID number, (b) material property labels, (c) weld toe notch factors, (d) weld root notch factors, (e) weld toe S-N curve slope and endurance limit

Notch factors for the new weld joint have been appropriately assigned to the weld toe and weld root, as seen in [Fig. 37 (c)] and [Fig. 37 (d)] respectively. Regarding the slope of the S-N curve at the weld toe, it was modified according to the slope from the literature example in [Table 9] since 4-point bending is used for fatigue testing which is a load setup in which the fatigue critical spot is the weld toe. The slope for the weld root was taken from the T-joint fillet weld between a sheet and a hollow section, see [Fig. 29 (b)], that already exists in the database under the SID 802, as is the rest of the data from [Fig. 37], including cycle endurance limits for both, weld toe and weld root.

Since the model for calculation of notch factors was created with a few modifications in regard to the *FEMFAT* modelling guidelines, such as using of 3D model instead of a 2D cross section and applying simple weld geometry rather than using microscopic measurements, the procedure of determining the notch factors wasn't described in full detail. The more detail calculation will be presented with the results of experimental fatigue testing for two different weld joints that will be assessed as the main topic of this thesis.

4.6 *FEMFAT Weld* fatigue assessment with the new weld joint

In order to finish the validation process, one final fatigue assessment was in order. The newly created weld joint needed to be tested to see how its results will compare with other joints used and, most importantly, how will it compare to the fatigue testing results for the literature example. The fatigue assessment was once again conducted using the *FEMFAT Weld* module with all of the basic parameters staying the same as in the simulations from chapter 4.4, including the material properties given in [Table 8]. The only thing that needed paying attention to, was the sheet thickness influence factor in *FEMFAT Weld*, because new notch factors were defined for the sheet thickness of $t = 3\,\mathrm{mm}$, so this influence had to be disabled for the purposes of this simulation. For it to stay enabled, new notch factors would need to be recalculated for a sheet thickness of $t = 10\,\mathrm{mm}$ using the reverse process from the one defined in the chapter 3.2.2.3. Whichever approach would have been chosen, the simulation results would be the same, so for the purposes of this example this influence will simply be disabled. Besides that, the only thing that distinguishes this assessment from those two earlier, is in fact the weld joint that was assigned to the geometry model of the welded specimen according to the procedure described in the beginning of chapter 4.4. T-joint fillet weld between two extruded profiles, defined with the data given in [Fig. 37], was simulated at two load levels with

stress ranges once again used for the creation of the S-N curve. The data obtained as a result of damage calculation using *FEMFAT Weld* is given in [Table 12] in the number of cycles to failure, together with the results of the fatigue testing from the literature of the same welded specimen. It is worth mentioning once more that the slope of the S-N curve of the newly created weld joint was given as a result by *FEMFAT Weld*, however it was only read out from the weld database, see [Fig. 37], by the software, no calculation for the slope was needed.

Table 12: *FEMFAT Weld* fatigue assessment results for literature example with new weld

	$\Delta\sigma_{\mathrm{n}}$ [MPa]	N_{f} [cycles]	k
Mann, T., Fatigue testing results [31]	50.0	$1.769 \cdot 10^6$	4.6
	100.0	$7.158 \cdot 10^4$	
FEMFAT Weld, T-joint circumferential fillet weld	50.0	$1.582 \cdot 10^6$	4.6
	100.0	$6.317 \cdot 10^4$	

The resulting S-N curve for the new weld joint is shown in [Fig. 38] along with all three S-N curves from the earlier fatigue assessment. All of the curves represent the survival probability value of $P_{\mathrm{S}} = 50\%$, as stated in the diagram. Comparing the final results, it can easily be seen that the S-N curve of the new welded joint shows almost perfect matching with the curve from the literature example. Even though the slope matching wasn't in question, the calculated notch factors have given an amazing correlation in terms of cycle numbers for each of the load levels. In terms of fatigue critical point from which the crack will initiate, with using the newly defined weld joint *FEMFAT Weld* gave a correct and expected prediction i.e., for both load levels the critical point obtained from the results was the weld toe at the horizontal extruded profile.

Through this analysis it has been proven that the calculated notch factors for the weld toe give outstandingly good results compared with the experimental data. However, for the notch factors describing the weld root, not much can be said because for their validation, another experiment would need to be performed with a different loading setup, this time with the fatigue critical area being in the weld root. If this was to be done, after obtaining experimental data for both, weld toe and weld root, the final calibration would need to be conducted so that the weld joint data written in the weld database can give reliable results regardless of where the fatigue critical

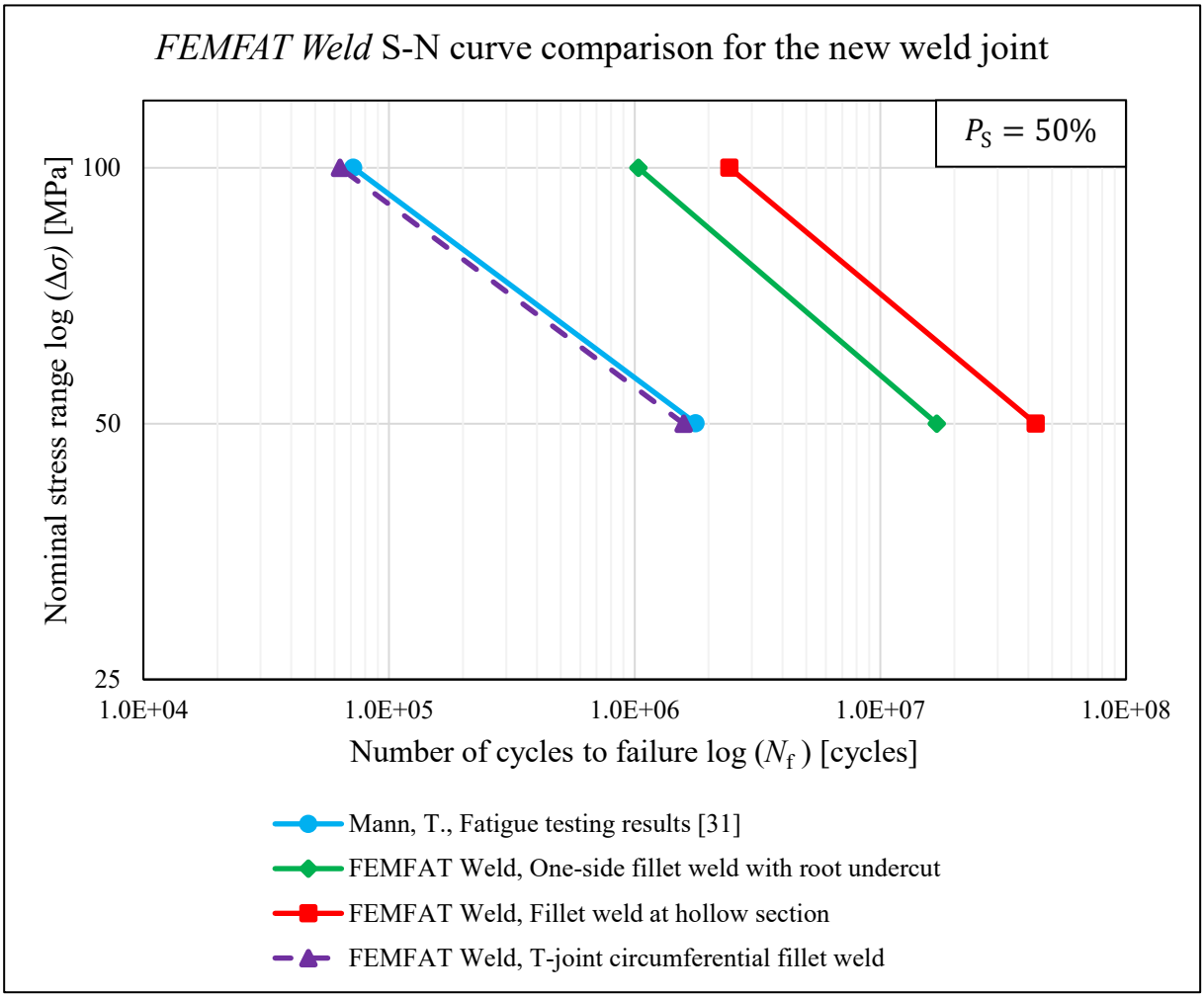

Figure 38: S-N curves for *FEMFAT Weld* fatigue assessment of the literature example using the new weld joint

point for crack initiation would be. The best-case scenario would be that the defined data gives reliable results with the first iteration for both, weld toe and weld root crack initiation examples. However, this would seldom be the case. So, final *FEMFAT* recommendation for extending the weld database is to conduct a calibration using only two parameters, notch factors and the slope.

By changing the values of notch factors, the S-N curve would shift from left to right, depending if the notch factors would be increased or decreased, see [Fig. 39 (a)]. On the other hand, changing the slope would change the number of cycles for the higher load level while the lower load level would remain at the same number of cycles to failure, as per [Fig. 39 (b)]. Maybe the simplest approach for calibration would be to calibrate the slope first and then by changing notch factors only shift the S-N curve in the desired direction.

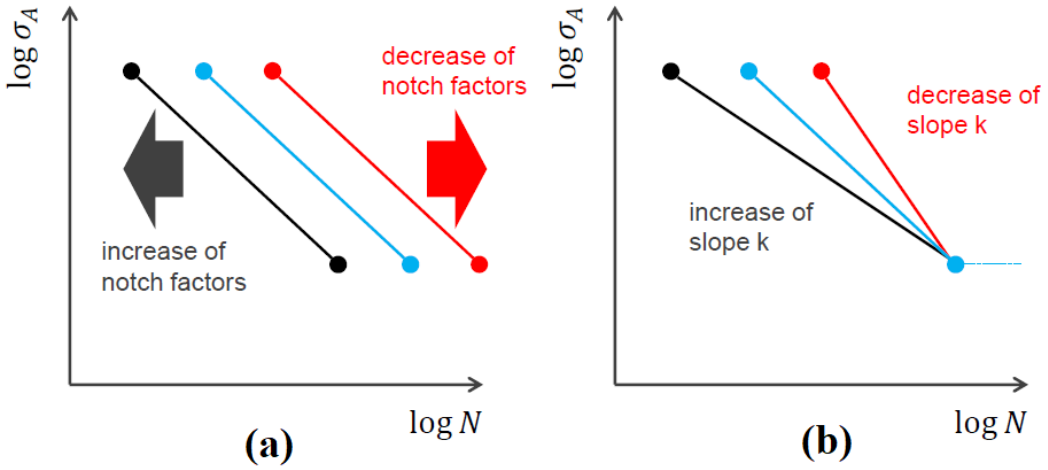

Figure 39: Effect on the S-N curve from [49] by changing: (a) notch factor values, (b) slope

The most important conclusion that can be drawn from this validation process is that extension of the weld database is a well-established process that could work properly if certain rules defined by *FEMFAT* are followed. Even with an example like this, where not all of the recommendations from *FEMFAT* could be followed, the resulting fatigue assessment showed almost perfect matching with the experimental data and provided the correct point of crack initiation in the results. Therefore, this validation process showed to be a great learning example for the successful use of the modelling guidelines in database extension. Regardless of the great results, it would be interesting to see how would notch factors between the three cross sections depicted in [Fig. 33] compare to each other if the 2D modelling approach for their calculation was applied to each of the shapes. Naturally, this would require further investigations that are not in the scope of this thesis. However, the method for calculating notch factors from a 2D detailed cross section of the weld will be applied in further chapters and compared with the results of high cycle fatigue tests that were conducted as a part of the investigation of *FEMFAT Weld*.

5 EXPERIMENTAL DATA AND RESULTS

After having successfully applied the weld database extension procedure proposed by *FEMFAT* to an example from the literature, a step further was taken in order to support the assumptions about the universal applicability of the *FEMFAT Weld* fatigue assessment stated in chapter 3. In order to substantiate these claims, high cycle fatigue testing of aluminum alloy welded specimens was conducted along with some additional experimental investigations including the microscopic measurements of the weld geometry for the purposes of weld database extension and hardness measurements of the different zones of the material around the weld.

All these investigations were conducted on two different type of specimens i.e., the butt joint and the T-joint welded joints, that were manufactured in cooperation with the Faculty of Mechanical Engineering and Naval Architecture at the University of Zagreb. For the geometry of the specimens, the limitations of the testing device were considered and in regard to the number of specimens needed for a meaningful high cycle fatigue testing, Technical Report ISO/TR 14345 [50] was used as a guideline. Hence, a total of 62 specimens were manufactured with more than half of them, 48 to be exact, predicted for the high cycle fatigue testing. As it was already mentioned, the main focus of this thesis is, in fact, the high cycle fatigue testing that was performed in cooperation with the AVL Material lab in Graz, Austria. For the testing procedures, geometry of the testing setups and planning, the ISO/TR 14345 [50] was consulted while for the statistical analysis of the high cycle fatigue testing the *Statistical Analysis of Fatigue Data* or SAFD tool, created by the university of Aachen in Germany, was used.

Through this chapter, the design and manufacturing of the specimens will be presented, as well as the testing program and corresponding results of each investigation that was performed. The results acquired from all these investigations, will later be used in the more detailed extension of the *FEMFAT* weld database.

5.1 Material data

In regard to the introduction in chapter 1 of this thesis, it was mentioned that various aluminum alloys are used throughout the automotive industry for all sorts of purposes. Generally speaking, aluminum alloys can be divided into two main categories, wrought, and cast alloys, with wrought alloys making up the vast majority of the market for the reason of their higher strength. Additionally, aluminum alloys can be divided into multiple different series depending on the main alloying element that is used. For example, 1xxx series is pure aluminum (99% or higher), in the 5xxx series magnesium is the principal alloying element, in 7xxx series it is zinc etc. Considering this classification, throughout many projects in AVL List GmbH, it has been noticed that many of the electrification related structural components, such as battery pack housings and integrated crash structures, see [Fig. 4], are often made of 6xxx series aluminum alloy. This series of aluminum alloys uses silicon and magnesium as the main alloying elements, which results in alloys that are formable, weldable and heat treatable. They also have good corrosion resistance and relatively high strength in comparison with other material series. Very often, this aluminum series is used for the production of extruded aluminum products which is also the reason why this series is interesting in regard to the topic of this thesis. As it was mentioned in chapter 1, battery pack housings and crash structures are mostly comprised of extruded aluminum profiles that are welded together. Hence, for the purposes of this thesis it has been chosen to use one of the aluminum alloys that is a part of the 6xxx series. It would be desirable to use the same alloy as in the literature example, however because of its unavailability at the time of material acquisition, a different alloy with the same application was chosen.

Considering all that has been said, extruded 6060-T66 aluminum alloy profile with rectangular hollow cross section (RHS) was acquired and used for the manufacturing of the test specimens. The geometry of the cross section is depicted in [Fig. 40], together with the manufacturing tolerances provided by the material manufacturer impol d.o.o. The wall thickness of $t = 3$ mm was chosen because thinner and thinner pieces of aluminum are being increasingly used in the manufacturing of already mentioned battery housings and other similar components. Due to the fact that this is a rather small wall thickness, it can also provide some conclusions in regard to the effects of welding on such thin aluminum components because standards and recommendations such as IIW [9] usually don't mention thicknesses below $t = 5$ mm. From [Fig. 40] it can also be seen that the chosen aluminum profile doesn't have curved edges which is certainly more beneficial for all the reasons described in chapter 4.5.

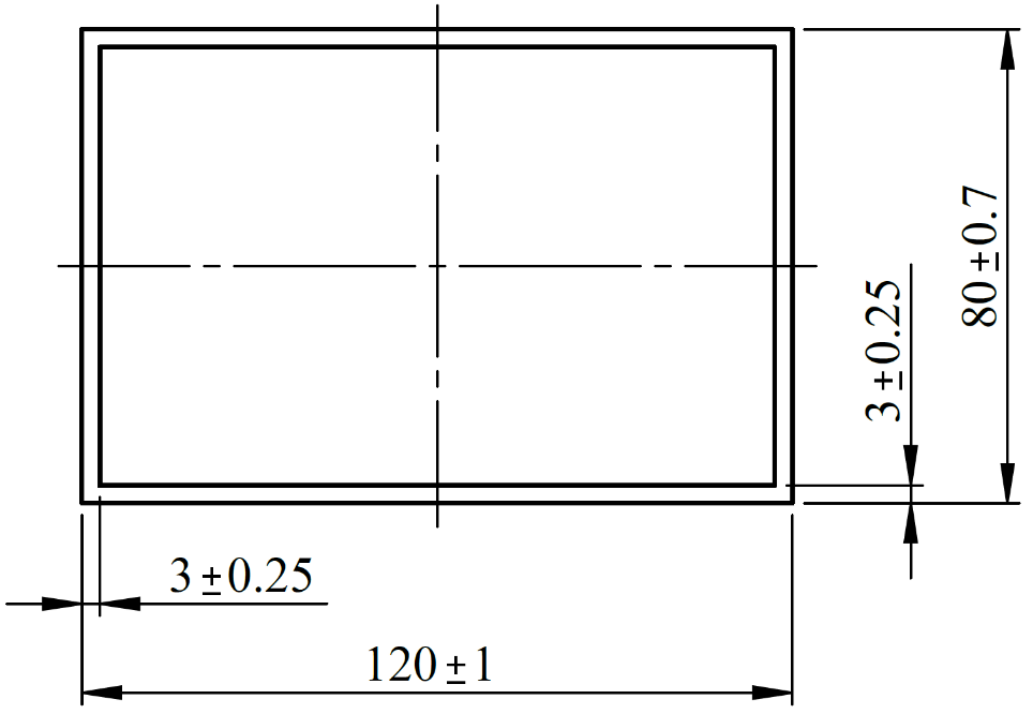

Figure 40: Extruded 6060-T66 aluminum alloy RHS profile acquired from impol d.o.o.

Basic mechanical properties of the material i.e., the ultimate tensile strength (UTS) R_m, yield strength $R_{p0.2}$ and elongation A are defined according to EN-755-2 and provided by impol d.o.o. as well as the chemical composition of the material defined according to EN-573-3. Both are given here in [Table 13] and [Table 14] respectively.

Table 13: Mechanical properties of extruded 6060-T66 RHS profile, from impol d.o.o.

R_m [MPa]	$R_{p0.2}$ [MPa]	A [%]
218.0	195.0	14.0

Table 14: Chemical composition of extruded 6060-T66 RHS profile, from impol d.o.o.

Si %	Fe %	Cu %	Mn %	Mg %	Cr %	Zn %	Cd %	Hg %	Pb %	Al %
0.45	0.21	0.01	0.02	0.50	0.01	0.02	0.001	0.001	0.01	rest

5.2 Test specimen manufacturing

The housing and the crash structure of the battery pack are often integrated together into one large, welded structure. However, the welding in such complicated structures hardly ever includes only one type of weld joint, and not only that but multiple different welds can often be connected with each other due to the complexity of the structure. Hence, it is hard to define one unique weld joint that could be considered for the sake of welding investigations applied to battery packs or similar structures. However, with performing the fatigue investigations for two relatively simple and commonly applied weld joints, the findings from such investigations could be much more beneficial for the appropriate fatigue assessment of more complex welded structures. Therefore, two weld joints were chosen for the experimental fatigue assessment, the first one being the one-sided butt joint I-seam weld and the second one the one-sided T-joint fillet weld. These two weld joints are basically fundamental welds used as a basis for many other types of weld joints that were derived from them. As they are quite common in various welded structures, including the mentioned battery packs, they can sure be a great benchmark for a successful fatigue assessment of more complex welded structures.

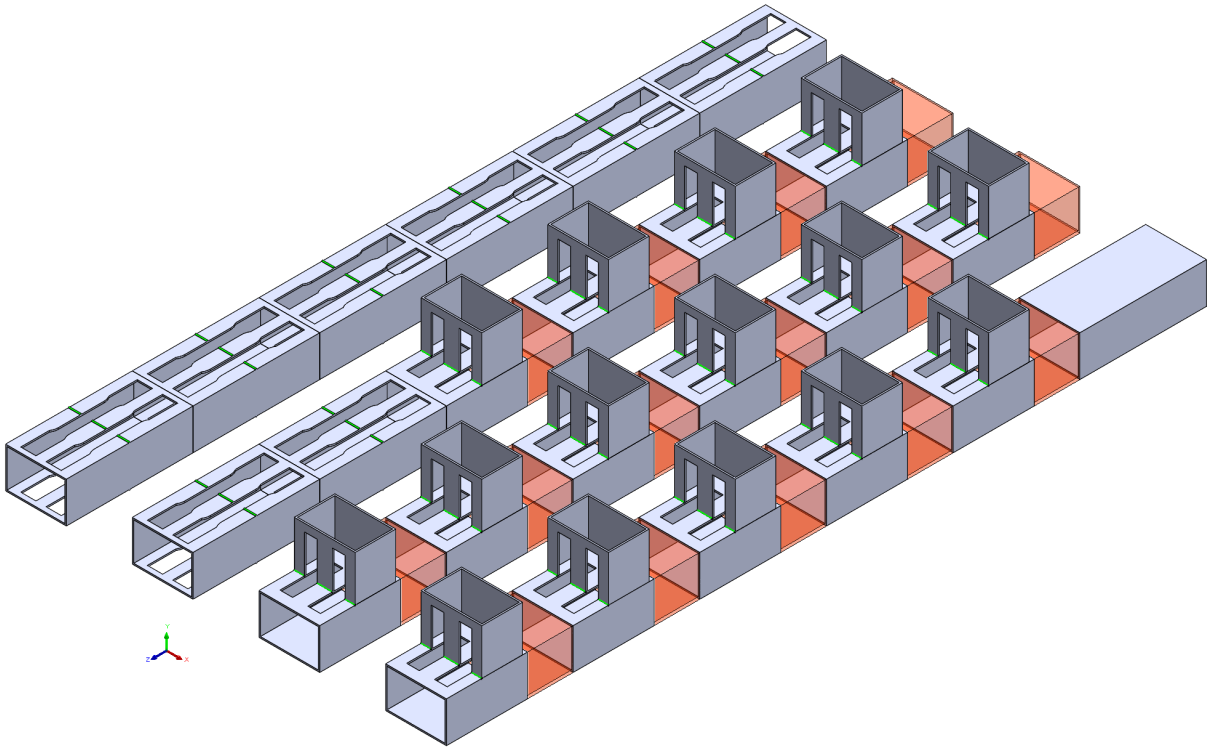

Figure 41: Manufacturing layout of the extruded 6060-T66 aluminum profiles

In order to investigate these weld joints, test specimens were manufactured from a total of 6000 mm of the ordered extruded 6060-T66 aluminum profile. The process of the manufacturing started with cutting the whole length of the ordered material into smaller sections. To be precise, a total of 24 equal sections, each 250 mm in length, with the entire layout of the material used for the manufacturing depicted in [Fig. 41]. Each section would then be additionally cut depending on the weld joint that is to be applied to that same section e.g., red transparent sections representing the sections welded for the T-joint specimens. Then, the section in question is subjected to the welding process and only after this is done, the final specimens were cut out from the extruded aluminum by using electrical discharge machining (EDM), also known as wire erosion. This cutting process was used because it is extremely precise with tolerances only in μm and the heat input during the process is minimized with equal current distribution and proper cooling. Thanks to such characteristic of EDM, the cutting process has no effect on the properties of the aluminum used for the specimen production.

From all of the sections created, as seen from [Fig. 41], one was left intact for the purposes of detailed material investigations of the extruded 6060-T66 aluminum which are not in the scope of this thesis.

5.2.1 Welding procedure and parameters

The idea was to conduct welding between extruded profiles while keeping their original shape in order to simplify the welding process and to ensure that the welding is done as uniformly as possible. Instead of welding each specimen individually, one weld seam along the extruded profile would provide two specimens after cutting which should be of more similar quality in the weld. Also, this way, the effects caused by the welding process, both the good and the bad, will be more evenly distributed through the material. The fact that the extruded aluminum with rectangular cross section was used for the welding will also provide better alignment of the finished specimens. For instance, if the profile was first cut into smaller plates and then welded, the whole process would be much more expensive, and the satisfactory level of weld equality would be much harder to achieve.

As it is one of the most common welding procedures, metal inert gas (MIG) welding also known as gas metal arc welding (GMAW), was chosen for the purposes of this thesis. The welding itself was performed by hand at the Department of welded structures within the Faculty of Mechanical Engineering and Naval Architecture (FAMENA) in Zagreb.

An example of the welding procedure for the butt joint specimen can be understood better with looking at [Fig. 42] where one of the mentioned sections that were cut from the overall length of the material, wasn't cut in half but a rather small cut through the thickness of the material in the middle of the section was made, perpendicular to the extruding direction of the material. With the section clamped in place, the cut was then welded back together resulting in the one-sided butt weld. The procedure was than repeated on the other side of the same section so multiple specimens could be cut from only one section.

Figure 42: Welding procedure for the one-sided butt joint I-seam weld

For the filler material, 4043 aluminum wire was used, with the basic mechanical properties' values for ultimate tensile strength R_{m}, yield strength $R_{\mathrm{p0.2}}$ and elongation A provided by the Department of welded structures at FAMENA given in [Table 15].

Table 15: Mechanical properties of 4043 aluminum filler wire provided by FAMENA

R_{m} [MPa]	$R_{\mathrm{p0.2}}$ [MPa]	A [%]
120.0	40.0	8.0

The chemical composition of the 4043 aluminum filler material was also provided by the same department at FAMENA, with the data presented here in [Table 16.].

Table 16: Chemical composition of 4043 aluminum filler wire provided by FAMENA

Si %	Fe %	Cu %	Mn %	Mg %	Zn %	Ti %	Al %
4.5 - 6.0	< 0.60	< 0.30	< 0.15	< 0.20	< 0.10	< 0.15	rest

Shielding gas used during the welding process was Argon 5.0, while the rest of the main welding parameters such as the electric current I, voltage V, welding speed v_{weld} and the shielding gas flow $q_{\text{v, gas}}$ are given in [Table 17.]

Table 17: Welding parameters

I [A]	V [U]	v_{weld} [cm/min]	$q_{\text{v, gas}}$ [l/min]
84	19.8	35	20

After the welding was conducted at each of the 23 sections of the extruded aluminum used for specimen manufacturing, see [Fig. 41], no additional treatments other than cleaning of the weld were applied i.e., all of the specimens were left in as-welded state. Reason for this is that in most real-life applications, weld joints used for such structures as battery pack or similar housings, won't go through any additional treatment as well.

5.2.2 Butt joint specimen geometry

As it was mentioned, multiple specimens can be cut out of each of the extruded sections presented in [Fig. 41]. Regarding the butt joint specimens, they are manufactured in two already described steps as seen in [Fig. 43]. First step implies the welding on each side of the extruded profile section, see green line in [Fig. 43 (a)], with the second step of cutting the defined geometry depicted in [Fig. 43 (b)]. The exact geometry and the isometric view of the final butt joint specimen can be seen in [Fig. 44 (a)] and [Fig. 44 (b)] respectively.

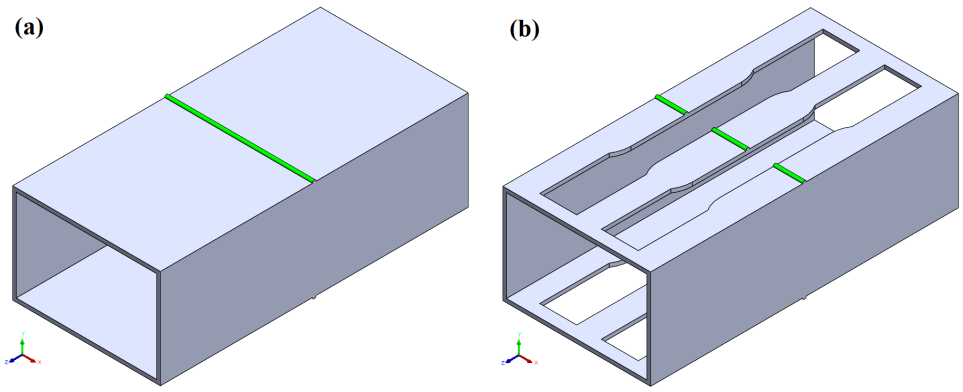

Figure 43: Butt joint specimen manufacturing steps: (a) MIG welding, (b) EDM cutting

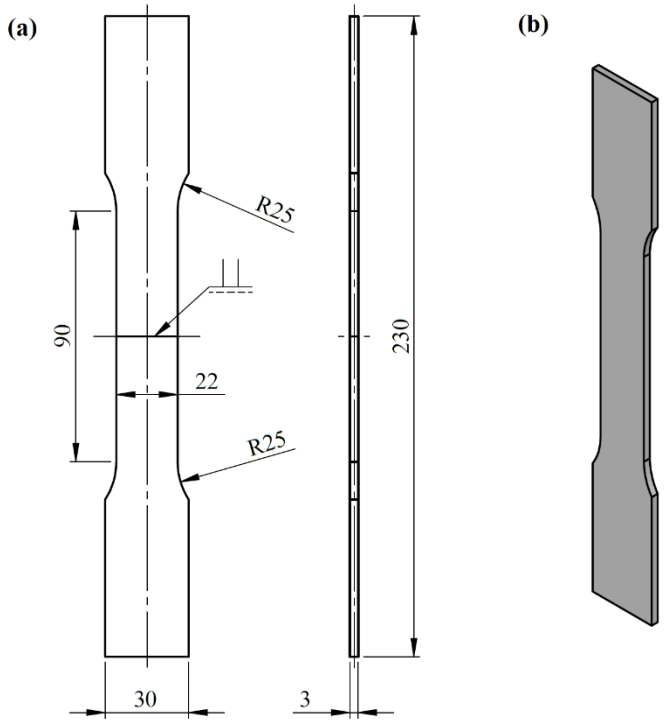

Figure 44: Butt joint welded specimen geometry: (a) technical drawing, (b) isometric view

5.2.3 T-joint specimen geometry

Similar to the butt joint specimen, the T-joint is also manufactured through two steps depicted in [Fig. 45]. First, the extruded profile section is cut into two pieces which are then welded together to form a 90° T-joint as it can be seen from [Fig. 45 (a)]. After that the welded section is subjected to the EDM procedure for cutting the final specimens. In [Fig. 46 (a)], T-joint specimen geometry is presented, with the isometric view of the specimen given in [Fig. 46 (b)].

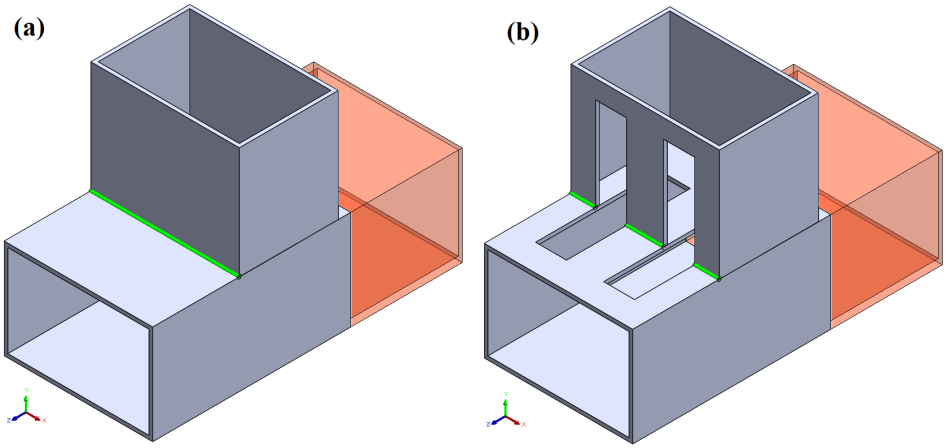

Figure 45: T-joint specimen manufacturing steps: (a) MIG welding, (b) EDM cutting

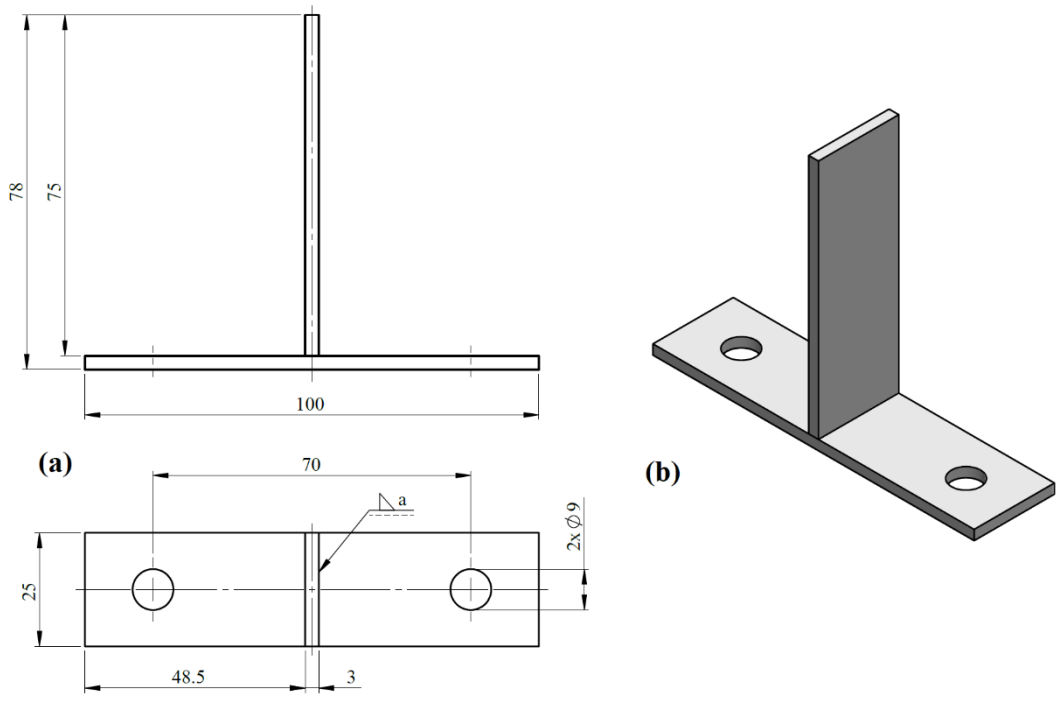

Figure 46: T-joint welded specimen geometry: (a) technical drawing, (b) isometric view

5.3 Pre-testing investigations

During the welding process, components are joined together by means of a large heat input which causes melting and consequent fusion of the materials being welded together. Considering the fact that an additional material is added to the structure through the welding process i.e., the welding material also known as the filler material, it is no surprise that significant changes can occur in the material around the weld.

Generally speaking, each weld joint can be divided in three different zones in regard to its metallurgical properties. The first one is of course the fusion zone, the exact area where the welding was performed and where two materials, base material, and filler wire, were joined together. The fusion zone is rather small in comparison with the second zone which is maybe the most important one and it was already mentioned in the chapter 2.1.3. The heat affected zone or HAZ for short, basically represents a transition area between the completely fused material and the unaffected base material of the welded structure which is also considered to be the third zone where no effects of the welding process can be observed. Size of the HAZ naturally depends on the heat input during the welding process but in any case, it will be present in the structure if no post weld heat treatment for the removal of HAZ is conducted. Although there is no exact way of measuring the size of the HAZ, there are some investigations that can be performed in order to approximately determine the size and position of the HAZ. Therefore, few of the specimens described in chapter 5.2, were randomly selected for the microscopic analysis to try, and see the change in the microstructure of the material which could indicate the boundary between the HAZ and the base material. Also, hardness measurements were conducted to see if there is any change in hardness around the weld as a consequence of the welding process, which could also indicate how large the HAZ really is.

Comparing the mechanical properties of the base material 6060-T66 with the filler material 4043, given in [Table 13] and [Table 15] respectively, a significant difference in strength can be spotted. For example, yield strength of the base material is more than twice the value of the same strength of the filler material. However, due to the heat input during the welding process and the change in the microstructure of the material, welds in general significantly improve the static strength of the welded structure. With this in mind, in static loading conditions, the HAZ will always be the most critical area for failure. Therefore, a few of the butt joint specimens were subjected to static tensile tests to see what is in fact the strength of the HAZ i.e., what is the strength drop between the base material and the HAZ.

5.3.1 Microscopic analysis of the microstructure around the weld

Two random specimens from each group of the weld joints manufactured for the purposes of this thesis were randomly chosen and microscopic analysis was performed. Unfortunately, even the microscopic images couldn't show the difference in microstructure of the base material and the heat affected zone, most probably because of the high purity of the 6060-T66 aluminum alloy, see [Table 14]. However, the boundary of the fusion zone i.e., the welding material, is visible even to the naked eye for both types of the weld specimens, butt joint in [Fig. 47] and T-joint in [Fig. 48].

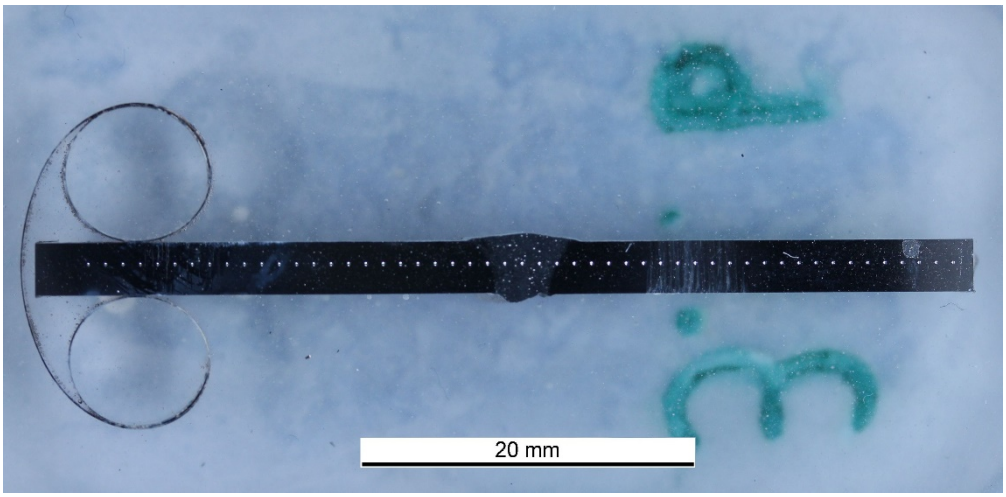

Figure 47: Butt joint specimen for microscopic analysis of the microstructure

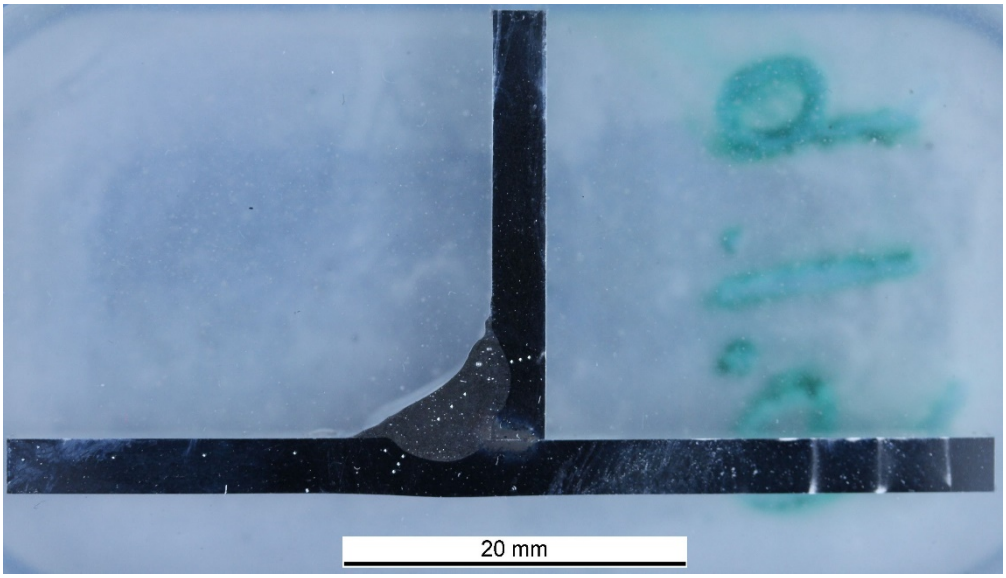

Figure 48: T-joint specimen for microscopic analysis of the microstructure

5.3.2 Hardness measurement

So, a clear difference can be seen between the weld material and the heat affected zone, however it seems that there is no visible boundary between the heat affected zone and the base material. Since the specimens were left in as-welded state after the welding was finished, the heat affected zone most certainly exists, but it can't be seen just from looking directly into the cross section of the specimen. Therefore, additional investigations were performed to find out more about the location of the heat affected zone, first of them being the hardness measurement.

For the hardness measurement the Vickers hardness test was applied to cross sections of the welded specimens. A total of three measurements were conducted i.e., three specimens were tested, with the hardness scale of HV1 and dwell time of 10 s used for each of them. The HV1 hardness scale means that each measurement point was loaded with a force of 9.807 N in order to determine the value for the hardness.

As the main goal of the measurements was to prove that the heat affected zone exists, first measurements were done at two butt joint specimens. Reason for that is the simple and straight shape of the specimen, which makes it is easy to measure hardness at large number of points along the same line in order to cover a wide area around the weld itself. Exactly that was done,

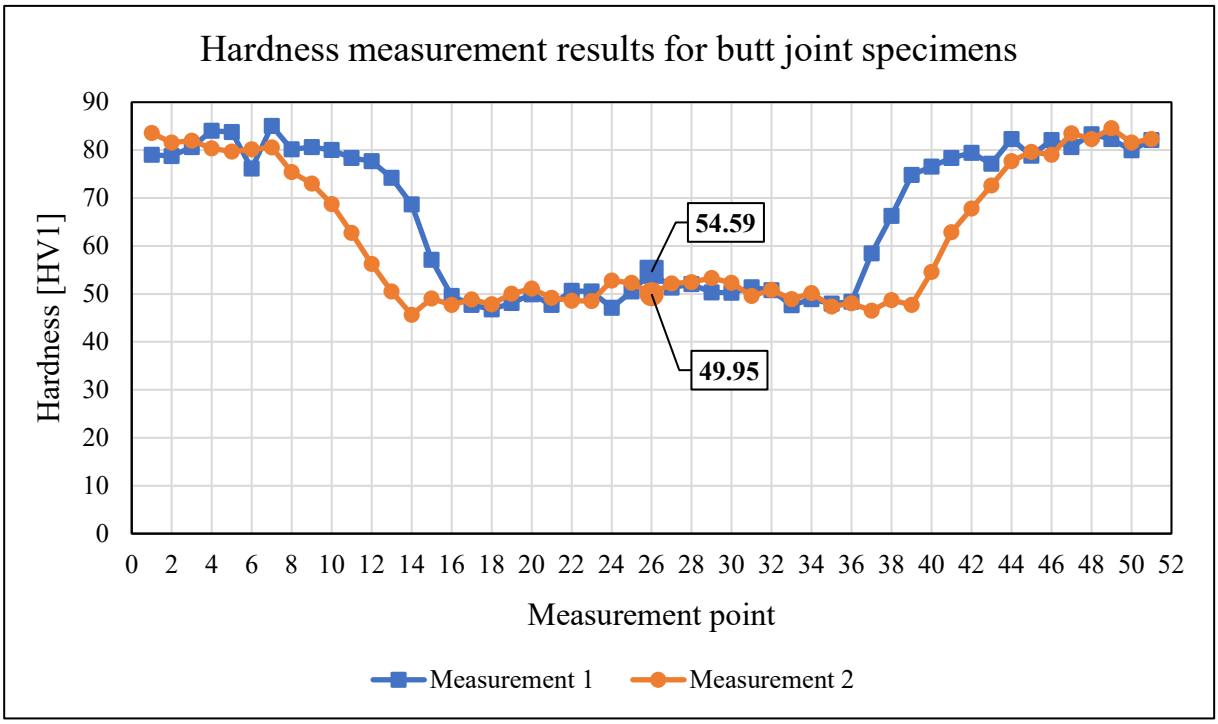

Figure 49: Hardness measurements diagram for the butt joint specimens

a total of 51 measurement points were assessed with 1 mm distance between each of them which covers an area 50 mm wide. One of the hardness tested butt joint specimens can be seen in [Fig. 47] with all of the indentations caused by the pyramidal indenter clearly visible. The results for these two measurements are given in [Fig. 49] from which it can be immediately seen that there is a visible difference in hardness between the middle of the assessed area and the ends of the same area. The measurement point number 26 marks the middle of the weld in both measurements and the exact hardness value at that spot is shown in the diagram for both specimens at [Fig. 49]. Considering the distances between the measurement points and possible variations in weld quality among all of the specimens that were manufactured, a conclusion can be made that the HAZ covers an area that is around 20 mm wide i.e., 10 mm from each side of the weld. This basically divides the specimen into two areas, in regard to hardness, with the first area including the weld and the HAZ, and the second one including only the base material. The mean, minimum and maximum hardness values for each of the two areas that can be differentiated by this analysis are given in [Table 18]. The measurement points at the transition from the base material to the HAZ are disregarded for this calculation. Therefore, for each zone listed in [Table 18], a range of the assessment points used for the calculation is given. From both, [Table 18] and [Fig. 49], it can be seen that in the first area the value for hardness gravitates around 50HV1 which indicates that no difference in hardness exists between the weld and the HAZ. However, in the far ends of the measurement area, which include the base material without welding effects, the value is moving around 80HV1 and the transition between these two values clearly marks the boundary of the HAZ area. Comparison of the results for both measurements leads to a conclusion that both specimens show similar hardness values at the same areas around the weld, which can be argued as valid for other specimens as well.

Table 18: Mean, min. and max. HV1 values for different zones in butt joint specimens

Butt joint	Material zone (assessed points)	Mean	Min.	Max.
Measurement 1 [HV1]	Weld and HAZ (16-36)	49.63	46.78	54.59
	Base material (1-10, 40-51)	80.51	76.13	85.05
Measurement 2 [HV1]	Weld and HAZ (13-39)	49.64	45.66	53.30
	Base material (1-7, 44-51)	81.23	77.68	84.54

In order to corroborate the conclusions reached with the first two specimens, one T-joint specimen that can be seen in [Fig. 48] was also subjected to the same hardness measurement with the results given in [Fig. 50]. A total of 9 measurement points was assessed, with points 4, 5 and 6 being directly in the weld and the rest positioned across the wall thickness of the specimen. Looking at the results in [Fig. 50] it is easy to see that no difference in hardness exists and in regard to the results acquired from butt joint specimens, the only explanation for this must be that the HAZ in T-joint specimens covers the whole corner area of the joint including the whole thickness of the material. As it was for the butt joint specimens, in [Table 19] certain values for hardness of the T-joint specimen are presented. If compared to the data in [Table 18] it can be seen that values do not differ significantly which means that the hardness of the weld and the HAZ stays the same for this material combination, regardless of the specimen geometry.

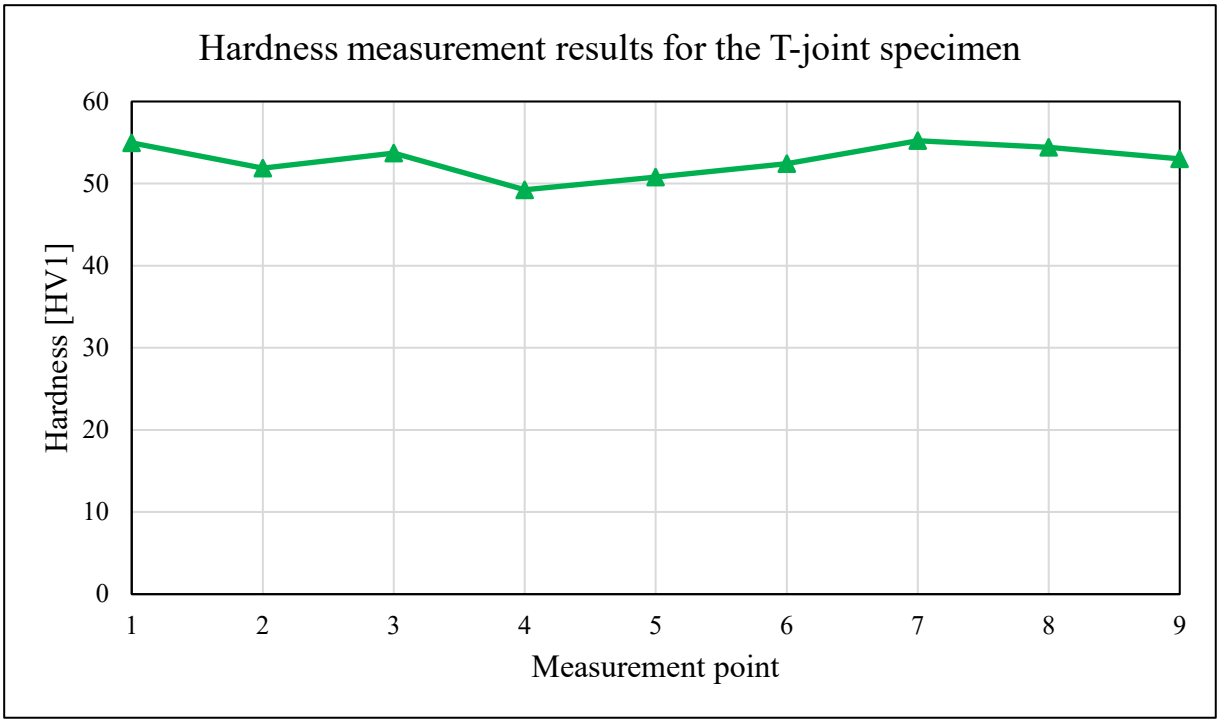

Figure 50: Hardness measurements diagram for the T-joint specimen

Table 19: Mean, min. and max. HV1 values for different zones in the T-joint specimen

T-joint	Material zone (assessed points)	Mean	Min.	Max.
[HV1]	Weld and HAZ (16-36)	52.85	49.25	55.22

5.3.3 Static tensile tests of the butt joint specimens

Similar conclusion to the one from the hardness measurements was obtained through the static tensile tests of butt joint specimens. In total three specimens were subjected to this type of test and all of them failed at the same spot i.e., at the transition between the base material and HAZ, see [Fig. 51], which was approximately 20 mm wide. This type of failure was expected because the HAZ is in fact the weakest point of the welded structure when static loadings are in question. The results acquired from these tests are given in [Table 20] and were very helpful with the allowable load determination for the HCF tests that were conducted next.

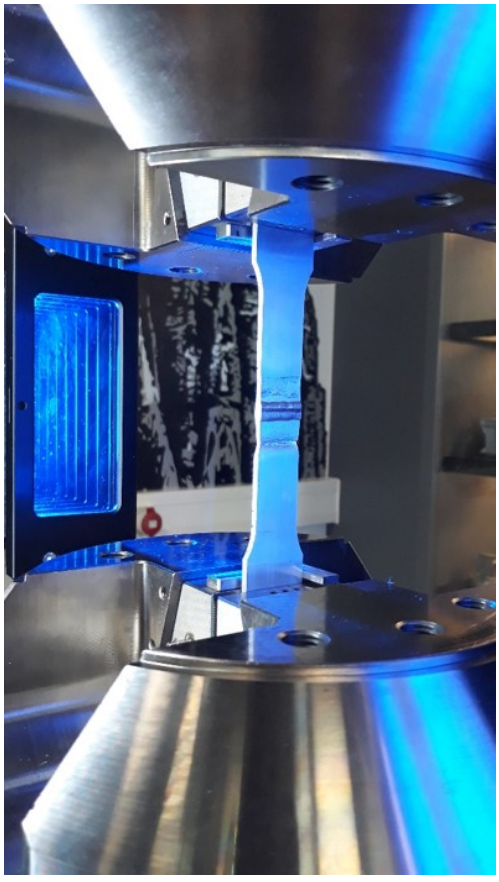

Figure 51: Butt joint specimen subjected to the static tensile test

Table 20: Mechanical properties of the HAZ in the butt joint specimen

R_{m} [MPa]	$R_{\mathrm{p0.2}}$ [MPa]
129.0	87.0

5.3.4 Microscopic measurements of the weld geometry

Throughout this thesis, it was mentioned more than once that the procedure for the extension of the weld database in *FEMFAT* recommends the use of a detailed 2D model of the weld geometry for the calculation of the notch factors for each weld joint that is to be added into the database. Therefore, in order to apply this procedure to the welded joints manufactured for the purposes of this thesis and introduced in the chapter 5.2, microscopic measurements were conducted on both types of specimens, butt joint and T-joint. Measurements acquired through this procedure were then used for the creation of the detailed 2D model which will be used later on for the calibration of the notch factors for each of the welded joints.

5.3.4.1 Butt joint specimen microscope measurements

From all of the specimens manufactured for the purposes of various investigations presented in this chapter, a total of two butt joint specimens were taken for the microscopic measurement of the weld geometry. As per [Fig. 44], each butt joint weld is 22 mm wide so in order to get more data, each of the two randomly chosen specimens was cut into different sections so that a total of four different measurements of the cross-sectional weld geometry could be conducted.

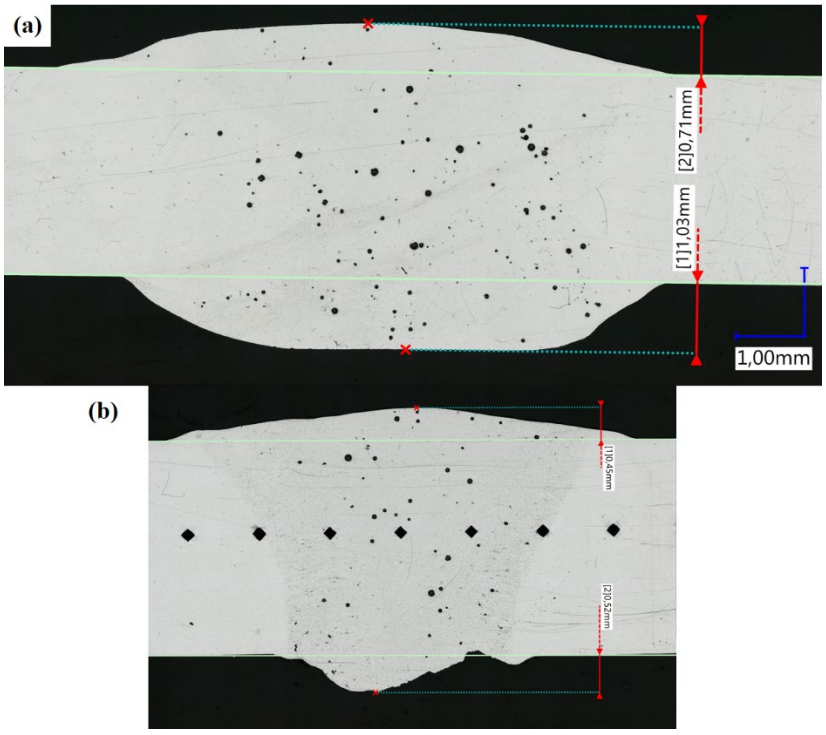

Figure 52: Microscopic measurements of the butt joint weld: (a) good quality, (b) bad quality

An example of two microscopic images obtained from such measurements is given in [Fig. 52]. As it was expected, a great deal of differences in the geometry could be found even in just the four measurements conducted here. This can be seen by simply comparing the two butt joint specimens given in [Fig. 52 (a)] and [Fig. 52 (b)] respectively. The former shows a weld of pretty good quality with a sufficient amount of weld material, but the latter is of such a bad quality that no useful data for the representation of the whole group of specimens could be acquired from the microscopic images. Therefore, the two measurements obtained from that same specimen were disregarded. The values obtained from the other two measurements conducted at the specimen of good weld quality, see [Fig. 52 (a)], were used for the definition of the detailed 2D model of the butt joint depicted in [Fig. 53]. From looking at the cross section of the valid specimen, the conclusion can be made that butt joint specimens differ a great deal in regard to the side of the specimen. The welding was conducted only from one side, because given the small thickness of the material welding from both sides is really not necessary, which makes the weld on that side much smoother, a little bit wider and it can be described with only one curve through the width L and height H of the top extrusion of the weld, see [Fig. 53]. On the other hand, the bottom side of the specimen has a larger height of the extrusion h and after a curved shaped protrusion from the base material, the surface flattens and needs to be described with an additional radius R and the height r_c at which the curvature of the surface changes.

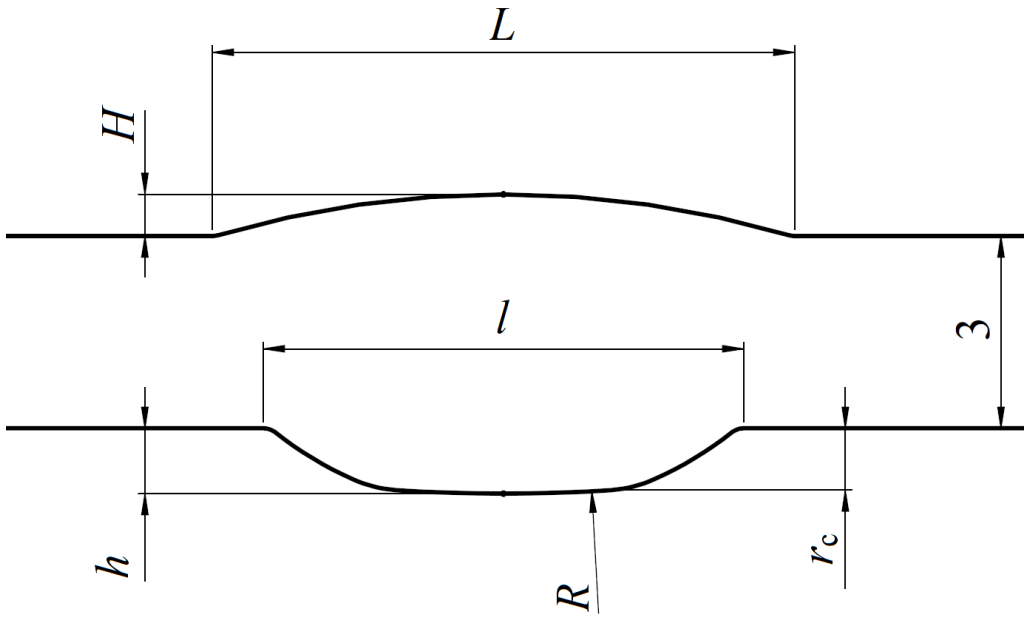

Figure 53: Sketch of the final butt joint weld geometry in the 2D detailed model

The measured values for the two good cross sections are given in [Table 21] along with their average values which were used for the exact weld geometry in the detailed 2D model. The radius of the weld toe at each side of the specimen is not given here because the analysis showed that it differs a lot. For example, weld toe radius at the bottom of the specimen varies from 0.2 to 1 mm, while the radius on the top side varies all the way from 0.5 to 3 mm. When the notch effect of the shape is considered, it makes sense that the top surface with a smaller notch effect has a larger weld toe radius and vice versa. All in all, the weld toe radius will be approximated when modelling the 2D detailed weld geometry according to recommendations by *FEMFAT*.

Table 21: Measurements of the butt joint weld geometry used for the 2D detailed model

	L [mm]	l [mm]	H [mm]	h [mm]	R [mm]	r_c [mm]
Measurement 1	8.76	6.25	0.58	1.00	14.7	0.90
Measurement 2	9.10	7.90	0.72	1.05	23.9	0.96
Average	8.93	7.08	0.65	1.03	19.3	0.93

5.3.4.2 T-joint specimen microscope measurements

The same procedure described already for the microscope measurements of the butt joint specimens was applied to randomly selected T-joint specimens. In this case, also two specimens were selected and cut into four different cross sections that were subjected to the microscopic imaging. Interestingly enough, as it can be seen from [Fig. 54], one of the chosen specimens was again of poor weld quality in comparison with the other one. The specimen depicted in [Fig. 54 (a)] shows very good penetration in both, the vertical and the horizontal plate of the joint, while the specimen in [Fig. 54 (b)] barely has any penetration of the weld material into the base plates. For this reason, the two measurements from the second presented specimen were disregarded. In order to define the sketch of the 2D detailed weld geometry of the T-joint specimens given in [Fig. 55], the measurements obtained from the two cross sections of the good quality specimen were used. More detailed examination of the valid specimen depicted in [Fig. 54 (a)], showed that the middle of the fillet weld took on a convex shape. This is most probably a consequence of the softness of the material during the cooling process after the welding. Another interesting characteristic is the so-called cold lap at the each of the two welds

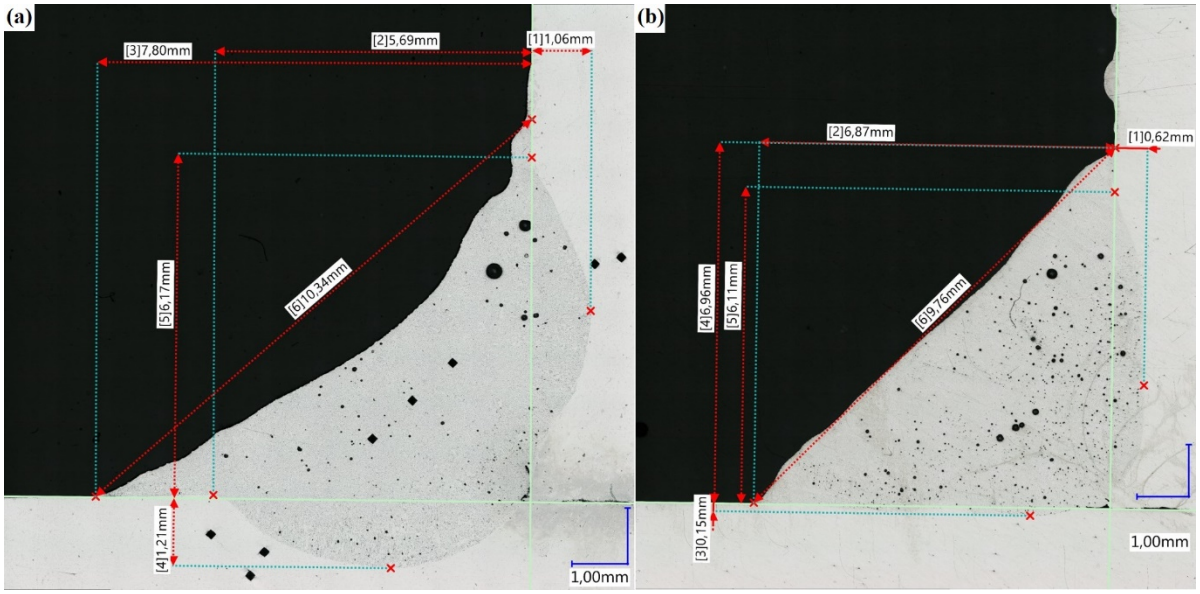

Figure 54: Microscopic measurements of the T-joint weld: (a) good quality, (b) bad quality

toes that exist in a fillet weld. Cold lap represents the area where no fusion between the base material and the weld material happened and it is a common occurrence in such welded joints. Even though cold lap is an area with no real fusion between the materials, it needed to be included into the measurements because exactly this cold lap is what gives the fillet weld its characteristic triangular shape. Basically, the fillet weld of the T-joint specimen group can be described with two main dimensions, width *L* and the height *H* but in order to include the shape

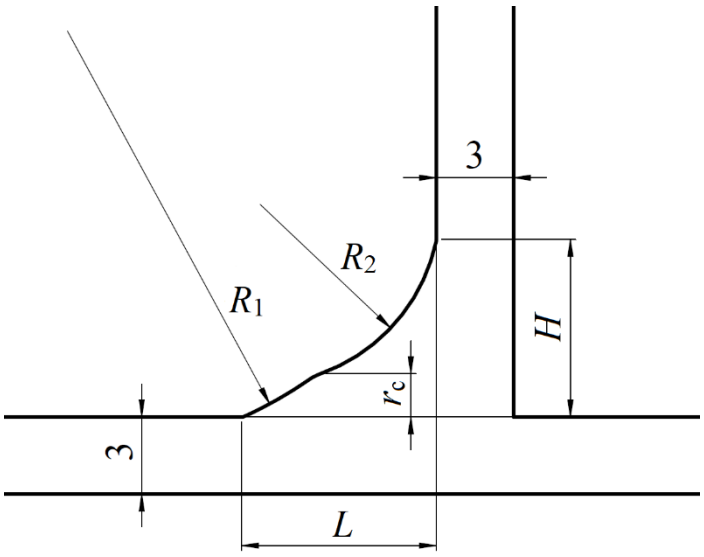

Figure 55: Sketch of the final T-joint weld geometry in the 2D detailed model

of the convex recess in the middle of the weld, additional values for two radiuses R_1, R_2 and the height where they change r_c need to be included. The measured values for the two good cross sections are given in [Table 22] along with their average values which were used for the exact weld geometry in the detailed 2D model.

Table 22: Measurements of the T-joint weld geometry used for the 2D detailed model

	L [mm]	H [mm]	r_c [mm]	R_1 [mm]	R_2 [mm]
Measurement 1	7.22	6.96	1.40	16.00	6.00
Measurement 2	7.80	6.79	1.80	17.00	8.00
Average	7.51	6.87	1.60	16.50	7.00

Regarding the weld toe radius, variations exist in the T-joint weld geometry as well, but they are far less pronounced than that is the case with the butt joint weld geometry. General measurements of the weld toe radius showed variations between 0.3 and 1 mm which is a rather small range to cover but as in the case of butt joint welded specimens, because of the radius variation and the fact that the radius will be assumed according to certain recommendations, the values for the weld toe radius aren't given here.

5.4 High cycle fatigue (HCF) testing

Since welded structures do not represent the best solutions for static loading conditions as it was mentioned in the chapter 5.3.3, it is more interesting, and it makes much more sense, in regard to their application, to investigate their behavior during the dynamic loading conditions as they are always susceptible to fatigue failure caused by various types of notches at the welded structures.

Even though various different experimental investigations were conducted as it has already been shown through the chapter 5, the main focus of the experimental investigations conducted as a part of this thesis was on the high cycle fatigue testing, or HCF for short. It was already mentioned that in order for the weld database used by *FEMFAT Weld* to be extended using the procedure described in chapter 3 and chapter 4, a sufficient amount of data needed to be obtained. From everything said so far about the database extension procedure, it can be concluded that there are two main sets of data that are necessary for each weld joint to be created, notch factors, and local S-N curve data i.e., slope and endurance cycle limit. Furthermore, such a set of data is needed for both weld toe and weld root individually since they can behave quite differently in regard to fatigue life of the welded structure that is being analyzed.

In order to obtain the needed data, a total of 48 specimens were provided for HCF testing, with 24 of the butt joint specimens and the same number of the T-joint welded specimens. Since the location of the failure, being at the weld toe or at the weld root, depends on the loading setup, each group of the specimens was additionally divided into two sets of 12 specimens. This way it was possible to use each set of 12 for a different setup in order to induce the fatigue failure at a different location. For the T-joint specimens, the fatigue failure can occur in the weld root or at the weld toe, so tensile and 3-point bending HCF tests respectively, were used for obtaining the results. In the case of the butt-joint specimen there is no weld root, however because of the asymmetry of the specimens, two different weld toes can be investigated depending on the side of the specimen that is being analyzed, so tensile and 3-point bending HCF tests were applied to the butt joint specimens as well. Before deciding on the 3-point bending setup, the 4-point bending was considered, however due to small distortion of some specimens as a consequence of welding, it wasn't possible to achieve contact in all four points at the same time so that approach was abandoned. For each of the four setups, a separate S-N curve could be created from which all the necessary data for the *FEMFAT Weld* database extension can be acquired.

The number of specimens chosen for the creation of the corresponding S-N curves was determined according to the ISO/TR 14345 [50] which states that in order to create an S-N curve from test results, a minimum of 8 to 10 tests are needed with two or more tests at each stress level. In respect to the ISO/TR 14345 [50], multiple different load levels were used for each set of twelve specimens, and the testing was performed with the aim of having as many tests as possible at each load level. The testing procedure was conducted in a way that after each test would finish, according to the result it would be decided if it is necessary to change the load level or additional tests at the same load level would be beneficial. All of the specimens were tested with the pulsating stress ratio of $R = 0.1$, but the results have been plotted in force range ΔF versus number of cycles to failure N_f. Reason for this is that the stress range $\Delta\sigma$ or the stress amplitude σ_a would be quite simple to calculate for the butt joint specimen geometry, but in the case of the T-joint it would be harder to determine the exact stress amplitude in the cross section of the weld because of the specimen geometry. Therefore, it was decided to plot the curves using the force-based values rather than stress-based values, so that a certain consistency exist through all four S-N curve diagrams that will be obtained.

Regarding the testing itself, both types of the manufactured welded specimens were subjected to HCF testing which was conducted in the AVL Material lab in Graz using the Zwick-Roell HC25 servo hydraulic testing machine. The aim of the test was to investigate the finite life of the specimens, so the runout limit was set to 5,000,000 cycles rather than the usual double value. The criterion for stopping the test was the crack initiation point in fatigue life of the specimens, ensured with a small value of elongation that must be exceeded in order to stop the tests. If such a value is not met, and the test continues even though the crack already initiated, through the postprocessing of the plotted elongation versus cycle number from the device, it is

Table 23: Mode 1 frequencies for each HCF loading setup

Specimen type	HCF loading setup	Mode 1 frequency [Hz]
Butt joint specimen	tension	324.93
	3-point bending	392.54
T-joint specimen	tension	2352.8
	3-point bending	706.68

possible to see when the crack initiated. The maximum achievable testing frequency of the device used for the tests is $f = 100$ Hz. In order to avoid any possible resonances, some modal simulations for the purpose of finding the mode 1 frequency were conducted using *Abaqus 2019.HF4* with the results given in [Table 23] from which it can be clearly seen that no concern about resonances needs to be raised.

The statistical analysis of the results obtained for each of the four different setups was conducted using the SAFD tool which provides the S-N curves for three different survival probabilities $P_S = 10\%$, $P_S = 50\%$ and $P_S = 90\%$. However, the important thing to note is that this tool doesn't plot the survival probabilities but rather failure probabilities so what is considered to be 10% failure probability line in SAFD is in fact the 90% survival probability curve in *FEMFAT* and testing results. The curves are calculated from the input data which includes the force range ΔF applied in the test and the number of cycles to failure N_f, both values provided for each of the 12 specimens tested with the corresponding setup. The curves are presented in the SAFD tool via the following equation:

$$\log N_f = a + k \cdot \log \Delta F \,, \tag{30}$$

which can be transformed into the expression for exact calculation of the number of cycles N_f, from the applied force range ΔF as follows:

$$N_f = 10^a \cdot \Delta F^k \,, \tag{31}$$

where k is the slope of the corresponding S-N curve and a the exponent value of the equation. Since the SAFD tool doesn't provide the value for the range of dispersion $T_{10/90}$, it must be calculated as a ratio between force range for 10% survival probability $\Delta F_{P_S=10\%}$ and force range for 90% survival probability $\Delta F_{P_S=90\%}$ with the following equation:

$$T_{10/90} = \frac{\Delta F_{P_S=10\%}}{\Delta F_{P_S=90\%}}, \tag{32}$$

with the already calculated stress ranges $\Delta F_{P_S=10\%}$ and $\Delta F_{P_S=90\%}$ from equation (31) for the same, arbitrary chosen, number of cycles to failure N_f.

Through this chapter, all four of the used setups will be presented along with the final testing results for each of them. Also, the calculations of the number of cycles N_f for each of the three survival probability lines and the corresponding range of dispersion $T_{10/90}$ will be presented.

5.4.1 Butt joint specimen – tension

For the first set of fatigue tests, the simplest test from the four planned was chosen, that being the tension loading of the butt joint specimen. Since the geometry of the butt joint specimen was modeled according to the standard tensile specimen dimensions, the first testing setup was quite simple to prepare, see [Fig. 56]. The setup consists of two clamping points with the lower one being fixed and the upper one performing the cyclic loading of the butt joint specimen. A sketch of the setup is given in [Fig. 56 (a)] where it can be seen that the length of the clamping is 30 mm, while [Fig. 56 (b)] shows the specimen in the device during the test. Since the geometry of the weld isn't symmetrical, it can be said that the specimens have two different sides, with the top side being the one from which the welding was conducted, see [Fig. 56].

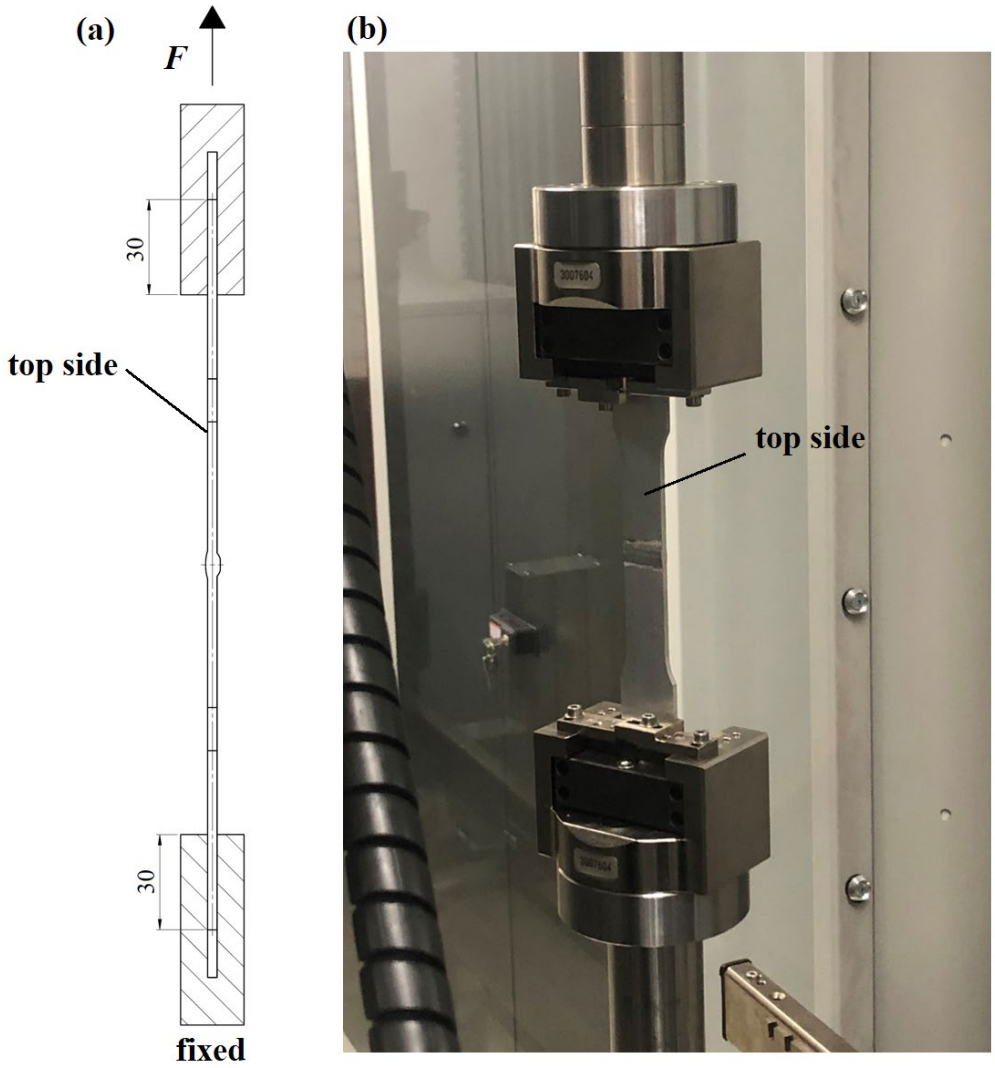

Figure 56: Butt joint specimen HCF tension: (a) testing setup, (b) specimen in the device

In respect to the ISO/TR 14345 [50], a total of four different load levels were used for the twelve specimens that were tested with this setup, each of them but one having at least two successful test results. Since the aim was to investigate the finite fatigue life, after the first load level with $\Delta F = 4158$ N had finished the test as a runout, no more specimens were tested at this load level. All of the results together with the applied load levels are given in [Table 24] which shows that all tests were conducted at the frequency of $f = 40$ Hz with the stress ratio of $R = 0.1$.

Table 24: HCF tension testing results for the butt joint specimen

Specimen ID	$F_{\min}$ [N]	$F_{\max}$ [N]	ΔF [N]	R	f [Hz]	N_f [cycles]
1.1	462	4620	4158	0.1	40	5,000,000
1.2	660	6600	5940	0.1	40	436,247
1.3	660	6600	5940	0.1	40	2,454,934
1.4	660	6600	5940	0.1	40	2,755,731
1.5	660	6600	5940	0.1	40	671,277
1.6	660	6600	5940	0.1	40	318,539
1.7	792	7920	7128	0.1	40	152,488
1.8	792	7920	7128	0.1	40	398,615
1.9	792	7920	7128	0.1	40	306,325
1.10	792	7920	7128	0.1	40	258,009
1.11	594	5940	5346	0.1	40	1,295,534
1.12	594	5940	5346	0.1	40	3,516,243

As it was expected from this test, all of the specimens, except the 1.1 which was a runout, had a failure i.e., crack initiation point, at the weld toe of the bottom side of the butt joint weld. Since the welding was performed only from one side, rather than both sides which is usually the case with butt welds, the geometry of the weld isn't symmetrical. The top side from which the welding was conducted is much smoother while the bottom side has a larger extrusion of the weld material, hence the notch effect at the bottom side is also larger. Therefore, for the simple tensile pulsating load, the bottom side weld toe is the crack initiation point.

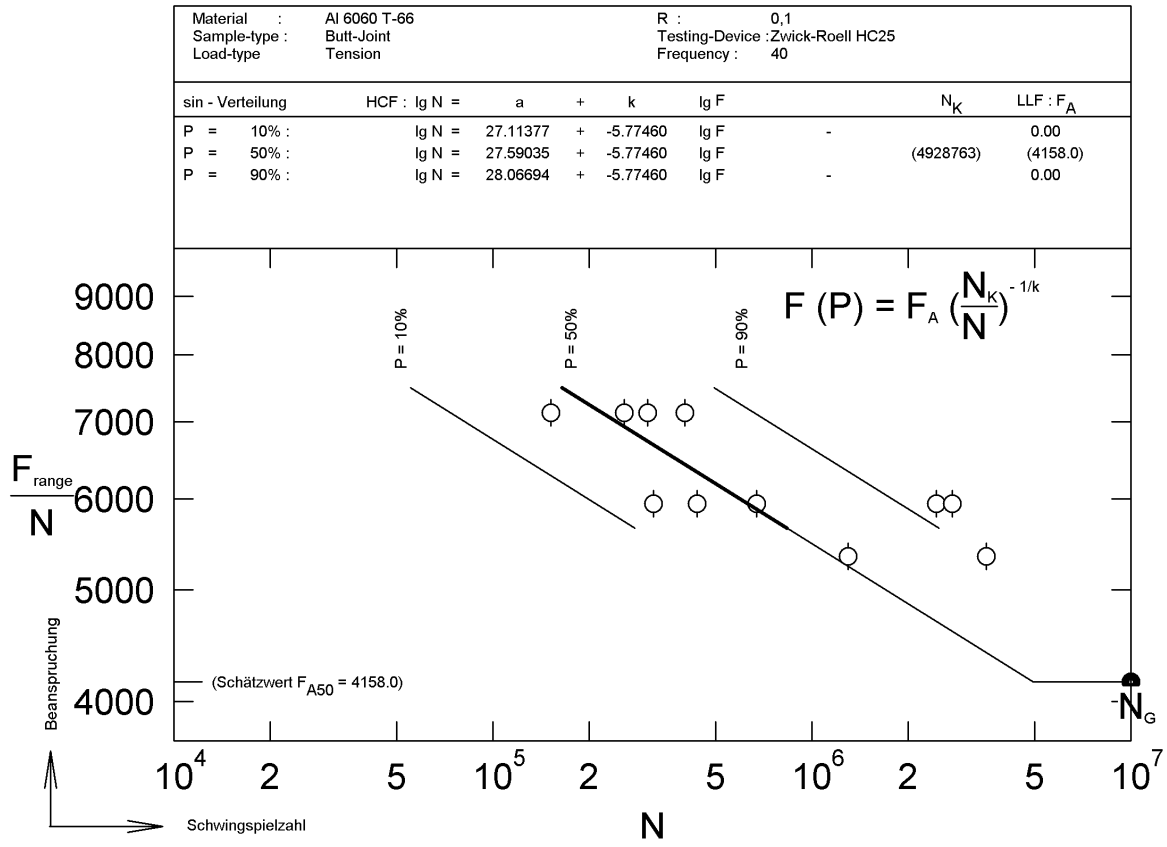

Figure 57: HCF tension testing S-N curves for the butt joint specimen from SAFD

The statistical analysis of the results presented in [Table 24] was conducted using the SAFD tool and the resulting S-N curves are given in [Fig. 57] with the slope of $k = 5.8$. Using the equation (31) along with the data for a and k from [Fig. 57], values for the number of cycles N_f depending on the load levels and survival probability P_S are calculated and given in [Table 25].

Table 25: N_f values depending on P_S and ΔF, for the tension tested butt joint

N_f [cycles]		$\Delta F = 4158$ N	$\Delta F = 5346$ N	$\Delta F = 5940$ N	$\Delta F = 7128$ N
P_S	90%	$1.64 \cdot 10^6$	$3.85 \cdot 10^5$	$2.1 \cdot 10^5$	$7.32 \cdot 10^4$
	50%	$4.93 \cdot 10^6$	$1.15 \cdot 10^6$	$6.28 \cdot 10^5$	$2.19 \cdot 10^5$
	10%	$1.48 \cdot 10^7$	$3.46 \cdot 10^6$	$1.88 \cdot 10^6$	$6.57 \cdot 10^5$

Using the values from [Table 25] and the equation (32), the range of dispersion for the butt joint specimens in HCF tension testing can be calculated i.e., $T_{10/90} = 1.46$.

5.4.2 Butt joint – 3-point bending

The 3-point bending setup for the butt joint specimens was prepared as depicted in [Fig. 58]. Three steel pins with the mutual distance of 20 mm, were arranged in such a way that the bottom loading pin pushes the specimen from the bottom side. Also, the specimen needs to be positioned in a way that the loading pin lies below the weld toe of the top side, with the center of the pin at least 1 mm away from the top side weld toe radius, see [Fig. 58 (a)]. This distance can't be measured during the test, so it is taken as an approximation that should be obeyed as much as possible. Since the first setup with tensile loading resulted in the failure at the weld toe of the bottom side, the aim of this setup was to induce the crack initiation at the weld toe of the top side of the specimen because the bottom side is being compressed during testing which won't result in crack initiation. Specimen mounted into the device is depicted in [Fig. 58 (b)], where it can be seen that the setup is reversed in regard to the [Fig. 58 (a)], because only the upper arm of the machine can be loaded. So, from the perspective of the machine the specimen is being compressed but with the right specimen orientation, the wanted setup can be achieved. Also, a small bending deformation can be noticed due to the nature of the setup, but it didn't show any significant influence on the final results. It was impossible to avoid this effect since the geometry of the specimen is not suitable for any real-life bending applications.

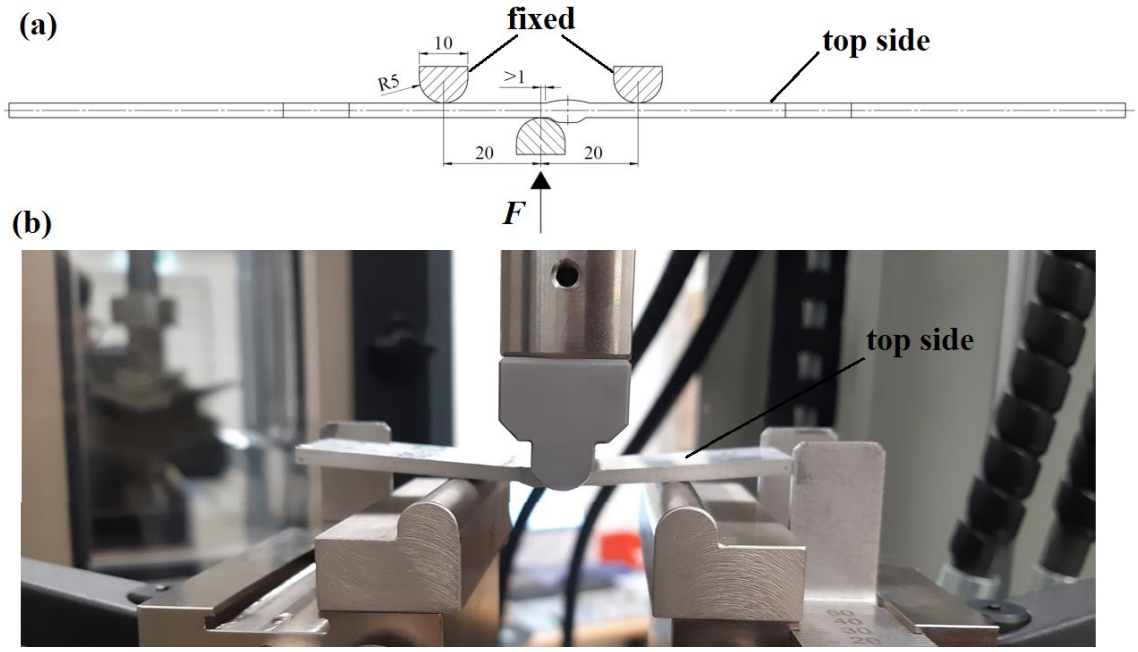

Figure 58: Butt joint specimen HCF 3-point bending: (a) testing setup, (b) specimen in the device

From the testing results given in [Table 26], it can clearly be seen that not much bending force is needed to completely deform the specimen. The forces used for the 3-point bending setup are much smaller than for the tension setup. Again, four different load levels were used for the twelve specimens that were tested with this setup, and only the lowest load level which turned out to be a runout has only one test from the same reason mentioned in the case of the tension setup. All of the results together with the applied load levels are given in [Table 26] which shows that the tests were conducted at the frequency of $f = 100$ Hz and with the stress ratio of $R = 0.1$.

As mentioned in the beginning, the desired crack initiation site for this setup was the weld toe at the top side of the specimen which confirmed to be a correct expectation since all of the specimen failed at that spot, except the 2.1 which was a runout. If the specimen would be turned upside down, the results would show the crack initiation at the bottom side weld toe with a lower number of cycles to failure since the notch effect at the bottom side is larger, however, this is just an assumption based on data acquired so far and it wasn't investigated.

Table 26: HCF 3-point bending testing results for the butt joint specimen

Specimen ID	$F_{\min}$ [N]	$F_{\max}$ [N]	ΔF [N]	R	f [Hz]	N_f [cycles]
2.1	30	300	270	0.1	100	5,000,000
2.2	50	500	450	0.1	100	4,801,246
2.3	50	500	450	0.1	100	2,835,338
2.4	70	700	630	0.1	100	108,707
2.5	70	700	630	0.1	100	134,136
2.6	60	600	540	0.1	100	159,201
2.7	60	600	540	0.1	100	403,378
2.8	60	600	540	0.1	100	348,710
2.9	60	600	540	0.1	100	253,317
2.10	50	500	450	0.1	100	2,058,218
2.11	50	500	450	0.1	100	592,385
2.12	50	500	450	0.1	100	350,583

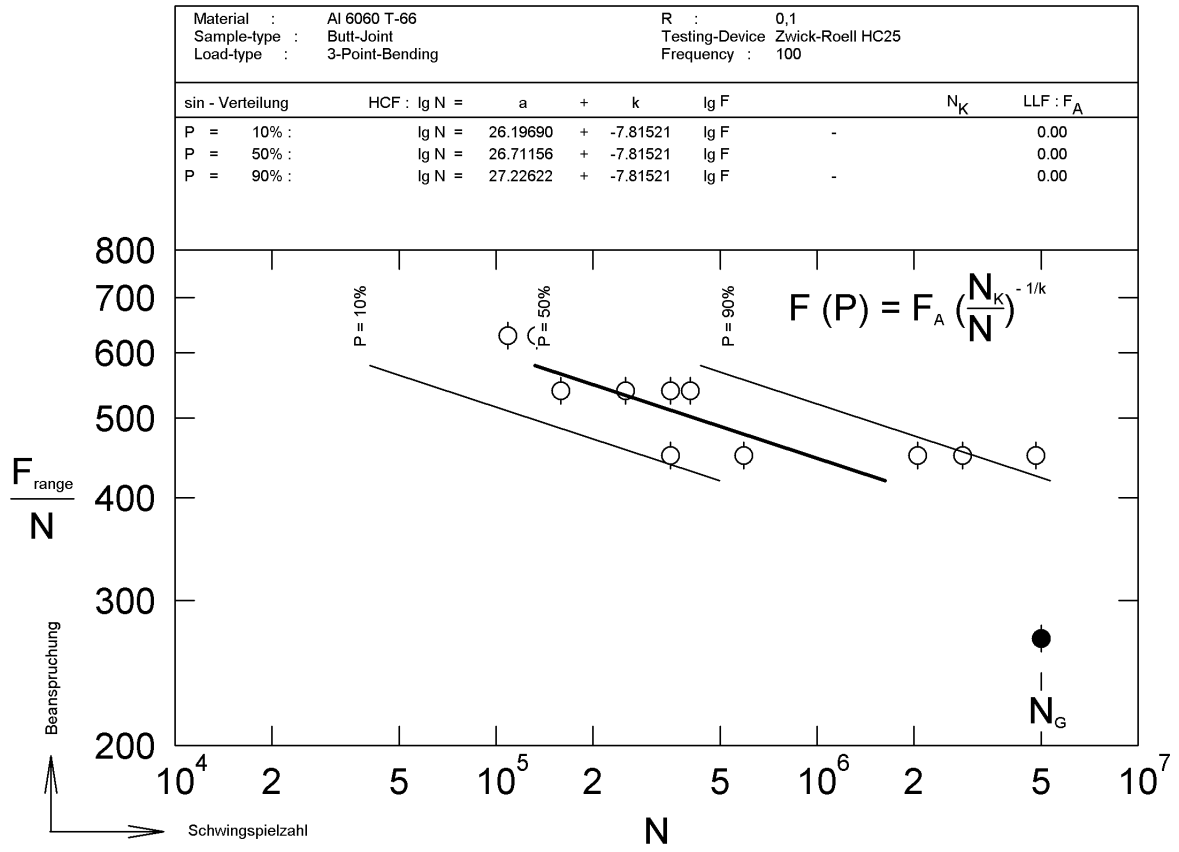

Figure 59: HCF 3-point bending testing S-N curves for the butt joint specimen from SAFD

The statistical analysis of the results presented in [Table 26] resulted in the S-N curves given in [Fig. 59] with the slope of $k = 7.8$. Using the equation (31) along with the data for a and k from [Fig. 59], values for the number of cycles N_f depending on the survival probability P_S and load level are calculated and given in [Table 27].

Table 27: N_f values depending on P_S and ΔF, for the 3-point bending tested butt joint

N_f [cycles]		$\Delta F = 270$ N	$\Delta F = 450$ N	$\Delta F = 540$ N	$\Delta F = 630$ N
P_S	90%	$1.57 \cdot 10^7$	$2.89 \cdot 10^5$	$6.96 \cdot 10^4$	$2.09 \cdot 10^4$
	50%	$5.13 \cdot 10^7$	$9.47 \cdot 10^5$	$2.28 \cdot 10^5$	$6.83 \cdot 10^4$
	10%	$1.68 \cdot 10^8$	$3.10 \cdot 10^6$	$7.45 \cdot 10^5$	$2.23 \cdot 10^5$

Value of the range of dispersion for this setup is $T_{10/90} = 1.35$, from [Table 27] and (32).

5.4.3 T-joint specimen – tension

With the testing of the butt joint specimens finished it was in order to apply the same two setups for the T-joint specimens. Therefore, the first set of T-joint fatigue tests was subjected to the tension loading with the setup given in [Fig. 60]. Similar to the butt joint tension setup, the upper arm of the device was clamped to the vertical plate of the T-joint in the length of 30 mm. However, the horizontal plate was fixed in place with two bolts and washers, one on each side of the specimen, see [Fig. 60 (a)]. The specimen mounted in the device according to the presented sketch can be seen in [Fig. 60 (b)].

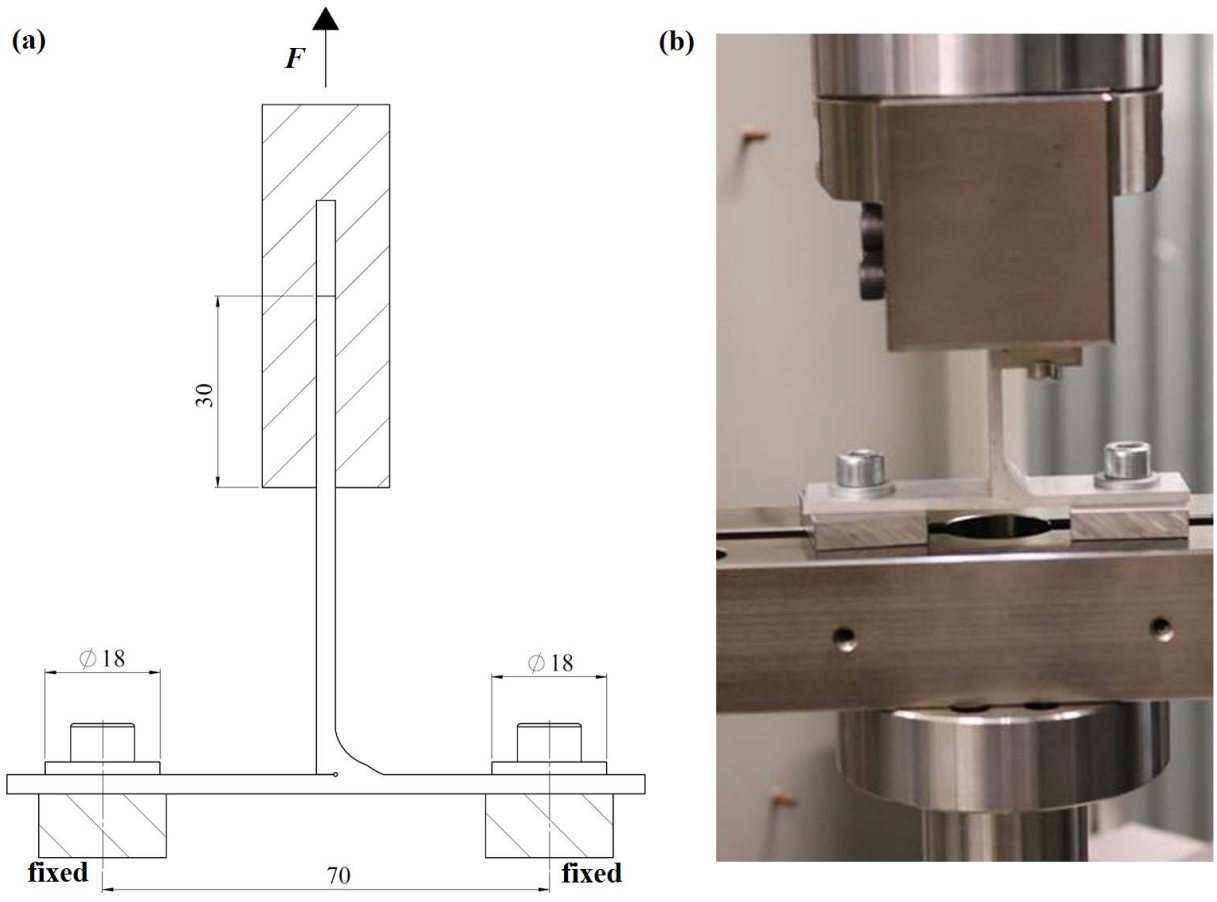

Figure 60: T-joint specimen HCF tension: (a) testing setup, (b) specimen in the device

This setup was designed to induce the crack initiation site in the weld root of the T-joint fillet weld which eventually turned to be the case. However, there was a problem in the sense that the test hardly ever stopped automatically. The reason for it is that, when the crack initiates in the weld root it will more often propagate through the thickness of the bottom plate rather than

to propagate through the weld. This eventually causes a failure at the horizontal plate which brakes in half at the left side of the T-joint which has no welding, but the test continues because there is still enough material in the weld area to endure the loading, even though the load isn't distributed through two bolts anymore but only one.

Nevertheless, the data needed for the crack initiation number of cycles could still be found through the diagrams created automatically by the machine software and it is presented here along with other testing data and results in [Table 28]. Four different load levels were used with all of them having at least two test results this time since there was no test in which the crack initiation didn't happen i.e., there was no runout from the crack initiation point of view. As in all testing setups so far, the tests were conducted with the stress ratio of $R = 0.1$ but this time with the frequency of $f = 60$ Hz.

Table 28: HCF tension testing results for the T-joint specimen

Specimen ID	$F_{\min}$ [N]	$F_{\max}$ [N]	ΔF [N]	R	f [Hz]	N_f [cycles]
4.1	100	1000	900	0.1	60	55,000
4.2	100	1000	900	0.1	60	48,000
4.3	100	1000	900	0.1	60	105,000
4.4	100	1000	900	0.1	60	55,000
4.5	50	500	450	0.1	60	4,000,000
4.6	50	500	450	0.1	60	1,750,000
4.7	75	750	675	0.1	60	150,000
4.8	75	750	675	0.1	60	75,000
4.9	75	750	675	0.1	60	135,000
4.10	60	600	540	0.1	60	700,000
4.11	60	600	540	0.1	60	680,000
4.12	60	600	540	0.1	60	1,450,000

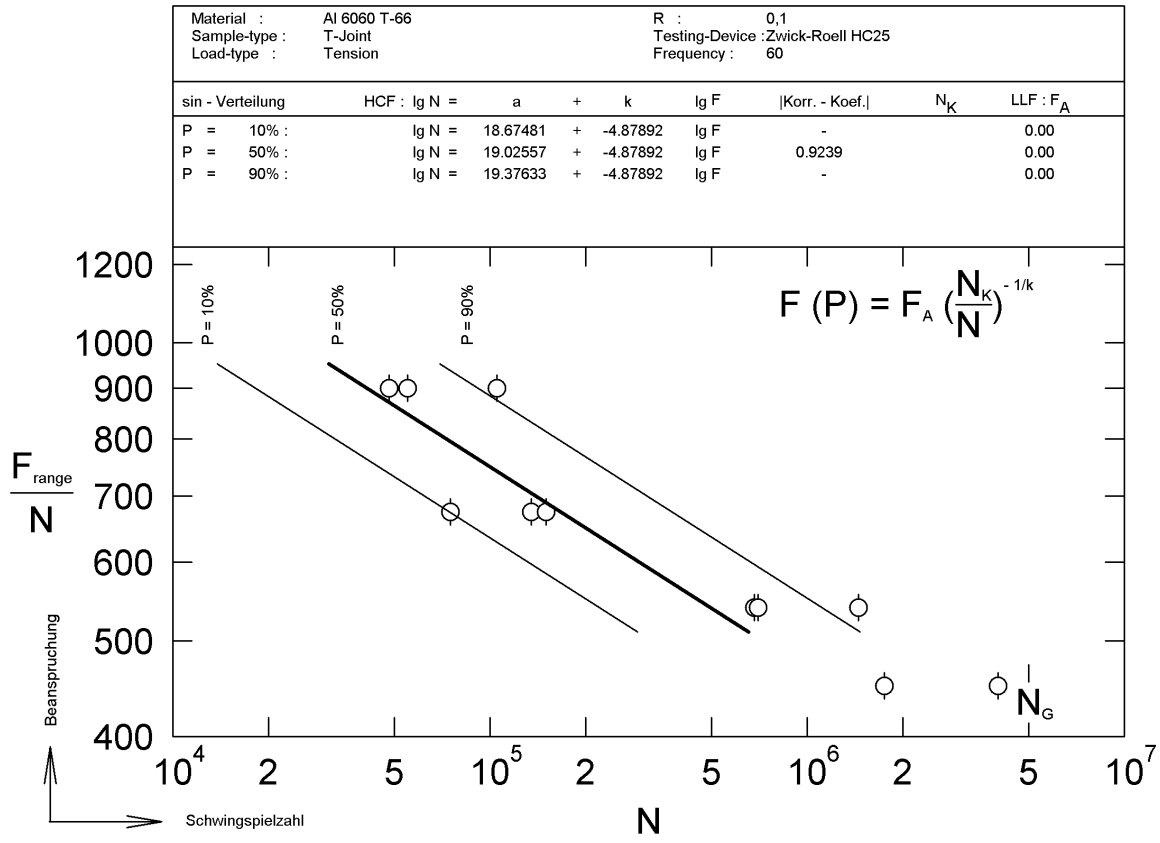

Figure 61: HCF tension testing S-N curves for the T-joint specimen from SAFD

Once again, the statistical analysis with the SAFD tool was used to create S-N curves given in [Fig. 61] from the data in [Table 28]. The slope of the curves is $k = 4.9$ and using this together with the values for a from SAFD and the equation (31), leads to the values for the number of cycles N_f depending on the survival probability P_S and load level given in [Table 29].

Table 29: N_f values depending on P_S and ΔF, for the tension tested T-joint

N_f [cycles]		$\Delta F = 450$ N	$\Delta F = 540$ N	$\Delta F = 675$ N	$\Delta F = 900$ N
P_S	90%	$5.37 \cdot 10^5$	$2.21 \cdot 10^5$	$7.43 \cdot 10^4$	$1.83 \cdot 10^4$
	50%	$1.20 \cdot 10^6$	$4.95 \cdot 10^5$	$1.67 \cdot 10^5$	$4.09 \cdot 10^4$
	10%	$2.70 \cdot 10^6$	$1.11 \cdot 10^6$	$3.74 \cdot 10^5$	$9.18 \cdot 10^4$

Using the values from [Table 29] and applying the equation (32), the range of dispersion for the T-joint specimens in HCF tension testing is calculated with a value of $T_{10/90} = 1.39$.

5.4.4 T-joint specimen – 3-point bending

With three setups already presented, final setup left for the HCF testing is in fact the 3-point bending setup for the T-joint specimens. Since the HCF tension tests of the T-joint specimens resulted in the fatigue failure in the weld root, the 3-point bending setup needed to be created in a way that induces the fatigue failure in the weld toe of the fillet weld. Since similar demand needed to be met with the butt joint specimens it is no surprise that this setup is quite similar to the one already described for the butt joint specimen testing, and it is presented in [Fig. 62]. The three pins of the same geometry, with the radius of $r = 5$ mm, were used in the same layout as for the already conducted 3-point bending tests of the butt-joint specimens. Once again, they are arranged in such a way that the loading pin achieves contact with the specimen directly below the weld toe of the fillet weld but with keeping in mind that the distance between the center of the pin and the weld toe shouldn't be less than 1 mm. If the loading pin was placed a little bit closer to the weld root, the critical point for the fatigue failure would shift from the toe to the root so during testing it was of the most importance to put the specimen into the machine as depicted in the sketch from [Fig. 62 (a)]. A closer look at the specimen correctly put into the machine is given in [Fig. 62 (b)] and as it was already described in chapter 5.4.2, because only the upper arm of the machine can be loaded, the specimen needs to be put into the machine opposite from the given sketch.

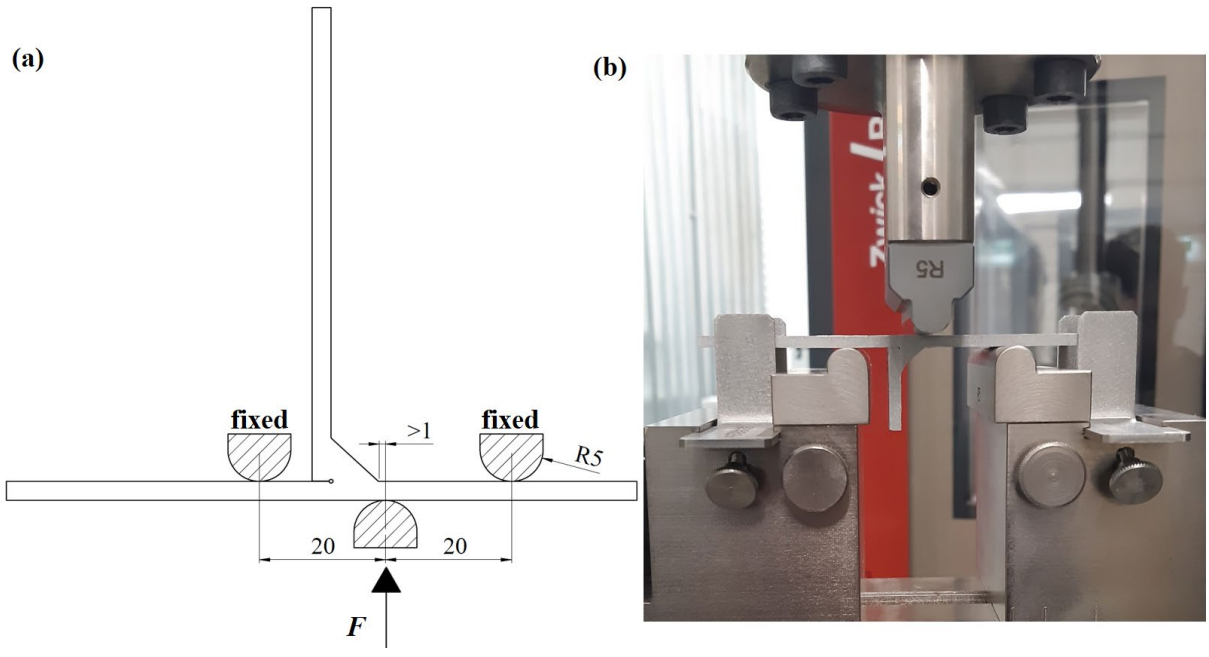

Figure 62: T-joint specimen HCF 3-point bending: (a) testing setup, (b) specimen in the device

The testing results are given in [Table 30], and in comparison, with the results of the tension testing for the same specimen given in [Table 28], the conclusion can be made that there is no significant difference in forces needed to cause the fatigue failure in both, the weld root and the weld toe. As well as in other three setups, four different load levels were used for the twelve T-joint specimens subjected to 3-point bending, and only the lowest load level which turned out to be a runout has only one test from the same already mentioned reason. Tests were performed at the frequency of $f = 100$ Hz and with the stress ratio of $R = 0.1$ with the final results together with the applied load levels given in [Table 30].

Table 30: HCF 3-point bending testing results for the T-joint specimen

Specimen ID	$F_{\min}$ [N]	$F_{\max}$ [N]	ΔF [N]	R	f [Hz]	N_f [cycles]
5.1	30	300	270	0.1	100	5,000,000
5.2	50	500	450	0.1	100	2,335,774
5.3	50	500	450	0.1	100	3,679,277
5.4	70	700	630	0.1	100	91,101
5.5	70	700	630	0.1	100	299,880
5.6	70	700	630	0.1	100	172,189
5.7	50	500	450	0.1	100	3,211,693
5.8	60	600	540	0.1	100	1,218,390
5.9	60	600	540	0.1	100	420,603
5.10	60	600	540	0.1	100	548,860
5.11	60	600	540	0.1	100	2,058,034
5.12	70	700	630	0.1	100	134,110

As it was already expected, the crack initiation site for all of the specimens used with this setup was the weld toe of the fillet weld at the horizontal plate of the joint. This only proves that the approach taken for the HCF testing was indeed the correct one.

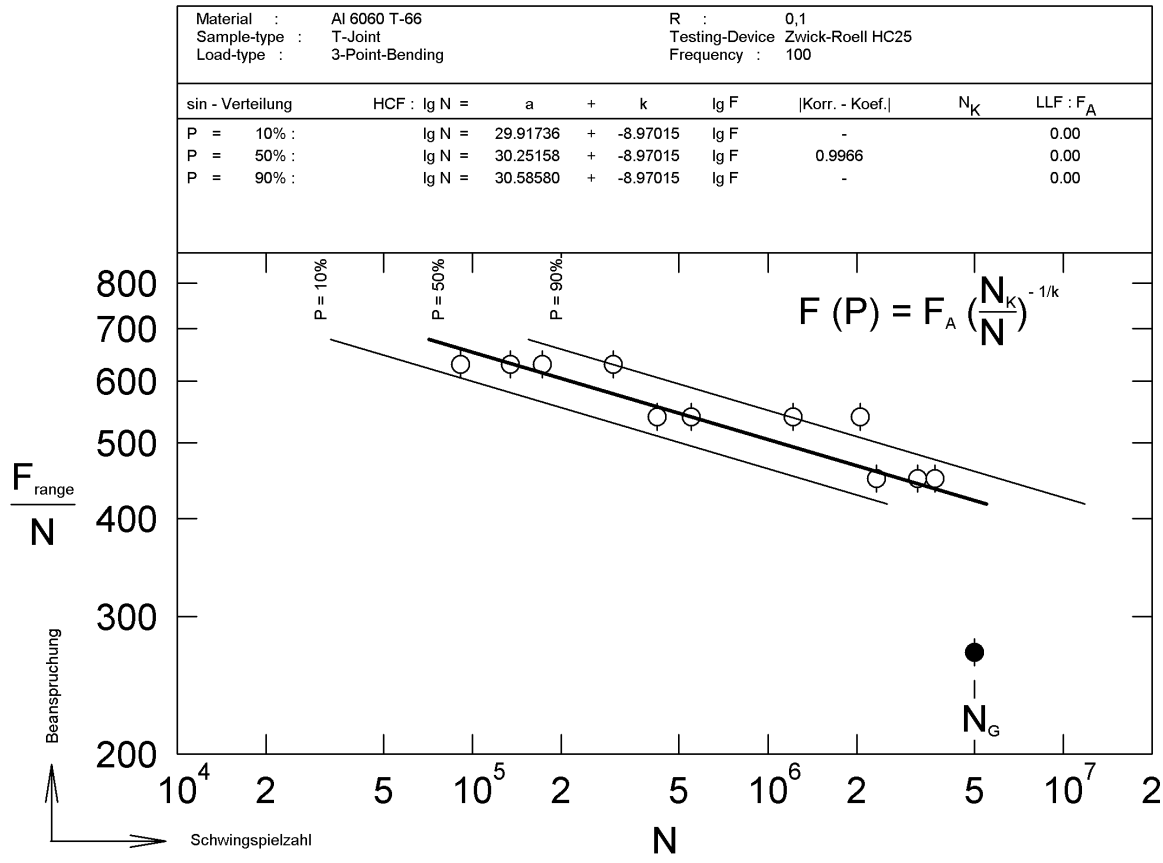

Figure 63: HCF 3-point bending testing S-N curves for the T-joint specimen from SAFD

In [Fig. 63] the S-N curves obtained from the statistical analysis tool called SAFD are given together with the data for the equations of these curves i.e., the exponent a and the slope with a value of $k = 9.0$. Using this data with the equation (31), number of cycles to failure N_f in dependance to the different load levels and different survival probabilities P_S is calculated with the values given in [Table 31]. Finally, all that is left is to calculate the range of dispersion using the equation (32) and the data from [Table 31] which gives the value of $T_{10/90} = 1.18$.

Table 31: N_f values depending on P_S and ΔF, for the 3-point bending tested T-joint

N_f [cycles]		$\Delta F = 270$ N	$\Delta F = 450$ N	$\Delta F = 540$ N	$\Delta F = 630$ N
P_S	90%	$1.28 \cdot 10^8$	$1.31 \cdot 10^6$	$2.55 \cdot 10^5$	$6.41 \cdot 10^4$
	50%	$2.77 \cdot 10^8$	$2.83 \cdot 10^6$	$5.52 \cdot 10^5$	$1.38 \cdot 10^5$
	10%	$5.97 \cdot 10^8$	$6.11 \cdot 10^6$	$1.19 \cdot 10^6$	$2.99 \cdot 10^5$

6 *FEMFAT* WELD DATABASE EXTENSION

With the literature example used for the validation of the database extension procedure itself, pretty much each important aspect of *FEMFAT Basic*, *FEMFAT Weld* and the whole procedure was clarified in much detail. The only thing left unexplained is the exact process of the notch factor calculation which will be more thoroughly explained in this chapter.

Even though *FEMFAT* database extension procedure states that a 2D model of the weld geometry should be used for determining the notch factors, for reasons described in chapter 4.5, a detailed 3D model was used for that purpose with the literature example during the validation of the procedure. Additionally, few more recommendations from *FEMFAT* needed to be bypassed for different reasons which are also explained in the chapter 4.5. However, in the case of two weld joints that were investigated in the scope of this thesis, microscopic measurements of the weld cross sections were conducted, therefore a detailed 2D model of each joint has been created as recommended by *FEMFAT* modelling guidelines. In order to completely verify the process of database extension, all of the given recommendations will be obeyed for the two mentioned weld joints.

For the modeling of detailed weld geometry, the average values of the cross-sectional dimensions given in chapter 5.3.4 were used, for each of the two investigated weld joints respectively. Each of the defined 2D models was created as a 2D shell model with the use of eight-node plane stress elements designated with CPS8 (8-node biquadratic). Although the thickness of these shell models could be adjusted to suit the exact width dimension given in [Fig. 44] and [Fig. 46] for both, butt joint and T-joint specimens respectively, for the purpose of notch factor calculation the thickness was set to 1 mm. Such modeling is chosen as a direct recommendation by *FEMFAT* for the reason of simplifying the modeling process. As notch factors are defined through static linear analyses in FEM software in which stress change is purely linear, because of that the change of notch factors is also linear with its value depending on the applied load. Therefore, the idea behind such recommendations is that by using a unitary thickness of the weld cross section and a load that will provide unitary stresses at a certain distance from the notch, either weld toe or weld root, the value of the stress at the notch will in fact be equal to the value of the corresponding notch factor when the corresponding stress values are entered into the equation (14). For the distance from which the reference nominal stress for the equation (14) is taken, the same approach as in the literature example was applied i.e., stress

was read from the FE model at a distance of $1t$ from the notch, which equals to 3 mm in the case of both weld joints investigated here. Additional reasoning for this will be provided with the results of notch factor calculation.

Each of the two detailed weld models was subjected to multiple FEM analyses according to the different load cases from [Fig. 35] that could be applied to that particular weld joint. Keeping in mind that the thickness of the 2D shell model refers in fact to the width of the real specimen, it can be concluded that the cross section to which the load is applied is the same for both investigated weld joints when the thickness in the FE model is set to be unitary. Therefore, for the loading conditions, the same values for the applied force F_{unitary} and the moment M_{unitary} were used for both models. Both were calculated using simple analytical equations with the applied force F_{unitary} calculated from the nominal stress equation:

$$\sigma_{\text{n}} = \frac{F_{\text{unitary}}}{A}. \tag{33}$$

When the values of unitary nominal stress $\sigma_{\text{n}} = 1$ MPa and the surface $A = 3\ \text{mm}^2$ are applied into the equation the value of the force is equal to $F_{\text{unitary}} = 3$ N. Similarly, the M_{unitary} was calculated using the beam theory equation (25) which when rearrange gives:

$$M_{\text{unitary}} = \frac{\sigma_{\text{n}} \cdot I}{y}. \tag{34}$$

Again, when calculating for the unitary nominal stress $\sigma_{\text{n}} = 1$ MPa, using the values for the maximum distance from the center of the cross section $y = 1.5$ mm and the moment of inertia for the unitary thickness of the model $I = 2.25\ \text{mm}^4$, the value of the applied moment can be calculated as $M_{\text{unitary}} = 1.5$ Nmm. With the values for the loads that induce unitary stresses in the specimen obtained, all of the boundary and loading conditions needed for the final definition of each load case that is applied to a specific weld joint can be found in [Fig. 35].

With all the information acquired, the notch factors were calculated for each of the weld joints with the fictious notch radius of $\rho_{\text{f}} = 0.3$ mm for weld toe and weld root, according to the *FEMFAT* recommendations from equation (29). Additionally, the same procedure was conducted for an assumption of the notch radius equal to $\rho_{\text{f}} = 1$ mm according to IIW [9] which recommends this value to be used for sheet thickness of $t = 5$ mm or larger but it will be investigated here how does it suit for the smaller sheet thickness. All of these calculations are based on the notch factors for the weld nodes in the middle of the weld seam since the start or end of the weld weren't investigated for the work in this thesis.

6.1 Butt joint specimen

The detailed shell model of the butt joint specimen was created according to the geometry of the specimen given in [Fig. 44] with an addition of the detailed weld geometry created using the average values from [Table 21] and the value of $\rho_f = 0.3$ mm for the notch radius. Through the modelling process all of the mentioned recommendations proposed by *FEMFAT* have been implemented and the final result is given in [Fig. 64]. The [Fig. 64 (a)] shows only the geometry of the whole model, while the extra fine mesh applied to the area around the weld is depicted in [Fig. 64 (b)]. It can be seen that the, as in the literature example, the mesh was created in a way that the extraction of stresses at certain distances from the weld toe is as simple as possible.

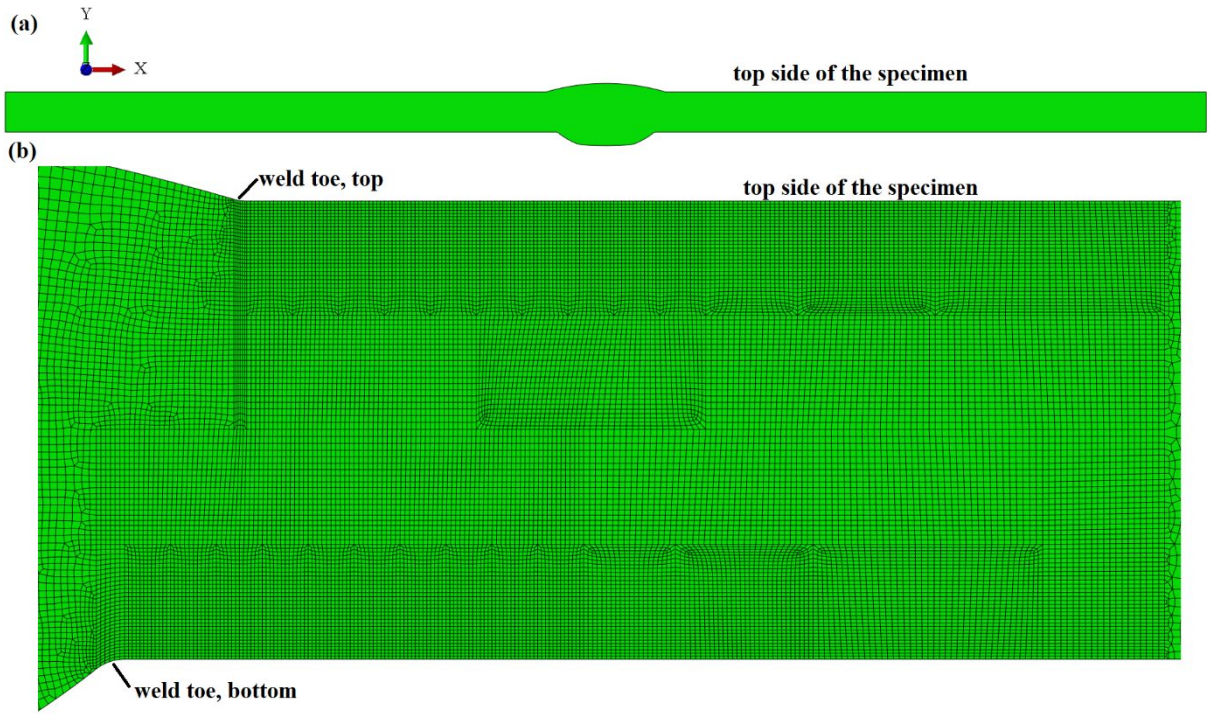

Figure 64: Butt joint specimen FE model used for notch factor calculation: (a) shape of the model, (b) extra fine mesh of the weld area

In regard to the possible load cases for the calculation of the notch factors that are presented in [Fig. 35] and designated in [Table 10], only two load cases are needed for this type of geometry. Because of the simplicity of the butt joint, only the load cases lc1 and lc2 are needed in order to obtain the notch factors. Since the butt joint in question isn't symmetrical, notch factors for the weld toe at the top surface as well as notch factors for the weld toe at the bottom surface will be calculated and introduced into the weld database.

6.1.1 Tension load case, lc1

For the first load case designated with lc1, tension in the plates of the joint was investigated with the FE model being fixed on one side and the force $F_{\text{unitary}} = 3$ N applied on the other side of the butt joint specimen. As per the guidelines provided by *FEMFAT* the principal stress S11 was calculated using the finite element analysis for the purpose of notch factor calculation. Principal stress distribution for the tension load case lc1 is given in [Fig. 65] along with the stress values at each of the two weld toes and stress values at the distance of $1t$ from them. Values in black refer to the weld toe at the top side of the specimen, while the ones in red refer to the values assessed for the weld toe at the bottom side of the specimen. The stresses at the distance of $1t$ were measured on both sides of the specimen in order to confirm that the stress distribution is equal through the thickness of the material at the given distance.

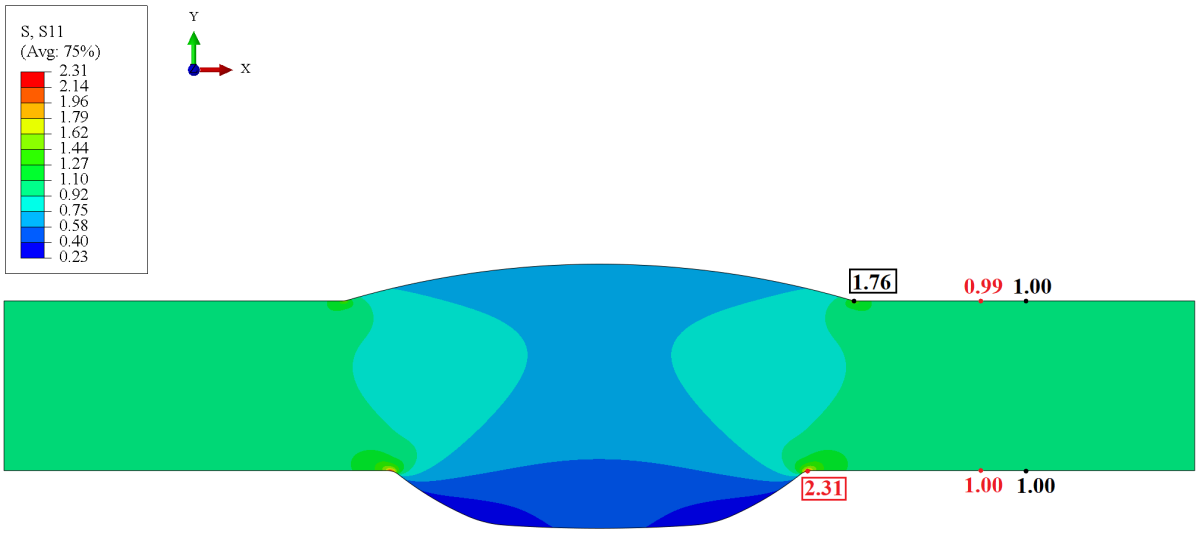

Figure 65: Principal stress S11 distribution in the butt joint specimen for lc1

From the values depicted in [Fig. 65], notch factors can be determined even without the use of the equation (14). Therefore, resulting notch factor for the weld toe at the top surface has a value of $K_{\text{f, t-lc1}} = 1.76$, and the notch factor at the bottom surface is equal to $K_{\text{f, b-lc1}} = 2.31$. As it was expected, due to the weld geometry described in chapter 5.3.4.1, the notch effect is larger at the bottom side of the specimen.

6.1.2 Bending load case, lc2

The effect of bending loading conditions to notch factors has been investigated with the second load case, designated with lc2. The FE model was fixed on one side as in the load case lc1, butt for the bending analysis, the moment of $M_{\text{unitary}} = 1.5$ Nmm was applied on the other side as per [Fig. 35]. Again, the principal stress S11 was calculated since both plates in the joint lie parallel in regard to the principal X axis. Distribution of the principal stress S11 for the load case lc2 is given in [Fig. 66] with all the stress values needed for the notch factor calculation as well. From the stresses at the distance of $1t$ from each weld toe it can be nicely seen how exactly the specimen was loaded since the stresses at each side have the same unitary absolute value with a different sign, which indicates a correct stress distribution through the thickness of the material.

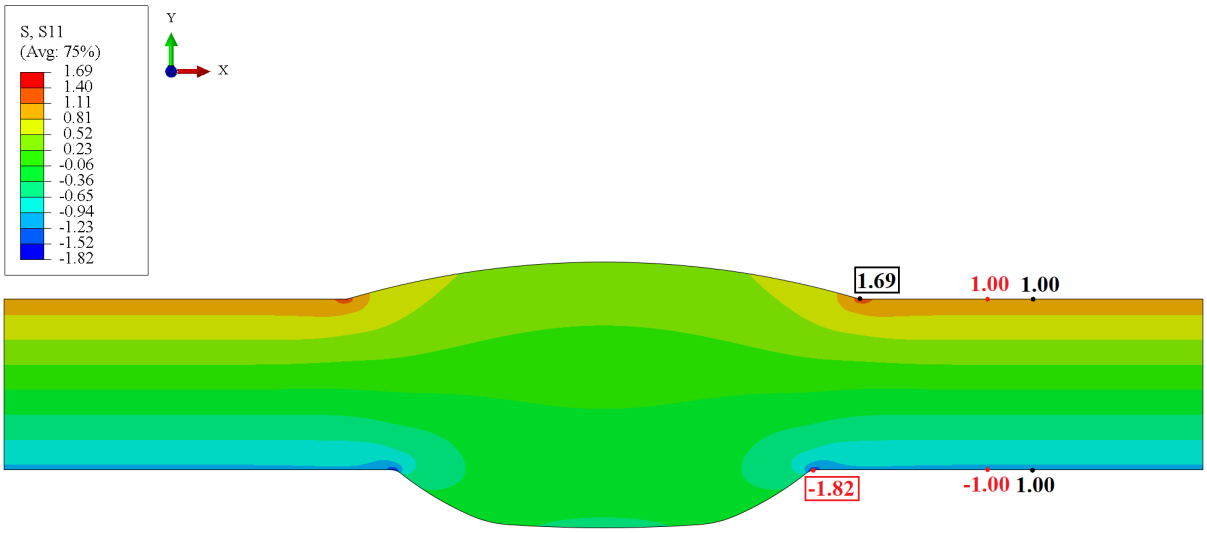

Figure 66: Principal stress S11 distribution in the butt joint specimen for lc2

As well as in the last load case, there is no need for the equation (14) since the notch factor values are seen directly from [Fig. 66] which is a direct consequence of the unitary modelling approach. For the weld toe at the top of the butt joint specimen the notch factor has a value of $K_{\text{f, t-lc2}} = 1.69$, while the notch factor at the bottom equals to $K_{\text{f, b-lc2}} = 1.82$. Even though the stress value is in fact indicative of compression at the bottom side weld toe, for the calculation of notch factors only the absolute value of the stress is considered.

Since the butt joint specimen investigated in this thesis isn't symmetrical, an additional analysis for the bending investigation in load case lc2 was conducted. Basically, all the boundary conditions were left the same with only the acting direction of the moment $M_{\text{unitary}} = 1.5$ Nmm switched in regard to [Fig. 35] in order to see if any changes in the values of the notch factors would occur. However, by looking at the [Fig. 67] where the principal stress S11 distribution for such loading conditions is presented, it is clear that no change whatsoever was caused in the absolute values of the stresses at any given point that was assessed for this load case.

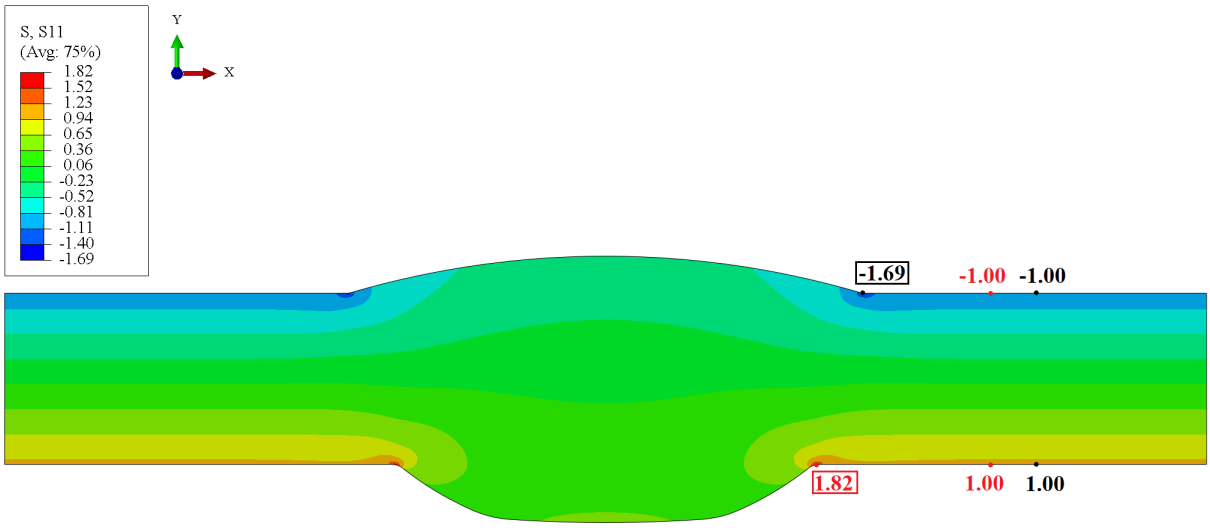

Figure 67: Principal stress S11 distribution in the butt joint specimen for reversed lc2

6.1.3 Non-symmetrical I-seam weld with ρ_f = 0.3 mm

Before finally defining the new non-symmetrical I-seam weld with a fictious notch radius of $\rho_f = 0.3$ mm, it is necessary to present why was the nominal stress needed for the notch factor calculation read from the FE model at a distance of $1t$. The distribution of the principal stress S11 along the increasing distance from the weld toe is given in [Fig. 68]. Each of the weld toes is represented with its own curve for each load case, while the stress at the weld toe is assigned an arbitrary distance of -0.5 mm just for the purposes of the graphical presentation. It is clear from the diagram in [Fig. 68] that the nominal stresses are already achieved at the distance of $0.5t$ which just confirms that the nominal stresses used for the calculation of notch factors were correctly applied and the notch effect of the weld geometry was successfully captured within the FE analyses.

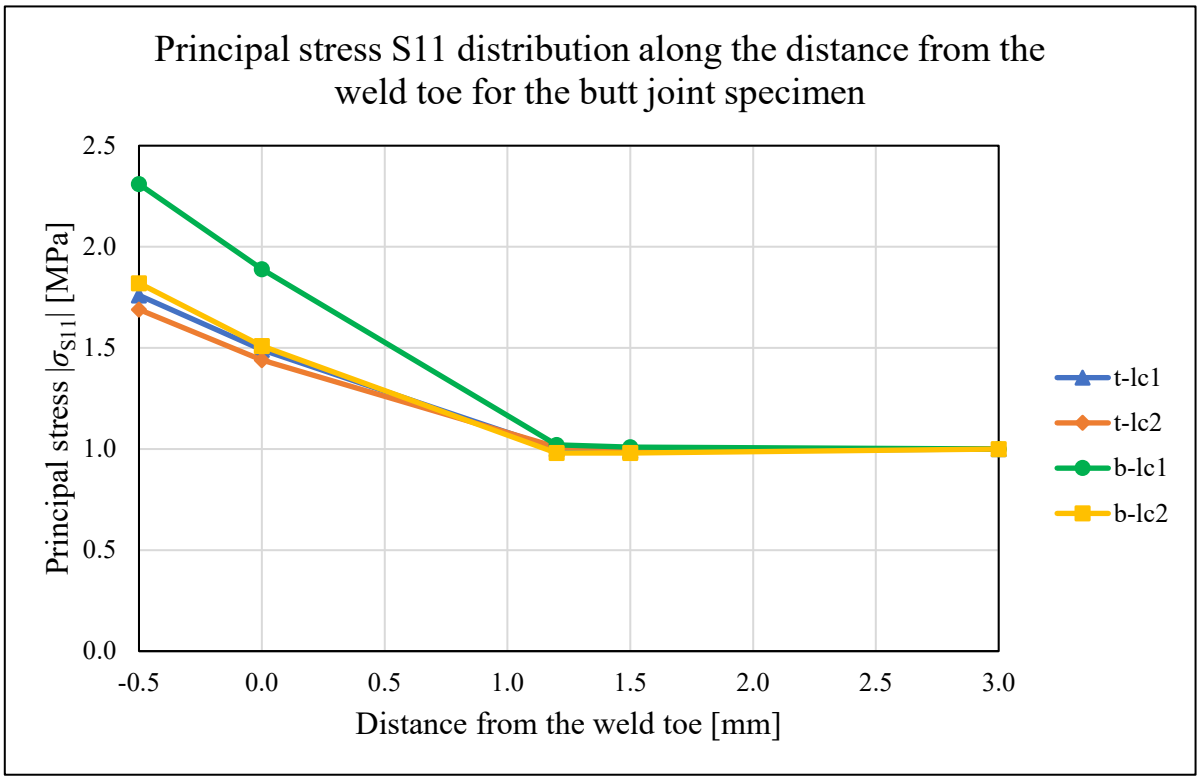

Figure 68: Principal stress S11 distribution along the distance from the weld toe for the butt joint specimen with $\rho_f = 0.3$ mm

Table 32: Calculated notch factors for non-symmetrical I-seam weld with $\rho_f = 0.3$ mm

	lc1	lc2
Weld toe at the top	1.76	1.69
Weld toe at the bottom	2.31	1.82

With the both load cases conducted, all notch factors that are needed to describe the non-symmetrical butt joint I-seam weld can be obtained. Therefore, the notch factors calculated for weld toes at both sides of the butt joint in question are given in [Table 32]. However, before these notch factors can be introduced into the weld database, they need to be recalculated in regard to the sheet thickness influence presented in chapter 3.2.2.3, otherwise the notch factors from [Table 32] could only be used for sheet thickness of $t = 3$ mm. As it was described in said chapter, when the sheet thickness influence factor is enabled, all the notch factors are multiplied by a certain value calculated from the polygon course given in [Fig. 23]. For the thickness of $t = 3$ mm, this factor has a value $G = 0.667$, so if the calculation is to be applied

in reverse, all of the notch factors calculated for the sheet thickness of $t = 3$ mm need to be multiplied by a reciprocal sheet influence factor of $1/G = 1.5$ in order to comply with the polygon course given in [Fig. 23]. Therefore, the final notch factors, ready to be introduced in the weld database as a part of a new weld joint are given in [Table 33].

Table 33: Weld database notch factors for non-symmetrical I-seam weld with $\rho_f = 0.3$ mm

	lc1	lc2
Weld toe at the top	2.64	2.54
Weld toe at the bottom	3.47	2.73

Final values that need to be defined in order for the new joint to be successfully implemented into the weld database are the slope and the endurance cycle limit. Generally speaking, both of these parameters are obtained through the experimental HCF testing, however in all of the tests conducted in this thesis and presented in chapter 5, the finite fatigue life was investigated which refers to the cycles below the endurance cycle limit. Because of this no meaningful endurance cycle limit could be determined and an arbitrary value of $N_{\text{end}} = 2 \cdot 10^6$ was chosen since the same value exists in IIW [9] for the FAT class definition. The slopes were taken from the SAFD results with the values of $k = 7.8$ for the top side weld toe, see [Fig. 59] and $k = 5.8$ for the bottom one, see [Fig. 57]. The final definition of the newly created weld joint in the weld database is given in [Fig. 69].

```
$ Butt Weld, Non-Symmetrical I-Seam  (Master Thesis MV)                                  Situation: 2021-11-26
$ -----------------
SID 110 Butt Weld, non-symmetrical I-seam, r=0.3 mm
MIDSQ 909 907
$
$ Data for a node in the middle of the weld seam
$
$    MNT MNB UTL1 UTL2 UTL3 UBL1 UBL2 UBL3 WTL1 WTL2 WTL3 WBL1 WBL2 WBL3 SPTO SPBO SSTO SSBO
$    ---------------------------------------------------------------------------------
 907         2.64 2.54      3.47 2.73
 908         2.64 2.54      3.47 2.73
 909         2.64 2.54      3.47 2.73
 910         2.64 2.54      3.47 2.73
$
$         BEPKT 1        BEPKT 2        BEPKT 3        BEPKT 4      SHEAR Top    SHEAR Bottom
$     Inclination    Inclination    Inclination    Inclination    Inclination    Inclination   Survival Probability in Perc.
$     Cycle Endur.   Cycle Endur.   Cycle Endur.   Cycle Endur.   Cycle Endur.   Cycle Endur.  Range of Disp. 10-90 Percent
$    ------------------------------------------------------------------------------------------------------------------------
N907         7.80           5.80           4.00           4.00           5.00           5.00           50.0
E907      2000000        2000000        1000000        1000000        1800000        1800000          1.260
N908         7.80           5.80           4.00           4.00           5.00           5.00           50.0
E908      2000000        2000000        1000000        1000000        1800000        1800000          1.260
N909         7.80           5.80           4.00           4.00           5.00           5.00           50.0
E909      2000000        2000000        1000000        1000000        1800000        1800000          1.260
N910         7.80           5.80           4.00           4.00           5.00           5.00           50.0
E910      2000000        2000000        1000000        1000000        1800000        1800000          1.260
```

Figure 69: Weld database for non-symmetrical I-seam weld with $\rho_f = 0.3$ mm

6.1.4 Non-symmetrical I-seam weld with ρ_f = 1 mm

The whole procedure of calculating the notch factors described through the chapter 6.1 so far was repeated for a different fictious notch radius with a value of $\rho_f = 1$ mm. Notch factors obtained through the repeated procedure and already recalculated for the compliance with the sheet thickness influence polygon course are given in [Table 34]. Naturally, the values of the notch factors are smaller than with the weld joint described in the chapter 6.1.3 because the fictious notch radius used for this model was larger and therefore the notch effect of the weld toe was less pronounced.

Table 34: Weld database notch factors for non-symmetrical I-seam weld with ρ_f = 1 mm

	lc1	lc2
Weld toe at the top	2.12	2.03
Weld toe at the bottom	2.55	2.09

The values for the slope and the endurance cycle limit stay the same regardless of the fictious notch radius since they are based either on the literature references like the endurance cycle limit in this case or on the testing results like the slopes for each of the two different weld toes. The definition of this weld joint in the weld database is given in [Fig. 70].

```
$ Butt Weld, Non-Symmetrical I-Seam  (Master Thesis MV)                                  Situation: 2021-11-26
$ ----------------
SID 111 Butt Weld, non-symmetrical I-seam, r=1 mm
MIDSQ 913 911
$
$ Data for a node in the middle of the weld seam
$
$    MNT MNB UTL1 UTL2 UTL3 UBL1 UBL2 UBL3 WTL1 WTL2 WTL3 WBL1 WBL2 WBL3 SPTO SPBO SSTO SSBO
$    ---------------------------------------------------------------------------------
 911         2.12 2.03      2.55 2.09
 912         2.12 2.03      2.55 2.09
 913         2.12 2.03      2.55 2.09
 914         2.12 2.03      2.55 2.09
$
$         BEPKT 1        BEPKT 2        BEPKT 3        BEPKT 4      SHEAR Top    SHEAR Bottom
$      Inclination    Inclination    Inclination    Inclination    Inclination    Inclination   Survival Probability in Perc.
$     Cycle Endur.   Cycle Endur.   Cycle Endur.   Cycle Endur.   Cycle Endur.   Cycle Endur.  Range of Disp. 10-90 Percent
$    ------------------------------------------------------------------------------------------------------------------------
N911          7.80           5.80           4.00           4.00           5.00           5.00           50.0
E911       2000000        2000000        1000000        1000000        1800000        1800000          1.260
N912          7.80           5.80           4.00           4.00           5.00           5.00           50.0
E912       2000000        2000000        1000000        1000000        1800000        1800000          1.260
N913          7.80           5.80           4.00           4.00           5.00           5.00           50.0
E913       2000000        2000000        1000000        1000000        1800000        1800000          1.260
N914          7.80           5.80           4.00           4.00           5.00           5.00           50.0
E914       2000000        2000000        1000000        1000000        1800000        1800000          1.260
```

Figure 70: Weld database for non-symmetrical I-seam weld with ρ_f = 1 mm

6.1.5 Symmetrical I-seam weld with ρ_f = 0.3 mm

During the set of HCF testing where butt joint specimens were subjected to pulsating tensile load which was described in chapter 5.4.1, the critical location for the failure of the specimen was the weld toe at the bottom side. The reason for that was already explained but in order to investigate how would a symmetrical specimen perform in such loading conditions, an additional weld joint was added to the weld database. The new joint is based on the non-symmetrical I-seam weld with the fictious notch radius of $\rho_f = 0.3$ mm, in a way that both sides of the joint are considered to have the same notch factors as the top side of the reference joint, see [Table 33]. So, the notch factors for this symmetrical I-seam weld are given in [Table 35].

Table 35: Weld database notch factors for symmetrical I-seam weld with ρ_f = 0.3 mm

	lc1	lc2
Weld toe at the top	2.64	2.54
Weld toe at the bottom	2.64	2.54

From [Fig. 71] where the weld joint in the format in which it is incorporated in the weld database is given, it can be seen that the slope taken for this weld joint is the one from the HCF tension test since the joint will be used for the comparison with exactly these results. The endurance cycle limit remained at the value of $N_{end.} = 2 \cdot 10^6$ taken from IIW [9].

```
$ Experimental Butt Weld, Symmetrical I-Seam  (Master Thesis MV)                                    Situation: 2021-11-26
$ ----------------
SID 112 Experimental Butt Weld, symmetrical I-seam, r=0.3
MIDSQ 917 915
$
$ Data for a node in the middle of the weld seam
$
$    MNT MNB UTL1 UTL2 UTL3 UBL1 UBL2 UBL3 WTL1 WTL2 WTL3 WBL1 WBL2 WBL3 SPTO SPBO SSTO SSBO
$    ------------------------------------------------------------------------------------
 915         2.64 2.54      2.64 2.54
 916         2.64 2.54      2.64 2.54
 917         2.64 2.54      2.64 2.54
 918         2.64 2.54      2.64 2.54
$
$         BEPKT 1        BEPKT 2        BEPKT 3        BEPKT 4      SHEAR Top    SHEAR Bottom
$      Inclination    Inclination    Inclination    Inclination    Inclination    Inclination   Survival Probability in Perc.
$      Cycle Endur.   Cycle Endur.   Cycle Endur.   Cycle Endur.   Cycle Endur.   Cycle Endur.  Range of Disp. 10-90 Percent
$     ------------------------------------------------------------------------------------------------------------------------
N915         5.80           5.80           4.00           4.00           5.00           5.00           50.0
E915      2000000        2000000        1000000        1000000        1800000        1800000          1.260
N916         5.80           5.80           4.00           4.00           5.00           5.00           50.0
E916      2000000        2000000        1000000        1000000        1800000        1800000          1.260
N917         5.80           5.80           4.00           4.00           5.00           5.00           50.0
E917      2000000        2000000        1000000        1000000        1800000        1800000          1.260
N918         5.80           5.80           4.00           4.00           5.00           5.00           50.0
E918      2000000        2000000        1000000        1000000        1800000        1800000          1.260
```

Figure 71: Weld database for symmetrical I-seam weld with ρ_f = 0.3 mm

6.1.6 Symmetrical I-seam weld with ρ_f = 1 mm

Based on the principle used for the creation of the symmetrical butt joint in the chapter 6.1.5, another symmetrical butt joint was created. Using the notch factors at the top side of the specimen from the non-symmetrical I-seam weld with the fictious notch radius of $\rho_f = 1$ mm, a symmetrical joint with the same value for the radius was created. The notch factors for this weld joint are given in [Table 36].

Table 36: Weld database notch factors for symmetrical I-seam weld with ρ_f = 1 mm

	lc1	lc2
Weld toe at the top	2.12	2.03
Weld toe at the bottom	2.12	2.03

The format in which the joint was defined in the database can be seen in [Fig. 72] with the same values for the slope and the endurance limit as in the symmetrical I-seam weld with the fictious notch radius of $\rho_f = 1$ mm.

```
$ Butt Weld, Symmetrical I-Seam  (Master Thesis MV)                                  Situation: 2021-11-26
$ -----------------
SID 113 Butt Weld, symmetrical I-seam, r=1 mm
MIDSQ 921 919
$
$ Data for a node in the middle of the weld seam
$
$    MNT MNB UTL1 UTL2 UTL3 UBL1 UBL2 UBL3 WTL1 WTL2 WTL3 WBL1 WBL2 WBL3 SPTO SPBO SSTO SSBO
$    ---------------------------------------------------------------------------------------
 919         2.12 2.03      2.12 2.03
 920         2.12 2.03      2.12 2.03
 921         2.12 2.03      2.12 2.03
 922         2.12 2.03      2.12 2.03
$
$         BEPKT 1        BEPKT 2        BEPKT 3        BEPKT 4      SHEAR Top    SHEAR Bottom
$      Inclination    Inclination    Inclination    Inclination    Inclination    Inclination   Survival Probability in Perc.
$      Cycle Endur.   Cycle Endur.   Cycle Endur.   Cycle Endur.   Cycle Endur.   Cycle Endur.  Range of Disp. 10-90 Percent
$     ---------------------------------------------------------------------------------------------------------------------
N919         7.80           5.80           4.00           4.00           5.00           5.00           50.0
E919      2000000        2000000        1000000        1000000        1800000        1800000          1.260
N920         7.80           5.80           4.00           4.00           5.00           5.00           50.0
E920      2000000        2000000        1000000        1000000        1800000        1800000          1.260
N921         7.80           5.80           4.00           4.00           5.00           5.00           50.0
E921      2000000        2000000        1000000        1000000        1800000        1800000          1.260
N922         7.80           5.80           4.00           4.00           5.00           5.00           50.0
E922      2000000        2000000        1000000        1000000        1800000        1800000          1.260
```

Figure 72: Weld database for symmetrical I-seam weld with ρ_f = 1 mm

6.2 T-joint specimen

Using the geometry of the T-joint specimen given in [Fig. 46] along with the detailed weld geometry defined with the average values from the microscopic measurements in [Table 22] the detailed shell model of the T-joint fillet weld was created. The weld toe and the weld root were modeled in the geometry with the fictious notch radius of $\rho_f = 0.3$ mm. In [Fig. 73 (a)] the whole geometry of the detailed shell model is presented with the extra fine meshing of the weld root and the weld toe given in [Fig. 73 (b)] and [Fig. 74 (c)] respectively. As it was the case with the butt joint model, all *FEMFAT* recommendations are included here as well.

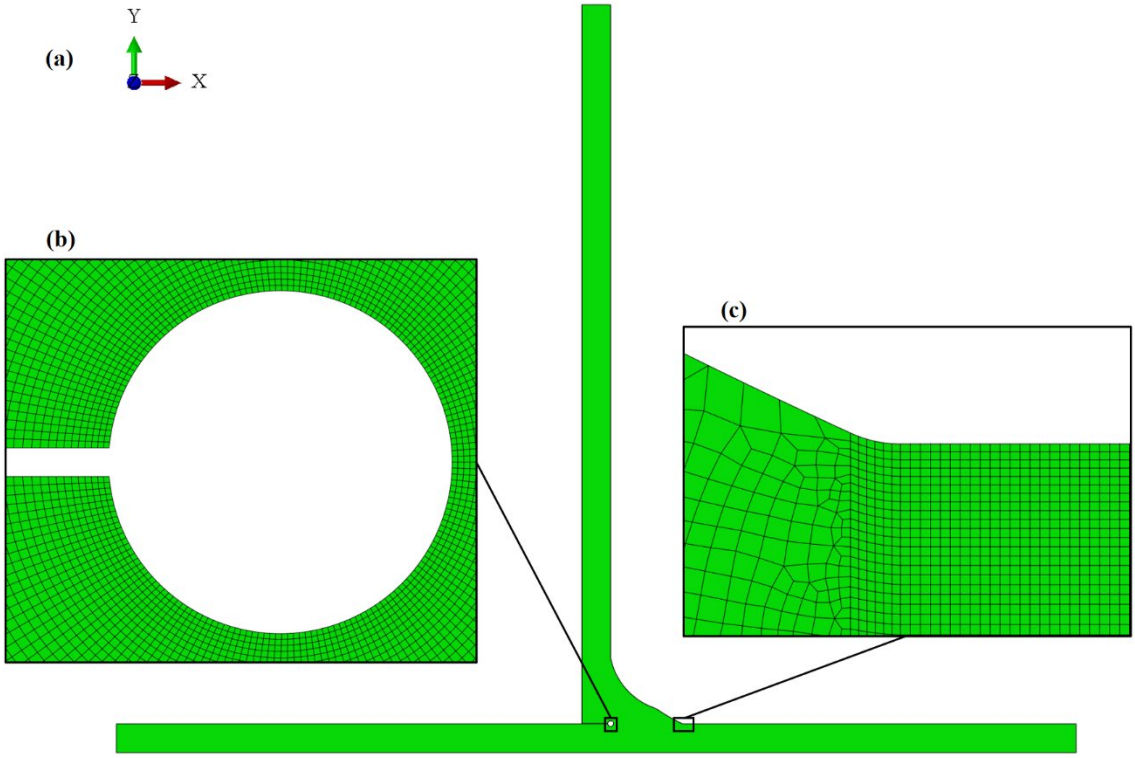

Figure 73: T-joint specimen FE model used for notch factor calculation: (a) shape of the model, (b) extra fine mesh of the weld root, (c) extra fine mesh at the weld toe

For the calculation of the notch factors for this kind of weld joint, all of the load cases depicted in [Fig. 35] and named in [Table 10] need to be applied. Through all six load cases, corresponding notch factors for the weld toe at the horizontal and vertical plates, and in the weld root, will be calculated in regard to different loading conditions and eventually distributed in the right way for the creation of the new weld joint in weld database.

6.2.1 Tension load case, lc1

The first load case defined in [Fig. 35] investigates the stresses in the horizontal plate of the weld joint induced by the tension applied to the joint through that same plate. In this case the horizontal plate of the weld joint is not loaded and therefore the weld toe at the top of the weld doesn't need to be evaluated. For the FEM analysis, the shell model was fixed on the left side with the force $F_{\text{unitary}} = 3$ N acting on the right side of the horizontal plate. According to *FEMFAT* recommendations, for the calculation of notch factors the principal stress S11 was evaluated with the stress distribution for the tension load case lc1 given in [Fig. 74]. Also, in the same figure, stress values in the bottom weld toe and weld root are presented. The distance for reading out the nominal stress values is yet again set at $1t$ away from the assessed notch. Values in black refer to the weld root, while the ones in red refer to the values assessed for the weld toe which is valid for all load cases.

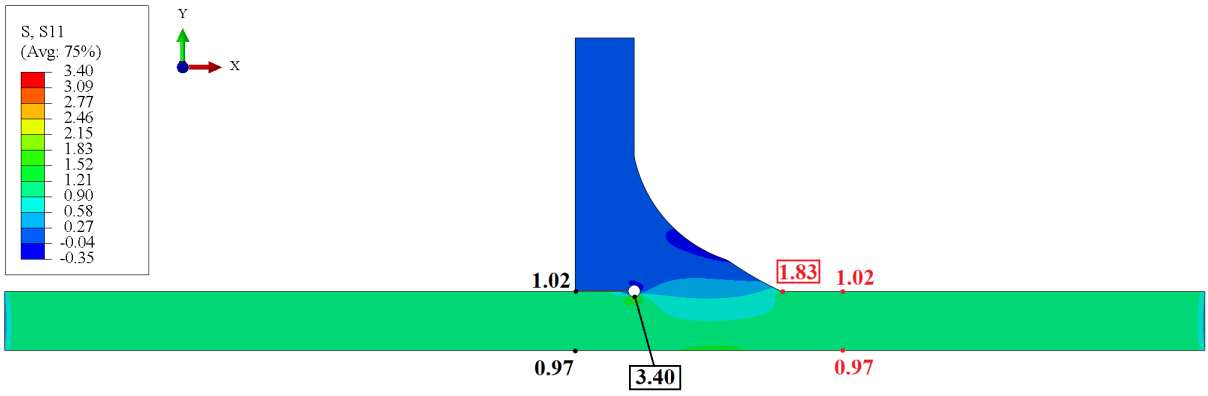

Figure 74: Principal stress S11 distribution in the T-joint specimen for lc1

Using the values depicted in [Fig. 74], notch factors need to be determined with the equation (14) since the nominal stresses aren't exactly $\sigma_{\text{n}} = 1$ MPa. Hence, the resulting notch factor for the weld toe has a value of $K_{\text{f, t-lc1}} = 1.79$. As for the root, because the radius was modelled with an undercut into the material of the horizontal plate, the notch factor calculated by dividing the stress at the root with the nominal stress at $1t$ i.e., $K_{\text{f, r-lc1}} = 3.32$, needs to be properly corrected as explained in chapter 2.4. Using the values of $\sigma_{\text{l}} = 0.97$ MPa and $\sigma_u = 1.02$ MPa from [Fig. 74] and applying them to the equation (15), the corrected notch factor for the root is calculated with the value of $K^*_{\text{f, r-lc1}} = 2.25$.

6.2.2 Bending load case, lc2

Similar to the load case lc1, the second load case lc2 also investigates the stresses in the horizontal plate of the weld joint but for the bending loading conditions. So yet again, the specimen was loaded from the side where the welding was performed but with the unitary stress inducing moment $M_{\text{unitary}} = 1.5$ Nmm as opposed to the force used in the load case lc1. The stress distribution of the principal stress S11 in the weld joint can be seen in [Fig. 75] along with the corresponding values of the stress at the weld toe of the horizontal plate and the weld root. In both of the load cases investigated so far, the principal stress S11 was used because the horizontal plate lying in the direction of the principal X axis was loaded. From the stresses at the distance of $1t$ at the weld toe, the distribution of stresses through the thickness of the material can be nicely seen, the same as in [Fig. 66].

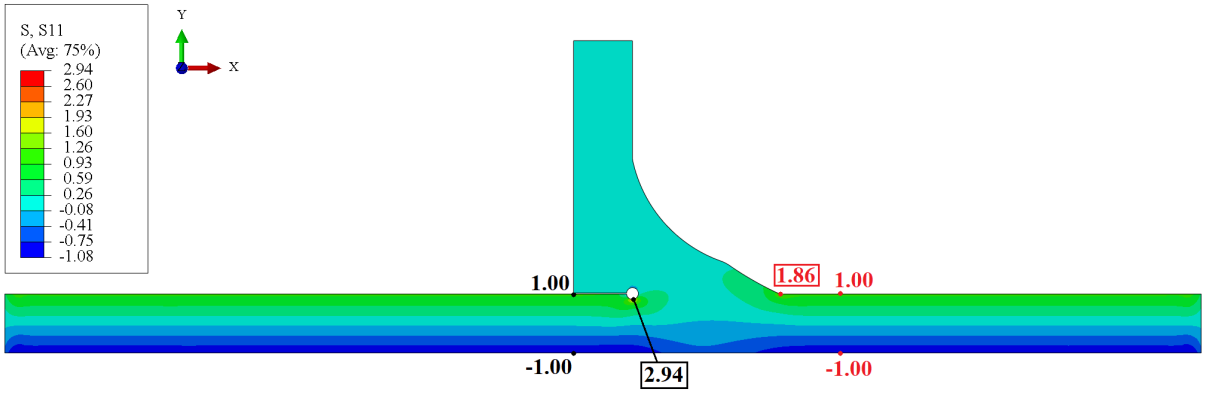

Figure 75: Principal stress S11 distribution in the T-joint specimen for lc2

Since the values of the nominal stresses at the distance of $1t$ from the evaluated notch are in fact unitary in this case, the notch factors can be taken from [Fig. 75] without the calculation using the equation (14). The notch factor at the horizontal weld toe is equal to $K_{\text{f, t-lc2}} = 1.86$ while the notch factor at the root has a value of $K_{\text{f, r-lc2}} = 2.94$ but it needs to be corrected again for the same reason. Applying the equation (15) to this load case, the corrected notch factor for the root is obtained with a value of $K^*_{\text{f, r-lc2}} = 2.38$. For the purpose of the undercut correction via the equation (15), the stresses at the top and bottom side of the investigated plate need to be included with their respective signs i.e., in this case the lower surface stress with the value of $\sigma_{\text{l}} = -1$ MPa and the upper surface stress with the value of $\sigma_{\text{u}} = 1$ MPa.

6.2.3 Tension load case, lc3

From the [Table 10] it can be seen that the load case lc3 is the second load case used to describe the effects of tensile loading at the weld joint in question. With the load case lc1 which defines the tension effects in the horizontal plate already investigated, to complete the notch factor definition for the tensile loading of the weld joint, load case lc3 was analyzed to define the tensile loading effects in the vertical plate of the joint. The boundary and loading conditions from [Fig. 35] where applied to the shell model of the weld geometry with the acting force $F_{\text{unitary}} = 3$ N positioned at the top of the vertical plate in the joint. Since this load case presents the loading conditions for the vertical plate in the joint, for calculation of corresponding notch factors, principal stress S22 was used and in [Fig. 76] the magnified deformation shape (deformation scale factor in *Abaqus 2019.HF4* was set to 200) of the joint in question can be seen. Immediately it can be noticed that the vertical plate of the joint isn't subjected only to tension but there is also a bending effect that is a consequence of the non-symmetrical welding in regard to the loading conditions i.e., the tensile load isn't evenly distributed on both sides of the specimen. For example, if welding was done from both sides of the vertical plate the bending effect probably wouldn't exist or it would be significantly smaller. Anyway, such bending effect

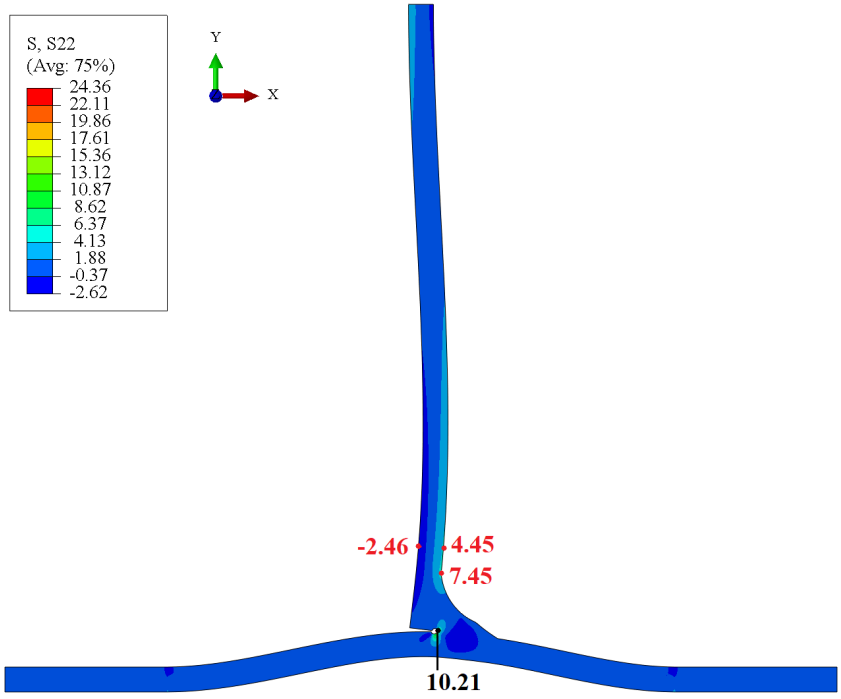

Figure 76: Magnified deformation shape of the T-joint specimen for lc3 with the S22 stress distribution

causes problems with the calculation of the notch factors. From [Fig. 76] it can be seen that the stress value at the distance of $1t$ from the weld toe at the vertical plate is no longer unitary. And not only that, because of the bending that occurs in the vertical plate, the stress is no longer equally distributed through its thickness as it should be for a tensile load case. With such effects active in the model, no meaningful notch factor calculation can be performed so *FEMFAT* proposed a solution for counteracting the negative bending effect which is shown in [Fig. 77]. So, the first simulation step, see [Fig. 77 (a)], results in unwanted bending effect which causes deformations depicted in [Fig. 76], but for that to be resolved another step must be added in which the inverted reaction forces from the first step would be applied, see [Fig. 77 (b)]. The inverted reaction forces would be taken from the reference points for the left fixing and the reference point for the acting force, both from the results in step 1. When these two steps are defined the new simulation can be conducted to obtain the results in step 2 as well. Finally, in order to get the valid stress results for the calculation of the notch factor caused by a purely tensile load, the field outputs for stress from the two described steps need to be added together as it is depicted in [Fig. 78]. The addition of these two stress field outputs results in the correct

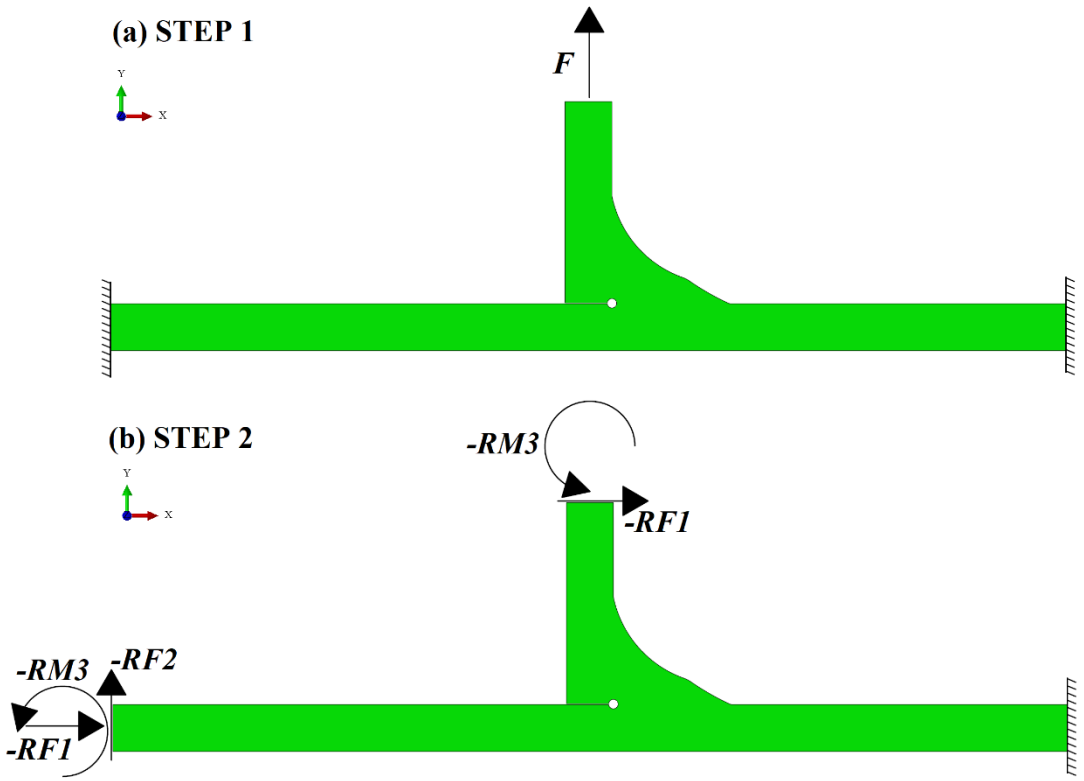

Figure 77: Solution for the unwanted bending effect in lc3 proposed by *FEMFAT*

distribution of the principal stress S22 through the vertical plate of the weld joint which is investigated in this load case. From [Fig. 78] it can be seen that the stress values at the distance of $1t$ from the weld toe at the vertical plate, are in fact unitary which means that the notch factor for the weld toe with the value of $K_{\text{f, t-lc3}} = 1.58$ is valid without any calculation. Since the bending correction was done as proposed by *FEMFAT*, the value for the root notch factor $K_{\text{f, r-lc3}} = 11.64$ doesn't need to be additionally corrected as well.

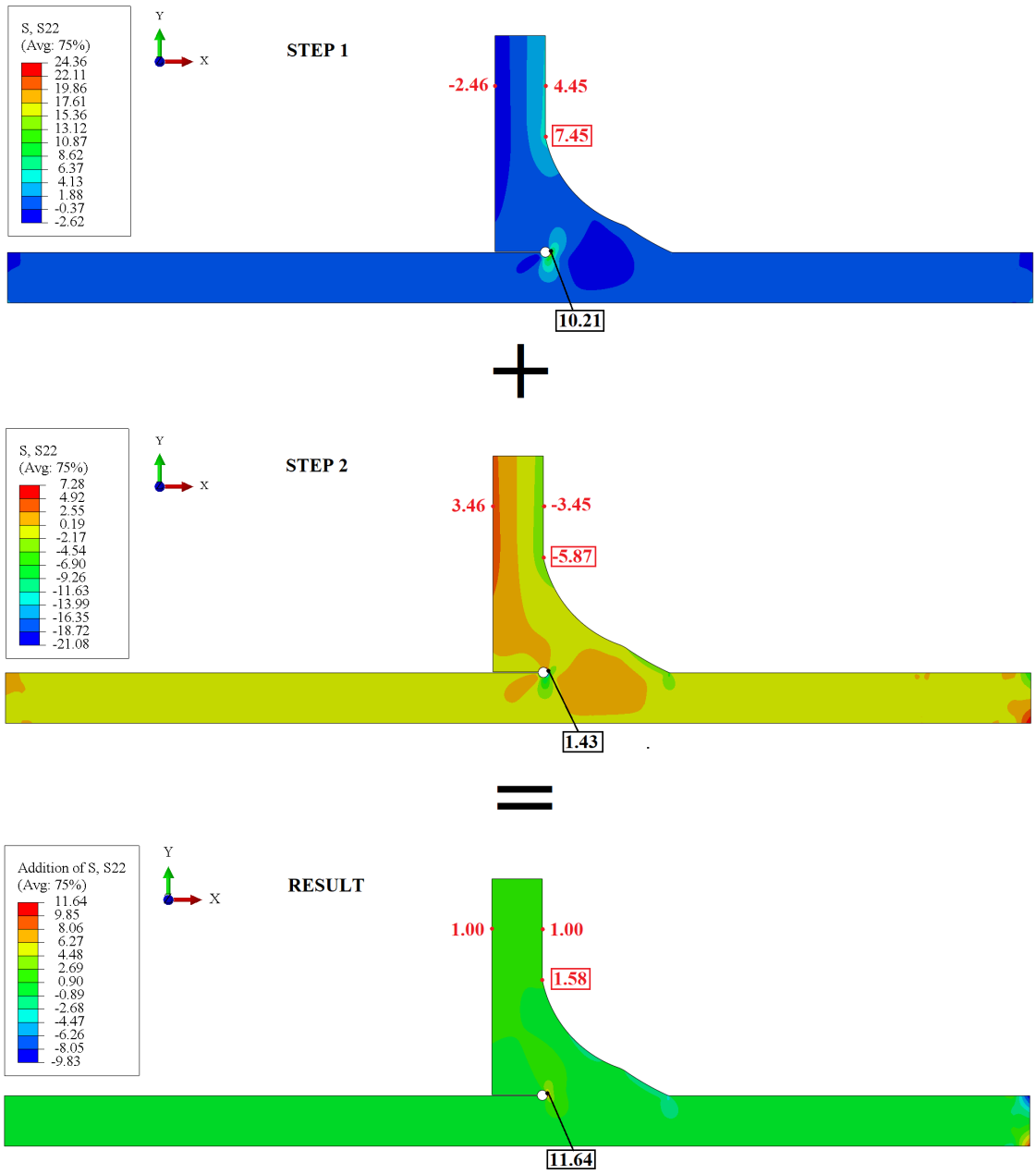

Figure 78: Principal stress S22 distribution and bending correction for the T-joint specimen in lc3

6.2.4 Bending load case, lc4

Similar to the load case lc2, the fourth load case lc4 also investigates the stresses in respect to the bending loading conditions, but for the vertical plate of the specimen since the horizontal plate was already assessed in the load case lc2. Once again, the specimen is loaded via the vertical plate of the weld joint with the moment $M_{\text{unitary}} = 1.5$ Nmm and boundary conditions according to [Fig. 35]. The stress distribution of the principal stress S22 in the weld joint can be seen in [Fig. 79] along with the corresponding values of the stress at the weld toe of the vertical plate and the weld root. In both load cases defined for the vertical plate of the joint, lc3 and lc4, the principal stress S122 was used because the said plate lies in the direction of the principal Y axis. From the stresses at the distance of $1t$ at the weld toe, the distribution of stresses through the thickness of the material can be nicely seen, the same as in [Fig. 75] but for the horizontal plate.

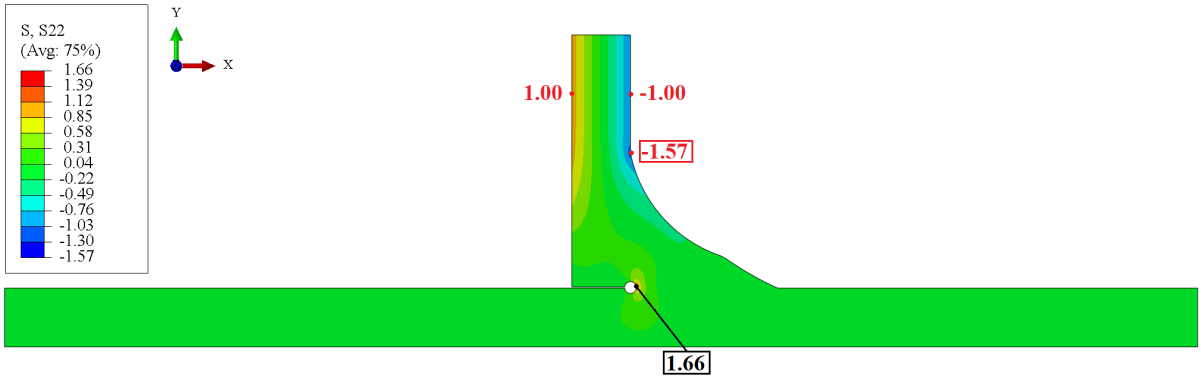

Figure 79: Principal stress S22 distribution in the T-joint specimen for lc4

The values of the nominal stresses at the distance of $1t$ from the evaluated notch are once again unitary, so the notch factors can be taken directly from [Fig. 79] with the notch factor at the vertical weld toe equal to $K_{\text{f, t-lc4}} = 1.57$. The notch factor at the weld root has a value of $K_{\text{f, r-lc4}} = 1.66$ but it needs to be corrected again because of the root undercut. The corrected notch factor for the root is obtained from the equation (15) with a value of $K^*_{\text{f, r-lc4}} = 1.35$. Since the critical stress in the root is positioned in the top part of the undercut modeled for the root notch effect description, for the values of the stresses at the lower and upper surface used for the undercut correction via the equation (15), the stresses from the vertical plate must be included.

6.2.5 Load flow load case, lc5

As one of the two load cases that defines the notch factor for the load flow, the load case lc5 is defined for the investigation of only one notch effect in the weld joint and that is the effect of the weld root. Because of the boundary conditions and loading setup as per [Fig. 35], the stresses in the weld joint are distributed in such a way that the stress values for both weld toes gravitate around zero. The whole moment $M_{\text{unitary}} = 1.5$ Nmm applied through the vertical plate simply flows through the weld root to the only fixing in this load case which is on the opposite side of the vertical plate from the weld itself. The described stress distribution of the principal stress S11 is given in [Fig. 80] together with the values for the corresponding S11 stresses in the weld root.

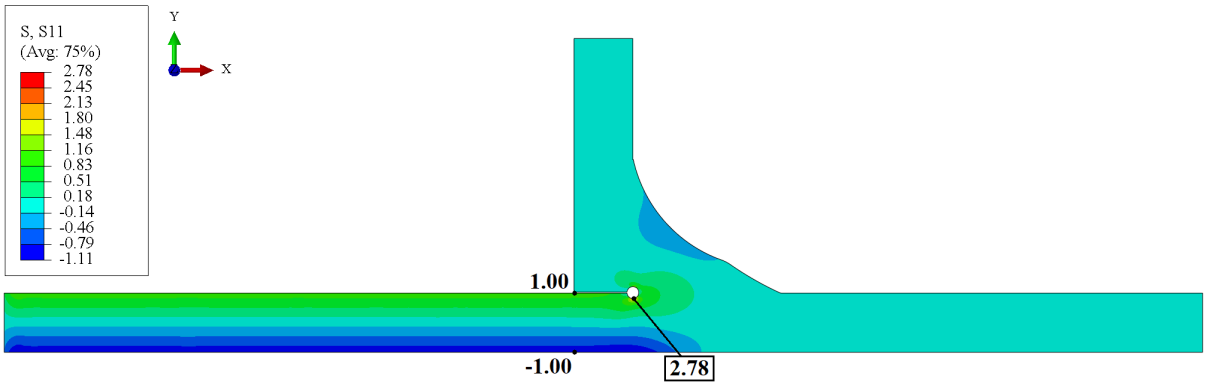

Figure 80: Principal stress S11 distribution in the T-joint specimen for lc5

Since the calculation of notch factors for the weld toe is meaningless in this case, only the notch factor for the weld root is calculated. This time, because the critical point of the root is positioned in the bottom part of the root undercut, the nominal stresses from the horizontal plate are used for the notch factor calculation. So, the notch factor for the weld root in the load case lc5 has a value of $K_{\text{f, r-lc5}} = 2.78$ but when corrected using the equation (15) and the adequate nominal stresses from both surfaces of the horizontal plate, it achieves a value of $K^*_{\text{f, r-lc5}} = 2.25$.

6.2.6 Load flow load case, lc6

The final load case for which the notch factors need to be defined is the load case lc6. The same as the previous one, this load case also investigates the effects of the load flow on the notch factors. However, because of the fixing of the specimen on the different side, this time on the side of the weld, see [Fig. 35], the load case serves as a tool for the definition of the notch factors at the weld toe rather than the weld root. Even though the stresses in the weld root exist and they are greater than zero, weld root doesn't need to be assessed in this load case since the already presented load case lc5 serves for that purpose. Given to the fact that there are two different weld toes in the T-joint fillet weld, and for the calculation of the notch factor only one is needed, both are assessed and the larger one is taken for the weld database incorporation. Each notch factor requires different principal stress for its proper assessment so in [Fig. 81] distributions of principal stresses in the weld joint for both, S11 stress in [Fig. 81 (a)] and S22 in [Fig. 81 (b)], are given. As it can be seen the larger notch factor is the one at the horizontal plate with a value of $K_{\mathrm{f,\,t\text{-}lc6}} = 1.85$, so this one will be taken into the database.

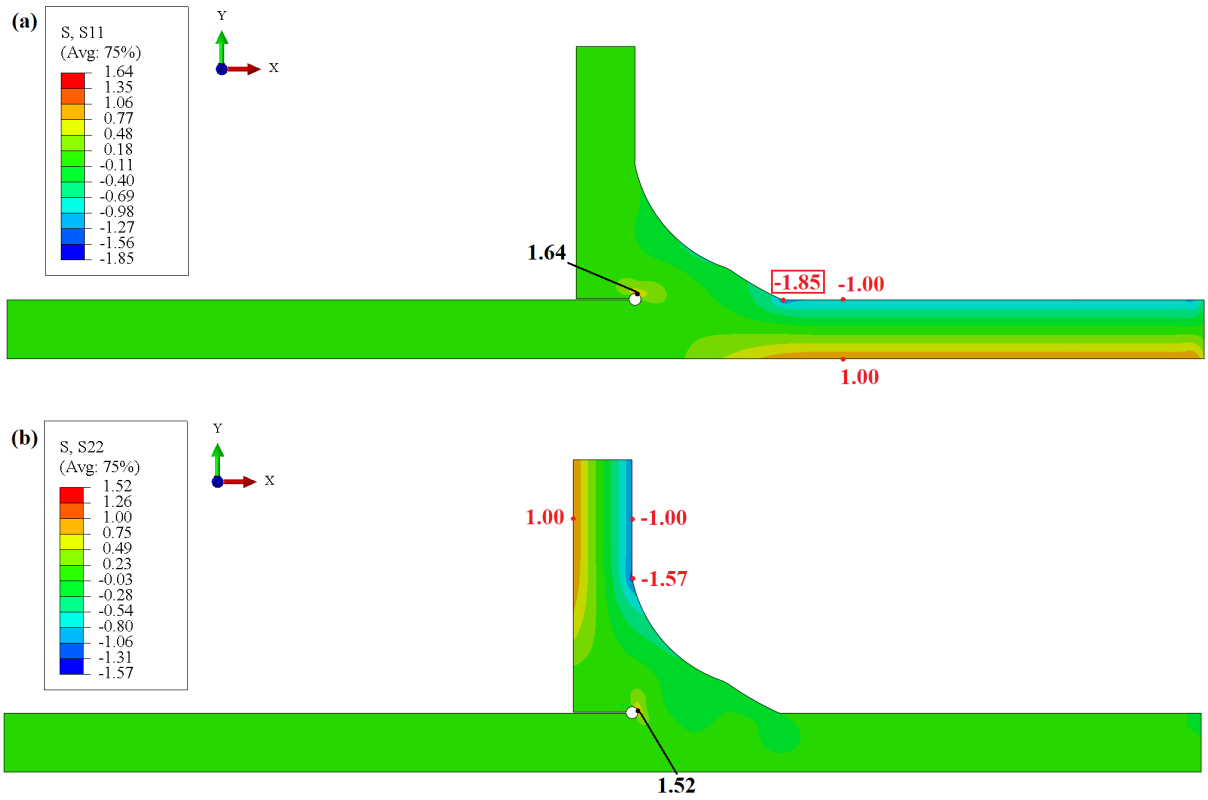

Figure 81: Principal stress distribution in the T-joint specimen for lc6 for: (a) S11, (b) S22

6.2.7 T-joint fillet weld with ρ_f = 0.3 mm

The distribution of corresponding principal stresses in each of the six load cases for the T-joint presented in this chapter along the increasing distance from the notch effect location, either weld toe or weld root, is almost identical to the distribution given in [Fig. 68] which is valid for the butt joint load cases so there is no need to visually represent it once more. In the case of the T-joint weld geometry, the nominal stresses also converge to the unitary value already at the distance of $0.5t$ which means that distance of $1t$ used for the calculation of the notch factors in each of the six load cases was justifiably applied. The similar behavior between both analyzed weld joints could be explained through the great quality of the mesh in each of the two models. The fine mesh with biquadratic elements allows for the fine distribution which can successfully capture the effect of the local stress concentrations caused by the notches defined with the fictious notch radius. If coarser mesh was used, it would be hard to keep the stress concentrations in very small areas therefore such fast convergence of the nominal stress would also be hardly possible.

Table 37: Calculated notch factors for T-joint fillet weld with ρ_f = 0.3 mm

	lc1	lc2	lc3	lc4	lc5	lc6
Weld toe	1.79	1.86	1.58	1.57	–	1.85
Weld root	2.25	2.38	11.6	1.35	2.25	–

With all of the load cases performed and analyzed, the new T-joint fillet weld with a fictious notch radius of $\rho_f = 0.3$ mm can be properly defined and imported into the weld database. All of the notch factors for this weld joint are gathered and presented in [Table 37] which includes all the corrections that needed to be done mostly for the reason of the root undercut in the model geometry. The only adaptation was done with the notch factor for the root from lc3 since the weld database format predicts only three digits for each notch factor i.e., the factor was rounded from 11.64 to 11.6. In order to include these notch factors into the weld database, they need to be recalculated in regard to the sheet thickness influence presented in chapter 3.2.2.3. If this step of the database extension procedure was to be skipped, the notch factors from [Table 37] could only be used for sheet thickness of $t = 3$ mm. As it was described in the case of butt joint specimens in chapter 6.1, all of the notch factors calculated for the sheet thickness of $t = 3$ mm

Table 38: Weld database notch factors for T-joint fillet weld with $\rho_f = 0.3$ mm

	lc1	lc2	lc3	lc4	lc5	lc6
Weld toe	2.69	2.79	2.37	2.36	–	2.78
Weld root	3.38	3.57	17.4	2.03	3.38	–

need to be multiplied by a reciprocal sheet influence factor of $1/G = 1.5$ in order to fit with the polygon course given in [Fig. 23]. Therefore, the final notch factors, ready to be introduced in the weld database as a part of a new weld joint are given in [Table 38].

Final values that need to be defined in order for the new joint to be successfully implemented into the weld database are the slope and the endurance cycle limit of the S-N curve for each analyzed notch. For the same reason as the one described in chapter 6.1.3, and to keep the continuity in the weld database extension, an arbitrary value of $N_{\text{end.}} = 2 \cdot 10^6$ was chosen for the cycle endurance limit for both, weld toe and weld root, according to IIW [9] and their FAT class definition. The slopes were taken from the SAFD results with the values of $k = 9.0$ for the weld toe, see [Fig. 63] and $k = 4.9$ for the weld root, see [Fig. 61]. The final definition of the newly created weld joint in the weld database is given in [Fig. 82].

```
$ T-Joint, Fillet Weld  (Master Thesis MV)                Situation: 2021-11-26
$ ------------------------------------------------------------
SID 210 T-joint, fillet weld with root undercut, r=0.3 mm
MIDSQ 903 901 905
$
$ Data for a node in the middle of the weld seam
$
$    MNT MNB UTL1 UTL2 UTL3 UBL1 UBL2 UBL3 WTL1 WTL2 WTL3 WBL1 WBL2 WBL3 SPTO SPBO SSTO SSBO
$    ---------------------------------------------------------------------------------------
 901 906                                  3.38 3.57 3.38
 902     906                                           3.38 3.57 3.38
 903 905     2.69 2.79 2.78
 904     905                 2.69 2.79 2.78
 905 903 901 2.37 2.36                                 17.4 2.03
 906 901 903                 2.37 2.36      17.4 2.03
$
$         BEPKT 1        BEPKT 2        BEPKT 3        BEPKT 4      SHEAR Top    SHEAR Bottom
$      Inclination    Inclination    Inclination    Inclination    Inclination    Inclination   Survival Probability in Perc.
$     Cycle Endur.   Cycle Endur.   Cycle Endur.   Cycle Endur.   Cycle Endur.   Cycle Endur.  Range of Disp. 10-90 Percent
$    ---------------------------------------------------------------------------------------------------------------------
N901          9.00           9.00           4.90           4.90           5.00           5.00           50.0
E901       2000000        2000000        2000000        2000000        1800000        1800000          1.260
N902          9.00           9.00           4.90           4.90           5.00           5.00           50.0
E902       2000000        2000000        2000000        2000000        1800000        1800000          1.260
N903          9.00           9.00           4.90           4.90           5.00           5.00           50.0
E903       2000000        2000000        2000000        2000000        1800000        1800000          1.260
N904          9.00           9.00           4.90           4.90           5.00           5.00           50.0
E904       2000000        2000000        2000000        2000000        1800000        1800000          1.260
N905          9.00           9.00           4.90           4.90           5.00           5.00           50.0
E905       2000000        2000000        2000000        2000000        1800000        1800000          1.260
N906          9.00           9.00           4.90           4.90           5.00           5.00           50.0
E906       2000000        2000000        2000000        2000000        1800000        1800000          1.260
$
```

Figure 82: Weld database for T-joint fillet weld with $\rho_f = 0.3$ mm

6.2.8 T-joint fillet weld with ρ_f = 1 mm

Using the describe procedure, notch factors were calculated once more for the fictious notch radius of $\rho_f = 1$ mm. Therefore, newly calculated notch factors already recalculated for the compliance with the sheet thickness influence polygon course are given in [Table 39]. Since the $\rho_f = 1$ mm was used, in the weld root, an undercut hole of the diameter $d = 2$ mm was modeled which is quite a lot of material loss for the sheet thickness of $t = 3$ mm. This led to the notch factor for the weld root in lc3 having a value of $K_{f,\,r\text{-}lc3} = 59.8$ which is unrealistic and therefore the value for this notch factor was left the same as in [Table 39].

Table 39: Weld database notch factors for T-joint fillet weld with ρ_f = 1 mm

	lc1	lc2	lc3	lc4	lc5	lc6
Weld toe	2.12	2.18	2.06	2.04	–	2.18
Weld root	2.19	2.25	17.4	0.89	2.24	–

The values for the slope and the endurance cycle limit stay the same regardless of the fictious notch radius since they are based either on the literature reference from IIW [9] or on the testing results like the slopes for each notch, weld toe and weld root. The definition of the final weld joint in the weld database is given in [Fig. 70].

```
$ T-Joint, Fillet Weld  (Master Thesis MV)                Situation: 2021-11-26
$ ------------------------------------------------------------
SID 210 T-joint, fillet weld with root undercut, r=1 mm
MIDSQ 903 901 905
$
$ Data for a node in the middle of the weld seam
$
$    MNT MNB UTL1 UTL2 UTL3 UBL1 UBL2 UBL3 WTL1 WTL2 WTL3 WBL1 WBL2 WBL3 SPTO SPBO SSTO SSBO
$    ---------------------------------------------------------------------------------------
 901 906                                    2.19 2.25 2.24
 902     906                                               2.19 2.25 2.24
 903 905     2.12 2.18 2.18
 904     905               2.12 2.18 2.18
 905 903 901 2.06 2.04                                     17.4 0.89
 906 901 903               2.06 2.04      17.4 0.89
$
$         BEPKT 1        BEPKT 2        BEPKT 3        BEPKT 4      SHEAR Top    SHEAR Bottom
$      Inclination    Inclination    Inclination    Inclination    Inclination    Inclination   Survival Probability in Perc.
$      Cycle Endur.   Cycle Endur.   Cycle Endur.   Cycle Endur.   Cycle Endur.   Cycle Endur.  Range of Disp. 10-90 Percent
$     ---------------------------------------------------------------------------------------------------------------------
N901         9.00           9.00           4.90           4.90           5.00           5.00           50.0
E901      2000000        2000000        2000000        2000000        1800000        1800000          1.260
N902         9.00           9.00           4.90           4.90           5.00           5.00           50.0
E902      2000000        2000000        2000000        2000000        1800000        1800000          1.260
N903         9.00           9.00           4.90           4.90           5.00           5.00           50.0
E903      2000000        2000000        2000000        2000000        1800000        1800000          1.260
N904         9.00           9.00           4.90           4.90           5.00           5.00           50.0
E904      2000000        2000000        2000000        2000000        1800000        1800000          1.260
N905         9.00           9.00           4.90           4.90           5.00           5.00           50.0
E905      2000000        2000000        2000000        2000000        1800000        1800000          1.260
N906         9.00           9.00           4.90           4.90           5.00           5.00           50.0
E906      2000000        2000000        2000000        2000000        1800000        1800000          1.260
$
```

Figure 83: Weld database for T-joint fillet weld with ρ_f = 1 mm

7 COMPARISON OF HCF TESTING WITH *FEMFAT Weld*

After the successful application of the weld database extension to the literature example in the chapter 4, the whole procedure for the expansion of the weld database has now been completed in much more detail for both of the specimen types investigated in this thesis while abiding to all given *FEMFAT* recommendations. As a result, notch factors for various different weld joints were obtained and together with the data gathered from the high cycle fatigue testing, multiple new weld joints were created and implemented in the existing weld database. In order to see how accurate these newly created weld joints are in terms of fatigue assessment, a comparison of the *FEMFAT Weld* analysis which uses them with the results of HCF testing needs to be performed. As described through the chapter 3, *FEMFAT Weld* uses the data given in the weld database for the fatigue assessment of welded structures, therefore for each of the setups that were tested for high cycle fatigue in the scope of this thesis and presented in chapter 5.4, a corresponding *FEMFAT Weld* analysis will be conducted. With using the weld joints of the same type, created for different assumptions of the fictious notch radius ρ_f, the main question to be answered is how well these assumptions predict the behavior of the real specimens in regard to fatigue life. In addition to the comparison of the newly created weld joints, an analysis with the existing weld joints for the I-seam and the fillet weld that are defined in the database by *FEMFAT* will be conducted to see how they compare with the assessment using the newly created weld joints.

Before presenting the comparison analyses for each of the four setups from chapter 5.4 separately, some mutual characteristics of said analyses can be mentioned. As it was already mentioned *FEMFAT Weld* uses the results of the FEM analysis in order to conduct its fatigue assessment based on the data from the weld database. Therefore, an FE model was created for each setup with considerations to the modelling guidelines proposed by *FEMFAT*, especially in regard to the meshing of each model, presented in the chapter 3. Since these finite element analyses are in fact within the static and linear domain of behavior, the material properties from [Table 6] were used for their purposes. With the FEM results obtained through *Abaqus 2019.HF4*, each setup i.e., each tested weld joint, could be properly assessed in respect to fatigue life using the *FEMFAT Weld* module. Since fatigue assessment in *FEMFAT Weld* implies a dynamically loaded welded structure, a different set of material data from the one used in static analyses is needed. Hence, material data for 6060-T66 aluminum alloy, which was used for the specimen manufacturing, is taken from AVL material library, see [Table 40].

Table 40: Material data for 6060-T66 aluminum from AVL material library

	Static [MPa]		Fatigue, $P_S = 50\%$ [MPa]	
Strengths	UTS R_m	Yield $R_{p0.2}$	Pulsating	Alternating
Tension	215.0	160.0	131.4	77.2
Compression	215.0	160.0	0.0	77.2
Bending	256.5	191.7	139.3	96.9
Shear	124.1	92.3	80.6	44.5

For each setup, the weld seam in the model geometry was defined using the procedure in *FEMFAT Visualizer* described in the chapter 4.4. As in [Fig. 40] where the weld joint for the FE model from the literature example was defined, the newly created weld joints were also assessed only for the nodes in the middle of the weld seam i.e., if they were to be used for the assessment of the start or end of the weld in any given welded structure, notch factors from the database for each new weld joint would need to be adapted. However, this type of assessment is something only to be considered for future reference, since it is not in the scope of this thesis, hence all of the weld joints that will be assessed are deemed to be applied as circumferential weld seams.

Furthermore, each of the setups from the HCF testing has four different load levels defined through four different force ranges ΔF with each force range consisting of the minimum and maximum force applied in a pulsating sequence. For the *FEMFAT Weld* fatigue assessment two different force levels need to be applied to the model that is being assessed in order to get meaningful fatigue assessment results i.e., one simulation with *FEMFAT Weld* is valid for one force range that was applied during the corresponding HCF test. This gives the results needed for one point in the S-N curve diagram, therefore each setup was simulated in *FEMFAT Weld* for two different force range ΔF values in order for the full S-N curve to be created. Each of the two points for the definition of the S-N curve is obtained using the damage calculation analysis in *FEMFAT*. All of the fatigue assessments conducted in *FEMFAT* for various setups were performed for the survival probability value of $P_S = 50\ \%$, therefore the comparison of the obtained S-N curves will be presented in respect to the S-N curve for $P_S = 50\ \%$ for each of the four setups used in the testing respectively.

7.1 Butt joint specimen - tension

The first setup from the HCF tests conducted for this thesis was the HCF tensile test of the butt joint welded specimen. The FE model for this setup was created and defined according to the boundary and loading conditions given in [Fig. 56 (a)] with all four load levels used in the testing, see [Table 24], included into the FE analysis. The mesh that was created as per *FEMFAT Weld* recommendations can be nicely seen from [Fig. 84] where the stress distribution of the Max. Principal stress in the specimen in question is shown for the maximum force from the HCF tests loading data i.e., F_{max}=7920 N. For the *FEMFAT Weld* fatigue assessment, the highest and lowest force range ΔF values were taken from the HCF testing data which can be found in [Table 24], and used as the two needed load levels in order to get the necessary results

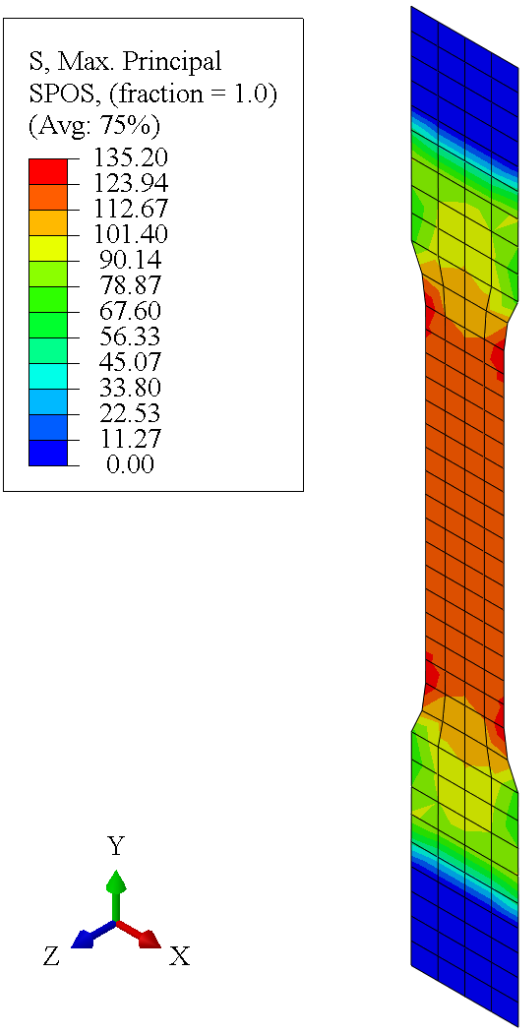

Figure 84: Max. Principal stress distribution in the butt-joint specimen for the tension setup with the maximum force

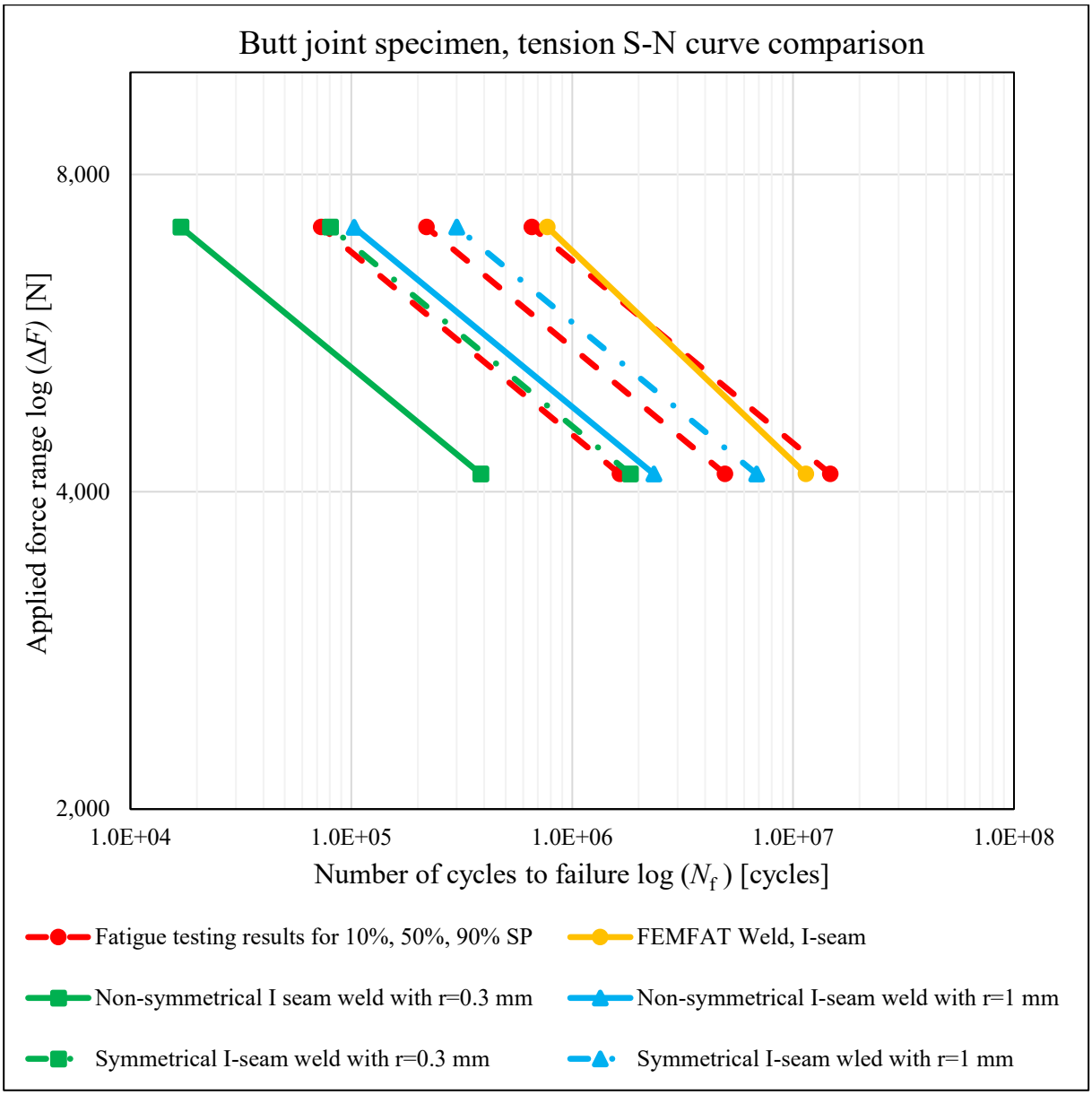

Figure 85: S-N curve comparison for the butt join specimen in tension setup

for the creation of the corresponding S-N curves. All four newly created butt joint welds introduced into the database and presented in the chapter 6.1, were assessed with *FEMFAT Weld* resulting in four different S-N curves that are depicted in [Fig. 85]. Also, the S-N curves created from the HCF testing results given in [Fig. 57] and [Table 25] and the S-N curve for the I-seam weld joint already existing in the weld database, are shown in [Fig. 85] as well.

From looking at the curves given in [Fig. 85] several conclusions can be drawn. First one is that the existing weld joint created by *FEMFAT* shows more optimistic results for the fatigue assessment in comparison to the 50% survival probability S-N curve obtained with HCF testing.

As for newly created I-seam weld joints, the most conservative results overall are obtained from the I-seam weld with $\rho_f = 0.3$ mm, which shows the reduction in fatigue strength with a factor of more than 10 in respect to the experimental 50% survival probability line. On the other hand, using the $\rho_f = 1$ mm for the I-seam weld, the S-N curve is shifted to the right which could be expected since the notch effect included in the notch factor is smaller due to the larger notch radius. However, the results are still a little conservative in respect to the 50% survival probability line from the test. When applying the symmetrical I-seam weld for whichever value of fictious notch radius ρ_f, the results show to be less conservative in respect to the non-symmetrical weld joint with the same ρ_f. This is only logical since the symmetrical I-seam weld joint was derived from the non-symmetrical one by using only the smaller notch factors from the two sets available in the non-symmetrical joint, see chapter 6.1, and smaller notch factors must result in higher fatigue strength for the same loading conditions. Both of the S-N curves for the symmetrical I-seam weld joints fall in between the 10% and 90% survival probability lines from HCF testing with the I-seam weld joint defined for $\rho_f = 0.3$ mm showing more conservative results than the I-seam with the $\rho_f = 1$ mm. Overall, the most fitting result for the 50% survival probability S-N curve obtained by HCF testing is the one from the simulation with the symmetrical I-seam weld defined with $\rho_f = 1$ mm.

In order to achieve better matching with the test results, the non-symmetrical I-seam weld joint would need to be recalculated for a fictious notch radius greater than $\rho_f = 1$ mm. This could be done either by repeating the process of notch factor calculation for a larger notch radius or by using the values obtained from the two analyzed notch radii with linear extrapolation to find out the exact notch radius fitting to the 50% survival probability curve from the test. The same could be stated for the symmetrical I-seam weld joint except in this case the most suitable notch radius is somewhere between the two analyzed radii so linear interpolation should be used instead. Similar linear approximations can already be found in the weld database e.g., with the base and weld material correlation, see [Fig. 19] and sheet thickness influence, see [Fig. 23].

In regard to the overall test results, the existing *FEMFAT* I-seam weld gives too optimistic assessment while the non-symmetrical welds from the manufactured specimens result in rather conservative fatigue strengths. This would mean that the real radii in both weld toes of the butt joint specimen are in fact much larger than the *FEMFAT* assumption $\rho_f = 0.3$ mm which the equation (29) assumes i.e., equation (29) seems to be too conservative for the I-seam weld.

7.2 Butt joint specimen – 3-point bending

As described through the chapter 5, the tension setup for the butt joint specimen was used to analyze the notch effect at the bottom of the specimen, which had larger notch effects due to the nature of the welding process. So, in order for the notch effect at the top of the specimen to be analyzed, the 3-point bending setup was defined. Using the boundary and loading conditions given in [Fig. 58 (a)], the FE model for the setup in question was created. Once again, all four load levels used in the testing, see [Table 26], were included into the FE analysis. The mesh for the modelling of the butt joint specimen was created as per *FEMFAT Weld* recommendations while the pins were modeled with solid elements. The modelling approach for this setup was the same to the one described in the case of literature example used for the database extension procedure validation in chapter 4. The stress distribution of the Max. Principal stress in the butt joint specimen for the 3-point bending setup can be seen in [Fig. 86], showing the stresses resulting from the maximum force of $F_{\max}$=700 N from [Table 26]. The same as it was the case with the tension setup, the highest and lowest force range ΔF values were taken from the HCF testing data and used for the *FEMFAT Weld* fatigue assessment for the creation of the characteristic S-N curves for each analyzed weld joint.

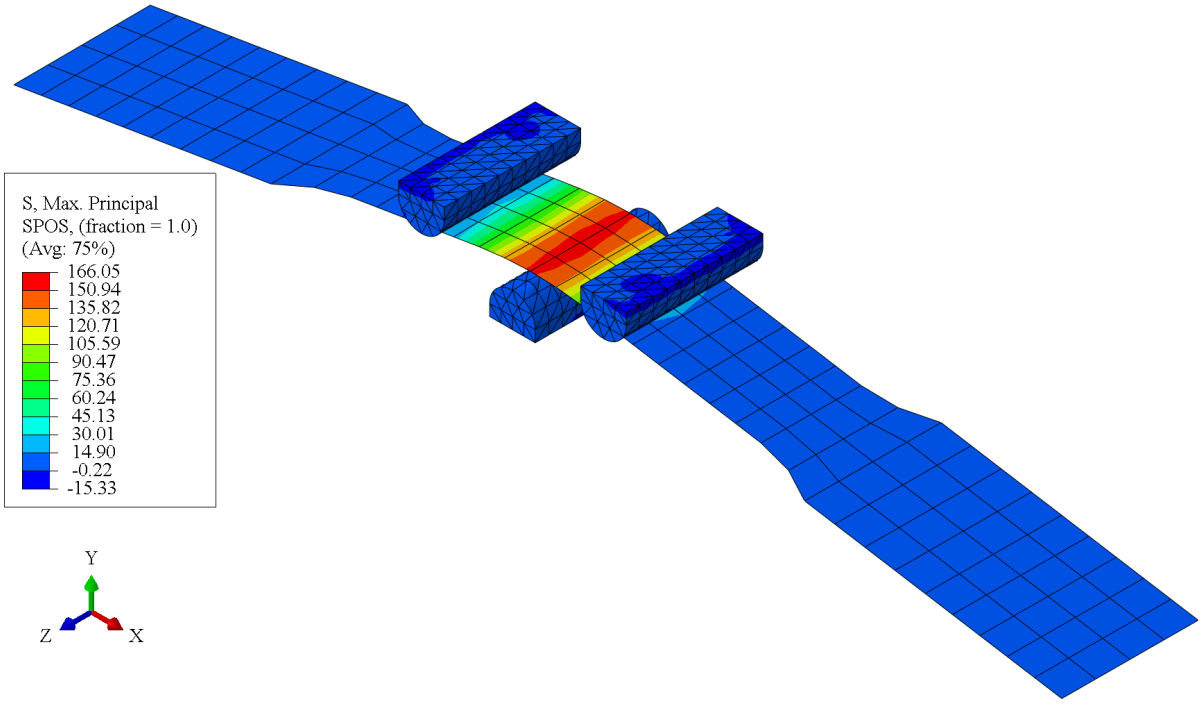

Figure 86: Max. Principal stress distribution in the butt-joint specimen for the 3-point bending setup with the maximum force

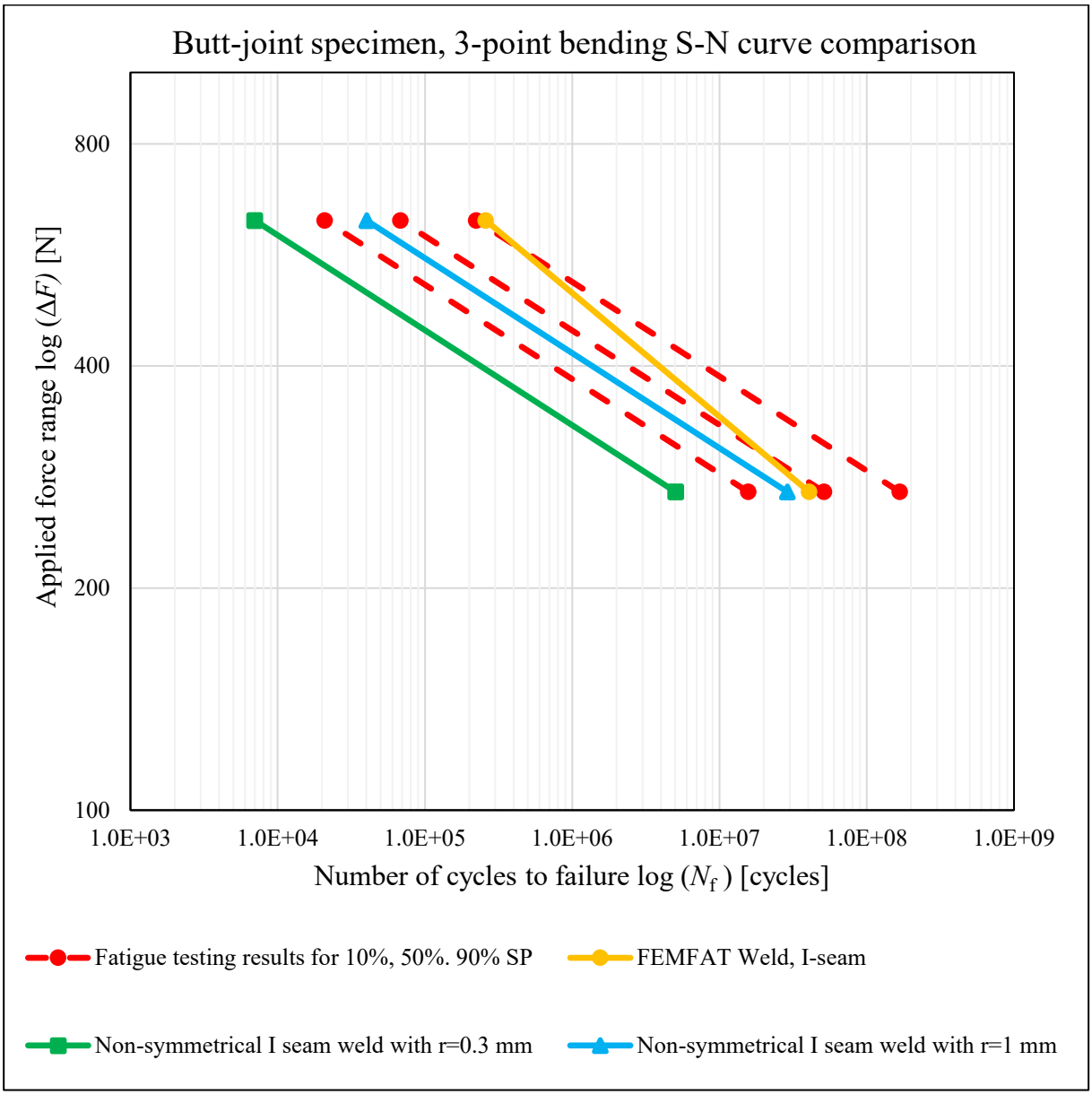

Figure 87: S-N curve comparison for the butt joint specimen in 3-point bending setup

Opposite to the tension setup assessment where all four newly created I-seam welds from the chapter 6.1 were investigated, in the case of the 3-point bending setup only the non-symmetrical weld joints created based on the original shape of the butt joint specimen were taken into the assessment. Since the 3-point bending setup was defined in a way to induce the crack initiation at the top side of the specimen i.e., at the weld toe with a smaller notch effect, the notch factors that describe this behavior are in fact the same notch factors that were used for the definition of the symmetrical butt joint I-seam weld. Therefore, whichever butt joint I-seam weld is used for the 3-point bending setup fatigue assessment, the results would be the same because the critical

notch factors that are taken from the database are the same. So, in order to prevent confusing visualizations in [Fig. 87] where the results are presented, only the results for the *FEMFAT Weld* fatigue assessment with the non-symmetrical I-seam welds are presented. Naturally, the S-N curves created from the HCF testing results given in [Fig. 59] and [Table 27] and the S-N curve for the already existing I-seam weld joint, are shown in [Fig. 87] as well.

By first glance at the S-N curves in [Fig. 87], it can be seen that similar to the results of the tension setup in [Fig. 85], all curves but one, are positioned inside the range of dispersion between the 10% and 90% survival probability lines from the experiment. The one curve that falls out of this range is the S-N curve from the non-symmetrical I-seam weld with the fictious notch radius of $\rho_f = 0.3$ mm, and once again fatigue assessment with this type of I-seam weld gives conservative results with a reduction factor of around 10 in respect to the 50% survival probability S-N curve from HCF testing. The non-symmetrical I-seam weld with $\rho_f = 1$ mm on the other hand, shows far better matching with the test values for 50% survival probability with a little bit more conservative S-N curve. Final result presented in [Fig. 87] is the one for fatigue assessment with the existing *FEMFAT* I-seam weld which lies quite nicely in the area of the test results, but it has a different slope. However, if a closer look is given to the point in the curve for the lowest force range, it can be seen that the cycle values for both the existing I-seam weld and the newly created one with $\rho_f = 1$ mm, are quite similar. In fact, if the *FEMFAT* recommendation about the S-N curve slope modification given in [Fig. 39 (b)] would be applied to the data of the existing I-seam weld, it would be possible to almost match the results of the existing I-seam perfectly with the newly created one for the fictious notch radius of $\rho_f = 1$ mm.

For the non-symmetrical I-seam weld joint to achieve better matching with the HCF results it would be needed to recalculate the notch factors for a notch radius greater than $\rho_f = 1$ mm, the same as in the case of butt joint tension loading results. Again, the same two methods could be applied to achieve this, either the linear extrapolation or to repeat the database extension procedure.

Looking at the overall results, the non-symmetrical I-seam weld can be considered as the least conservative result of all that are presented here. The existing *FEMFAT* I-seam weld gives a bit too different slope for a proper comparison but if the slope would be adapted in line with the *FEMFAT* recommendations, it would also show good matching. Once again, the *FEMFAT* assumption of $\rho_f = 0.3$ mm from the equation (29) seems to be too conservative for the weld toes in the case of a non-symmetrical butt joint welded specimen.

7.3 T-joint specimen – tension

The first of two setups used for the investigation of the T-joint specimen with the HCF tests conducted in the scope of this thesis was the HCF tensile test. The FE model for this setup was created and defined according to the boundary and loading conditions given in [Fig. 60 (a)]. Included into the FE analysis were also all four load levels used in the testing, see [Table 28]. The mesh created according to *FEMFAT Weld* recommendations from the chapter 3.2.1 can be nicely seen from [Fig. 88] where the stress distribution of the Max. Principal stress in the given T-joint specimen is shown for the maximum force applied during the HCF testing i.e., $F_{\max}$=1000 N. Once again, the highest and lowest force range ΔF values were taken from the HCF testing data which can be found in [Table 24] and applied to the simulation model for the purposes of *FEMFAT Weld* fatigue assessment.

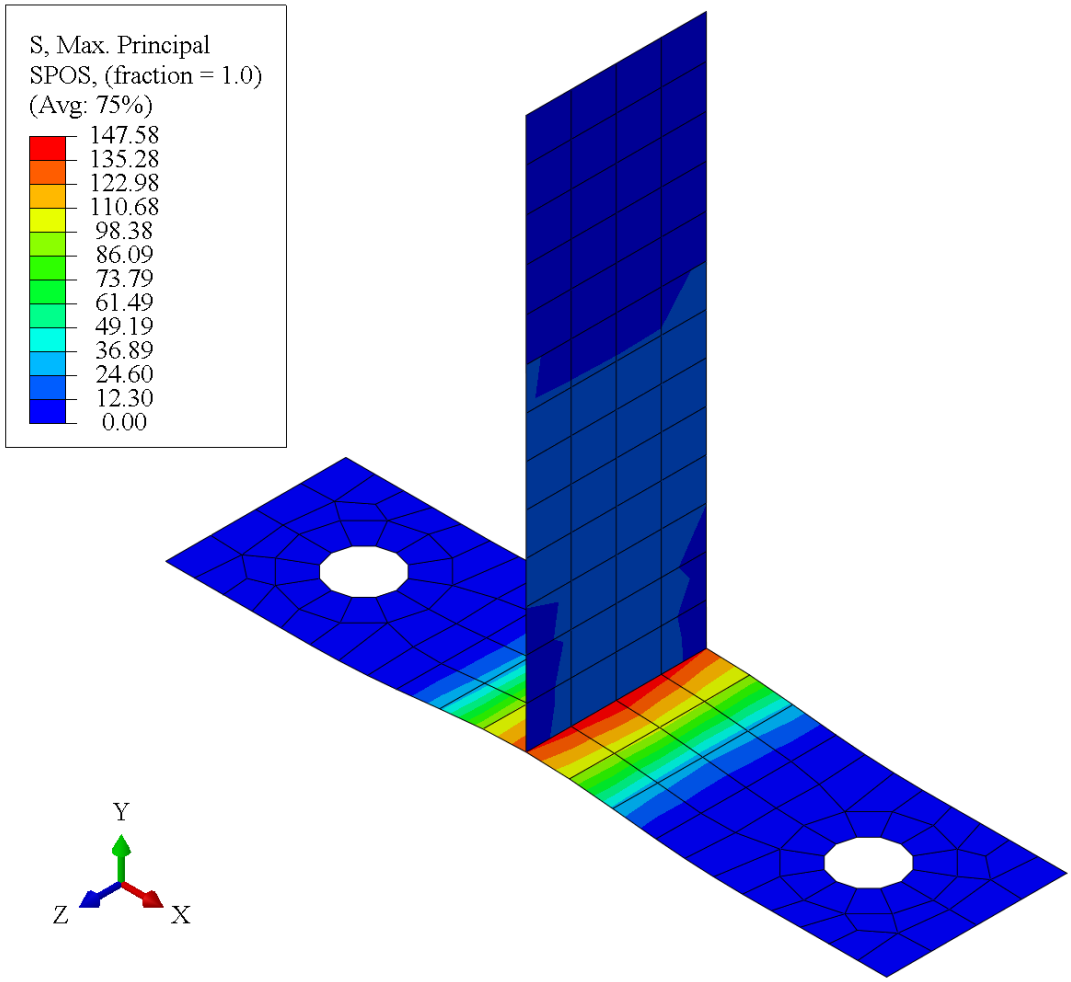

Figure 88: Max. Principal stress distribution in the T-joint specimen for the tension setup with the maximum force

Since for the T-joint specimen it wasn't possible to perform an assessment of the weld symmetry influence in regard to the fatigue assessment without creating a completely new FE model, only two new weld joints were defined in the weld database based on the two different fictious notch radii used throughout the whole thesis, $\rho_f = 0.3$ mm and $\rho_f = 1$ mm. The S-N curves obtained from the fatigue assessment using the *FEMFAT Weld* module for each of the two fillet weld joints defined in the chapter 6.2 are presented in [Fig. 89] along with the S-N curves created from the HCF testing results given in [Fig. 61] and [Table 29] and the S-N curve for the T-joint fillet weld with root undercut that already exists in the *FEMFAT* weld database.

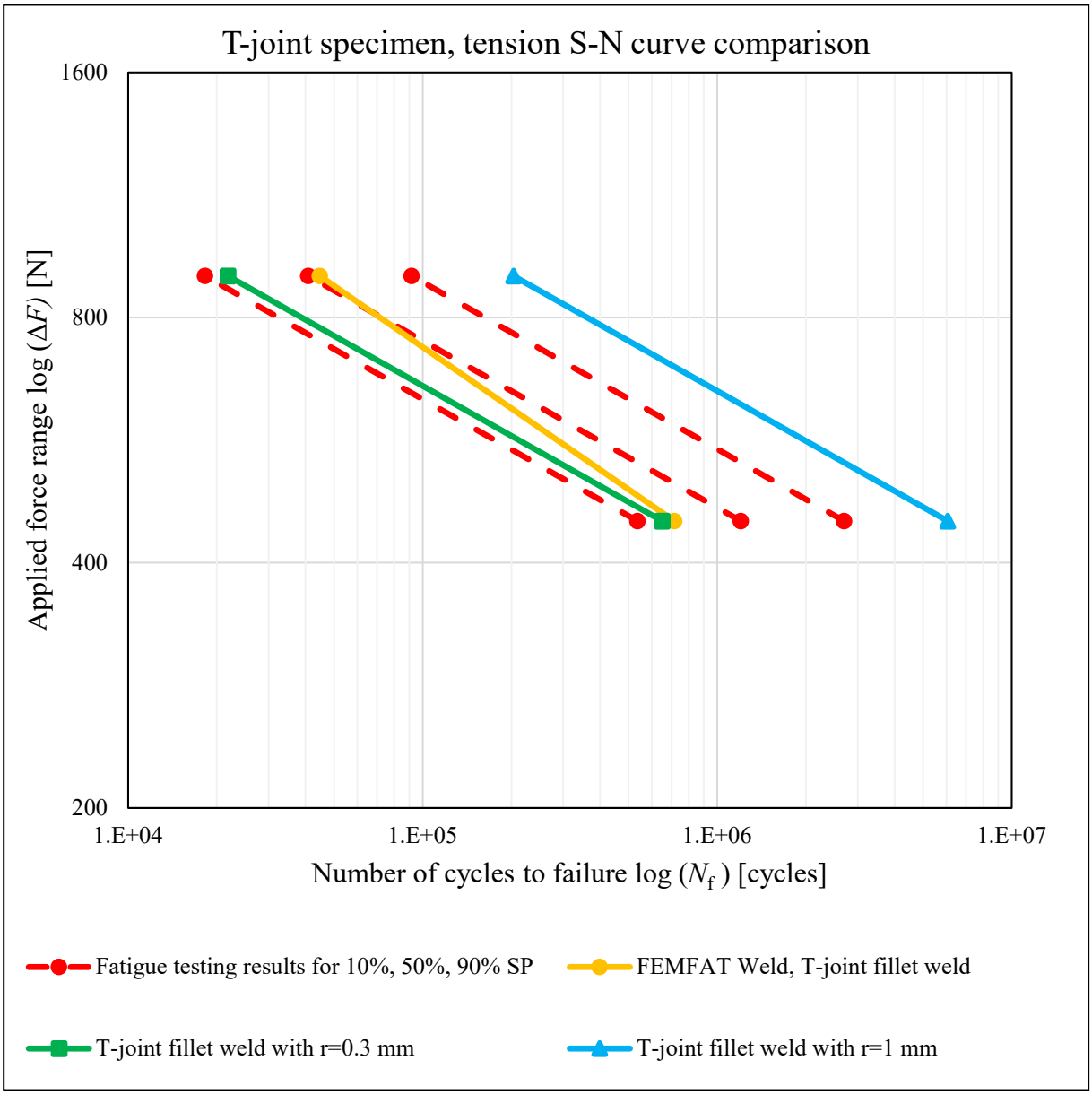

Figure 89: S-N curve comparison for the T-joint specimen in tension setup

From the comparison analysis of all the curves depicted in [Fig. 89] it can be noticed that a quite different layout of the curves is present in regard to the results presented so far with the butt joint specimen, specifically in regard to the positioning of the curves depending on the fictious notch radius. For the T-joint fillet weld with $\rho_f = 1$ mm the final S-N curve is overly optimistic in relation to the 50% survival probability curve obtained with HCF testing and it falls outside the range of dispersion for the tension setup. However, the S-N curve created from the fatigue assessment of the T-joint filet weld with the fictious notch radius of $\rho_f = 0.3$ mm provides rather good matching with being not too conservative in relation to the 50% survival probability S-N curve of the fatigue testing. As well as the newly created fillet weld joint, the fatigue assessment with the existing fillet weld with the root undercut lies nicely with the 50% survival probability line, however the slope of the existing fillet weld result doesn't match to the testing results. Nevertheless, with the points for the lower force range of the new and the existing fillet weld being so close as they are in [Fig. 89], the weld database calibration procedure for the slope modification given in [Fig. 39 (b)] could be applied. Using this procedure, the slope of the existing fillet weld would be adapted to the slope obtained from SAFD results in [Fig. 61] and the S-N curve would just pivot around the lower load level point until it aligns with the slope of the testing S-N curves. When aligned, the result would be pretty much the same as the one for the fatigue assessment with the new T-joint fillet weld.

Overall, the conclusion can be that in the case of the T-joint specimen, the assumption about the fictious notch radius $\rho_f = 0.3$ mm from the equation (29), isn't too conservative and that it provides results that are closer to the 50% survival probability curve than the assumption of the same radius with a value of $\rho_f = 1$ mm. If the exact radius that fits the testing curve would be calculated, it would lie somewhere between the two fictious radii analyzed in this thesis, and that would probably be much closer to the lower radius of $\rho_f = 0.3$ mm.

7.4 T-joint specimen – 3-point bending

The final set of S-N curves that needs to be assessed and compared is obtained with the 3-point bending setup of the T-joint welded specimen. This setup was used for the assessment of the weld toe in contrast with the tension setup of the same specimen which served for an assessment of the weld root. In order for the S-N curve data to be obtained, the FE model of the setup was created according to the boundary conditions given in [Fig. 62. (a)] with the loading data taken from [Table 30]. All eight force values that are distributed into four different pulsating load levels for the fatigue assessment were included in the FE model which can be seen in [Fig. 90] where the stress distribution for the Max. Principal stress in the T-joint specimen is given for the maximum force of $F_{\max}$=700 N for the 3-point bending setup of the HCF testing.

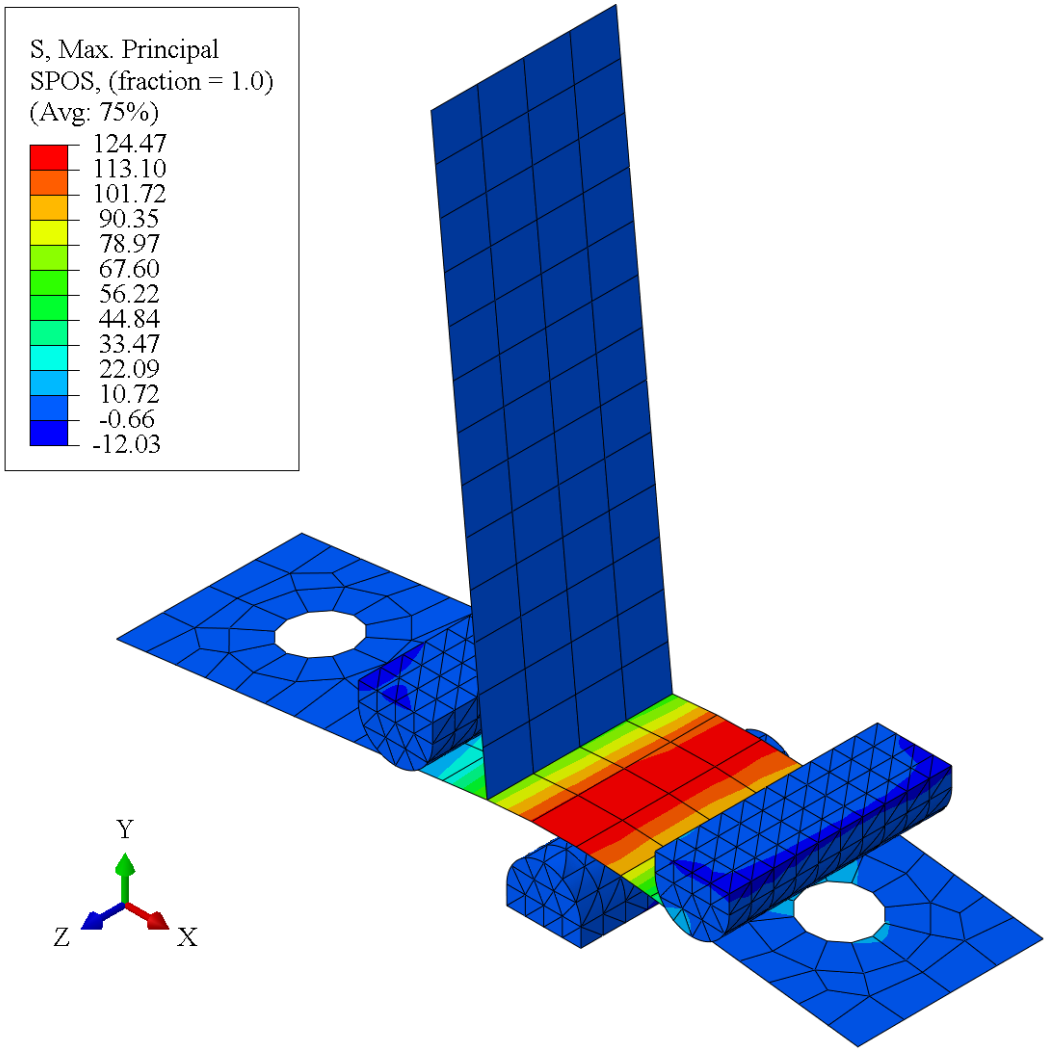

Figure 90: Max. Principal stress distribution in the T-joint specimen for the 3-point bending setup with the maximum force

From the statistical analysis of the HCF results for the 3-point bending setup with the T-joint specimen, see [Fig. 63], it is seen that the S-N curve is the closest to being flat compared to other four different statistical results in respect to the specimen and setup type. A slope this high leads to the fact that the number of cycles at the lowest load level used in this setup exceeds the mark of $N_f = 1 \cdot 10^7$ cycles by quite some margin for the 50% survival probability S-N curve of the HCF testing. Given to the fact that such a high number of cycles isn't a matter of investigation in this thesis, for the visualization of the corresponding S-N curves, along with the highest value of the force range ΔF, the second lowest force range will be used to avoid the

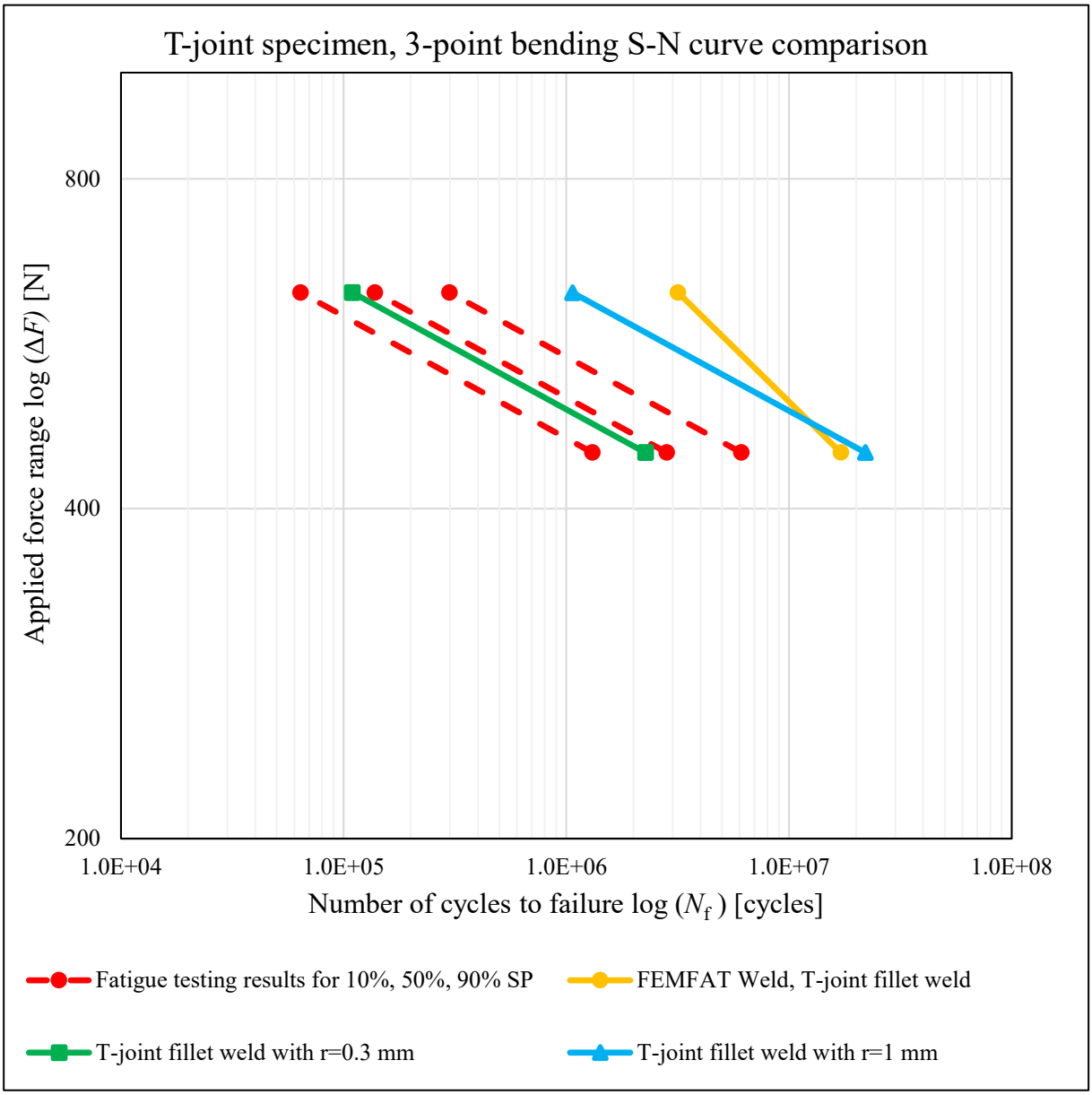

Figure 91: S-N curve comparison for the T-joint specimen in 3-point bending setup

extra high values of the cycles until failure. So, the S-N curves which correspond to this particular setup of the T-joint welded specimen are given in [Fig. 91] and they include two curves for the new fillet weld joints for the fictious notch radius $\rho_f = 0.3$ mm and $\rho_f = 1$ mm respectively, along with a curve for the existing fillet joint in *FEMFAT* and the results from HCF testing for each of the three characteristic survival probability values. From the diagram at [Fig. 91] the immediate conclusion could be drawn that the S-N curve obtained for the fillet weld with $\rho_f = 0.3$ mm shows almost perfect matching with the S-N curve for the 50% survival probability obtained from the HCF testing. The other two analyzed weld joints show similar results in regard to the position of their corresponding S-N curves in the diagram in the sense that both assessments provide overly optimistic evaluations of the fatigue life in comparison with the experimental data. The S-N curve for the fillet weld with $\rho_f = 1$ mm can be seen as shifted to the left from the 50% survival probability line meaning that the resulting notch stresses with such radius do not induce quite as much local concentrations as it was gathered from the testing data. Once again, the curve for the existing fillet weld from the weld database can be adjusted to match the curve for the newly created fillet weld with the fictious notch factor of $\rho_f = 1$ mm, by using the already mentioned *FEMFAT* weld database calibration procedure, see [Fig. 39].

The final results for the 3-point bending setup applied to the T-joint specimen show that the assumption of $\rho_f = 0.3$ mm has proven to be a good approximation for the T-joint. The reason for which this assumption could work better for the T-joint specimen is in fact the variation of the weld toe radius which seemed to be below 1 mm for all of the T-joint specimens used for the microscopic measurements. On the other hand, the weld toe radius for the butt joint varied even up to 3 mm, therefore the assumption of $\rho_f = 0.3$ mm was clearly way to conservative to be able to describe the fatigue life of multiple butt joint specimens that were tested.

8 CONCLUSION

Throughout the work of this thesis the whole fatigue assessment procedure used by *FEMFAT Weld* was thoroughly investigated and described in full detail. Even though the procedure was successfully validated with the use of a literature example, an experimental fatigue analysis of two different seam welds joining the 6060-T66 aluminum alloy was conducted in order to fully understand the calculation procedure based on the weld database which contains predefined weld joints with specifically assigned notch factors describing the notch effect in the weld. The high cycle fatigue results were then compared to the fatigue assessment from *FEMFAT Weld*.

The butt joint specimen with the welding conducted only from one side was subjected to two different setups in high cycle fatigue testing in order to obtain the results for two possible failure locations. As it was described, the two different possible crack initiation points exist due to the non-symmetry of the welding, since different notch effects occur on each side of the specimen. This non-symmetry is also reflected on the notch factor values in the weld database used for *FEMFAT Weld* fatigue assessment. Through the analysis of the high cycle fatigue results for each of the two setups, it could be observed that the basic assumption of the fictious notch radius calculated through equation (29) gives overly conservative results i.e., predicts a much shorter fatigue life in comparison with the S-N curve for the 50% survival probability from testing results. However, when fictious notch radius of $\rho_{\mathrm{f}} = 1\ \mathrm{mm}$ is applied, the fatigue assessment results obtained from *FEMFAT Weld* result in much better matching with the testing results even though still a little bit conservative in respect to the results. The reason for such conservative results could be found in the weld geometry of the butt joint specimen. From the measurements of the weld toe radii at each of the two different sides of the butt joint weld it has been found that weld toe radius varies a great deal from specimen to specimen, with some radii values going all the way up to $3\ \mathrm{mm}$. With that in mind, the conservative results for a fictious notch radius of $\rho_{\mathrm{f}} = 0.3\ \mathrm{mm}$ are then not that much surprising.

Equally as the butt joint specimen, the T-joint specimen welded with the one-sided fillet weld, was subjected to two different setups in high cycle fatigue testing in order to induce failure at both weld toe and weld root respectively. From the measurements of the T-joint weld geometry, a much smaller deviation up to only $1\ \mathrm{mm}$ in weld toe radius could be noticed as opposed to the butt joint, while for the notch size in the root no measurements could be taken but from the microscopic images a very small gap could be seen between the two welded extruded profiles,

justifying the geometry which was used to describe the notch radius in the weld root. In regard to the comparison of the high cycle fatigue results with the fatigue assessment results from *FEMFAT Weld*, the assumption of fictious notch radius with the value of $\rho_f = 0.3$ mm shows quite reliable fatigue results with good matching with the 50% survival probability values from testing results. With this being the case, introducing the fictious notch factor of $\rho_f = 1$ mm results in overly optimistic fatigue life in comparison to the high cycle fatigue results. Even though this may sound as a completely opposite conclusion from the one for the butt joint specimen, when the real radius at the location of the notch effect is considered, immediately it is clear that the assumption of $\rho_f = 0.3$ mm can be applied to describe the full set of the T-joint specimens without being too conservative. Therefore, it could be stated that the assumption given with the equation (29) can be used but with keeping in mind the size of the real notch i.e., for cases where larger radius variations are possible, the results may be too conservative.

As for the further calibration of the results from *FEMFAT Weld* with the goal of finding the correct notch radius that would perfectly describe the fatigue behavior of the testing results, two methods are proposed. Either to iterate the whole described procedure of weld database extension until the satisfactory value of the notch radius or simply to apply linear interpolation or extrapolation for the calculation of the fitting notch radius. In terms of time and cost efficiency, the latter most definitely seems better for the real-life engineering practice.

In the end, the most important conclusion that can be made from the work in this master thesis is in fact that *FEMFAT Weld* can be used for a reliable fatigue assessment of welded aluminum joints. The software provides great solutions for modifications of specific weld joints that can be adapted to the user's needs which is clearly seen from the way the symmetrical I-seam weld joint was derived from the non-symmetrical I-seam in order to obtain better matching results. By following all the defined steps for weld database extension, a total of six different weld joints was implemented into the weld database which provide enough data from which many more joints could be derived in a faster and simpler manner. Also, with all four setups, the weld joints already existing in the weld database were used for the fatigue assessment as well, and their respective results show to be rather optimistic in regard to the high cycle fatigue testing which means *FEMFAT* could be used for weld assessment without the concerns of too conservative results when additional safety factors apply to the structure. All of these observations confirm the fact that *FEMFAT Weld* is a powerful tool which can enhance and speed up the process of weld fatigue assessment in future work inside AVL GmbH.

LITERATURE

[1] Hashimoto, N.: *Application of Aluminum Extrusions to Automotive Parts*, KOBELCO Technology Review, 2017, 35, 69-75

[2] Schubert, E.: *Challenges in Thermal Welding of Aluminium Alloys*, World Journal of Engineering and Technology, 2018, 6, 296-303

[3] Naito, J., Suzuki, R.: *Multi-material Automotive Bodies and Dissimilar Joining Technology to Realize Multi-material*, KOBELCO Technology Review, 2020, 38, 32-37

[4] https://www.audi-mediacenter.com/en/audi-r8-72, October 14th, 2021

[5] EAA: *Aluminium in Cars – Unlocking the Light-weighting Potential*, European Aluminium Association, 2013

[6] https://www.audi-mediacenter.com/en/audi-e-tron-75, October 17th, 2021

[7] Almar-Næss, A.: *Fatigue Handbook*,Third edition, TAPIR, 1985

[8] CEN: *EN 1999-1-3: Eurocode 9: Design of aluminium structures – Part 1-3: Structures susceptible to fatigue*, European Committee for Standardization, 2011

[9] IIW: *Recommendations for Fatigue Design of Welded Joints and Components*, International Institute of Welding document IIW-1823-07, 2008

[10] ECCS: *European Recommendations for Aluminium Alloy Structures Fatigue Design*, European Convention for Constructional Steelwork, 1992

[11] Basquin, O. H.: *The Exponential Law of Endurance Tests*, Proceedings of the Thirteenth Annual Meeting, American Society for Testing Materials, 1910, 10, 625-630

[12] Mathers, G.: *The welding of aluminium and its alloys*, First edition, Woodhead Publishing, 2002

[13] Maddox, S. J.: *Fatigue strength of welded structures*, Second edition, Abington Publishing, 1991

[14] Pinho-da-Cruz, J. A. M., Ferreira, J. A. M., Costa, J. D. M., Borrego, L. F. P.: *Fatigue analysis of thin AlMgSi welded joints under constant and variable amplitude block loadings*, Thin-Walled Structures, 2003, 41, 389-402

[15] Radaj, D., Sonsino, C. M., Fricke, W.: *Fatigue assessment of welded joints by local approaches*, Second edition, Woodhead Publishing, 2006

[16] IIW: *Fatigue Design of Welded Joints and Components – Recommendations of IIW Joint Working Group XIII-XV*, International Institute of Welding document XIII-1539-96/XV-845-96, 2005

[17] Maddox, S. J.: *Review of fatigue assessment procedures for welded aluminium structures*, International Journal of Fatigue, 2003, 25, 1359-1378

[18] DNV: *Fatigue Design of Offshore Steel Structures*, Det Norske Veritas Recommended Practice DNV-RP-C203, 2010

[19] Lee, J.-M., Seo, J.-K., Kim, M.-H., Shin, S.-B., Han, M.-S., Park, J.-S., Mahendran, M.: *Comparison of hot spot stress evaluation methods for welded structures*, International Journal of Naval Architecture and Ocean Engineering, 2013, 2, 200-210

[20] Tveiten, B. W.: *The Fatigue Strength of RHS T-joints*, SINTEF report STF24A03220, 2003

[21] Radaj, D.: *Design and analysis of fatigue resistant welded structures*, First edition, Abington Publishing, 1990

[22] Pilkey, W. D., Pilkey, D. F., Bi, Z.: *Peterson's Stress Concentration Factors*, Fourth edition, John Wiley & Sons, 2020

[23] Dowling, N. E.: *Mechanical Behavior of Materials – Engineering Methods for Deformation, Fracture, and Fatigue*, Fourth edition, Pearson Education, 2013

[24] Lawrence, F. V., Mattos, R. J., Higashida, Y., Burk, J. D.: *Estimating the fatigue crack initiation life of welds* from *Fatigue Testing of Weldments*, American Society for Testing and Materials, 1978, STP 648, 134-158

[25] Peterson, R. E.: *Relation between stress analysis and fatigue of metals*, Proceedings of SESA, 1950, 11, 199-206

[26] Peterson, R. E.: *Notch sensitivity* from *Metal Fatigue*, McGraw Hill, 1959, 293-306

[27] Neuber, H.: *Kerbspannungslehre*, Springer, 1937

[28] Neuber, H.: *Über die Berücksichtigung der Spannungskonzentration bei Festigkeitsberechnungen*, Konstruktion, 1968, 20, 245-251

[29] Neuber, H.: *Theory of Notch Stresses*, Ann Arbor Mich, Edwards, 1946

[30] Thum, A., Buchmann, W.: *Mitteilungen der Materialprüfungsanstalt an der Technischen Hochschule Darmstadt*, Volume 1: *Dauerfestigkeit und Konstruktion*, VDI-Verlag, 1932

[31] Mann, T.: *Fatigue assessment methods for welded structures and their application to an aluminium T-joint*, Doctoral Thesis, Norwegian University of Science and Technology, 2006

[32] Sonsino, C. M., Radaj, D., Brandt, U., Lehrke, H. P.: *Fatigue assessment of welded joints in AlMg4.5Mn aluminium alloy (AA 5083) by local approaches*, International Journal of Fatigue, 1999, 21, 985-999

[33] Miller, K. J., de los Rios, E. R.: *The Behaviour of Short Fatigue Cracks*, Mechanical Engineering Publications, 1986

[34] Lee, Y.-L., Pan, J., Hathaway, R. B., Barkey, M. E.: *Fatigue Testing and Analysis (Theory and Practice)*, Elsevier, First edition 2005

[35] Gigliotti, L.: *Assessment of the applicability of XFEM in Abaqus for modeling crack growth in rubber*, Master Thesis, KTH School of Engineering Sciences, 2012

[36] Tada, H., Paris, P. C., Irwin, G. R.: *The Stress Analysis of Cracks Handbook*, Third edition, American Society for Testing and Materials, 2000

[37] Paris, P., Erdogan F.: *A Critical Analysis of Crack Propagation Laws*, Transactions of the American Society for Testing and Materials, 1963, 528-533

[38] Dijkstra, O. D., Soetens, F., van Straalen, I. J. J.: *Inventory of fatigue crack growth models and their data for aluminium alloy structures*, TNO Building and Construction Research, 1990

[39] El Haddad, M. H., Smith, K. N., Topper, T. H.: *Fatigue crack propagation of short cracks*, Journal of Engineering Materials Technology, 1979, 101, 42-46

[40] Härkegård, G.: *An effective stress intensity factor and the determination of the notched fatigue limit*, Proceedings of the International Symposium of Fatigue Thresholds, 1981, 867-879

[41] Maddox, S. J.: *An analysis of fatigue cracks in fillet welded joints*, International Journal of Fracture, Volume 11, 1975, 2, 221-243

[42] Bowness, D., Lee, M. M. K.: *Prediction of weld toe magnification factors for semi-elliptical cracks in T-butt joints*, International Journal of Fatigue, 2000, 22, 369-387

[43] https://femfat.magna.com/index.php?id=618, November 15th, 2021

[44] Tveiten, B. W., Sigmund, K. A., Fjeldstad, A.: *Fatigue Assessment of Aluminum Rectangular Hollow Section T-joints by Hot-Spot Stress Approach*, Proceedings of the Nineteenth International Offshore and Polar Engineering Conference, 2009, 392-399

[45] ECS: *FEMFAT 5.4 – WELD User Manual*, MAGNA 2019

[46] Tveiten, B. W., Fjeldstad, A., Härkegård, G., Myhr, O. R., Bjørneklett, B: *Fatigue life enhancement of aluminium joints through mechanical and thermal prestressing*, International Journal of Fatigue, 2006, 28, 1667-1676

[47] Avallone, E. A., Baumeister III, T., Sadegh, A. M.: *Marks' Standard Handbook for Mechanical Engineers*, Eleventh edition, McGraw Hill, 2006

[48] ECS: *FEMFAT 5.4 – WELD Modelling Guideline*, MAGNA, 2019

[49] ECS: *FEMFAT weld – advance training*, MAGNA, 2021

[50] ISO: *ISO/TR 14345 Technical Report*, International Organization for Standardization, 2012